

THE UNIVERSITY OF HULL

Macroporous polymers and Janus particles prepared  
via redox-initiated polymerisation of emulsion templates  
at room temperature

being a Thesis submitted for the Degree of Doctor of Philosophy  
in the University of Hull

by

Khaled Althubeiti

March 2018

MSc (University of Hull)

BSc (Taif University)

## **Acknowledgements**

First and foremost, I would like to express my massive gratitude to my supervisor Dr Tommy Horozov for his guidance, patience and help during my studies. I am extremely thankful to him for his support, understanding and building up my skills.

I would like massively to thank Taif University and Saudi cultural bureau in London for the financial support and giving me this opportunity to study abroad. I would like warmly to thank Tony Sinclair for the SEM images and the student Eun Sung Park for some of the experimental data collected during his Masters project with my help and guidance. Thanks also go to Chris and Nigel in the mechanical workshop for their help in some of the experiments. I would like to express my deepest gratitude to all my friends in the Chemistry department, past and present, who shared their time with me in and outside the lab, in particular, Ben, Ana Maria, Hui Shi, Robe, Osama, Ahmad, Connor, Jamie, Javen, Dain, Anump. I would like deeply to thank all my Saudi friends who shared the time with me here in the UK, especially Mohammed Aljohni, Nasser Alamrani, Sead Algrny and Sahala Alosamy. I would also thank all my friends who I met here in the UK during my study, in particular Sezgin Tunc who supported me and spend time together.

Finally, I would like deeply to thank all my family who supported me and did not hesitate a second to stand by me. I would like to thank my sisters and brothers for their encouragement and motivation during my studies. Special thanks go to my uncle Abudallah who supported me and stand beside me all the time in my life. There are no words to express my thanks and gratitude to my parents Mansi and Sarah Althubeiti for all their unreserved financial and emotional support. Special thanks also go to Rosy Althubeiti for her support, motivation and inspiration and who has been lighting my days. Without all the support of my family I would not reach this stage.

## Abstract

The main focus of this thesis is on the preparation of macroporous polymers and Janus particles using emulsion templates. Benzoyl peroxide – dimethyl-p-toluidine (BPO-DMPT) redox-initiation couple is used to polymerise the oil phase of water-in-oil (w/o) or oil-in-water (o/w) emulsion templates at room temperature and produce macroporous polymeric materials or Janus particles, respectively.

The preparation of macroporous polymers via emulsion templating usually uses water-in-oil emulsions. The polymerisation of the oil phase is initiated either by a thermo-initiator at elevated temperature (60-80 °C) or a photo-initiator by irradiating relatively thin transparent samples with UV light. Both approaches suffer from low energy efficiency and require tedious sample preparation (removal of inhibitors, inert atmosphere). Those drawbacks are addressed by us in Chapter 3 of the thesis, where the polymerisation of w/o emulsion templates with a BPO-DMPT redox-initiation system at room temperature is investigated. The morphology and mechanical properties of the porous materials obtained are compared to those synthesised from emulsion templates using the traditional thermo-initiated polymerisation in Chapter 4. It is demonstrated for the first time that MMA-based emulsion templates can be polymerised using BPO-DMPT redox-initiation to produce open cell macroporous polymeric materials at room temperature without the need of any complicated steps of preparation typical for other methods. The method developed by us is simpler, faster and cheaper in comparison to the existing methods. It allows for the preparation of materials with up to 93 % porosity and better mechanical properties than those produced with the thermo-initiation method.

The preparation of Janus particles in large quantities is still one of the most challenging problems in the field. Most of the preparation methods reported suffer from limited yields or Janus functionalities which could be achieved. The use of particle-stabilised (Pickering) emulsions of paraffin wax-in-water has been used with some success for making Janus particles in large amounts, but the paraffin wax has caused problems with the poor particle adhesion and the limited conditions for chemical modification. In Chapter 5, we use our knowledge for redox-initiated polymerisation of methacrylates gained in the macroporous polymer study to develop efficient and reliable procedures for the preparation of Janus particles using polymerised o/w Pickering emulsions. The feasibility of this approach is demonstrated by small-scale experiments conducted using high speed homogenisation in the emulsion preparation. The possibility of scaling up the process to achieve larger yields

of Janus particles is also demonstrated. Janus particles with hydroxyl-amine functionalities have been produced and their Janus character revealed by zeta-potential measurement in comparison to bare and fully aminated silica particles.

## PRESENTATIONS

The work in this thesis has been presented by the author at the following conferences:

1. Poster presentation (1<sup>st</sup> Prize), “Preparation of Janus particles using polymerised Pickering emulsions”, RSC International conference “Particles at interfaces”, 7-9 September 2016, Leeds, UK.
2. Oral presentation, “Macroporous polymers prepared at room temperature via redox-initiated polymerisation of high internal phase emulsion templates”, 16<sup>th</sup> European Student Colloid Conference, 18-22 June 2017, the University of Florence, Italy
3. Oral presentation, “Macroporous polymers prepared at room temperature via redox-initiated polymerisation of high internal phase emulsion templates”, UK Colloids 2017, 10-12 July 2017, Manchester, UK
4. Oral presentation, “Preparation of macroporous polymers and Janus particles using redox-initiated polymerisation of emulsion templates at room temperature”, Departmental Research Colloquium, 22<sup>nd</sup> January 2018, University of Hull, UK.

## Contents

<b>CHAPTER 1 - Introduction</b> .....	<b>1</b>
1.1 Emulsions .....	2
1.1.1 Surfactant-stabilised emulsions .....	2
1.1.2 Particle-stabilised emulsions .....	3
1.1.3 Emulsion stability .....	7
1.1.3.1 Creaming or sedimentation .....	7
1.1.3.2 Flocculation and coalescence .....	8
1.1.3.3 Ostwald ripening .....	8
1.2 High internal phase emulsions .....	8
1.3 Polymerised High Internal Phase Emulsions (polyHIPEs) .....	9
1.3.1 Preparation of macroporous polymers .....	17
1.3.1.1 PolyHIPEs produced by thermo-initiated or photo-initiated polymerisation .....	18
1.3.1.2 PolyHIPEs produced by room temperature polymerisation using redox- initiation .....	20
1.4 Mechanical properties of solid foams and their deformation .....	21
1.5 Applications of polyHIPEs .....	28
1.6 Janus particles .....	29
1.6.1 Preparation of Janus particles .....	30
1.6.1.1 Microfluidic fabrication of Janus particles .....	30
1.6.1.2 Janus particles prepared by selective surface modification .....	32
1.6.1.3 Preparation of Janus particles using Pickering emulsion .....	34
1.6.2 Properties and applications of Janus particles .....	38
1.6.2.1 Amphiphilic properties .....	38
1.6.2.2 Magnetic and catalytic properties .....	39
1.6.2.3 Self-assembly of Janus particles .....	40
1.7 Aims of the research .....	42
1.8 Presentation of thesis .....	43
1.9 References .....	44
<b>CHAPTER 2 - Experimental</b> .....	<b>50</b>
2.1 Materials .....	50

2.1.1 Solvents .....	50
2.1.2 Surfactants .....	50
2.1.3 Silica particles .....	51
2.1.4 Chemicals used in polymerisation experiments .....	51
2.2 Methods used in the preparation of macroporous polymer by emulsion templating	52
2.2.1 Preparation of w/o emulsion templates for redox-initiated polymerisation at room temperature .....	52
2.2.2 Preparation of macroporous polymer via redox-initiated polymerisation at room temperature .....	53
2.2.3 Preparation of macroporous polymer via thermo-initiated polymerisation at 70°C.....	53
2.2.4 Purification of macroporous polymer by Soxhlet extraction .....	55
2.2.5 Investigation of the curing dynamics of polymerising samples .....	55
2.2.6 Mechanical properties and porosity determination .....	62
2.2.7 Voids and pore throat determination .....	66
2.3 Methods used in the preparation of Janus particles .....	67
2.3.1 Cleaning of silica particles .....	67
2.3.2 Amination of silica particles.....	67
2.3.3 Zeta potential measurements for silica particles .....	68
2.3.4 Preparation of emulsions and investigation of their type and stability .....	68
2.3.5 Polymerisation of Pickering emulsions .....	68
2.3.6 Microscope images .....	69
2.4 Scanning electron microscope (SEM) images .....	69
2.5 References .....	69
<b>CHAPTER 3 - Preparation of macroporous polymers from emulsion templates using redox-initiated polymerisation at room temperature .....</b>	<b>70</b>
3.1 Introduction.....	70
3.2 Preparation of macroporous polymeric materials from water-in-oil emulsion templates with variable volume fraction of water.....	71
3.2.1 Porous polymers prepared at constant surfactant concentration in the oil phase .....	71
3.2.2 Macroporous polymers prepared at constant surfactant concentration in the emulsion template.....	84
3.3 Effect of surfactant concentration on the properties of polyHIPEs at a fixed volume fraction of water in the emulsion template.....	97
3.4 Effect of cross-linker concentration on the properties of polyHIPEs at a fixed volume fraction of water in the emulsion template.....	111
3.5 Applications of macroporous materials produced at room temperature .....	122

3.6 Conclusions .....	130
3.7 References .....	132
<b>CHAPTER 4 - Porous polymeric materials produced by thermo-initiated polymerisation of emulsion templates at elevated temperature .....</b>	<b>134</b>
4.1. Introduction .....	134
4.2. Preparation of porous polymeric materials using BPO as thermo-initiator .....	135
4.3. Preparation of porous polymeric materials using AIBN as thermo-initiator .....	136
4.4. Comparison of porous polymeric materials produced at room temperature to those produced at high temperature .....	148
4.5. Conclusions .....	155
4.6. References .....	156
<b>CHAPTER 5 - Preparation of Janus particles using polymerised particle-stabilised emulsions.....</b>	<b>157</b>
5.1 Introduction .....	157
5.2 Small scale experiments with Pickering emulsions prepared by high speed homogenisation .....	160
5.2.1 Type and stability of emulsions .....	161
5.2.2 Polymerisation of the Pickering emulsions .....	173
5.2.3 Release of silica particles from polymerised emulsion droplets .....	181
5.2.4 Particle immersion in the polymer and ‘Janus balance’ .....	186
5.3 Scaling-up the process of Janus particle preparation .....	187
5.4 Conclusions .....	195
5.5 References .....	197
<b>CHAPTER 6 - Summary of conclusions and future work.....</b>	<b>198</b>
6.1 Summary of main findings and conclusions .....	198
6.2 Future work .....	203

## **CHAPTER 1**

### **Introduction**

The main focus of this research is to fabricate porous polymeric materials and Janus particles by using the emulsion templating technique. Water-in-oil emulsions are commonly used to produce macroporous polymeric materials by polymerising the continuous oil phase. After the polymerisation is completed, the water phase is removed upon drying leaving behind pores in the polymer matrix. One of the most challenging aspects of producing porous polymeric materials by this method is to maintain the emulsion template stable during the polymerisation. Traditionally, the polymerisation of the oil phase is initiated by using thermo-initiators or photo-initiators. When thermo-initiators are used, the polymerisation has to be performed at elevated temperature (60-80 °C) which decreases the emulsion stability. In contrast, the photo-initiated polymerisation is usually performed at room temperature under UV light exposure. However, it can be only applied on thin samples in transparent moulds allowing for the light to penetrate in the emulsion template. The polymerisation of methyl methacrylate at room temperature using redox-initiators (benzoyl peroxide and amines) is well-known and has been used in dentistry, medical restoration and other applications since 1950s. Nevertheless, until very recently, this approach has not been applied for the preparation of porous polymers by emulsion templating. In this study, we investigate the use of peroxide-amine redox initiation for the polymerisation of emulsion templates containing acrylic monomers at room temperature.

In the last two decades, there is increased scientific interest in solid particles which have two surface regions with different properties (Janus particles) because of their unique properties and potential applications. One of the most challenging problems in Janus particle research is their preparation in large quantities. Most of the preparation strategies reported suffer from limited yields or Janus particle functionalities, thus hampering the large-scale applications. One of the most promising approaches addressing that problem is the use of particle-stabilised (Pickering) emulsions of paraffin wax-in-water as a tool for making Janus particles introduced by Granick's group in 2006. However, the paraffin wax causes problems due to poor particle adhesion and limited conditions for chemical modification. Here, we extend this approach to polymerised Pickering emulsions using a mixture of monomers as an oil phase.

In this introductory chapter, the fundamental subjects which are most relevant to this research are presented. The basic concepts of emulsion stabilisation by both surfactants and solid particles are introduced. The main characteristics of high internal phase emulsions (HIPEs) and their polymerisation to polyHIPEs discussed. The mechanical properties of solid foams are described and the applications of polyHIPEs considered. The definition of Janus particles, the most common methods of their preparation, their properties and potential applications are reviewed.

## **1.1 Emulsions**

An emulsion is a mixture of two immiscible liquid phases, such as oil and water. One of the phases is dispersed into the other phase as droplets of microscopic size (typically with diameters  $> 1 \mu\text{m}$ ). Although the size of the emulsion droplets is bigger than the range identified for colloidal dispersions (diameter  $< 1 \mu\text{m}$ ), their characteristics and behaviour are ordinarily colloidal in nature, so they could be characterized as colloidal systems. There are two main types of emulsion. Emulsions in which oil droplets are dispersed in a continuous water phase are called oil-in-water (o/w) emulsions; whereas, those in which water droplets are dispersed in an oil phase are called water-in-oil (w/o) emulsions. There are more complex types of double (or multiple) emulsions, such as oil-in-water-in-oil (o/w/o) and water-in-oil-in-water (w/o/w) emulsions.<sup>1,2</sup>

### **1.1.1 Surfactant-stabilised emulsions**

When oil and water are mixed together, they produce an unstable emulsion resulting in a complete separation of the mixture into bulk phases within seconds. To overcome this problem and to produce a stable emulsion, a third component is required as a stabiliser. Surfactants (surface-active agents) are often used as an emulsion stabiliser (emulsifier). Their role is to lower the interfacial tension between the two immiscible phases by adsorbing at the oil-water interface and to prevent the rapid coalescence (merging) of the droplets.<sup>3</sup> Surfactant molecules have two different parts with different affinities to the oil and water phases. The tail group is hydrophobic and prefers to stay in oil, while the head group is hydrophilic and therefore has high affinity to water (Fig. 1.1). For instance, in an oil-in-water emulsion, the surfactant molecules adsorption at the interface between the two phases allows the head group (hydrophilic) to be positioned in the water phase and the tail group (hydrophobic) to be positioned in the oil phase. There are different types of common surfactants with regard to the charge of the surface-active species present in their aqueous solutions. Those include anionic, cationic, non-ionic and amphoteric surfactants.

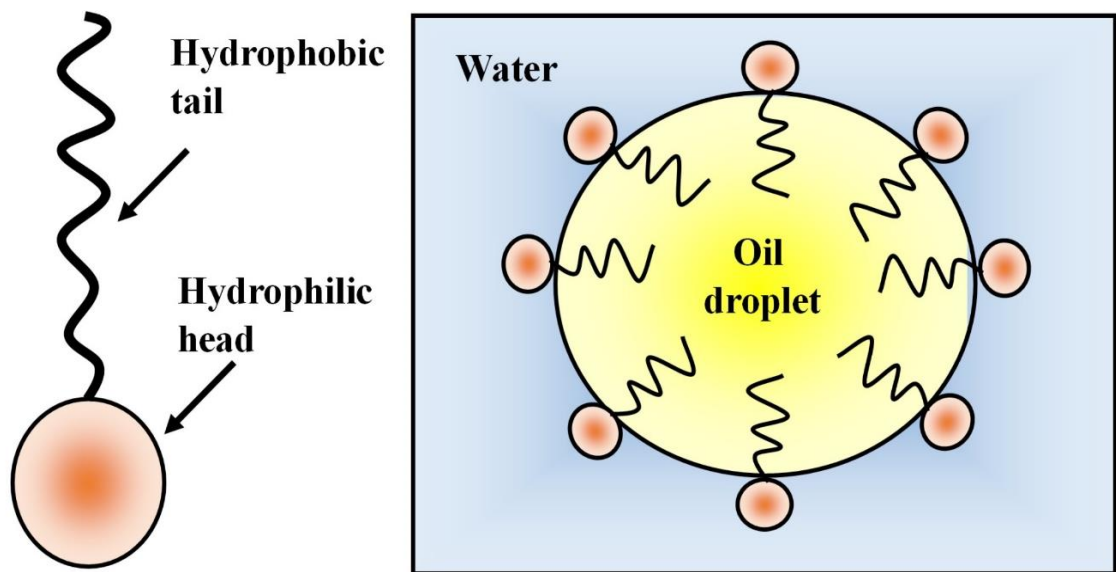


**Figure 1.1.** Schematic representation of surfactant molecule (left) and an oil droplet in water with surfactant adsorbed at the drop surface (right).

### 1.1.2 Particle-stabilised emulsions

In 1903, Walter Ramsden observed the ability of solid particles to stabilise emulsions, and in 1907, Pickering built upon that observation. Later, emulsions stabilised by solid particles have been named as Pickering emulsions.<sup>5</sup> The typical size of solid particles used as emulsion stabilisers is in the micrometre to nanometre range. In such systems, solid particles show some similarities to surfactants.

Similar to surfactant molecules, solid particles accumulate at the interface between oil and water forming mono- or multi-layers thus reducing the area of the high energy liquid interface. The position of a solid particle at the liquid interface depends on the three-phase contact angle ( $\theta$ ), which also influences the adsorption energy of the particles at the interface. The contact angle and the three interfacial forces are illustrated in Fig.1.2. The contact angle is linked to the interfacial tensions of the contacting phases by Young's equation (1.1).<sup>6 7</sup>

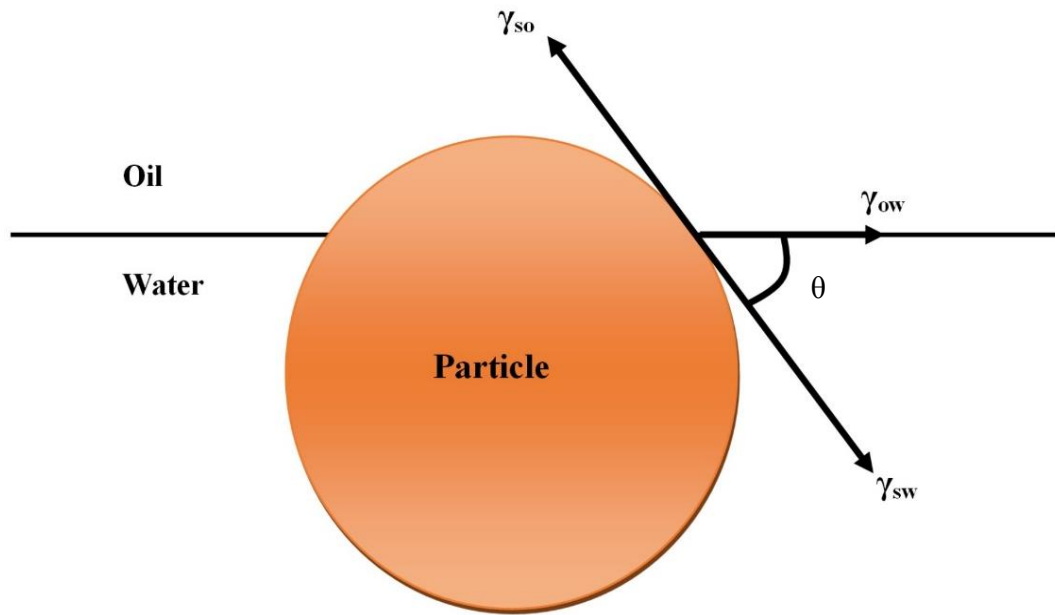


**Figure 1.2.** Schematic representation of a spherical solid particle at the interface between oil and water indicating the three interfacial tension forces acting at the three-phase contact line:  $\gamma_{so}$  - the interfacial tension between the solid and oil;  $\gamma_{ow}$  - the interfacial tension between the oil and water;  $\gamma_{sw}$  - the interfacial tension between the solid and water.  $\theta$  is three phase contact angle.

$$\cos \theta = \frac{\gamma_{so} - \gamma_{sw}}{\gamma_{ow}} \quad , \quad (1.1)$$

where  $\gamma_{so}$  is the interfacial tension between the solid and oil,  $\gamma_{ow}$  the interfacial tension between the oil and water,  $\gamma_{sw}$  the interfacial tension between the solid and water, and  $\theta$  is the contact angle (measured through the water phase) where the three phases meet (see Fig. 1.2).

The type of emulsion (oil-in-water, o/w, or water-in-oil, w/o) depends on the three-phase contact angle value which is related to the hydrophobicity of particles. For particles stabilising o/w emulsions, the contact angle  $\theta$  is less than  $90^\circ$ , whereas particles stabilising w/o emulsions have a contact angle greater than  $90^\circ$ . When the contact angle  $\theta = 90^\circ$ , the particle is wetting equally from the two phases. Emulsions with poor stability are formed when the particles have extreme wettability by one of the phases and the contact angle approaches  $180^\circ$  or  $0^\circ$  (see Fig.1.3).<sup>8</sup>

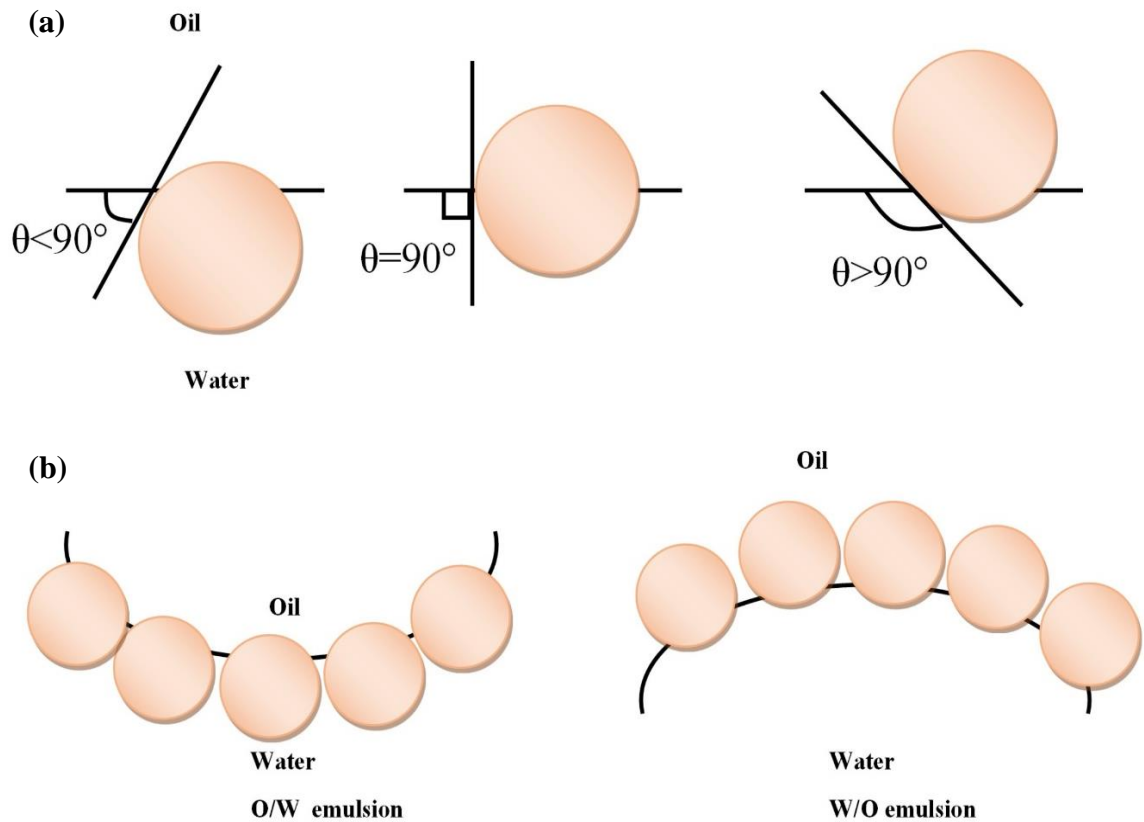


**Figure 1.3** (a) The contact angle measured through the aqueous phase showing the location of spherical particles at a planar oil-water interface. (b) The probability of solid particles positioned at curved oil-water interface. Particles stabilised in o/w emulsion have  $\theta < 90^\circ$ . Particles stabilised w/o emulsion have  $\theta > 90^\circ$  (redrawn from ref. 8).

Usually, the solid particles used as emulsifiers are less than a few micrometres in diameter. As result, the influence of gravity is negligible. In order to remove the particles from the interface, there is an essential energy required to achieve it. The energy required to remove a spherical particle from the interface into one of the bulk phases is defined by the following equation:

$$E = \pi r^2 \gamma_{ow} (1 \pm \cos \theta_{ow})^2 \quad (1.2)$$

Where  $\gamma_{ow}$  is the oil/water interfacial tension,  $r$  is the radius of the particles and  $\theta_{ow}$  is the three-phase contact angle measured via the water phase.

If the particles are moved into the water phase, the sign in the brackets should be negative; if the particles are moved into the oil phase, the sign should be positive. Emulsions stabilised by solid particles rely on factors such as particle wettability, interfacial tension between the two phases and particle sizes, as well as how strongly the particles are attached to the interface. For example, if the particles are completely hydrophobic or

hydrophilic, they will lose their ability to strongly adsorb at the interface. Other properties influence emulsion stability such as particle concentration, the interaction between the particles and particle shape. These properties expand the variety of particles used to stabilise emulsion, including clays,<sup>9</sup> silica,<sup>10</sup> carbon, microgels<sup>11</sup> and polymer particles.<sup>12, 13</sup>

Solid particles have the ability to adsorb at the interface between oil and water, which could form mono- or multi-layers at the interface and enhance emulsion stability by generating a physical barrier to prevent coalescence. The Fig.1.4 shows the energy of detachment of silica particles from the interface between oil-water against the contact angle  $\theta$  at  $\gamma = 50$  mN/m and  $r = 10$  nm. The particles attach strongly to the interface for  $\theta = 90^\circ$  as the energy of detachment is high. The energy is only 10 kT or less at contact angles between 0 to  $20^\circ$  and also between 160 and  $180^\circ$ .<sup>14</sup> The interaction between emulsion droplets through the particles in the continuous phase leads to an increase in viscosity. As result, the emulsion droplets are limited in movement, thus reducing the rate of emulsion instability.<sup>5, 15</sup>

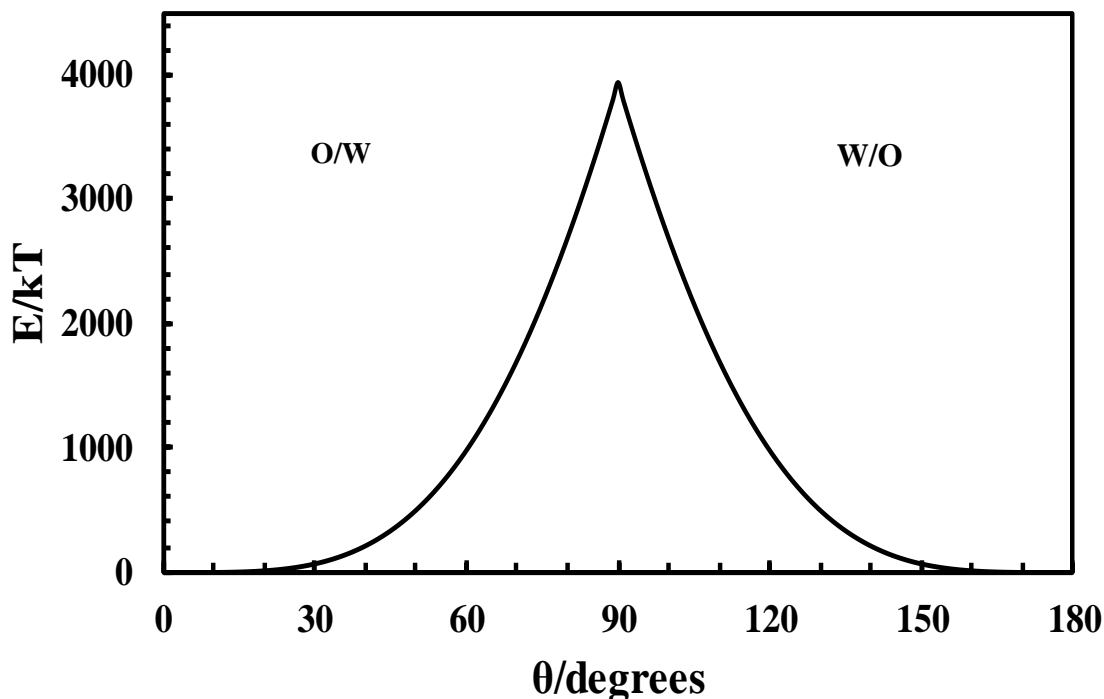


**Figure 1.4.** Energy of detachment versus the contact angle of 10 nm solid particles at the interface between oil-water with interfacial tension  $\gamma = 50$  mN/m. The emulsion formed at  $\theta$  less than  $90^\circ$  is oil-water; at  $\theta$  greater than  $90^\circ$ , the emulsion is water-oil. Redrawn from ref. 14.

### 1.1.3 Emulsion stability

Common emulsions (also called macro-emulsions) are thermodynamically unstable. This means that their free energy is greater than that of the two bulk liquid phases before emulsification; therefore, emulsion stability is considered to be a kinetic concept. A stable emulsion keeps its properties (concentration, distribution and size of the droplets) unchanged over a certain period of time. Figure 1.5 shows the four main processes that have the ability to destabilise an emulsion: creaming/sedimentation, flocculation, coalescence and Ostwald ripening.<sup>16</sup> These processes may occur at the same time or consecutively inside the emulsion.

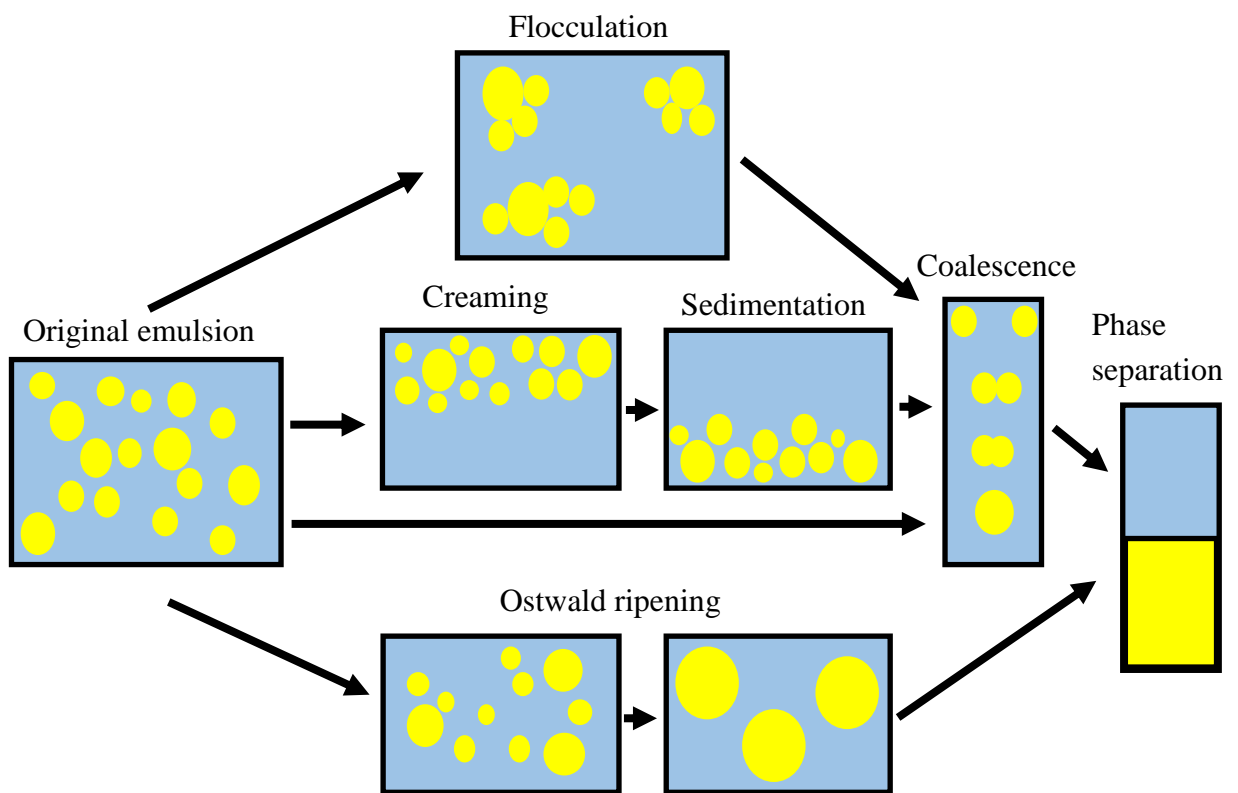


**Figure 1.5.** Different processes involved in the breakdown of an unstable emulsion (adapted from ref.16).

#### 1.1.3.1 Creaming or sedimentation

Creaming is a process in which the dispersed droplets move towards the top of the emulsion under the influence of gravity, forming a concentrated layer above a layer of clear continuous phase. This phenomenon occurs due to the density difference between oil and water. Usually creaming is observed in o/w emulsions because the oil (e.g. hydrocarbons) is less dense than water in most cases. However, in w/o emulsions, the

droplets of the dispersed phase (water) sediment to form a lower layer of dense emulsion below a layer of clear oil phase. This occurs when the dispersed droplets are denser than the continuous phase. This process is sedimentation, which is the opposite of creaming.<sup>2</sup>

### **1.1.3.2 Flocculation and coalescence**

The process in which the emulsion droplets aggregate without merging with each other is called flocculation. This aggregation of droplets (i.e. formation of flocs) speeds up the creaming (sedimentation) and may lead to coalescence. Coalescence occurs when two or more droplets merge together, forming larger droplets. Coalescence may lead to a complete phase separation after sufficiently long time. In contrast to creaming (sedimentation) and flocculation, coalescence is an irreversible process.<sup>2</sup>

### **1.1.3.3 Ostwald ripening**

Ostwald ripening is a destructive process caused by the different solubility of droplets in the continuous phases, which depends on the droplet size. The small droplets have greater solubility than the large droplets due to their bigger curvature. This may explain the disappearance of small droplets over time, the droplets may dissolved in the continuous phase and thus absorbed by the larger droplets. Whereas, the large droplets grow larger because the material from small droplets migrated (by diffusion) into them. This process is undesirable because the larger droplets are more likely to sediment or cream. As with coalescence, the Ostwald ripening is an irreversible process resulting in complete phase separation, but because the process is slow, takes much longer to occur.<sup>2</sup>

## **1.2 High internal phase emulsions**

High internal phase emulsions (HIPEs) are emulsions in which the internal droplet phase volume contributes to more than 74% of the total volume of the emulsion.<sup>17, 18</sup> These droplets are forming monodispersed droplets arranged in polyhedral symmetries. The system can reach 99% occupation by forming polydispersed droplets.<sup>17</sup> The viscosity of HIPEs is relatively high and they are paste-like emulsions. Surfactants are ordinarily used to stabilise HIPEs and include, for example, sorbitan monooleate (Span 80)<sup>19</sup>, Hypermer 2296 and trimethylammonium bromide (CTAB).<sup>20</sup> HIPE preparation usually requires a high amount of surfactant (5-50 vol.% with respect to the external phase) and/or solid particles to be used as stabilisers.<sup>21</sup>

### 1.3 Polymerised High Internal Phase Emulsions (polyHIPEs)

PolyHIPEs have been known for many years. Unilever researchers were the first to use the term “polyHIPEs” to define polymeric foams in 1982.<sup>22</sup> PolyHIPEs are made from high internal phase emulsions when the internal phase droplets occupy more than 74% of the total volume of emulsion.<sup>23</sup> The size distribution of the droplets is typically polydisperse and often the droplets have a non-spherical shape, resulting from their close contact and high concentration. Consequently, the external continuous phase is localised between droplets as thin films. Once the polymerisation of the external phase is completed, the internal phase is removed by evaporation and a porous polymer is formed. In many cases, the pores are interconnected through pore throats (windows) generated during the polymerisation of the external phase at the thinnest part of the film between the droplets.<sup>23, 24</sup>

A typical SEM image of polyHIPE with an open cell structure is shown in Fig. 1.6. The voids, also called pores or cells, are the cavities left behind of the evaporated droplets; the pore throats, or windows, are the small circular openings between them. The diameter of the droplets in the HIPE template dictates the diameter of pore throats (windows) and could vary from less than 1  $\mu\text{m}$  to over 100  $\mu\text{m}$ . The structure of polyHIPE materials is important for their specific application and can be tuned by adjusting the characteristics of the HIPE templates. In particular, tuning the void diameters is generally achieved by controlling the droplet size and stability of the HIPE template.<sup>25, 26</sup> The stability of HIPE template is a very important factor for the preparation of polyHIPE materials. The stability is affected by the droplet coalescence and Ostwald ripening, both leading to an increase of the pore diameter in comparison to the droplet diameter of the emulsion template.<sup>27</sup>

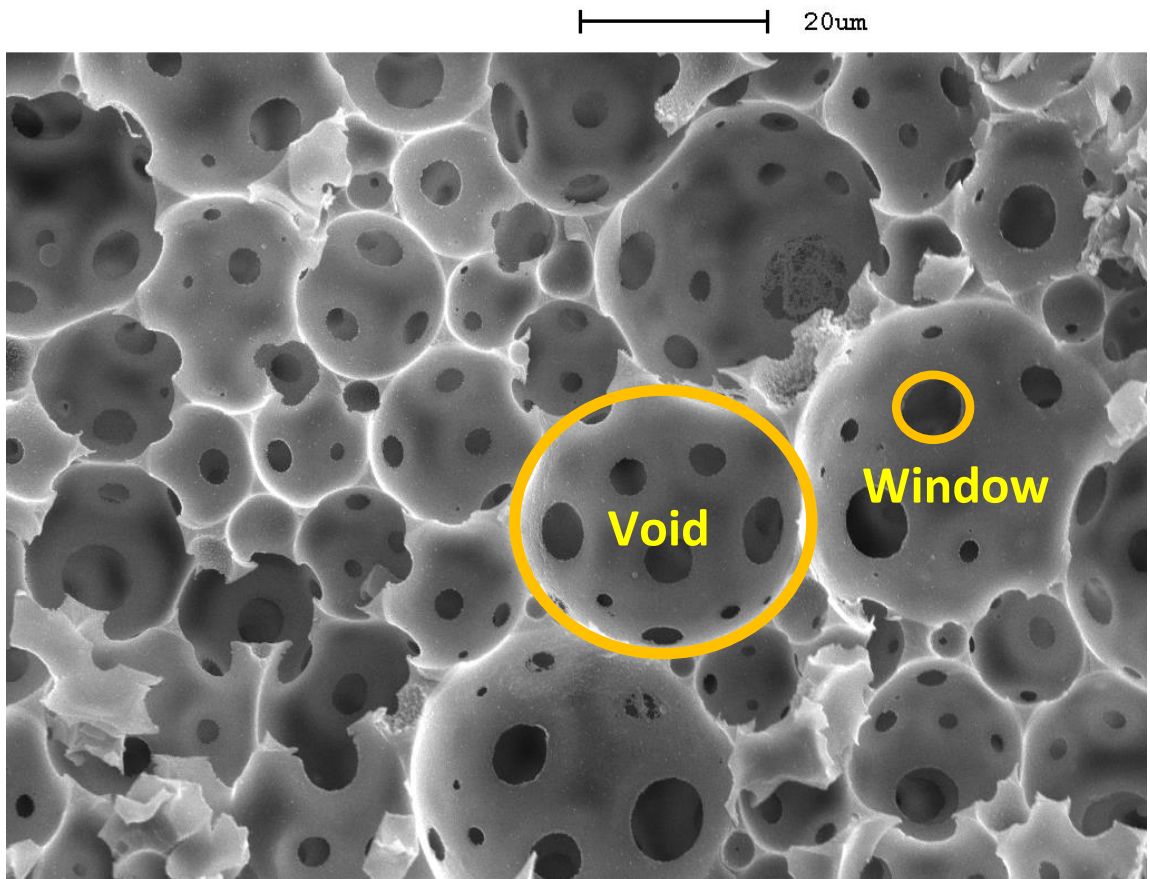
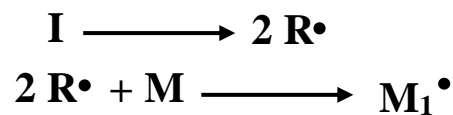


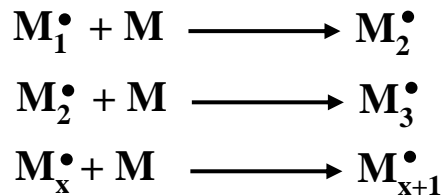
**Figure 1.6.** SEM images of a typical polyHIPE material with open cells where voids (pores) are connected by pore throats (windows).

Free radical polymerisation is a widely used method for making high molecular weight, polymeric materials from monomers such as, for example, acrylates or styrene. The monomers must have one or more reactive or unsaturated groups such as a reactive vinyl group. The three main steps for free radical polymerisation are illustrated in Fig. 1.7: initiation, when free radicals are generated; propagation, when oligomer chain growth is created; and termination, when the free radicals terminate.<sup>28</sup>

1- Initiation step



2- Propagation step



3- Termination step

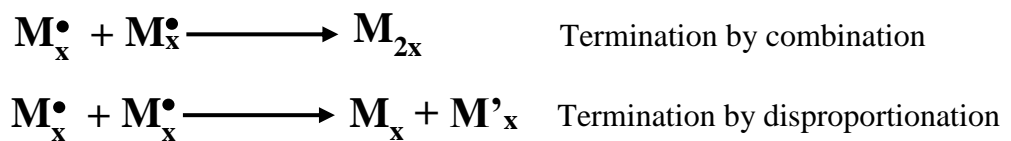


**Figure 1.7.** A general representation of free radical polymerisation steps. The initiator (I), Free radical (R) and the monomer (M).

For the preparation of polyHIPEs via free radical polymerisation, the HIPE templates must contain an initiator either in the water phase or in the oil phase to start the polymerisation. One of the most common thermo-initiators used in the oil phase is 2,2'-azobis (2- methylpropanenitrile) (AIBN, Fig.1.8). A common water soluble initiator is potassium peroxydisulphate (KPS). These initiators are used because they have a low dissociation energy of approximately 167 kJ/mol.<sup>29</sup> The properties and morphology of polyHIPEs could be affected by the type of initiator, whether in the oil phase or water phase (Williams *et al.*).<sup>30</sup> It has been shown that the polyHIPEs of styrene as the monomer and DVB as the crosslinker produced with KSP were 50% harder than those produced with AIBN, and their morphology was also different. Free radicals can be generated by thermal decomposition or photochemically as in AIBN (Fig1.8).The temperature at which the half-life of the thermo-initiator decomposition is equal to 10 hours is 60 °C for KPS and 65 °C for AIBN.<sup>29</sup>The redox processes can generate free radicals at room temperature, for example the reaction between cumene hydroperoxide (CHP, 2-hydroperoxypropan-2-ylbenzene) and ferrous sulphate (see Fig.1.9).<sup>31</sup>

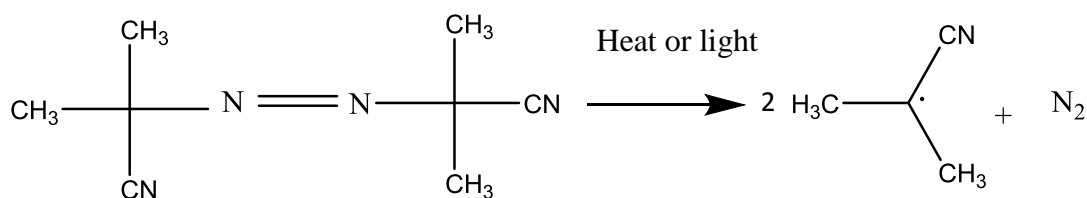


**Figure 1.8.** The decomposition of 2,2'-azobis(2-methylpropanenitrile) (AIBN) initiator for free radical polymerisation induced by heat or light.

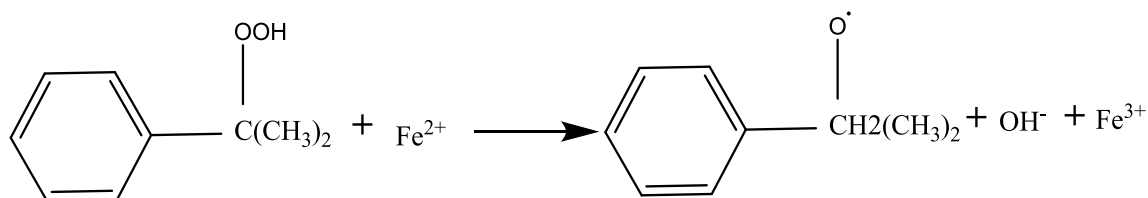


**Figure 1.9.** The one electron step involved in the redox reaction between cumene hydroperoxide (CHP) and  $\text{Fe}^{2+}$  producing a free radical.

For initiators to be suitable for generating free radical in the polymerisation of HIPEs, the reaction time and the temperature required for decomposition of the initiator are important factors to be considered. If the temperature required to initiate the polymerisation of the oil phase is higher than  $100^\circ\text{C}$ , the initiator cannot be used for the preparation of polyHIPEs as the internal water phase of the emulsion will boil. The temperature recommended to initiate polymerisation of the oil phase is in the range of  $50^\circ\text{C} - 70^\circ\text{C}$ , and heat produced by the reaction will also help to accelerate the polymerisation. Photochemical reactions follow a similar process as thermal polymerisation. In most cases, UV light is used to provide photons that break the weakest bond and provide free radicals for the reaction.<sup>32</sup> However, there are some limitations of photo polymerisation. If the sample or the block of emulsion layers is thick, then light penetration of the sample may not be successful, and the initiator will not decompose in the bulk of the sample. For this reason, photo polymerisation is not commonly used for polymerisation of emulsion templates. However, photo polymerisation has recently been used for fast polymerisation of thin emulsion samples.<sup>33-35</sup> Another option for polymerisation might be redox-initiators, which could be used to decrease the temperature required to begin the polymerisation.<sup>36</sup>

Benzoyl peroxide (BPO) and amines redox-initiated system has been studied for a long time since 1950s.<sup>37</sup> The redox-initiated system attracted many scientists due to the polymerisation can occur at room temperature. The acrylic monomers widely used to polymerise with redox-initiated systems.<sup>37</sup> This combination between the acrylic monomers and redox-initiation system has been used in many applications such as

dentistry<sup>38</sup> and bone surgery.<sup>39</sup> The mechanism of redox-initiated (BPO-amine) reaction is quite complex.<sup>40</sup> The initiation step starts by the nucleophilic attack from the tertiary amine towards the peroxide bond on the BPO molecules. Then, the redox reaction occurs, followed by the formation of benzoyloxy radical and a carbon centred radical derived from the tertiary amine (see Fig.1.10). There are also some side reaction of the redox-initiation of BPO and amine. The possible side reaction could be the free radical present (benzoyloxy radicals) in the system react with BPO to form free radical of phenyl radical and CO<sub>2</sub>. Another possible side reaction could be that the excess of nitroxides formed from the amine might react to generate free radicals (benzoyloxy radicals) see Fig.1.11.

40, 41

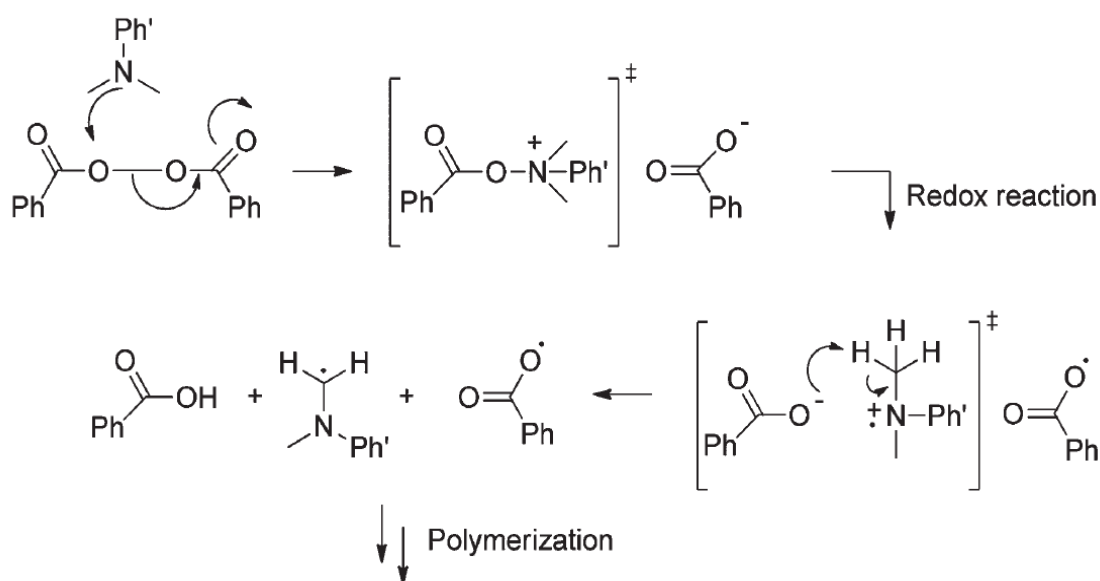


**Figure 1.10.** BPO activation and formation of radicals with a tertiary amine.<sup>37</sup>

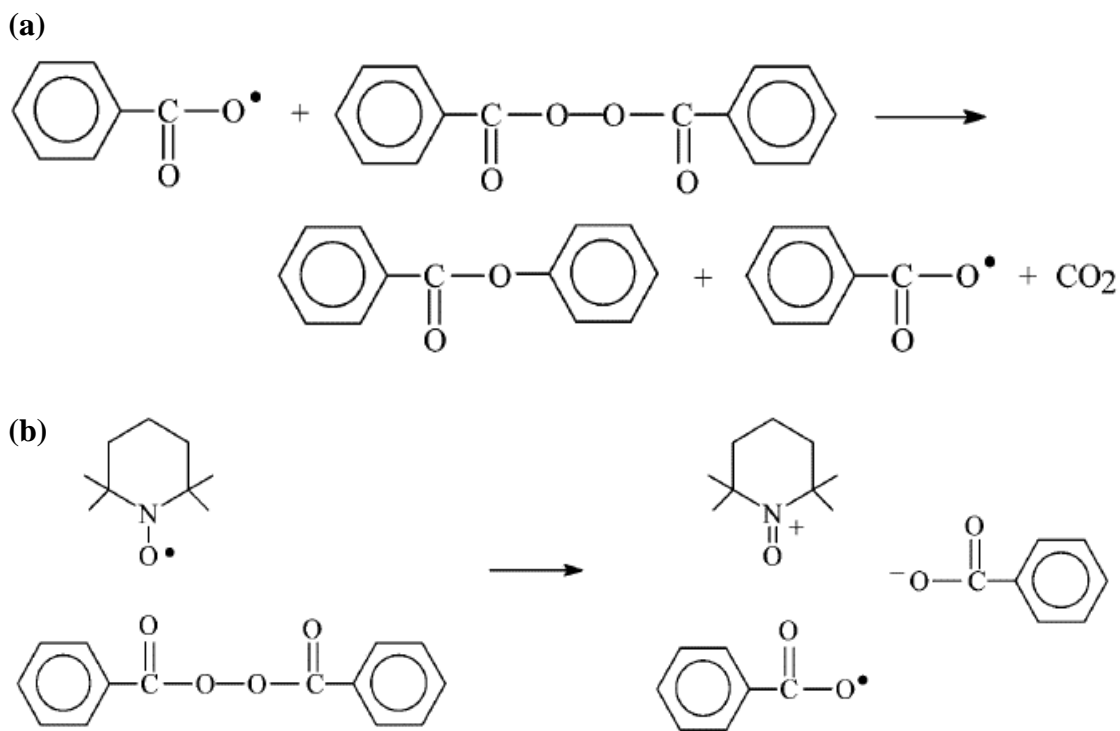


**Figure 1.11.** (a) The formation of benzoyloxy radical and  $\text{CO}_2$  as side reaction of presence of the benzoyloxy radical. (b) Nitroxides formed from an excess of amine.<sup>40</sup>

One of the most investigated systems for making polyHIPE materials consists of styrene (St, monomer) and divinylbenzene (DVB, crosslinker).<sup>42,43</sup> Such systems (St/DVB) have been extensively studied to understand which factors affect the 3D structure of the material produced. The concentration of surfactants is an important factor for controlling the formation and size of the pores and pore throats (windows).<sup>30</sup> Several hypotheses for the formation of the pore throats have been considered. According to the first hypothesis, the formation of pore throats occurs as a result of the shrinking of the external phase during polymerisation. It is suggested that increasing the surfactant concentration leads to thinning of the film between the droplets, so a hole forms in the film because of the shrinking of the external phase. To support this hypothesis, the St/DVB system was studied using different concentrations of the surfactant Span 80. The concentration of the surfactant was adjusted to produce closed-cell and open-cell materials. Concentrations in the range of 3 to 5 wt% produced closed-cells with no connection between the voids. When the concentration of the surfactant was increased to between 7 and 10 wt%, open-cell materials were produced. The pore throat diameter increased with the surfactant concentration. Cryo-SEM was used for studying the formation of pore throats.<sup>43</sup> The HIPE samples were frozen at different points of polymerisation, and SEM images were taken. The findings indicated that the gel point (at the point where the HIPE becomes

highly viscous or almost gel-like network) of the polymer corresponds to the creation of the pore throat.

The second hypothesis attributes the formation of pore throats to the mechanical action in the process of purification.<sup>44</sup> To test their hypothesis, the authors prepared polyHIPEs with 80vol.% aqueous internal phase and polymerised at 70°C for 24 h. The external phase contained 30vol.% styrene, 50vol.% DVB and 20vol.% Hypermer 107 (polymeric surfactant). The pore throats appeared during the purification step as the droplets of the internal phase seemed to be completely covered by the external phase for the whole polymerisation. The purification step was performed using a Soxhlet extractor, then the polyHIPEs were dried at an elevated temperature. The explanation for the opening pore throats was that the thin polymer film between droplets ruptured in the process of purification and drying (see Figs 1.12).<sup>44</sup>

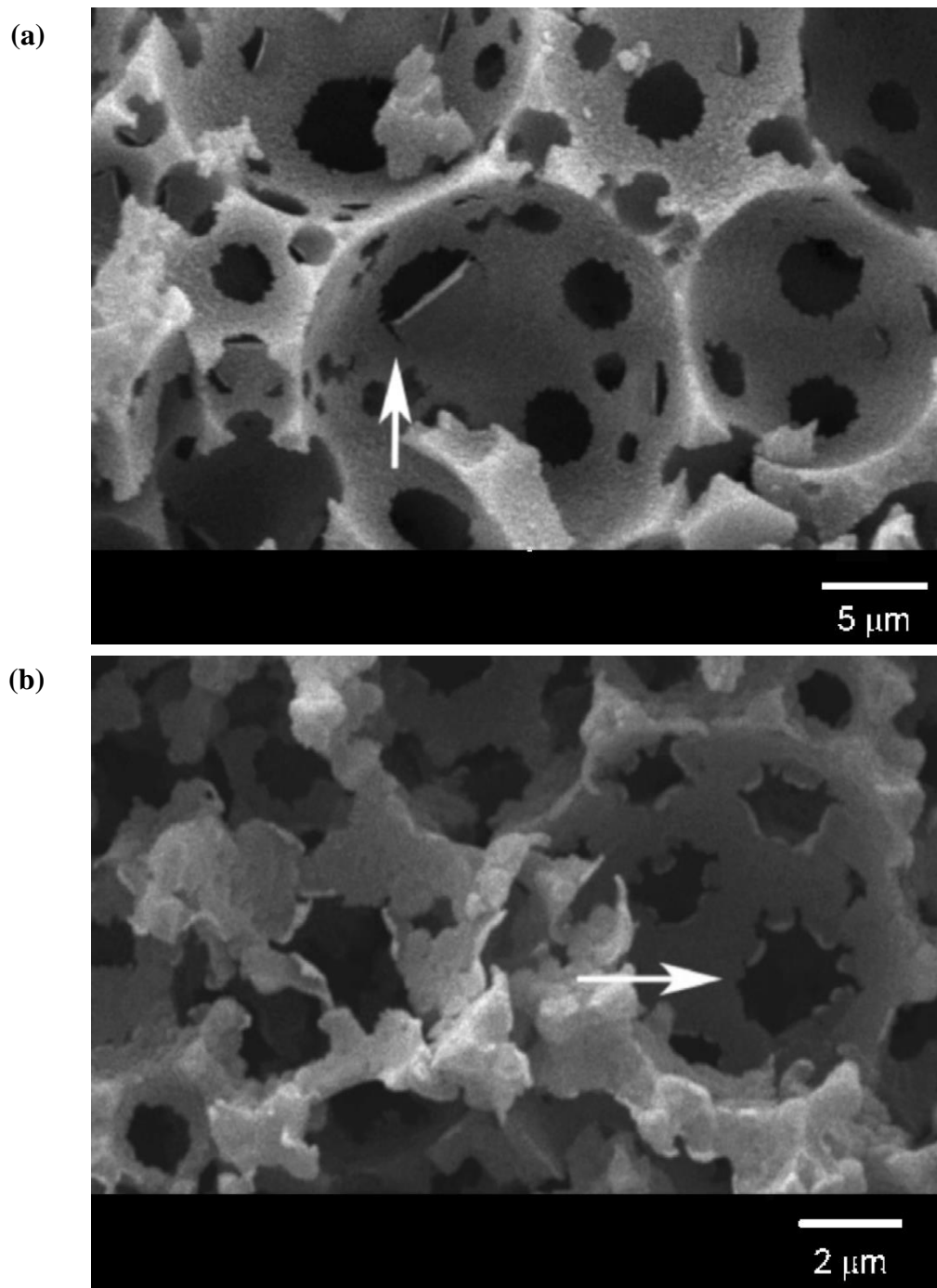


**Figure 1.12.** (a) PolyHIPE with pore throats partially covered by a thin, solid film, the arrow pointed to the film peeled during the purification step. (b) PolyHIPE with burst polymer films, which were initially covering the faces between two adjacent aqueous droplets and the arrow pointed to sharp edges of the pore throat indicated that the pore throat opened during the purification step. The external phase contained 30vol.% styrene, 50vol.% DVB and 20vol.% Hypermer 107 (polymeric surfactant) and the water phase made of 80vol.%. The polymerisation of the external phase carried out at 70°C.<sup>44</sup>

PolyHIPE materials can be designed in any desired shape through the moulding process. Before the polymerisation step, the HIPE is transferred into a mould where it stays until polymerisation is completed. As a result, the polyHIPE produced retains the shape and size of the mould. Many different mould sizes and shapes have been used. It has been reported that the morphology of the St/DVB polyHIPE surface was affected by the mould material. Glass was found to be unsuitable mould material because it interacted with the polymer surface, creating a surface morphology different from the polyHIPE interior. Some plastic moulds such as polypropylene and PTFE have been investigated, and a closed-cell pores were formed at the area in contact with the polypropylene mould, possibly because of the good wetting of the mould material by the external phase. PTFE was found to be one of the best mould materials to use because it did not affect the polyHIPE morphology. The final shape of polyHIPE materials can be controlled and adjusted for any application requiring a specific shape.<sup>23</sup>

### **1.3.1 Preparation of macroporous polymers**

There are specific methods that produce porous polymers, such as chemical or physical foaming or blowing,<sup>45, 46</sup> particle leaching,<sup>47, 48</sup> and emulsion templates.<sup>23</sup> The emulsion templating is considered to be one of the easiest and most efficient method for producing porous materials.<sup>49</sup> The ability to control the pore size by changing the emulsion composition and functionality of the emulsion template is a remarkable advantage of this method over the others.

The preparation of polyHIPEs is straightforward. Typically, the external phase contains monomers, crosslinker(s) and an appropriate surfactant. The internal phase is added a drop at a time during stirring. The emulsion is then stirred for a period of time. After the internal phase has been added, the emulsion is then stirred for a period of time for better homogenisation. The external phase of the emulsion is polymerised using a suitable curing method. The polymer obtained is washed in a Soxhlet extractor with an appropriate solvent to remove impurities and then dried (Fig. 1.13).<sup>23</sup>

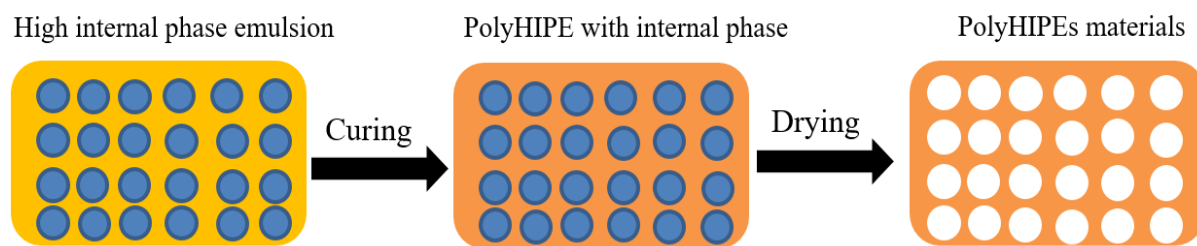


**Figure 1.13.** Schematic representation for preparation of polyHIPE porous materials. The fraction of internal phase has been reduced for clarity.

The polymerisation of the external phase in a typical polyHIPE preparation occurs via free radical polymerisation (FRP). Other polymerisation methods have also been studied, including atom transfer radical polymerization (ATRP) and reversible addition-fragmentation chain transfer polymerization (RAFT). The type of monomers used in preparation of polyHIPEs is important in free radical polymerisation. One of the most commonly used monomers to produce polyHIPEs is styrene, which is not soluble in water, thus, water-in-oil HIPEs are used as templates. Other hydrophobic monomers also have the ability to produce polyHIPEs, including butyl acrylate (BA), isobornyl acrylate (IBA), 2-ethylhexyl methacrylate (EHMA), 2-ethylhexyl acrylate (EHA) and methyl methacrylate (MMA).<sup>23, 50</sup>

Thiol-ene and thiol-yne reactions are also used to produce polyHIPEs via photopolymerisation of a trithiol with either an aliphatic diyne or triacrylate. The pore structure corresponds to typical polyHIPEs, and pore size is in the micrometre range. The mechanical properties of these polyHIPEs have been improved because the materials had a high degree of crosslinking. The porosity of these polyHIPEs ranges between 80 and 90%.<sup>51</sup>

Macroporous polystyrene have also been produced via the RAFT polymerisation mechanism. The structure is anticipated to be more homogeneous than polyHIPEs produced with conventional FRP due to the control of the radical polymerisation. The materials prepared by RAFT display higher mechanical properties compared to the materials produced by FRT preparation of polyHIPEs.<sup>52</sup>

### 1.3.1.1 PolyHIPEs produced by thermo-initiated or photo-initiated polymerisation

In most cases, the free radical polymerisation (FRP) of HIPE templates is thermally initiated. Bismarck and co-workers produced polyHIPEs using AIBN as thermo-initiator. Their external phase contained styrene monomer, DVB as a crosslinker, AIBN (initiator) and the Hypermer 2296 surfactant. The internal phase used was  $\text{CaCl}_2 \cdot 2\text{H}_2\text{O}$  dissolved in

deionised water. The electrolyte was needed to prevent the Ostwald ripening. Once the emulsion (HIPE) was formed, it was transferred into a polyethylene mould and polymerised in an oven at 70°C for 24 h., followed by a purification process using a Soxhlet extractor. Finally, the polyHIPE materials were dried. The authors found that the pore hierarchy influenced the mechanical properties of the polyHIPEs produced, and the concentration of surfactants significantly affected the size and structure of the pores, which also affected the mechanical properties.<sup>49</sup>

Krajnc *et al.* has produced polyHIPEs monoliths with a mixture of monomers in the external phase, EGDMA, GMA and EHA. The polymerisation was thermally initiated. The external phase was made up of GMA, EHA and EGDMA (crosslinker), and the Pluronic surfactant, PEL-121. The internal phase consisted of water, potassium persulphate and CaCl<sub>2</sub>·2H<sub>2</sub>O. After completing the addition of the internal phase, N,N,N',N'-tetramethylethylenediamine (TEMED) was introduced and stirred continuously for one hour. Polymerisation occurred at 40°C for 24 h. The polyHIPEs monolith exhibited a high porosity of 75% to 90%, and mechanical properties improved as EHA enhances the stability of the polyHIPEs.<sup>53</sup> In a separate study, Krajnc *et al.* also produced polyHIPE monoliths using GMA monomer and EGDMA crosslinker for the external phase, and the initiator, Potassium persulphate, in the aqueous internal phase was used as an initiator. Polymerisation occurred at 55°C for 48h. The highest porosity achieved was 90%.<sup>54</sup>

The elevated temperature used in thermo-initiated polymerisation has a significant detrimental effect on the stability of HIPEs leading to increased coalescence of the internal phase droplets. In addition, polymerisation at high temperatures requires a significant amount of surfactant, from 5vol.% to 50vol.% in the oil phase.<sup>55</sup> Those negative effects could be avoided if the FRP can be initiated at room temperature. Min Li *et al.* produced two types of polyHIPEs using St/DVB or methyl methacrylate/DVB at room temperature through radiation-induced polymerisation using  $\gamma$ -ray from <sup>60</sup>Co source. The amount of surfactant was reduced by a significant extent to 1.4wt%. Potassium peroxydisulfate (KPS) was used as the initiator and the emulsion was stabilised by Span 80.<sup>56</sup> Krajnc *et al.* produced a polyHIPEs monolith at room temperature by using the photo-initiator Irgacure 819 exposed to UV light. The external phase used was MMA, EGDMA and PEL-121 surfactant. The internal phase contained water and CaCl<sub>2</sub>. The mechanical properties improved significantly in comparison to other polyHIPEs produced at high temperature, and the porosity up to 85% was achieved.<sup>57</sup>

### 1.3.1.2 PolyHIPEs produced by room temperature polymerisation using redox-initiation

Cosgriff-Hernandez *et al.* has investigated the preparation of polyHIPEs at body temperature for tissue-engineered scaffolds using the advantage of polyHIPEs that they can fill any asymmetrical defects or gaps in the bone. The study team adjusted the polymerisation of the external phase to be polymerised at 37°C (body temperature). The synthesised propylene fumarate dimethacrylate (PFDMA) macromers (see Fig.1.14), which have the same end groups for methacrylate. This PFDMA is biodegradable and nontoxic. The preparation of polyHIPEs was as follows. The external phase of the HIPE template used was a 5wt% solution of an oil soluble initiator (BPO) in PFDMA containing also 5wt% of the surfactant polyglycerol polyricinoleate (PGPR 4125). The internal phase was an aqueous solution of calcium chloride (1wt%). HIPEs were transferred to an aluminium bead bath at 37°C for polymerisation overnight. The HIPE templates could be stored at 4°C for 1 week before use without affecting the size and the connectivity of the pores of the polyHIPEs produced.<sup>58</sup>

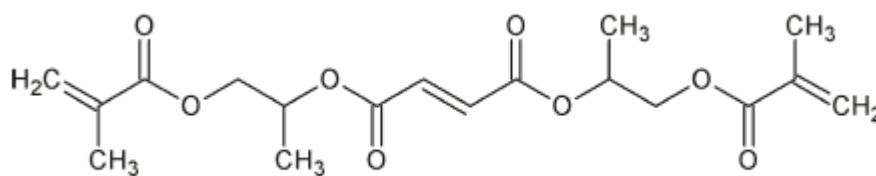


**Figure 1.14.** Propylene fumarate dimethacrylate (PFDMA) macromer synthesised and used in ref. 58. for making polyHIPEs.

Later the same group prepared polyHIPEs with a rapid cure time of the external phase. They prepared two HIPEs. The external phase was purified. The first HIPE contained the macromere (PFDMA), 10 wt% of PGPR4125 and different concentrations of benzoyl peroxide (0.5-5 wt%) in the external phase, and the internal phase contained an aqueous solution of calcium chloride (1 wt %). The second HIPE contained macromere (PFDMA), 10wt% of PGPR and different concentrations of trimethylaniline (TMA, 0.5–5.0 wt %) in the external phase and the internal phase contained an aqueous solution of calcium chloride (1 wt %). Once the HIPEs were formed, they were transferred to a double-barrel syringe, each barrel containing one of the two HIPEs prepared. The syringe had a static mixing head (1:1 ratio), and, as the injection took place, the two HIPEs mixed. The HIPEs were then left in a bath at 37°C to initiate polymerisation. The volume fraction of the water phase and porosity were maintained at 75%. The polymerisation of the two HIPEs upon mixing at 37°C was rapid, and the curing completed within a few minutes. The effect of increasing the concentration of BPO was negligible for the pore size but

significant for the mechanical properties of polyHIPEs. As the concentration of BPO increased, the mechanical properties improved.<sup>59</sup>

#### **1.4 Mechanical properties of solid foams and their deformation.**

The mechanical properties of polymeric materials depend on the chemical composition. However, knowing the chemical structure is essential for understanding the behaviour of different polymers; for instance, some polymers are glassy and others are elastic. This understanding allows scientists to modify the chemical structure to obtain materials for the desired application.<sup>60</sup>

In most applications, materials are subject to forces (loads). It is important that when force is applied, the resulting deformation (compression, elongation, twisting, and breaking) of these materials is calculated and analysed. Therefore, scientists have developed standard material testing methods that take into account the size, shape and handling of the sample (specimen).

The so-called engineering tensile or compressive stress is defined as the force applied perpendicular to a specimen divided by its original cross-sectional area and used to compare the mechanical response of specimens of different sizes and shapes. In compression and tension tests, the force is applied perpendicular to the cross-sectional area as shown in Fig.1.15 and the stress is calculated by equation 1.3.<sup>61</sup>

$$\sigma = \frac{F}{A} \quad (1.3)$$

where F is the normal force applied to the cross-sectional area A. The units of stress are N/m<sup>2</sup> or Pa.

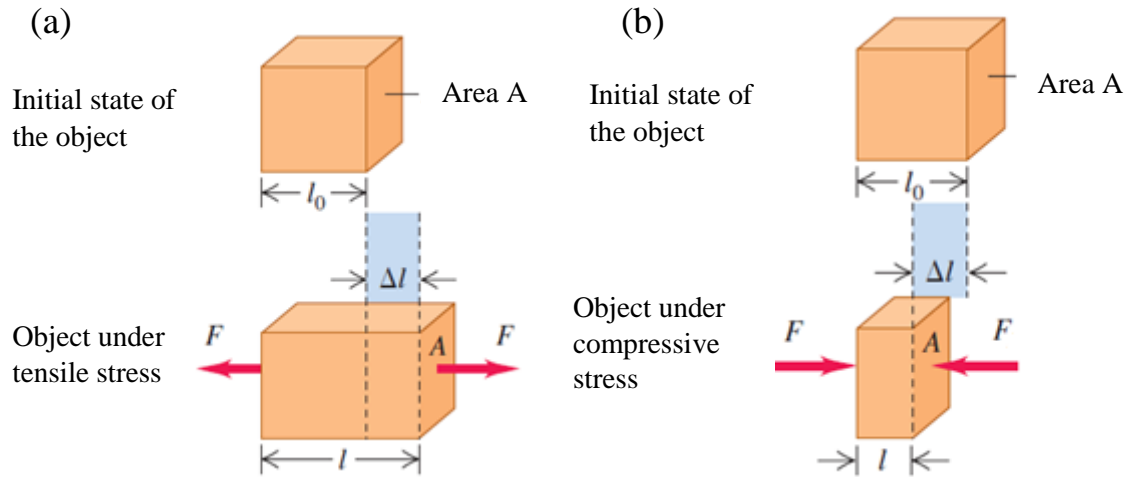


**Figure 1.15.** Schematic representation of materials under applied forces. (a) The material is under tensile stress. (b) The material is under compressive stress.<sup>61</sup>

The dimensions of the specimen change depending on whether the test type is compressive or tensile stress. The tensile or compressive strain can be defined as the ratio of the length change because of the applied stress, divided by the original length of the specimen (eq. 1.4). Hence, the strain is unitless.<sup>61</sup>

$$\varepsilon = \frac{l - l_0}{l_0} = \frac{\Delta l}{l_0} \quad (1.4)$$

where  $l$  is the length of the loaded specimen and  $l_0$  is the original length of the unloaded specimen.

To determine the strength and how the materials behave when subjected to force, Young's modulus can provide information about the elastic properties of the materials if it obeys Hooke's law. The Young modulus can be defined as the ratio of the stress divided by the strain, as shown in equation 1.5. For tension, the tensile stress is divided by the tensile strain; and for compression, the compressive stress is divided by the compressive strain.<sup>61</sup>

$$E = \frac{\sigma}{\varepsilon} \quad (1.5)$$

Here,  $\sigma$  is the stress in Pa and  $\varepsilon$  is the strain (unitless), hence the units of E are also Pa.

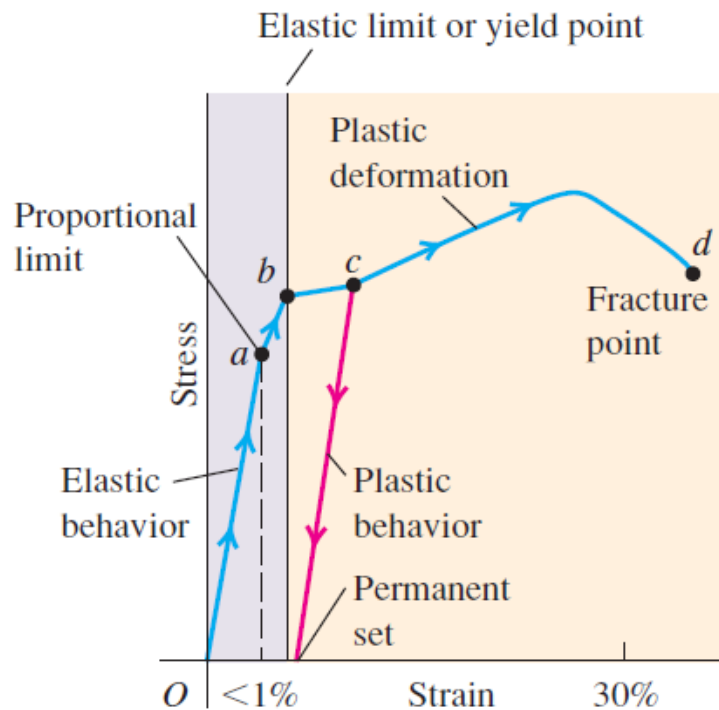


**Figure 1.16.** Typical stress-strain diagram for a ductile metal under tension.<sup>61</sup>

In Hook's law, the stress versus strain should be a straight line, and the slope should give the value of Young's modulus. The graph in Fig.1.16 corresponds to a tensile test of metal, and the strain is indicated in percentage of elongation. However, the same principle could apply for the compression test. The behaviour of materials could be explained from this graph when force is applied. Hook's law is followed in the first region from (O) to (a) as stress versus strain is a straight line. The end of this linear region (a) is called the proportional limit. After the point (a), the line is no longer straight, and Hook's law is not followed. Between the point (O) and (b), if the load is removed, the material will gradually return to its original length. So, the process of deformation is reversible, and when the stress is no longer applied, the materials have the ability to recover the energy input. The material shows elastic behaviour in the region from (O) to (b). The yield point is at the point (b) and the stress at this point (b) is named as the elastic limit. If the stress increases past the point (b), the strain will increase, and when the load is removed, the materials will not go back to its original length. The red line shows that the length of the materials at zero stress is now greater than the original length. As a consequence, the deformation is permanent and irreversible. The increase of load beyond (b) leads to a small rise in stress with a large rise in the strain. When the line approaches the point (d), fracture occurs, and the region between (b) and (d) is plastic deformation, which is

irreversible. The material deformed in the region between (b) and (d) can no longer return to its original length when the load is removed.<sup>60, 61</sup>

When a solid is formed by an interconnected network of struts, it is called a cellular solid. The structure of a honeycomb is the simplest cellular solid, with a two-dimensional hexagonal structure. Most cellular solids have a three-dimensional polyhedral structure and are referred to as solid foams. Open-cell solids refer to materials which have only cell edges, and the cells are interconnected; whereas, in the closed-cell foams, the cell faces are still present between the neighbouring cells. Gibson and Ashby explained that the relative density is the most important feature of these materials.<sup>62</sup> The relative density  $\frac{\rho}{\rho_s}$  is defined by the density of the cellular materials ( $\rho$ ) divided by the density of polymer forming the edges or faces of cells ( $\rho_s$ ). In the traditional way of making cellular solid materials, the gas bubbles are introduced to a molten polymer or a liquid monomer followed by solidification, either by cooling the hot polymer melt or polymerising the monomer. The foams produced can be either closed- or open-cell as shown in Fig. 1.17. Applications for cellular materials are numerous. For instance, they can be used for thermal insulation or packaging. Nature also has cellular materials such as cork, wood, bone and sponge. The preparation of cellular solid materials can be achieved by using high internal phase emulsions as templates to produced polyHIPEs.<sup>62, 63</sup>

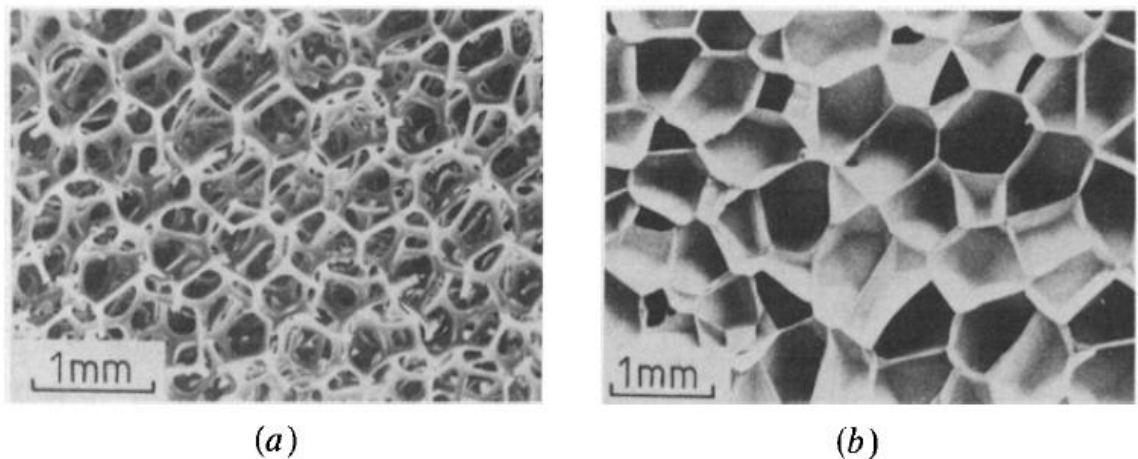


**Figure 1.17.** SEM images of typical polyHIPEs material structures. a) an open-cell polyurethane and b) a closed-cell polyurethane.<sup>62</sup>

The mechanical properties of polymeric foams are important to many applications. Ashby and Gibson provided a remarkable study about the mechanical behaviour of polymeric foams and described the behaviour of honeycomb materials. The structure and the materials used for making the cell walls strongly affect the mechanical behaviour of

polymeric foams. In addition, porosity and the type of pores (open-cell or closed-cell) are also very important.<sup>60</sup> Polymeric foams show three main regions in the stress-strain curve when the compression test is performed (Fig.1.18). In the first region, when the stress is low, the material deforms in a linear-elastic way. This is followed by a plateau region at approximately constant stress, which indicates that the foams are collapsing by elastic buckling for elastomeric foams (Fig.1.18 a), or by plastic yielding in elastic-plastic foams (Fig.1.18 b), or by brittle crushing in an elastic-brittle foam (Fig.1.18 c). The last region is where the foam collapses as a result of the crush of the cell walls, which is defined as densification. Most polymeric foams (plastic foams, brittle foams and elastic foams) obey the three-part, stress-strain curves.

The linear-elastic region is characterised by Young's modulus,  $E$ , which is related to the foam density. According to Gibson and Ashby,  $E$  for open-cell foams is given by equation 1.6.<sup>62</sup>

$$\frac{E}{E_s} = C_1 \left( \frac{\rho}{\rho_s} \right)^2 \quad (1.6)$$

where,  $E$  is Young's modulus of foam (MPa),  $E_s$  is Young's modulus of cell wall material (MPa),  $\rho$  is the density of foams ( $\text{kg/m}^3$ ),  $\rho_s$  is the density of cell wall material ( $\text{kg/m}^3$ ) and  $C_1$  is a constant, which includes all the geometric constants of proportionality. It has been shown that  $C_1 \approx 1$  is a good approximation in agreement with experimental data for open-cell foams.<sup>62</sup> The respective dependence for close-cell foams is more complex. In the open-cell foams the stiffness of the materials completely rely on the cell edges. However, in the close-cell foams, the solid materials not only contain in the edges of the cell but also in the cell faces. This fraction of the solid in the cell faces participate to the stiffness of the materials (equation 1.7).

$$\frac{E}{E_s} = C_1 \emptyset^2 \left( \frac{\rho}{\rho_s} \right)^2 + C'_1 (1 - \emptyset) \frac{\rho}{\rho_s} \quad (1.7)$$

where,  $E$  is Young's modulus of foam (MPa),  $E_s$  is Young's modulus of cell wall material (MPa),  $\rho$  is the density of foams ( $\text{kg/m}^3$ ),  $\rho_s$  is the density of cell wall material ( $\text{kg/m}^3$ ),  $C_1$  and  $C'_1$  are the constant proportionality and  $\emptyset$  is the volume fraction of the solid contain in the cell edges. Gibson and Ashby have shown that the elastic collapse stress of open-cell elastomeric foams is also related to a  $(\rho/\rho_s)^2$  factor. However, at

high relative densities the corrected version is given by equation 1.8.

$$\frac{\sigma_{el}}{E_s} = C_4 \left(\frac{\rho}{\rho_s}\right)^2 \left(1 + \left(\frac{\rho}{\rho_s}\right)^{1/2}\right)^2 \quad (1.8)$$

where  $\sigma_{el}$  is the elastic collapse stress of elastomeric foam (MPa),  $E_s$  is the elastic stress of the polymers wall.  $C_4$  is including all the constants of proportionality. It has been shown that  $C_4 \approx 0.03$  is a good approximation in agreement with experimental data for open-cell foams.

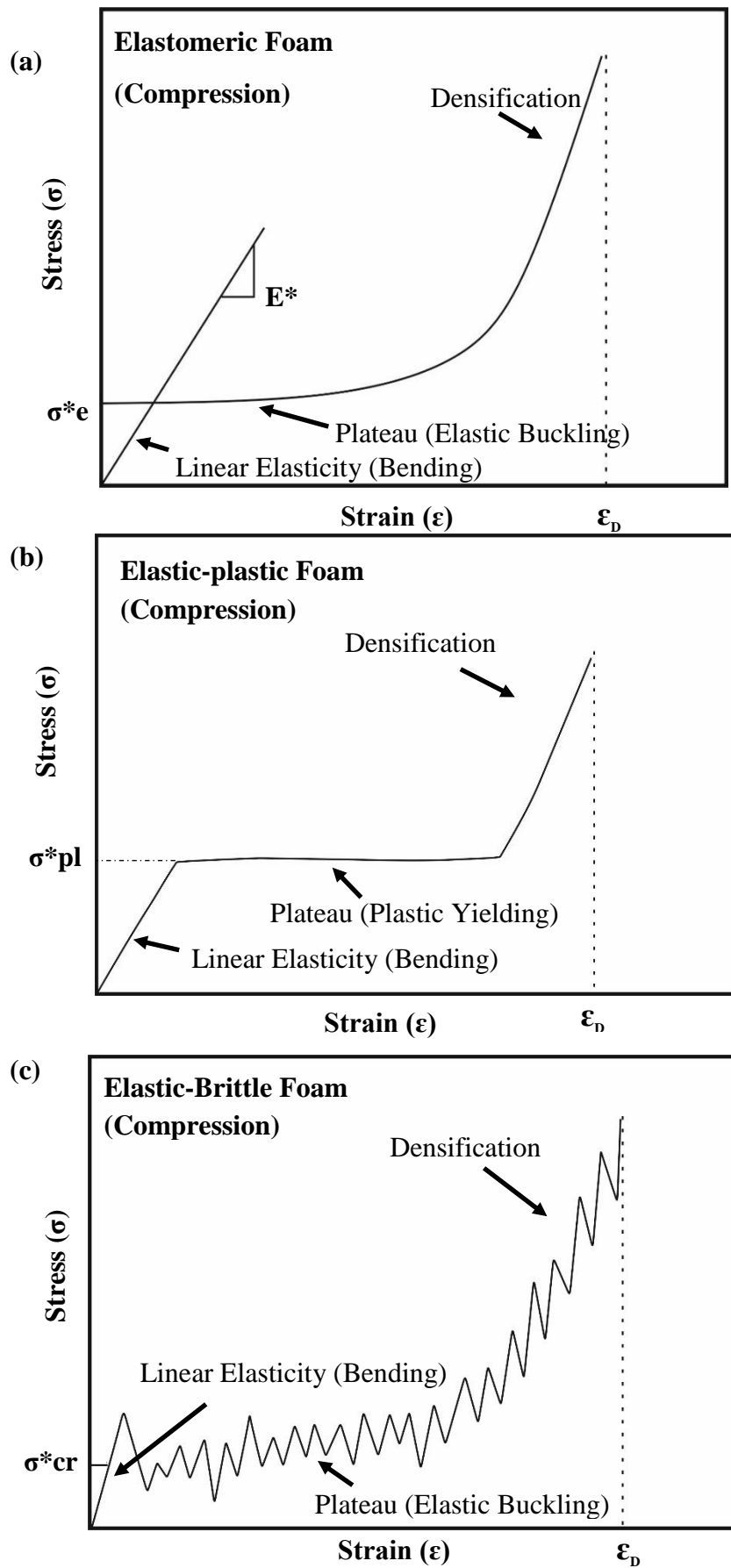


**Figure 1.18.** Compressive stress/strain curves for (a) elastomeric foams, (b) an elastic-plastic foam, (c) an elastic-brittle foam.<sup>62</sup>

The plastic yield stress for elastic-plastic foams has been found to be proportional to  $(\rho/\rho_s)^{3/2}$ , as shown in equation 1.9. The collapse of plastic occurs when the load on the cell walls is larger than the full plastic load at the cell edges.<sup>64</sup>

$$\frac{\sigma_{pl}}{\sigma_{ys}} = C_5 \left( \frac{\rho}{\rho_s} \right)^{3/2} \left( 1 + \left( \frac{\rho}{\rho_s} \right)^{1/2} \right)^2 \quad (1.9)$$

where  $\sigma_{pl}$  is the plastic collapse stress of plastic foam (MPa),  $\sigma_{ys}$  is the Yield strength of cell-wall material (MPa) and  $C_5$  is a constant, which includes all the geometric constants of proportionality. It has been shown that  $C_5=0.23$  is a good approximation in agreement with experimental data for open-cell foams.

The crush strength for brittle foams with open-cell structure is proportional  $(\rho/\rho_s)^{3/2}$  as shown in equation 1.10.

$$\frac{\sigma_{cr}}{\sigma_{fs}} = C_6 \left( \frac{\rho}{\rho_s} \right)^{3/2} \quad (1.10)$$

where  $\sigma_{cr}$  is the crushing strength of brittle foam (MPa),  $\sigma_{fs}$  is the modulus of rupture of cell-wall material (MPa) and  $C_6$  is including all the constant proportionality. It has been shown that  $C_6 = 0.2$ , there is wide variation in the intercepts of the data sets. It could be related to the value of cell wall modulus of rupture used.<sup>62</sup>

The analogues of equations 1.7 – 1.10 for close-cell foams are more complex because the mechanical response depends also on the distribution of the material between the cell faces and edges and the compression of the gas (or liquid) inside the pores.<sup>62</sup>

### 1.5 Applications of polyHIPES

PolyHIPE materials have been used as supporting for catalysis,<sup>65, 66</sup> separation media,<sup>67, 68</sup> scaffolds for tissue engineering,<sup>69, 70</sup> and for gas storage.<sup>68, 71</sup>

PolyHIPE materials have a highly organised structure and big voids. These voids are interconnected through the small pore throat (window). It can be used in chromatography for the separation of viruses<sup>72</sup> or removal of the heavy metal ion.<sup>73, 74</sup> PolyHIPES membrane were produced with (poly[(glycidyl methacrylate)-*co*-(ethylene glycol dimethacrylate)-*co*-(ethylhexyl methacrylate)] and the HIPES made of w/o (75vol.% water phase). The ethylhexyl methacrylate and ethyleneglycol dimethacryl affect the

flexibility of the membrane. The chemical modification were successfully applied to yield functional support for ion exchange.<sup>75</sup>

PolyHIPEs can produce highly porous scaffolds for tissue engineering. Perfect scaffold materials are expected to provide excellent support for growing new tissue and enhance cell migration to the areas which have defect site.<sup>76</sup> Controlling the architecture of polymeric foams offers a remarkable opportunity for tissue-engineered bone grafts. Styrene-based and unsaturated polyester-based macromeres have dominated the most recent research for developing polyHIPEs bone grafts. The pore morphology of styrene-based polyHIPE systems is one of the most suitable for those applications. Yet, they have been limited for use as a scaffold for tissue engineering because are made of non-biodegradable materials.<sup>58,77</sup> PolyHIPEs prepared from styrene and divinylbenzene in the external phase of HIPEs were modified by hydroxyapatite to enhance the diffusion and reproduction rates of osteoblasts.<sup>69</sup> PolyHIPEs with different pore size were tested for *in vitro* cell-polymer compatibility. Multicellular layers of osteoblasts were formed on the polymer surface; after 35 days the osteoblasts travelled inside the scaffold to 1.4 mm.

The preparation of biodegradable polyHIPEs that can be polymerised at body temperature and are also nontoxic was reported by Moglia *et al.* The distinctive characteristic of these polyHIPEs was that the emulsions (HIPEs) had high viscosity, providing a significant advantage as injectable materials before curing. These polyHIPEs could be used in many applications such as tissue-engineered bone grafts.<sup>58</sup>

## 1.6 Janus particles

Janus particles are particles with two different regions. Recently, these particles have attracted scientists' attention because of their interesting properties and applications. The Janus particle was introduced in Pierre-Gilles de Gennes's Noble lecture in 1991.<sup>78</sup> Janus refers to the Roman god with two faces placed back to back, one looking forward and the other backward. Similarly, the Janus particles have two different regions, which may differ in hydrophobicity, functionality or charges (Fig.1.19). There are other types of Janus particles that are determined by their shape (Fig1.20).<sup>79</sup> When Janus particles were introduced in the 1990s, there were a limited number of publications related to the field because of the difficulty fabricating Janus particles. However, recently preparation of Janus particles has become a subject of study by scientists using different methods for a variety of applications.

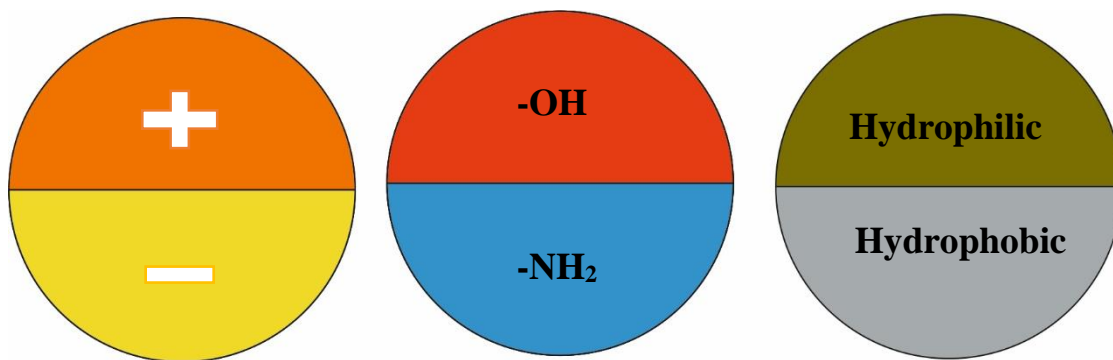


**Figure 1.19.** Janus particles with two different hemispheres based on their charges, functionality and hydrophobicity.

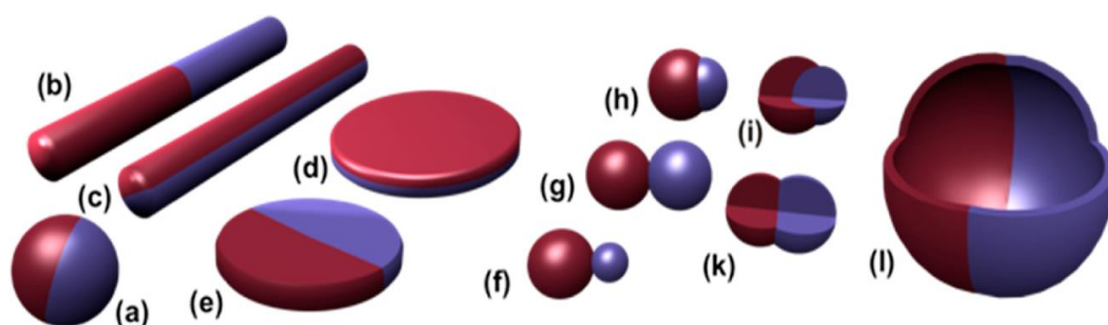


**Figure 1.20.** Spherical, (a) two types of cylindrical (b,c), and disc-shaped (d,e) JPs. Various kinds of dumbbell-shaped JPs (f–k) with an asymmetric or snowman character (f), symmetrical appearance (g,k), attached nodes (h) and eccentric encapsulation (i). Janus vesicles or capsules (l).<sup>79</sup>

## 1.6.1 Preparation of Janus particles

### 1.6.1.1 Microfluidic fabrication of Janus particles

The preparation of Janus particles via microfluidic method requires two different monomers that are not miscible with each other. The two monomers meet at a junction in capillary channels, creating a droplet that has both monomers without mixing, join together side by side and when the polymerisation takes place, Janus particles are produced. The immiscibility of the two monomers offers remarkable advantages for keeping the two regions of Janus particles distinctive. The polymerisation of Janus particles may occur within the microfluidic channel. Once the droplet is formed, the polymerisation can be started by ultraviolet radiation or thermal polymerisation. The two phases must be separated and flow in parallel to obtain a sharp boundary.<sup>80</sup>

Takizawa *et al.* developed a Y-shaped microfluidic channel by using the sheath-flow system. Janus droplets are made when the two monomers enter the channel from the two

inlets, with the aqueous phase creating a neck in the two-monomer stream to form Janus droplets (Fig. 1.21). Takizawa used this technique to generate bi-coloured Janus particles by using carbon black and titanium oxide pigments dispersed into acrylic monomers. Once the droplets are formed, a thermal polymerisation takes place by pouring droplets into a hot bath and are polymerised within 20 s. However, photo polymerisation could be applied by loading the droplets with a photo initiator and then exposing them to ultraviolet radiation.<sup>81</sup>

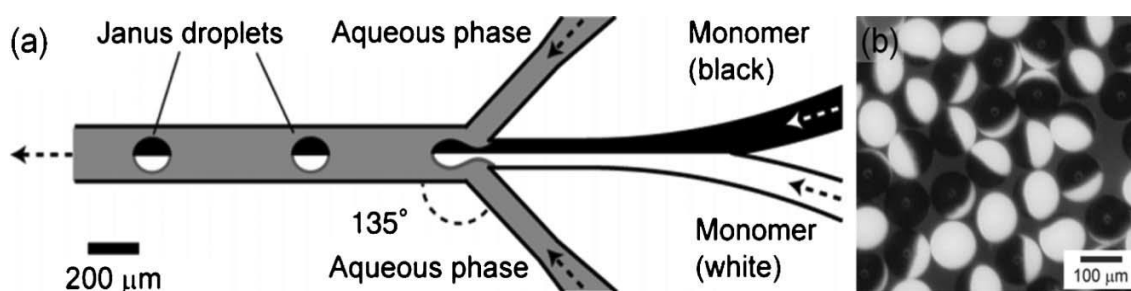


**Figure 1.21.** (a) Channel and flow configuration to generate the bicolored Janus droplets in a planar microfluidic geometry. (b) Synthesized bicoloured Janus particles.<sup>81</sup>

The advantages of the immiscibility between the two phases could be exploited to generate a sharp interface with Janus particles. This could be reached by using the microfluidic technique as demonstrated in Fig.1.22a. Two liquid monomers, preloaded with a photoinitiator force, join together, side-by-side at the central channels. The sheath flow sodium dodecylsulfate (SDS) solution is used from the side of the channel. At the central channel exit, Janus droplets are formed, then droplets are exposed to UV light for rapid polymerisation. The Janus particles produced have a sharp interface within the particles (Fig. 1.22b–d). The flow rate and ration between the two phases could be adjusted to produce different structures of Janus particles. Janus particles prepared with microfluidic methods are around 100μm in size and suffer from low yield because the flow rate is sometimes slow to prevent mixing of different phases by convection.<sup>80</sup>

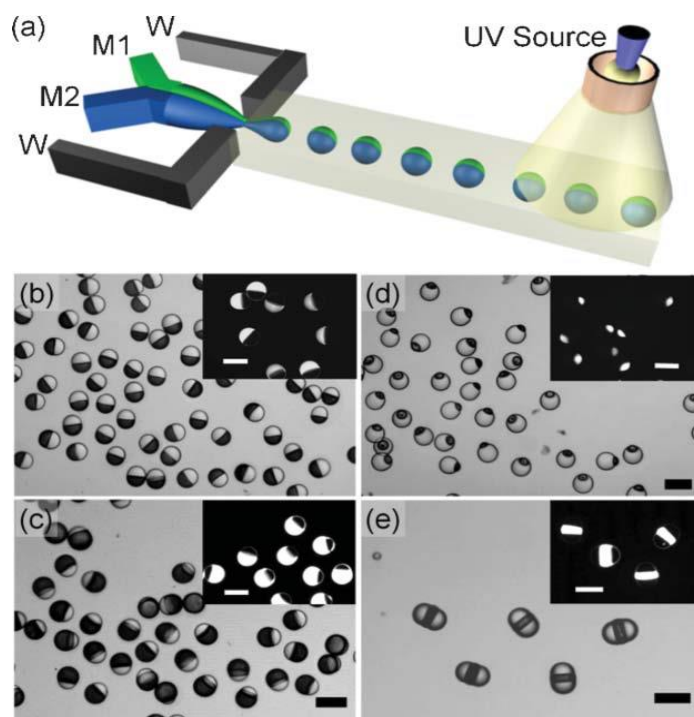


**Figure 1.22.** (a) Schematic of formation of droplets with ternary structures. Monomers M1 and M2 are injected in intermediate and central channels, respectively. (b, c, d). Optical microscopy images of Janus particles; the bright and dark phases are polymers of M1 and M2, respectively. (e) Janus particles with ternary structures.<sup>80</sup>

#### 1.6.1.2 Janus particles prepared by selective surface modification

Janus particles are produced with a variety of methods based on the treatment of one surface and protection of the other one, which may be one of the simplest ways of producing Janus particles. This technique has been widely used in microcontact printing,<sup>82, 83</sup> metal deposition,<sup>84-86</sup> plasma treatments,<sup>87, 88</sup> the binding of metals to Janus particles<sup>89, 90</sup>, etc.<sup>91-93</sup> with this method, the particles have to be firmly attached to the surface without any damage to the particles and with the top surface exposed for modifications. There are some methods for embedding particles at the surface through physical attraction, gel interface or polymer films, etc.<sup>82, 87, 88</sup>

Veysié and Casagrande produced Janus particles by using commercial glass particles (50-90 $\mu$ m diameter) and protected one side with cellulose varnish to obtain a hydrophilic side. The other side was made hydrophobic by applying octadecyltrichlorosilane.<sup>94</sup> In recent years, Paunov and Cayre have used a gel trapping technique to produce Janus particles.<sup>82</sup> This method is simple. Firstly, the silica particles are positioned at the gellan-oil interface at 50°C. Then the system is cooled down to room temperature to allow the aqueous phase to gel and trap the particles. PDMS then replaces the oil phase and the particles become embedded in the PDMS interface after curing. This allows particle

modification via gold sputtering. Later, Kretzschmar *et al.* introduced a faster, simpler method for trapping the 2.4 $\mu$ m polystyrene particles in PDMS. The polystyrene particles are stuck to a glass slide and placed face down on the precured PDMS mould. The depth of immersion may be controlled by the extent of precuring. The strong attraction between the polystyrene particles and the PDMS mould allow later modification in the Ag solution to generate Ag Janus particles as half shells. Janus particles could then be lifted from the PDMS stamp by using a metal blade to scratch them off.<sup>92</sup>

Yang *et al.* introduced particles from nano- to submicrometer.<sup>90</sup> They used aminated silica particles covalently located on poly[styrene-*ran*-(acrylic acid)] surface via active ester ester-mediated amidation chemistry. The reaction between the particles and the polymer film allows the particles to sink and controlled the depth of immersion in the polymer film (Fig. 1.23a). The silica particles used in this method were 460, 230, and 106 nm in diameter. Once the particles were covalently linked and immersed into the polymer film, the exposed surface of the particles was modified by applying acid-functionalised gold NPs linked through electrostatic interactions in water. The production of this step provides patchy coverage for the unmasked surface. Tuning the balance of the Janus particles could be achieved by using silica particles locked into electrospun fibre mats, which would allow them to generate triphasic particles. Silica particles (450 nm diameter) embed into PMMA/P4VP [Poly(4-vinylpyridine)] nanofibers and then the surface modification is applied to the exposed surface (Fig.1.23b).<sup>95</sup> The immersion depth for silica particles can be controlled by varying the temperature and the time of embedding into the fibre mats. This method illustrated the even behaviour of embedding and produced homogeneity of the particles above 80%.

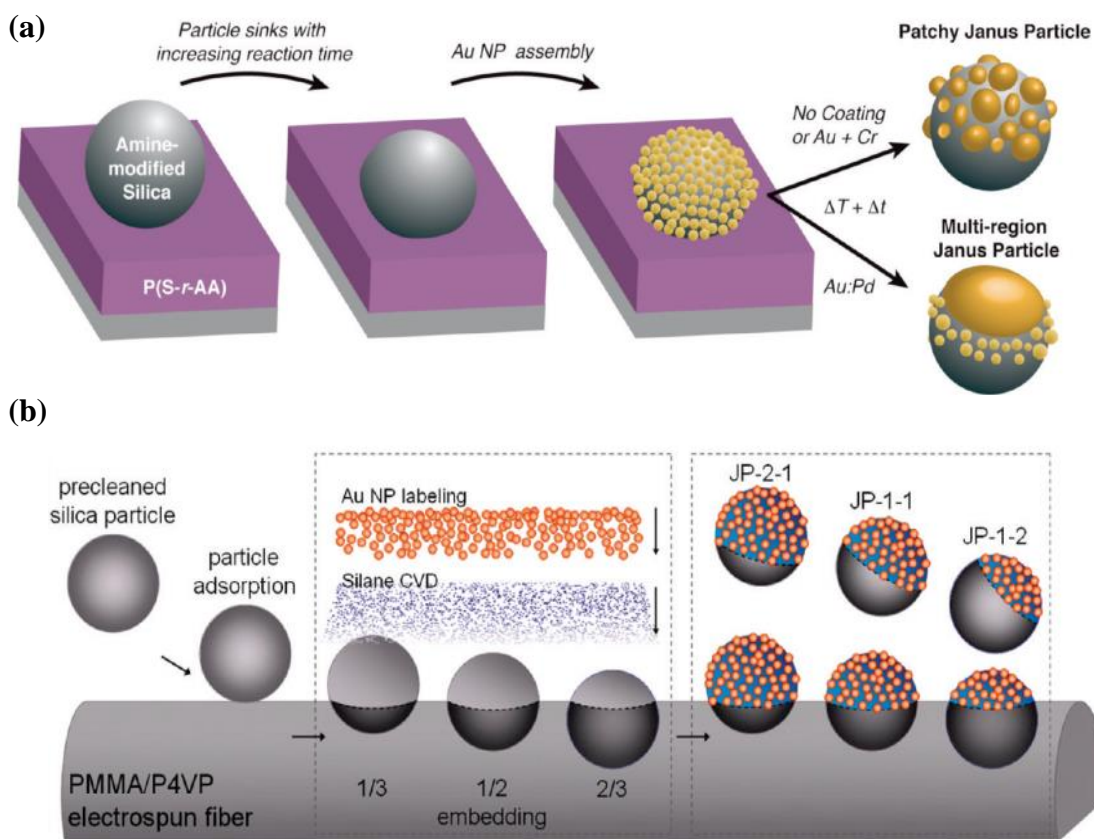


**Figure 1.23.** (a) Schematic representation of the self-assembled formation of patchy and multi-region Janus particles. 230 nm silica particles were covalently attached to the surface of P(S-r-AA) and subsequently sunk into the polymer film as a function of reaction time. 15 nm gold NPs were then electrostatically assembled onto the surface of 230 nm amine modified silica particles. These hybrid particles were then annealed with and without compatibilizing agents to form the Janus particles.<sup>90</sup> (b) The silica particles embedded into PMMA/P4VP, then, treated with silane CVD and Au.<sup>95</sup>

The modification technique of the exposed surface with the other one protected on a flat surface is fairly simple and quick for producing Janus particles. The advantages of this method control the Janus balance of the particles obtained. The disadvantage of this method is using the monolayer on a flat surface, which limits the production of a large yield of Janus particles. This method is not to be used for industrial applications because the production is only a few milligrams.

### 1.6.1.3 Preparation of Janus particles using Pickering emulsion

Pickering emulsion is one of the most promising methods for producing Janus particles in large quantities. The Pickering emulsion stabilises particles by locating them at the interface between oil and water. Granick *et al.* used Pickering emulsion to produce Janus particles by stabilising the oil-water emulsion with silica particles.<sup>96</sup> Paraffin wax was used as the oil phase. He began by mixing untreated silica particles with melted wax and

then homogenised them with water to form an oil/water emulsion (Fig. 1.24A). The silica particles are positioned at the interface between oil and water. Once the emulsion is stabilised with silica particles, the temperature is decreased to room temperature to trap the particles at the interface and solidifying the wax. The particles are thus half immersed in wax and half exposed for any desired chemical modifications (Fig. 1.24B and C). To release the particles after the modifications, the wax is dissolved by an organic solvent, freeing the particles. This technique has some advantages. Solidifying the oil phase improved the chance for better modification because the particles are trapped at the interface while the other half is protected. After modification, the particles are easy to retrieve by dissolving the solid core. A large amount of Janus particles is produced with only a few steps of preparation. Later, the same group demonstrated how they can control the silica particles immersion depth in the wax beads by adjusting the number of different surfactants that have an opposite charge (Fig.125a, b). Varying the concentration of didodecyl dimethyl ammonium bromide (DDAB) offers the ability to control Janus particles from 37° to 75°. The variations of Janus balance is demonstrated by the use of fluorescent labelling.<sup>97</sup>

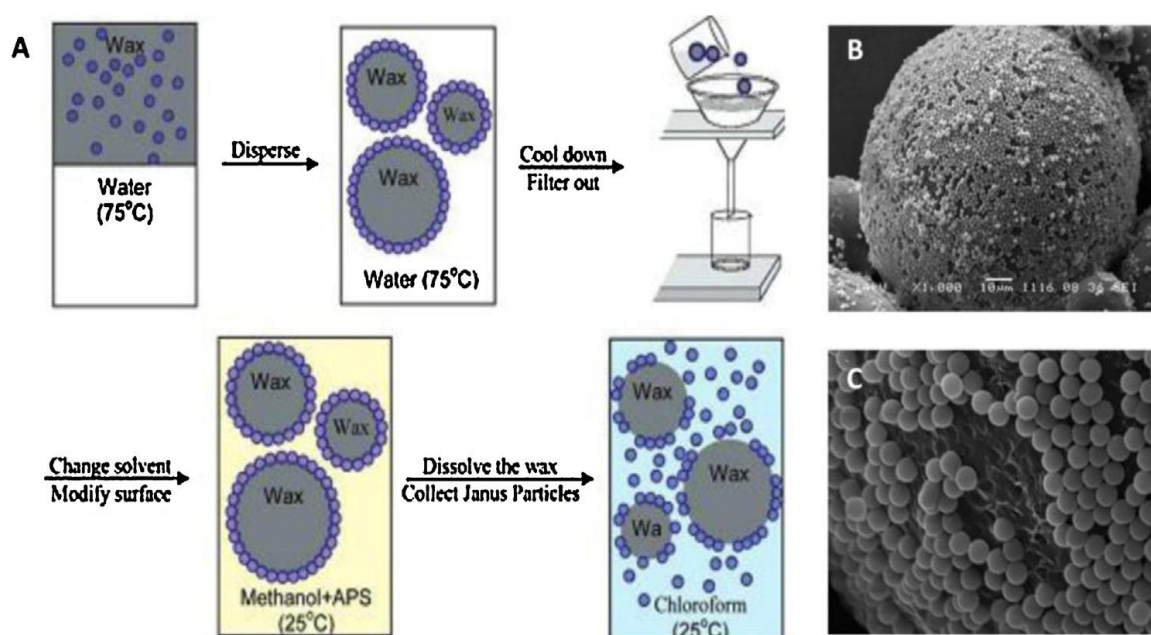


**Figure 1.24.** Schematic representations for (A) preparation of Janus particles by functionalizing particles adsorbed into o/w emulsion, followed by cooling so that the oil crystallizes to form a wax, and then filtered from water, (B) scanning electron microscopy (SEM) images of colloidosomes filtered from water, and (C) particles adsorbed onto the wax surface of colloidosomes.<sup>96</sup>

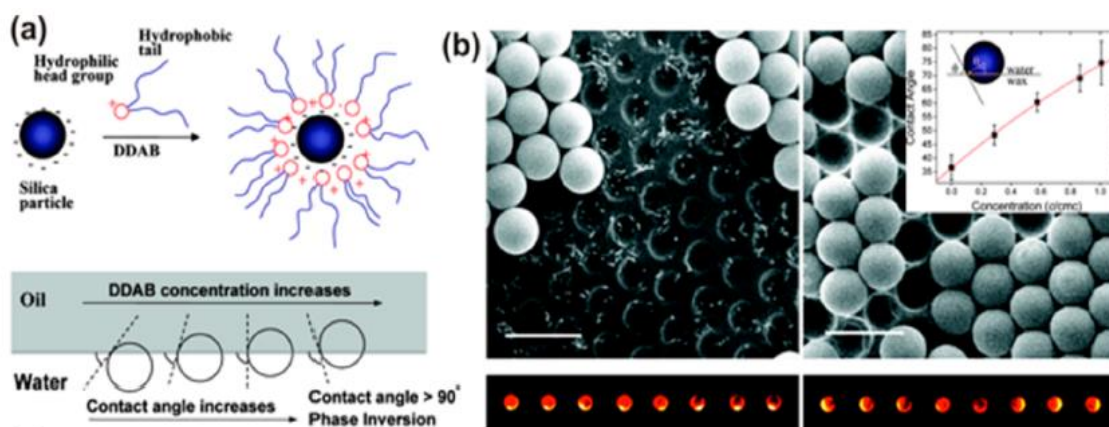


**Figure 1.25.** Modification of particles at Pickering emulsion interfaces. (a+b) Tuning the Janus balance: (a) The cationic surfactant DDAB adsorbs strongly on the SiO<sub>2</sub> beads and renders the particle more hydrophobic, causing them to penetrate deeper into the oil phase. (b) Comparison of SEM images of particles with different Janus balance (top panels) and corresponding epi-fluorescence images in water after fluorescent labelling. The epifluorescence images show the different character of the Janus particle. The fluorescent areas agree well with the size of the holes shown in the SEM images. The system on the right contains more DDAB. Scale bar = 5  $\mu\text{m}$ .<sup>97</sup>

There are some other research groups followed Granick who are using the Pickering emulsion to produce Janus particles. Recently, more work in the use of polymers to produce Janus particles via Pickering emulsion has been studied. Because the particles adsorbed strongly and irreversibly at the oil/water interface, the polymerisation of the oil phase trapped the particles at the interface, which allowed for further modification of the exposed surface. Li *et al.* used the Pickering emulsion to produce Janus particles. He used styrene as an oil phase and stabilised the emulsion with Cu<sub>2</sub>(OH)<sub>2</sub>CO<sub>3</sub> microspheres in water. The polymerisation then takes place, and polystyrene particles are modified with thioacetamide to produce Janus Cu<sub>2</sub>(OH)<sub>2</sub>CO<sub>3</sub>/CuS microspheres.<sup>98</sup> Wu *et al.* used the Pickering emulsion to produce SiO<sub>2</sub>-PS Janus particles in one step. Silica particles were stabilised in water through acid-base and electrostatic interaction, with styrene as an oil phase.<sup>99</sup> In Fig. 1.26, the formation of Pickering emulsion began by mixing 1-vinylimidazole (1-VID) with silica particles, water and styrene. Ultrasonication was then applied to form the Pickering emulsion. The silica particles were located at the interface through interaction with the amino groups (basic) on 1-VID and the hydroxyl groups on the surface of silica particles. The silica particle at this stage can be smoothly modified.

The polymer beads grew after adding the potassium persulfate, and the polystyrene-silica particles spheres were thus produced.

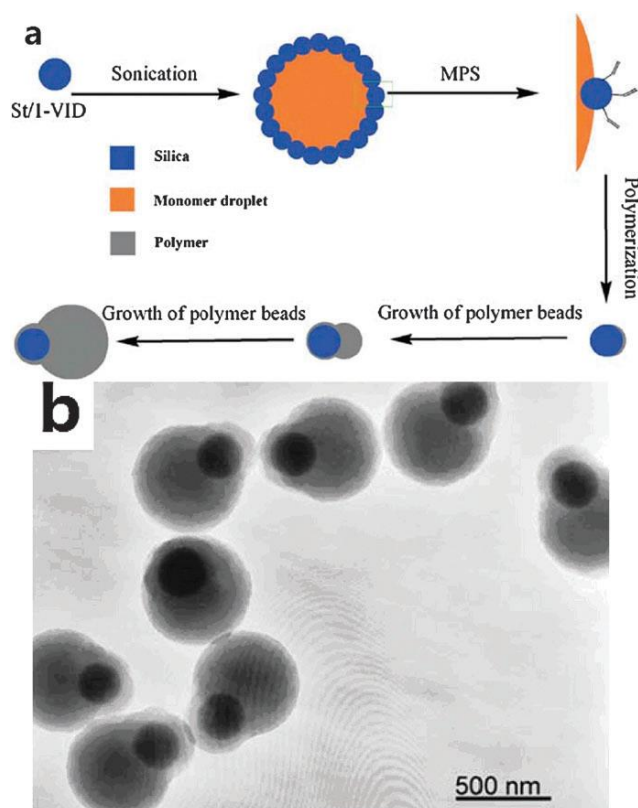


**Figure 1.26.** Synthetic procedure of PS–SiO<sub>2</sub> anisotropic colloid particles. (a) Silica particles, styrene, 1-vinylimidazole and water mixed by sonication to form droplets stabilised by silica particles. Then, the polymerisation for the growth of the polymer beads. (b) SEM images for Janus particles produced.<sup>99</sup>

Liu *et al.* produced Janus particles with controlled shapes. The Pickering emulsion was made and the wax solidified to trap the silica particles at the interface. The silica particles, which were previously treated with amino groups (silica-NH<sub>2</sub>) were then etched by applying the aqueous NH<sub>4</sub>F solution to the exposed surface of the silica particles. After separation, spherical Janus particles were obtained. The smooth side and the coarse side were distinguishable, with the clear circular showing the etching groove. Increasing the etching of Janus particles could change the shape from spherical to non-spherical (Fig.1.27).<sup>100</sup>

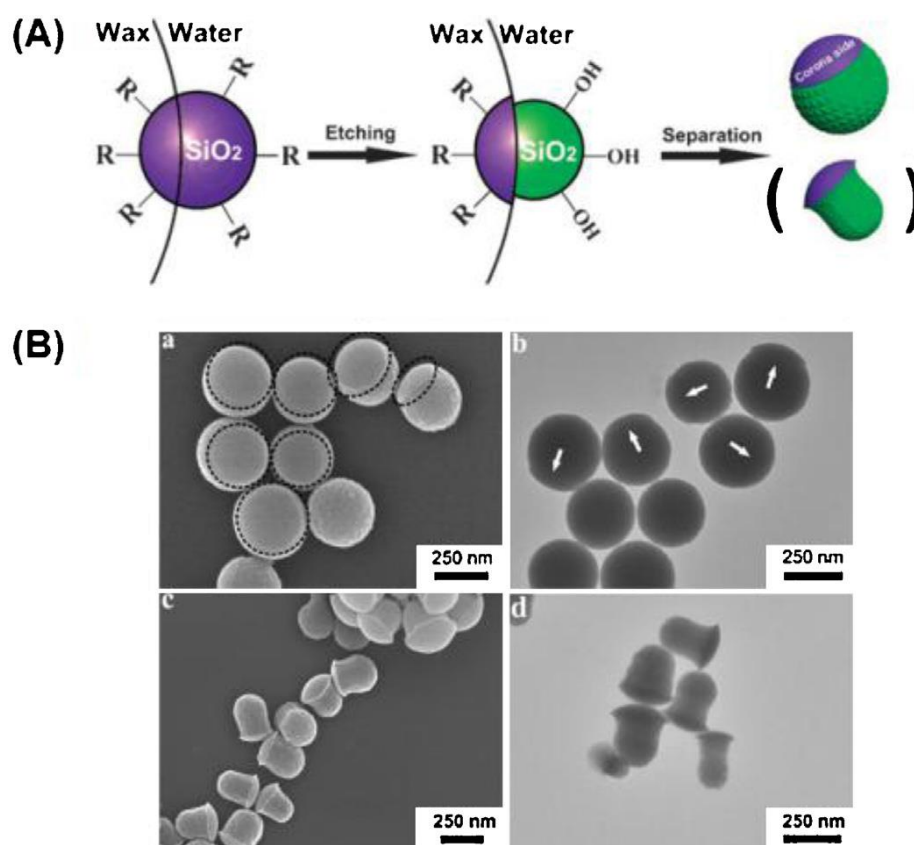


**Figure 1.27.** (A) Synthesis of Janus non-spherical colloids by asymmetric etching of the exposed side of the silica colloids at a Pickering emulsion interface. (B) SEM (a) and TEM (b) images of the as-prepared spherical Janus silica colloids by asymmetric etching the silica-NH<sub>2</sub> colloid for 21 h, (the smooth side is indicated by the arrow in (b)); SEM (c) and TEM (d) images of the as-prepared mushroom-like Janus silica colloids made by repeatedly etching for 42 d.<sup>100</sup>

## 1.6.2 Properties and applications of Janus particles

### 1.6.2.1 Amphiphilic properties

Janus particles have the ability to stabilise the emulsion due to their amphiphilic nature. This means they could replace the surfactant or work as a mixture of surfactant and particles. Janus particles have two different regions: one could be hydrophobic, or positively charged; and the other could be hydrophilic, or negatively charged.<sup>101, 102</sup> Janus particles positioned at the interface as a monolayer could resolve the problems of micelles created by surfactant.<sup>103</sup> Moreover, particles with improved surface chemistry show a higher adsorption energy at the interface compared to homogenised particles, as shown by Binks.<sup>104</sup>

Janus particles produced by the Pickering emulsion method using wax as an oil phase have been studied for their capability of producing a stable emulsion.<sup>105</sup> The hydrophobicity of the particles can be controlled by tuning the surfactant concentrations.

Pickering emulsion was made by dispersing Janus particles in toluene and then homogenising with water. The emulsion was kept at room temperature, and photos were taken at different times to monitor changing emulsion stability. Janus particles showed high emulsion stability for up to three weeks, as opposed to the control emulsion, which destabilised (Fig.1.28). This indicates the need for Janus functionalisation as the particles without any chemical modifications fail to make a stable emulsion.<sup>106</sup>

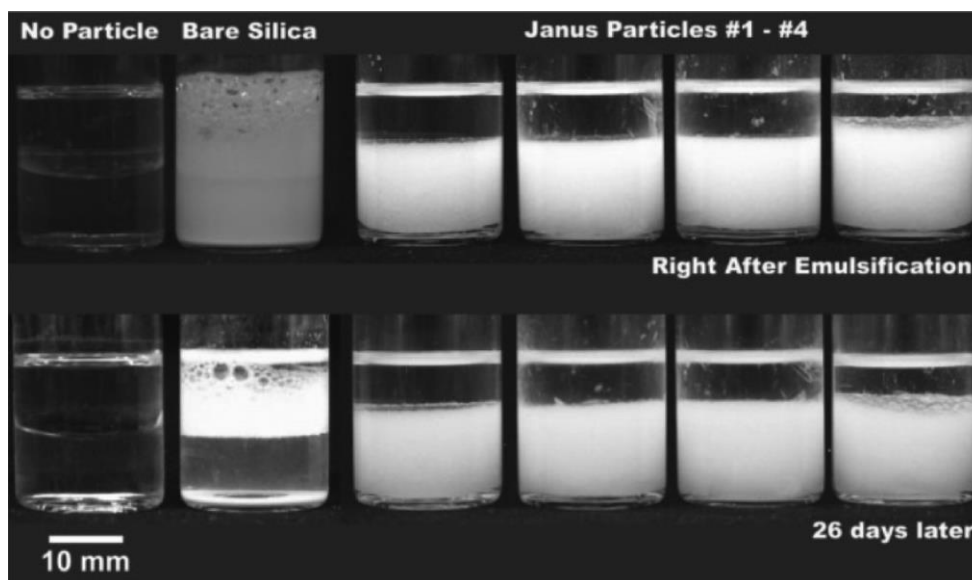


**Figure 1.28.** Photographs of emulsions. Emulsification was performed by dispersing the element running under 18 000 rpm for 1 min. Particles were 500 nm in diameter. The relative portion of hydrophobic and charged regions was parametrized by an angle  $\alpha$ , the inclination angle corresponding to the radian from the centre of the hydrophobic part to its edge. Janus particles #1–#4 had  $\alpha = 45, 47, 57,$  and  $72^\circ$ , respectively. The emulsions stabilized by Janus particles could be dispersed in toluene but not water, thereby indicating that the emulsion type is water in oil.<sup>105</sup>

### 1.6.2.2 Magnetic and catalytic properties

Janus particles display a remarkable magnetic responsiveness because they are created from magnetic components. These magnetic properties could be exploited in some applications, including biological imaging, biological probes and drug delivery. Janus magnetic particles also exhibited unusual rotational moves when an external magnetic field was applied.<sup>107-109</sup>

Janus particles with optical properties and made of magnetic components can be tuned by an external magnetic field. The two different regions of the Janus particles have magnetic nanoparticles in one region and quantum dots in the other region. The particles produced also have bifunctional magnetic fluorescence. When an electric field is applied, the orientation of the magnetic of  $\text{Fe}_3\text{O}_4$  nanoparticles is influenced by the direction of the

electric field. The reddish-brown colour appears when  $\text{Fe}_3\text{O}_4$  nanoparticle-dropped hemispheres face upward during the daylight and black under a UV light. In contrast, the panel displays the colour white for QD hemispheres when positioned upward in daylight and bright blue under a UV light. (Fig.1.29).<sup>110</sup> The catalytic properties of Janus particles have some potential applications, including fuel cell electrochemistry and degradation of organic pollutants. Janus particles made of  $\text{TiO}_2$  coated with Au nanoparticles exhibit catalytic activity and were able to reduce the 4-nitrophenol by using sodium borohydride to 4-aminophenol. At 400 nm, the absorption intensity of 4-nitrophenol quickly declined with time as a result of the reduction of product 4-aminophenol, achieving 99% conversion in 6 min.<sup>111, 112</sup>

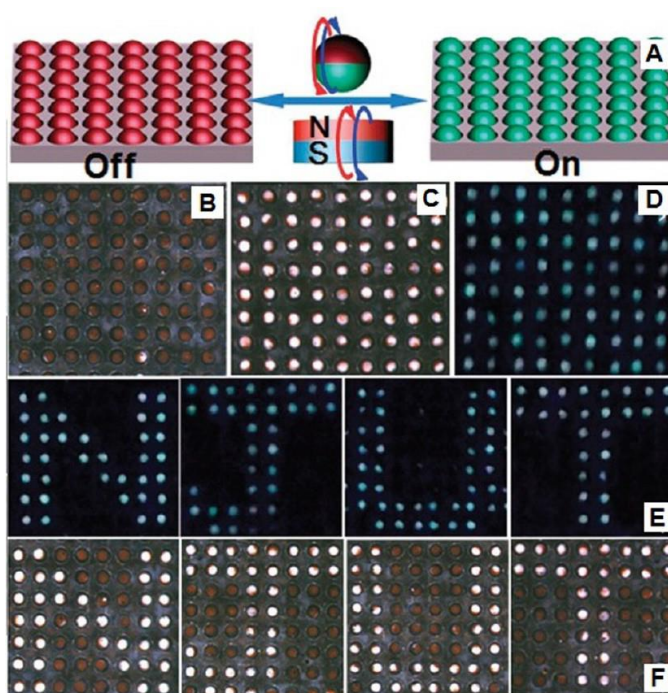


**Figure 1.29.** (A) Schematic representation of a fluorescent switch of Janus particles controlled by varying the direction of an external magnetic field. (B–F) Optical images of the magneto-responsive bead display prepared from Janus particles: (B, C, F) under daylight and (D, E) under UV irradiation.<sup>110</sup>

### 1.6.2.3 Self-assembly of Janus particles

Self-assembly of homogeneous spherical particles have been widely studied.<sup>113, 114</sup> Recently, Janus particles have attracted scientists because of the particles' ability to self-assemble.<sup>115-117</sup> Granick *et al.* illustrated how Janus particles are able to make a complex colloidal crystal. In addition, Triblock Janus spheres for designing micrometre-sized with the interaction between them. The poles exert hydrophobic attraction, and the middle exerts electrostatic repulsion. This allows particles to self-assemble into a colloidal kagome lattice (see Fig.30a).<sup>103, 118</sup> The attraction of triblock Janus particles occurs at

their poles, and the size of the particles influences their arrangement into geometrical order. The attraction in the middle is avoidable because of the charged middle band. In the Granick study, sedimentation occurred overnight due to the density discrepancy between the water and the Janus particles. After sedimentation, the particles arranged themselves into a quasi-two-dimensional order. Salt added to the suspension (3.5 mM NaCl), screened the electrostatic repulsions and allowed the hydrophobic attraction to take place. The order process has to reach the final stage to be thermodynamically stable, as shown in the fluorescence images (Fig. 1.30b). The hexagonal or triangular structure of the lattice has different microenvironments on the pore rims. This application of colloidal particles encourages scientists to fabricate structures more hierarchically, which can be used in different applications.

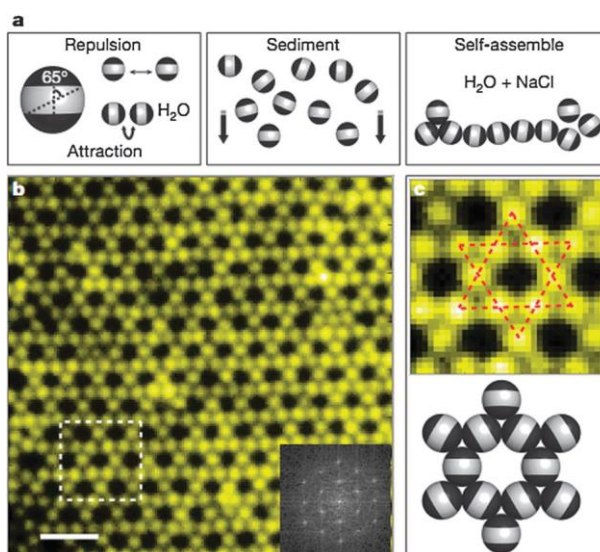


**Figure 1.30.** Colloidal kagome lattice after equilibration. (a) Triblock Janus spheres hydrophobic on the poles (black, with an opening angle of  $65^\circ$ ) and charged in the equator section (white), are allowed to sediment in deionized water. Then NaCl is added to screen electrostatic repulsion, allowing self-assembly by short-range hydrophobic attraction. (b) Fluorescence image of a colloidal kagome lattice (main image) and its fast Fourier transform image (bottom right). Scale bar is 4 mm. The top panel in (c) shows an enlarged view of the dashed white rectangle in (b). Dotted red lines in (c) highlight two staggered triangles. The bottom panel in (c) shows a schematic illustration of particle orientations.<sup>118</sup>

## 1.7 Aims of the research

The aim of the research presented in this thesis is to prepare macroporous polymers and Janus particles via emulsion templating by polymerising the oil phase at room temperature. This could help to maintain the emulsion stability better in comparison to high temperature polymerisation methods and to reduce the costs for the preparation of such materials which is of great practical importance.

Traditionally, polyHIPE materials are prepared by thermally induced polymerisation of the continuous emulsion phase at elevated temperature (60–80°C) or photoinitiated polymerisation of relatively thin transparent samples. Both approaches are energy inefficient and require tedious sample preparation (removal of inhibitors, inert atmosphere, etc.). There are redox initiator systems which have been used to initiate polymerisation at room temperature without the need of the external source of energy supply. Although such systems (e.g. benzoyl peroxide, BPO – dimethyl-p-toluidine, DMPT) have been used in MMA based bone cement compositions for many years and some other application as shown in the literature, their application for making a limited number of polyHIPEs for bio-applications was demonstrated only a few years ago. The present study aims to investigate the polymerisation of monomer and HIPE systems using a BPO-DMPT initiator couple at room temperature, to prepare polyHIPE materials from widely used monomer (MMA) and investigate the effect of crosslinker and surfactant concentration on the mechanical properties and the morphology of the materials produced. Then, try to produce polyHIPEs at high temperature using the thermo-initiator system. The polyHIPEs produced at room temperature will be compared those polyHIPE materials produced by the traditional high temperature thermo-initiation.

One of the most challenging problems in Janus particle research is their preparation in large quantities. Most of the preparation strategies reported suffer from limited yields or Janus particle functionalities which could be achieved, thus hampering their large scale applications. The use of particle-stabilised (Pickering) emulsions of paraffin wax-in-water as a tool for making Janus particles introduced by the group of Granick could give large yields, but the paraffin wax causes problems due to the poor particle adhesion and the limited conditions for chemical modification. Here we aim to extend this approach to polymerised Pickering emulsions using a mixture of monomers as an oil phase and silica particles as an emulsifier.

## **1.8 Presentation of thesis**

Chapter 2 describes all of the materials and experimental techniques used throughout the research. Chapter 3 considers the preparation of macroporous polymers at room temperature via emulsion templating using redox-initiated polymerisation. The effects of different factors (volume fraction of the internal water phase, concentrations of surfactant and crosslinker) on the mechanical properties and morphology of polyHIPEs produced are discussed. Finally, results demonstrating the flexibility and feasibility of our method for various applications are presented.

Chapter 4 concerns the preparation of polyHIPEs at high temperature using thermo-initiation systems. BPO and AIBN have been tested as thermo-initiators to produce polyHIPEs at high temperature using the traditional method. The mechanical properties and morphology of polyHIPEs produced at high temperature are studied and compared to those of polyHIPEs produced by redox-initiated polymerisation at room temperature.

The preparation of Janus particles via emulsion templating is presented in Chapter 5, divided into four sections according to the method used: results for the stability of o/w emulsions stabilised by a mixture of silica particles and a cationic surfactant; polymerisation of Pickering emulsions; optimisation of the silica particle release from the polymer beads followed by evidence for producing Janus particles by zeta potential measurements. The summary of main findings, conclusions and directions for future work are presented in the final chapter of the thesis.

## 1.9 References

1. J. Bibette, F. Leal-Calderon, V. Schmitt and P. Poulin, *Emulsion Science: basic principles. An overview*, Springer, New York, 2003.
2. B. P. Binks, *Modern aspects of emulsion science*, Royal Society of Chemistry, Cambridge, 1998.
3. D. Schuster, *Encyclopedia of emulsion technology*, CRC Press, New York, 1996.
4. D. Myers, *Surfactant science and technology*, John Wiley & Sons, New Jersey, 2006.
5. S. U. Pickering, *J.Chem. Soc.*, 1907, **91**, 2001-2021.
6. B. P. Binks and J. H. Clint, *Langmuir*, 2002, **18**, 1270-1273.
7. R. Aveyard, B. P. Binks and J. H. Clint, *Adv. Colloid Interface Sci.*, 2003, **100–102**, 503-546.
8. B. P. Binks, *Curr. Opin. Colloid Interface Sci.*, 2002, **7**, 21-41.
9. B. P. Binks, J. H. Clint and C. P. Whitby, *Langmuir*, 2005, **21**, 5307-5316.
10. N. Yan, M. R. Gray and J. H. Masliyah, *Colloids Surf., A*, 2001, **193**, 97-107.
11. T. Ngai, S. H. Behrens and H. Auweter, *Chem. Commun.*, 2005, 331-333.
12. Y. Zhu, Q. Hu, W. Wei, C. Yi and X. Liu, *Colloids Surf., A*, 2016, **504**, 358-366.
13. Z. Ao, Z. Yang, J. Wang, G. Zhang and T. Ngai, *Langmuir*, 2009, **25**, 2572-2574.
14. B. P. Binks and T. S. Horozov, *Colloidal Particles at Liquid Interfaces*, Cambridge University Press, Cambridge, 2006.
15. B. Braisch, K. Köhler, H. P. Schuchmann and B. Wolf, *Chem. Eng. Technol.*, 2009, **32**, 1107-1112.
16. B. P. Binks and T. S. Horozov, in *Colloidal particles at liquid interface* eds. R. Lopetinsky, H. M. Jacob and X. Zhenghe, Cambridge University Press, Cambridge 2006, ch. 6, p. 189.
17. K. Lissant, *J. Colloid Interface Sci.*, , 1966, **22**, 462-468.
18. K. J. Lissant, B. W. Peace, S. H. Wu and K. G. Mayhan, *J. Colloid Interface Sci.*, 1974, **47**, 416-423.
19. US 10/795,663, 2005.
20. S. Zhang, J. Chen and V. T. Perchyonok, *Polymer*, 2009, **50**, 1723-1731.
21. X. Zheng, Y. Zhang, H. Wang and Q. Du, *Macromolecules*, 2014, **47**, 6847-6855.
22. H. Zhang and A. I. Cooper, *Soft Matter*, 2005, **1**, 107-113.

23. N. R. Cameron, *Polymer*, 2005, **46**, 1439-1449.
24. R. Pons, I. Carrera, P. Erra, H. Kunieda and C. Solans, *Colloids Surf., A*, 1994, **91**, 259-266.
25. J. M. Williams, A. J. Gray and M. H. Wilkerson, *Langmuir*, 1990, **6**, 437-444.
26. J. M. Williams and D. A. Wroblewski, *Langmuir*, 1988, **4**, 656-662.
27. M. G. Freire, A. M. Dias, M. A. Coelho, J. A. Coutinho and I. M. Marrucho, *J Colloid Interface Sci*, 2005, **286**, 224-232.
28. H. G. Elias and H. G. Elias, in *Macromolecules*, Wiley-VCH Verlag GmbH, New York, 2005, pp. 309-367.
29. E. H. I. J. Brandrup, E. A. Grulke. , *Polymer Handbook*, John Wiley, New York, 4th edn., 2003.
30. J. M. Williams, *Langmuir*, 1991, **7**, 1370-1377.
31. W.-F. Su, in *Principles of Polymer Design and Synthesis*, Springer Berlin Heidelberg, Berlin, 2013, pp. 137-183.
32. M. Chen, M. Zhong and J. A. Johnson, *Chem. Rev.*, 2016, **116**, 10167-10211.
33. H. Pelletier, N. Belgacem and A. Gandini, *J. Appl. Polym. Sci*, 2006, **99**, 3218-3221.
34. S. D. Kimmins, P. Wyman and N. R. Cameron, *React. Funct. Polym.*, 2012, **72**, 947-954.
35. F. Schüler, D. Schamel, A. Salonen, W. Drenckhan, M. D. Gilchrist and C. Stubenrauch, *Angew. Chem., Int. Ed.*, 2012, **51**, 2213-2217.
36. N. Kohut-Svelko, R. Pirri, J. M. Asua and J. R. Leiza, *J. Polym. Sci., Part A: Polym. Chem.*, 2009, **47**, 2917-2927.
37. A. Zoller, D. Gigmes and Y. Guillemeuf, *Polym. Chem.*, 2015, **6**, 5719-5727.
38. P. K. Vallittu, I. E. Ruyter and S. Buykuilmaz, *Eur. J. Oral. Sc.i*, 1998, **106**, 588-593.
39. D. S. Zhao, N. Moritz, P. Laurila, R. Mattila, L. V. J. Lassila, N. Strandberg, T. Mäntylä, P. K. Vallittu and H. T. Aro, *J. Biomed Eng.*, 2009, **31**, 461-469.
40. I. D. Sideridou, D. S. Achilias and O. Karava, *Macromolecules*, 2006, **39**, 2072-2080.
41. T.-Y. Kwon, R. Bagheri, Y. K. Kim, K.-H. Kim and M. F. Burrow, *J. Investig Clin. Den.t*, 2012, **3**, 3-16.
42. R. J. Carnachan, M. Bokhari, S. A. Przyborski and N. R. Cameron, *Soft Matter*, 2006, **2**, 608-616.

43. N. Cameron, D. Sherrington, L. Albiston and D. Gregory, *Colloid Polym. Sci.*, 1996, **274**, 592-595.
44. A. Menner, and Alexander Bismarck, *Macromol. Symp.*, 2006, **424**, 19-24.
45. Q. Li and L. M. Matuana, *J. Appl. Polym. Sci.*, 2003, **88**, 3139-3150.
46. B. Krause, H. J. P. Sijbesma, P. Münüklü, N. F. A. van der Vegt and M. Wessling, *Macromolecules*, 2001, **34**, 8792-8801.
47. Z. Pan, Z.-h. Qu, Z. Zhang, R. Peng, C. Yan and J.-d. Ding, *Chin. J. Polym. Sci.*, 2013, **31**, 737-747.
48. C.-J. Liao, C.-F. Chen, J.-H. Chen, S.-F. Chiang, Y.-J. Lin and K.-Y. Chang, *J Biomed Mater Res*, 2002, **59**, 676-681.
49. L. L. Wong, P. M. Baiz Villafranca, A. Menner and A. Bismarck, *Langmuir*, 2013, **29**, 5952-5961.
50. N. Shirshova, A. Bismarck and J. H. Steinke, *Macromol. Rapid Commun.*, 2011, **32**, 1899-1904.
51. E. Lovelady, S. D. Kimmins, J. Wu and N. R. Cameron, *Polym. Chem.*, 2011, **2**, 559-562.
52. Y. Luo, A.-N. Wang and X. Gao, *Soft Matter*, 2012, **8**, 1824-1830.
53. S. Jerenec, M. Šimić, A. Savnik, A. Podgornik, M. Kolar, M. Turnšek and P. Krajnc, *React. Funct. Polym.*, 2014, **78**, 32-37.
54. P. Krajnc, N. Leber, D. Štefanec, S. Kontrec and A. Podgornik, *J. Chromatogr A*, 2005, **1065**, 69-73.
55. K. J. Lissant and K. G. Mayhan, *J. Colloid Interface Sci.*, 1973, **42**, 201-208.
56. D. Mao, T. Li, H. Liu, Z. Li, H. Shao and M. Li, *Colloid Polym. Sci.*, 2013, **291**, 1649-1656.
57. S. Huš and P. Krajnc, *Polymer*, 2014, **55**, 4420-4424.
58. R. S. Moglia, J. L. Holm, N. A. Sears, C. J. Wilson, D. M. Harrison and E. Cosgriff-Hernandez, *Biomacromolecules*, 2011, **12**, 3621-3628.
59. R. S. Moglia, M. Whitely, P. Dhavalikar, J. Robinson, H. Pearce, M. Brooks, M. Stuebben, N. Cordner and E. Cosgriff-Hernandez, *Biomacromolecules*, 2014, **15**, 2870-2878.
60. R. F. Landel and L. E. Nielsen, *Mechanical properties of polymers and composites*, Marcel Dekker, Inc, New York, 2nd edn., 1993.
61. H. Young and R. Freedman, *Sears and Zemansky's university physics : with modern physics.*, Jim Smith, France, 13 edn., 2012.

62. G. Lorna, and M. Ashby, *Cellular Solids: Structure and Properties*, Cambridge University Press, Cambridge, 2nd edn., 1997.
63. M. F. Ashby and R. M. Medalist, *Metall. Trans. A*, 1983, **14**, 1755-1769.
64. M. F. Ashby, *Philos. Trans. R. Soc., A*, 2006, **364**, 15.
65. F. Fernández-Trillo, J. C. M. van Hest, J. C. Thies, T. Michon, R. Weberskirch and N. R. Cameron, *Adv. Mater.*, 2009, **21**, 55-59.
66. C. E. Chan-Thaw, A. Villa, P. Katekomol, D. Su, A. Thomas and L. Prati, *Nano Lett.*, 2010, **10**, 537-541.
67. P. Krajnc, N. Leber, D. Štefanec, S. Kontrec and A. Podgornik, *J. Chromatogr A*, 2005, **1065**, 69-73.
68. W. Lu, D. Yuan, D. Zhao, C. I. Schilling, O. Plietzsch, T. Muller, S. Bräse, J. Guenther, J. Blümel, R. Krishna, Z. Li and H.-C. Zhou, *Chem. Mater*, 2010, **22**, 5964-5972.
69. G. Akay, M. Birch and M. Bokhari, *Biomaterials*, 2004, **25**, 3991-4000.
70. J. Hu, X. Sun, H. Ma, C. Xie, Y. E. Chen and P. X. Ma, *Biomaterials*, 2010, **31**, 7971-7977.
71. B. Li, R. Gong, W. Wang, X. Huang, W. Zhang, H. Li, C. Hu and B. Tan, *Macromolecules*, 2011, **44**, 2410-2414.
72. A. Barbetta, M. Dentini, L. Leandri, G. Ferraris, A. Coletta and M. Bernabei, *React. Funct. Polym.*, 2009, **69**, 724-736.
73. I. Pulko, M. Kolar and P. Krajnc, *Sci. Total Environ.*, 2007, **386**, 114-123.
74. B. C. Benicewicz, G. D. Jarvinen, D. J. Kathios and B. S. Jorgensen, *J. Radioanal. Nucl. Chem.*, 1998, **235**, 31-35.
75. I. Pulko, V. Smrekar, A. Podgornik and P. Krajnc, *J. Chromatogr A*, 2011, **1218**, 2396-2401.
76. C. T. Laurencin, M. A. Attawia, H. E. Elgendy and K. M. Herbert, *Bone*, 1996, **19**, S93-S99.
77. W. Busby, N. R. Cameron and C. A. Jahoda, *Biomacromolecules*, 2001, **2**, 154-164.
78. P. G. de Gennes, *Science*, 1992, **256**, 495.
79. A. Walther and A. H. E. Müller, *Chem. Rev.*, 2013, **113**, 5194-5261.
80. S. Yang, F. Guo, B. Kiraly, X. Mao, M. Lu, K. W. Leong and T. J. Huang, *Lab Chip*, 2012, **12**, 2097-2102.
81. T. Nisisako, T. Torii, T. Takahashi and Y. Takizawa, *Adv. Mater.*, 2006, **18**, 1152-1156.

82. O. Cayre, V. N. Paunov and O. D. Velev, *Chem. Commun.*, 2003, **18**, 2296-2297.
83. S. Jiang and S. Granick, *Langmuir*, 2009, **25**, 8915-8918.
84. H. Takei and N. Shimizu, *Langmuir*, 1997, **13**, 1865-1868.
85. J. Choi, Y. Zhao, D. Zhang, S. Chien and Y. H. Lo, *Nano Lett.*, 2003, **3**, 995-1000.
86. P. Wu, Y. Dai, T. Sun, Y. Ye, H. Meng, X. Fang, B. Yu and L. Dai, *ACS Appl. Mater. Interfaces*, 2011, **3**, 1859-1864.
87. X. Y. Ling, I. Y. Phang, C. Acikgoz, M. D. Yilmaz, M. A. Hempenius, G. J. Vancso and J. Huskens, *Angew. Chem., Int. Ed.*, 2009, **48**, 7677-7682.
88. K. D. Anderson, M. Luo, R. Jakubiak, R. R. Naik, T. J. Bunning and V. V. Tsukruk, *Chem. Mater.*, 2010, **22**, 3259-3264.
89. L. Nagle, D. Ryan, S. Cobbe and D. Fitzmaurice, *Nano Lett.*, 2003, **3**, 51-53.
90. M. D. McConnell, M. J. Kraeutler, S. Yang and R. J. Composto, *Nano Lett.*, 2010, **10**, 603-609.
91. S.-H. Kim, S. Y. Lee and S.-M. Yang, *Angew. Chem., Int. Ed.*, 2010, **49**, 2535-2538.
92. J.-Q. Cui and I. Kretzschmar, *Langmuir*, 2006, **22**, 8281-8284.
93. J. Gong, X. Zu, Y. Li, W. Mu and Y. Deng, *J. Mater. Chem.*, 2011, **21**, 2067-2069.
94. C. Casagrande, P. Fabre, E. Raphaël and M. Veyssié, *Europhys. Lett.*, 1989, **9**, 251.
95. C.-C. Lin, C.-W. Liao, Y.-C. Chao and C. Kuo, *ACS Appl. Mater. Interfaces*, 2010, **2**, 3185-3191.
96. L. Hong, S. Jiang and S. Granick, *Langmuir*, 2006, **22**, 9495-9499.
97. S. Jiang and S. Granick, *Langmuir*, 2008, **24**, 2438-2445.
98. Y. He and K. Li, *J. Colloid Interface Sci.*, 2007, **306**, 296-299.
99. S.-W. Zhang, S.-X. Zhou, Y.-M. Weng and L.-M. Wu, *Langmuir*, 2005, **21**, 2124-2128.
100. B. Liu, C. Zhang, J. Liu, X. Qu and Z. Yang, *Chem. Commun.*, 2009, DOI: 10.1039/B905981D, 3871-3873.
101. Y. K. Takahara, S. Ikeda, S. Ishino, K. Tachi, K. Ikeue, T. Sakata, T. Hasegawa, H. Mori, M. Matsumura and B. Ohtani, *J. Am. Chem. Soc.*, 2005, **127**, 6271-6275.

102. L. Hong, A. Cacciuto, E. Luijten and S. Granick, *Nano Lett.*, 2006, **6**, 2510-2514.
103. Q. Chen, J. K. Whitmer, S. Jiang, S. C. Bae, E. Luijten and S. Granick, *Science*, 2011, **331**, 199.
104. B. P. Binks and P. D. I. Fletcher, *Langmuir*, 2001, **17**, 4708-4710.
105. S. Jiang, M. J. Schultz, Q. Chen, J. S. Moore and S. Granick, *Langmuir*, 2008, **24**, 10073-10077.
106. S. C. Glotzer and M. J. Solomon, *Nat. Mater.*, 2007, **6**, 557.
107. J. Ge, Y. Hu, T. Zhang and Y. Yin, *J. Am. Chem. Soc.*, 2007, **129**, 8974-8975.
108. K. P. Yuet, D. K. Hwang, R. Haghgooie and P. S. Doyle, *Langmuir*, 2010, **26**, 4281-4287.
109. S.-H. Hu and X. Gao, *J. Am. Chem. Soc.*, 2010, **132**, 7234-7237.
110. J. Kim, S. E. Chung, S.-E. Choi, H. Lee, J. Kim and S. Kwon, *Nat. Mater.*, 2011, **10**, 747.
111. N. Chaturvedi, Y. Hong, A. Sen and D. Velegol, *Langmuir*, 2010, **26**, 6308-6313.
112. G. Volpe, I. Buttinoni, D. Vogt, H.-J. Kummerer and C. Bechinger, *Soft Matter*, 2011, **7**, 8810-8815.
113. J. Hu, M. Chen, X. Fang and L. Wu, *Chem. Soc. Rev.*, 2011, **40**, 5472-5491.
114. F. Li, D. P. Josephson and A. Stein, *Angew. Chem., Int. Ed.*, 2011, **50**, 360-388.
115. Z. Nie, D. Fava, E. Kumacheva, S. Zou, G. C. Walker and M. Rubinstein, *Nat. Mater.*, 2007, **6**, 609.
116. H. Xing, Z. Wang, Z. Xu, N. Y. Wong, Y. Xiang, G. L. Liu and Y. Lu, *ACS Nano*, 2012, **6**, 802-809.
117. Y. Liu, W. Li, T. Perez, J. D. Gunton and G. Brett, *Langmuir*, 2012, **28**, 3-9.
118. Q. Chen, S. C. Bae and S. Granick, *Nature*, 2011, **469**, 381.

## CHAPTER 2

### Experimental

This chapter describes all the materials and experimental procedures used across the thesis.

#### 2.1 Materials

##### 2.1.1 Solvents

The water used in all the experiments is deionised water obtained from Elgastat Prima reverse osmosis unit unless otherwise stated. The solvents used are listed in Table 2.1.

**Table 2.1.** Purity and supplier of organic solvents used.

Solvent	Purity/%	Supplier
Ethanol (absolute)	99.8	VWR
Propan-2-ol	99.99	VWR
Acetone	99.8	VWR

##### 2.1.2 Surfactants

The non-ionic oil soluble surfactant Pluronic PEL-121 (density - 1.006 g/mL, Fig.2.1a) purchased from Aldrich was used to stabilise water-in-oil emulsion templates in the preparation of macroporous polymer.<sup>1</sup> The water soluble cationic surfactant tetradecyltrimethylammonium bromide (TTAB, Fig.2.1b) ordered from Sigma was used to tune the hydrophobicity of silica particles for stabilising oil-in-water emulsions needed for the production of Janus particles.

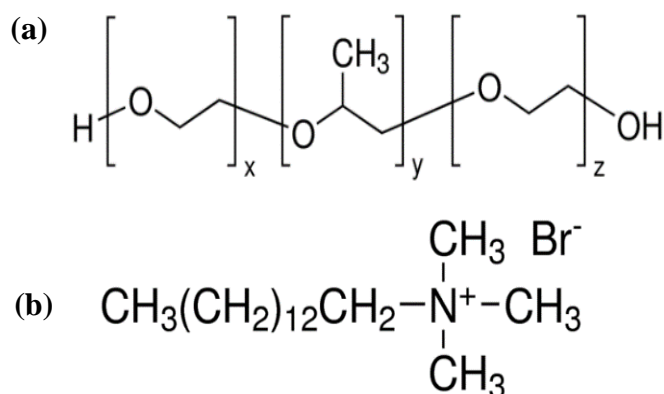


**Figure 2.1.**(a) Chemical structure of PEG-*b*-PPG-*b*-PEG triblock polymeric surfactant Pluronic PEL-121 where the average number of poly(ethylene glycol) units is  $x = z = 5$  and that of poly(propylene glycol) units is  $y=68.3$  (ref. 1). (b) Chemical structure of tetradecyltrimethylammonium bromide (TTAB).

### 2.1.3 Silica particles

Monodispersed silica particles were obtained from Fiber Optic Center Inc, USA as dry powders with diameters of 1.0  $\mu\text{m}$  and 0.1  $\mu\text{m}$ . According to the supplier, the particle density is 2.0  $\text{g/cm}^3$ , the purity is > 99.99% and the standard deviation of particle diameter is less than 10%.

The amination of silica particle surface was done by 3-aminopropyl triethoxysilane (APTES, 98%, Sigma). The pH in zeta potential measurements was adjusted using sodium hydroxide (analytical grade) and hydrochloric acid (HCl, 36%, analytical grade) both from Fisher Scientific.

### 2.1.4 Chemicals used in polymerisation experiments

The monomers and crosslinkers used in the polymerisation of the oil phase of emulsion templates are listed in Table 2.2. The benzoyl peroxide as solid mixture with ~50% dicyclohexyl phthalate (Sigma-Aldrich) used as the initiator at room temperature and accelerated by 4,*N,N*-trimethylaniline (DMPT,  $\geq 98.5$ , Aldrich ).the In all experiments for the preparation of macroporous polymer and Janus particles by a redox-initiated polymerisation at room temperature, the chemical were used as received. However, the monomers and crosslinkers used in the preparation of macroporous polymer by thermo-initiated polymerisation were purified by passing through basic alumina (Sigma-Aldrich) three times to remove inhibitors. Azobisisobutyronitrile (AIBN, 98%, Sigma-Aldrich) was used as a thermo-initiator in those experiments. Calcium chloride dehydrate (101.12, Fisher Scientific) was added to the water phase to enhance the emulsion stability during the polymerisation at high temperature.

**Table 2.2.** Formula, molar mass, density, purity and supplier of the monomers and crosslinkers used in the polymerisation of the oil phase of emulsion templates.

Chemical	Formula	Molar mass g/mol	Density g/mL	Purity %	Supplier
Methyl methacrylate (MMA)	$\text{C}_5\text{H}_8\text{O}_2$	100.12	0.936	99	Aldrich
Isobutyl methacrylate (IBMA)	$\text{C}_8\text{H}_{14}\text{O}_2$	142	0.886	9	Aldrich
1,6-hexanediol diacrylate (HDDA)	$\text{C}_{12}\text{H}_{18}\text{O}_4$	226.27	1.01	80	Aldrich
Ethylene glycol dimethacrylate (EGDMA)	$\text{C}_{10}\text{H}_{14}\text{O}_4$	198.22	1.0500	98	ACROS

## **2.2 Methods used in the preparation of macroporous polymer by emulsion templating**

### **2.2.1 Preparation of w/o emulsion templates for redox-initiated polymerisation at room temperature**

All chemicals in redox-initiated polymerisation experiments are used as received. The oil phase is a mixture of a monomer and crosslinker in which the initiator (BPO) and the surfactant (PEL-121) are dissolved. First, a stock solution of 4 wt/vol.% BPO in the monomer (MMA) is prepared. Then certain volumes of the stock solution, neat monomer and crosslinker (EGDMA) are mixed together to obtain a solution of BPO with the desired concentration (typically 1 wt/vol.% BPO as received). The actual concentration of BPO is a half of that prepared because the as received BPO contains 50 % dicyclohexyl phthalate as a stabiliser. Then the PEL-121 surfactant is dissolved in the BPO solution to the desired concentration. In most experiments, deionised water is used as an aqueous phase of the emulsions.

Emulsion templates are produced using the set-up shown in Fig.2.2. The oil phase is placed in a 500 mL three-neck flask and stirred with an overhead stirrer at 200 rpm. The water phase is added dropwise using a syringe pump set at a flow rate of 4 mL/min. Once all the water phase is added, the speed is increased to 700 rpm and the emulsion stirred further for a time equal to that spent for adding the water phase (for example, if it takes 10 min for the water phase to be added, the emulsion is stirred for another 10 min). Different volumes of oil and aqueous phases are used to make 50 mL emulsion containing 65-90 vol.% internal water phase.

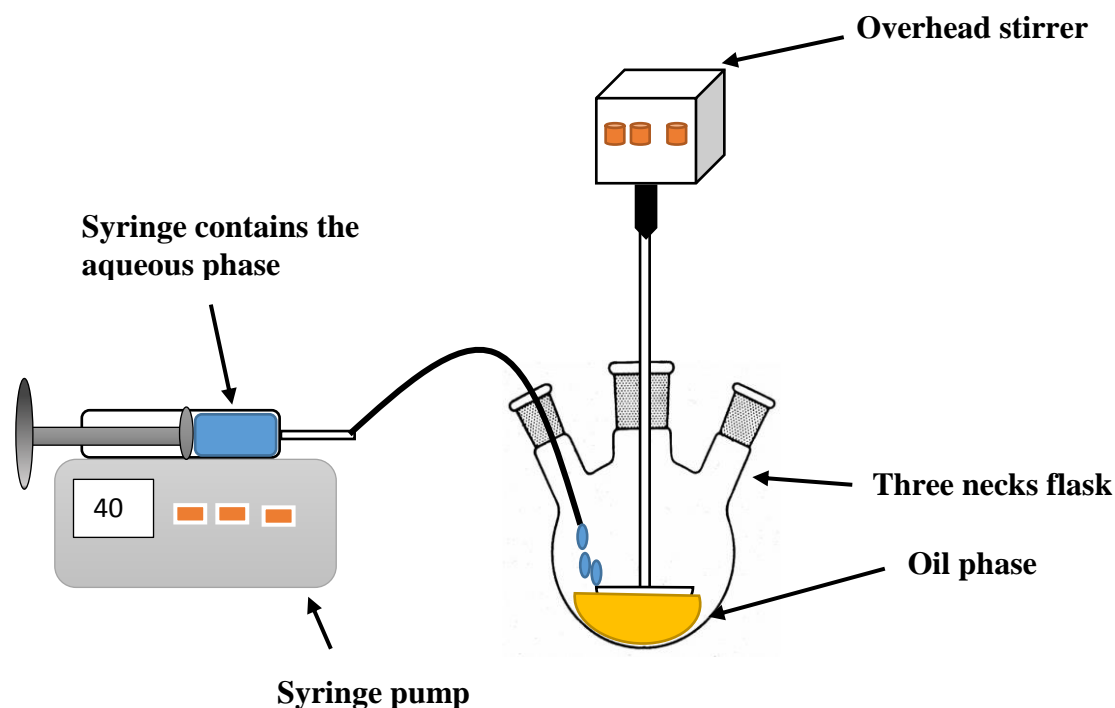


**Figure 2.2.** Schematic representation of the experimental set-up for producing HIPES.

### 2.2.2 Preparation of macroporous polymer via redox-initiated polymerisation at room temperature

In order to initiate the polymerisation, the DMPT accelerator (12  $\mu\text{L}$  per 1 mL oil phase) is added to the w/o emulsion template under continuous stirring for 4 to 7 min. Then the emulsion is poured into a cylindrical polypropylene mould made from the barrel of 5mL syringe and polymerised at room temperature overnight. After that, samples are inserted in a Soxhlet extractor loaded with absolute ethanol and purified overnight. Then, the sample is dried in air inside a fumed cupboard at room temperature overnight.

Alternatively, macroporous polymer are produced by mixing two emulsions - one containing BPO and the other DMPT only. The main advantage of this approach is that the emulsion templates are prepared in advance and used at a later time for making macroporous polymer materials when needed.

### 2.2.3 Preparation of macroporous polymer via thermo-initiated polymerisation at 70°C

The preparation of macroporous polymer by thermo-initiated polymerisation was found to be more challenging than that achieved by redox-initiated polymerisation. The inhibitors had to be removed from the monomers, oxygen expelled from the system and electrolyte added to the water phase. The water phase was prepared from deionised water

degassed under vacuum for 10 minutes. Then 1.78 g  $\text{CaCl}_2$  were dissolved in degassed deionised water to prepare 100 mL solution with concentration 0.12 M  $\text{CaCl}_2$ . For the preparation of the oil phase, the monomer (MMA) and the crosslinker (EGDMA) were passed three times through basic alumina to remove the inhibitors. The AIBN thermo-initiator was used as received. Firstly, a stock solution of 4wt/vol. % AIBN in MMA was prepared. Then, certain volumes of the stock solution, neat MMA and EGDMA were mixed together to obtain a solution containing 15vol.% EGDMA and 1.6 wt/vol.% AIBN (1 mol% with respect to the double bonds). Then the PEL-121 surfactant was added to the solution at a concentration of 5 wt/vol.%. The oil phase was purged with  $\text{N}_2$  for 10 minutes, then placed in a three-neck flask and stirred with an overhead stirrer at 200 rpm while  $\text{N}_2$  gas was purging through the flask. The water phase was added dropwise using a syringe pump set at a flow rate of 4 mL/min. After all of the water phase was added, the stirring speed was increased to 700 rpm and the nitrogen flow stopped. The emulsion was stirred for the time spent for adding the water phase (for example, if the water phase took 10 min to be added, the emulsion was stirred for another 10 min). The total volume of the emulsion produced was 50 mL. Then, the emulsion was poured into a mould (5 mL polypropylene syringe barrel or 15 mL centrifuge tube) and polymerised in a preheated oven at 70°C overnight. After completing the polymerisation, samples were inserted in a Soxhlet extractor loaded with ethanol and purified overnight. Finally, the samples were dried in air inside a fumed cupboard at room temperature overnight.

The samples were coded in order to distinguish between them see Table 2.3.

**Table 2.3.** The code sample and description for each systems.

Code sample	Description
<b>M65</b>	M = methyl methacrylate. 65 = the percentage of water phase.
<b>M65SE1</b>	M = methyl methacrylate. 65 = the percentage of water phase. SE= the surfactant concentration constant in the total volume of the emulsion. 1 = the number of sample was done.
<b>M80S3</b>	M = methyl methacrylate. 80 = the percentage of water phase. S = surfactant concentration is varied. 3 = the concentration of surfactant in the oil phase.
<b>M80C10</b>	M = methyl methacrylate. 80 = the percentage of water phase. C = the crosslinker concentration is varied. 10 = the concentration of crosslinker in the oil phase.
<b>MAIBN65</b>	M = methyl methacrylate. AIBN = the initiator used at high temperature. 65 = the percentage of water phase.

#### **2.2.4 Purification of macroporous polymer by Soxhlet extraction**

The sample is roped with filter paper and inserted in the Soxhlet extractor. 150 mL absolute ethanol are loaded in the extractor and heated in an oil bath set at 130°C. The condenser is cooled down by circulating water using a Grant thermostat set at 18°C. The sample is left in the Soxhlet extractor for 24 h. Then, it is taken out of the extractor and dried in air inside a fumed cupboard at room temperature overnight.

#### **2.2.5 Investigation of the curing dynamics of polymerising samples**

The curing process of polymerising samples (monomers or emulsion templates) was studied by a home-built experimental setup shown in Fig. 2.3. A cylindrical sample tube (inner diameter 16.2 mm) loaded with the liquid sample (5 mL) sits on a precision balance (Sartorius Entris 64-1S) connected to a computer. A cylindrical PTFE probe with a diameter of 3.175 mm is partially immersed in the sample. The probe is firmly attached to a platform which can be moved up or down with a constant speed by the step motor of a syringe pump (NE1000, New Era) controlled by the computer. The step motor is used to oscillate the probe at a constant amplitude of 0.6 mm and period of 6 s (Fig. 2.4a). This generates oscillations in the weight measured by the balance which are recorded by the computer (Fig. 2.4b). A K-type thermocouple mounted inside the probe (with its tip protruding 5 mm out from the probe) is used to monitor the temperature inside the sample using a digital thermometer (HH306A, Omega) also connected to the computer. Another thermocouple (not shown in Fig. 2.3) is used to measure the temperature in the air outside the sample. A water jacket connected to a Grant thermostat is used to control the temperature of the air surrounding the sample.

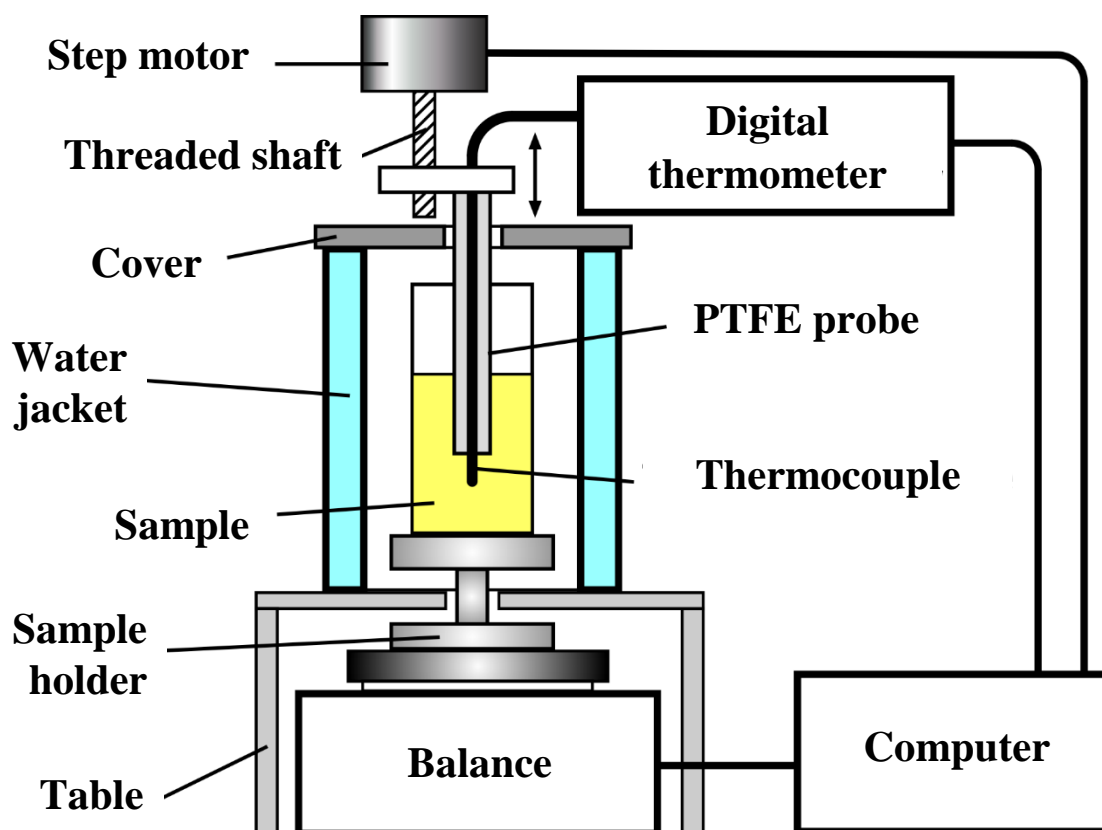


**Figure 2.3.** Experimental setup for studying the curing dynamics of polymerising samples.

In a typical experiment, the sample is placed on the sample holder over the balance pan. Then, the probe is immersed 10 mm inside the liquid sample and forced to oscillate by the step motor. Several factors contribute to the amplitude of the weight oscillations,  $A_w$ , detected by the balance. The first is the buoyancy which is proportional to the liquid density and the volume displaced by the probe. For the low density liquids used ( $\sim 1 \text{ g/cm}^3$ ) and the small amplitude of the probe oscillations (0.6 mm), the buoyancy contribution to  $A_w$  is very small ( $A_b \sim 0.005 \text{ g}$ ). The main contribution to the amplitude of weight oscillations ( $A_c$ ) corrected for buoyancy,  $A_c = A_w - A_b$ , is from the viscosity of the sample. Since the moving probe crosses the liquid interface, the proper quantitative analysis of the viscous contribution is difficult.<sup>2</sup> Both, the viscous drag on the probe moving inside the sample and the weight of the liquid film deposited on the probe during its withdrawal increase with the viscosity and contribute to  $A_c$ .<sup>1</sup> The surface tension would also contribute to the measured weight oscillations: (i) directly by the interfacial force due to the curved liquid surface around the probe and (ii) indirectly through the weight of the liquid film deposited on the probe.<sup>1</sup> In order to relate the amplitude of weight oscillations,

$A_c$ , to the liquid viscosity, measurements with a series of silicone oils with increasing viscosity (Table 2.4) have been made. The  $A_c$  measured for those silicone oils is plotted against their dynamic viscosity in a double logarithmic scale in Fig. 2.5. The data fit very well a power function ( $R^2 = 0.9991$ ).

**Table 2.4.** Properties of silicone oils at 25 °C used for linking the amplitude of weight oscillations,  $A_c$ , to the liquid viscosity.

Sample	Dynamic viscosity / Pa s	Density / g cm <sup>-3</sup>	Surface tension / mN m
AK 50 <sup>a</sup>	0.048 ± 0.001	0.96	20.8
AK 200 <sup>a</sup>	0.194 ± 0.002	0.97	21.1
AK 10000 <sup>a</sup>	9.7 ± 0.1	0.97	21.3
DC 30000 <sup>b</sup>	29.1 ± 0.3	0.97	21.3
DC 100000 <sup>b</sup>	97 ± 1	0.97	21.3
FT 300000 <sup>c</sup>	315 ± 2 <sup>d</sup>	0.97	21.3
FT 1000000 <sup>c</sup>	1048 ± 5 <sup>d</sup>	0.97	21.3

<sup>a</sup> from Wacker Chemie; <sup>b</sup> from Dow Corning, <sup>c</sup> from Lucas oil products Inc; <sup>d</sup> measured in this study using Bohlin CVO 120 rheometer with cone/plate geometry.

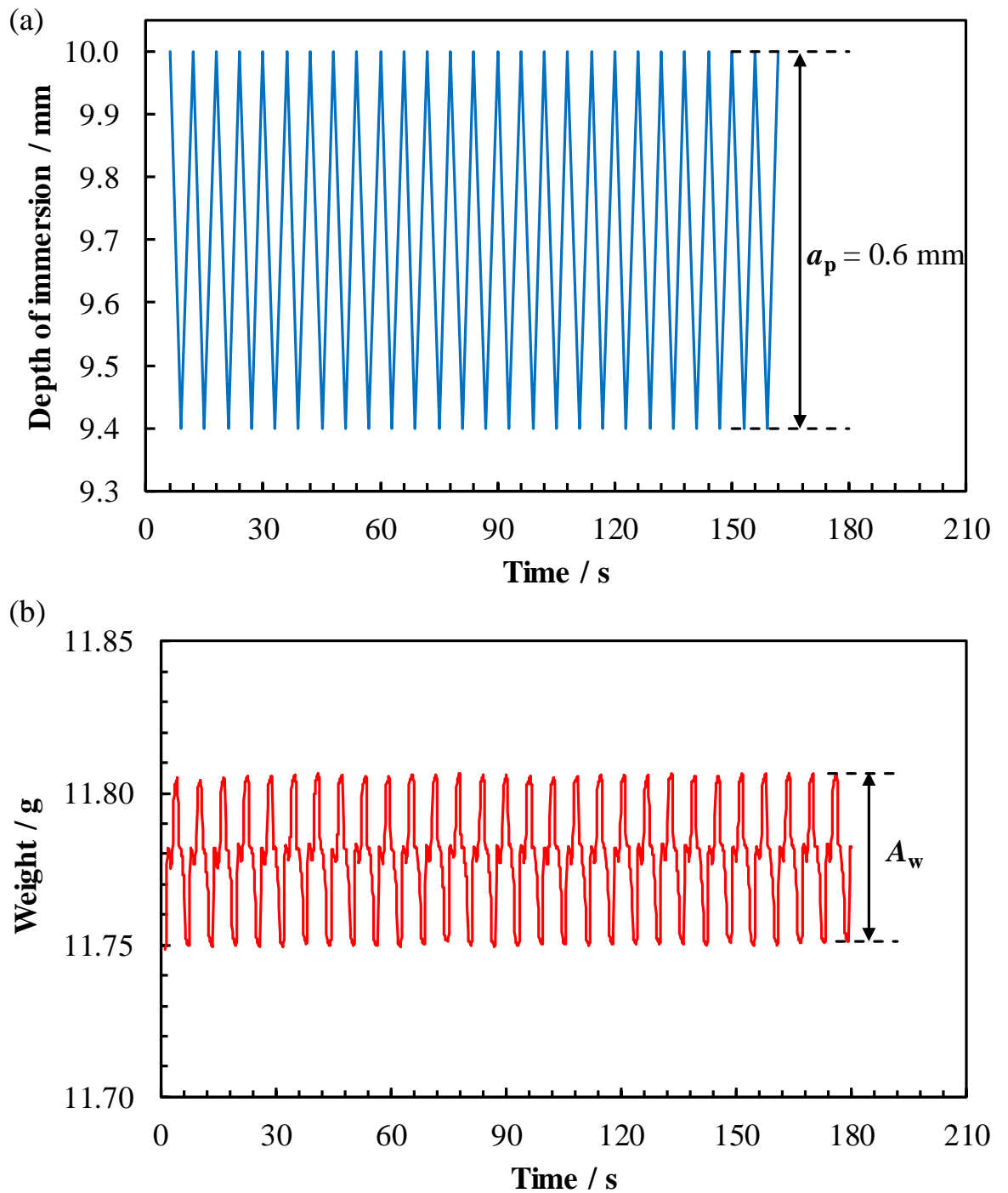


**Figure 2.4.** (a) Depth of immersion of the PTFE probe in the sample versus time in curing experiments. The probe oscillates with amplitude  $a_p = 0.6 \text{ mm}$  and a period of 6 s. (b) The sample weight oscillations with amplitude  $A_w$  registered by the balance due to the oscillations of the PTFE probe immersed in a silicone oil sample (see also Fig. 2.3).

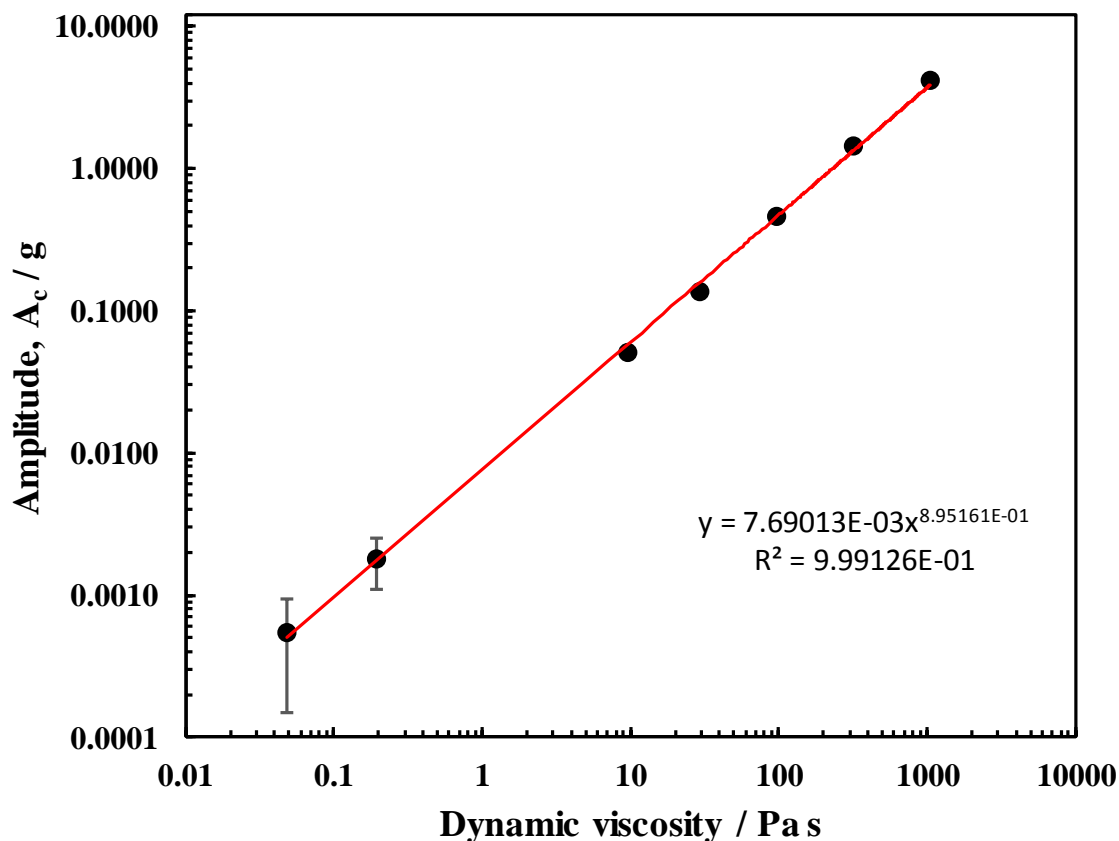


**Figure 2.5.** Amplitude of weight oscillations corrected for buoyancy,  $A_c$ , for silicone oil samples measured by the setup shown in Fig. 2.2 at 25 °C plotted against the dynamic viscosity of the oil (Table 2.3). The PTFE probe, immersed 10 mm in the liquid, oscillated with amplitude  $a_p = 0.6$  mm and a period of 6 s during the measurements. The solid line is the best power function fit.

The data show in Fig. 2.5 suggest that there is a direct correlation between the amplitude of weight oscillations  $A_c$  and the viscosity,  $\eta_a$ , of liquids with approximately the same surface tension. Therefore, the unknown viscosity of a liquid sample,  $\eta_a$ , could be determined from the value of  $A_c$  measured at the conditions in Fig. 2.5 by the equation

$$\eta_a = a(A_c)^b \quad (2.1)$$

where the constants  $b = 1.11614$  and  $a = 229.396 \text{ Pa s g}^{-1.11614}$  have been determined from the data in Fig. 2.5. The validity of eq. (2.1) has been tested by measuring liquids with known viscosities shown in Table 2.5. The viscosities of two silicone oil samples agree very well with the expected viscosities. Positive deviations are observed for liquids with larger surface tensions, however, the measured viscosity is overestimated by less than 13 % for liquid samples with surface tension in the range 21-33  $\text{mN m}^{-1}$ . The surface tensions of MMA, EGDMA and their mixtures fall in that range (Table 2.6), therefore one could

expect that the oscillating probe experiments can be used for measuring the viscosity (overestimated by less than 15 %) during the polymerisation of such systems. Typical results from such experiments are shown in Fig. 2.6.

**Table 2.5.** Properties of liquids used for testing eq. (2.1):  $\rho$  - density,  $\gamma$  - surface tension and  $\eta_e$  - expected viscosity (from the supplier);  $\eta_a$  - viscosity calculated from  $A_c$  by eq. (2.1), all at 25 °C.

Test liquid	$\rho / \text{g cm}^{-3}$	$\gamma / \text{mN m}$	Dynamic viscosity / Pa s		$\frac{\eta_a - \eta_e}{\eta_e} / \%$
			$\eta_e$	$\eta_a$	
Silicone oil, OH 1000 <sup>a</sup>	0.96	21.2	0.96	$0.99 \pm 0.08$	$3 \pm 8$
Silicone oil, DC 5000 <sup>b</sup>	0.97	21.3	4.85	$4.84 \pm 0.11$	$-0.2 \pm 2$
Pluronic, PEL-121 <sup>c</sup>	1.006	$33.2^{\text{d}}$	1.20	$1.35 \pm 0.09$	$13 \pm 8$
Glycerol	1.26	63.0	0.934	$1.76 \pm 0.09$	$88 \pm 10$

<sup>a</sup> from Wacker Chemie; <sup>b</sup> from Dow Corning, <sup>c</sup> neat liquid from Sigma; <sup>d</sup> measured in this study using Kruss K10 tensiometer with a platinum Wilhelmy plate.

**Table 2.6.** Surface tensions,  $\gamma$ , of MMA, EGDMA and their mixtures measured at 25 °C by using Kruss K10 tensiometer with a platinum Wilhelmy plate.

Liquid sample	$\gamma / \text{mN/ m}$
MMA	$25.83 \pm 0.02$
EGDMA	$30.20 \pm 0.02$
15 vol.% EGDMA in MMA	$26.54 \pm 0.03$
15 vol.% EGDMA in MMA + 5 wt/vol.% PEL-121 surfactant	$26.86 \pm 0.04$

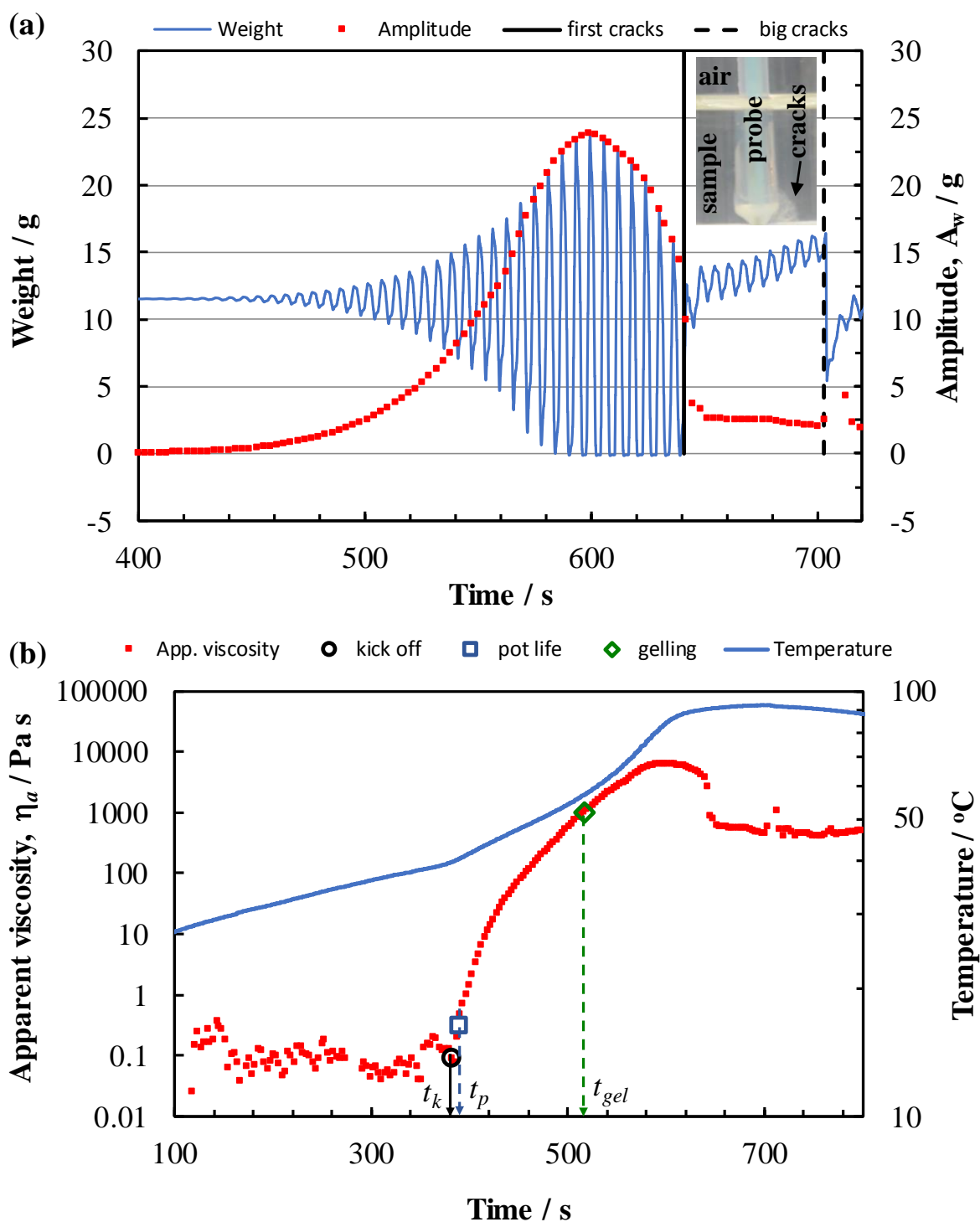


**Figure 2.6.** (a) A typical weight versus time plot recorded during the polymerisation of a liquid monomer sample (15 vol.% EGDMA, 1 wt/vol.% BPO, 120  $\mu$ L DMPT in MMA) using an oscillating probe. The probe immersed at 10 mm in the sample oscillates with a constant amplitude of 0.6 mm and a period of 6 s. The amplitude of weight oscillations,  $A_w$  (red squares) increases with time because the viscosity increases due to polymerisation. The vertical lines mark the appearance of cracks close to the probe tip (see inset). (b) Apparent viscosity and temperature of the sample during polymerisation. The vertical arrows point to the ‘kick off’ time,  $t_k$  (the time of rapid increase of viscosity), pot life,  $t_p$  (the time for doubling the initial viscosity) and the time at  $\eta_a = 1000$  Pa s adopted by us as the gelling time,  $t_{gel}$ . The time is measured from the moment of adding the DMPT to the sample to initiate the polymerisation.

A typical weight and amplitude of weight oscillations versus time plot recorded during the polymerisation of a liquid monomer sample (15 vol.% EGDMA, 1 wt/vol.% BPO, 120  $\mu$ L DMPT in MMA) using an oscillating probe is shown in Fig. 2.6a. The polymerisation of the oil phase started immediately after adding the accelerator (DMPT). The difference in weight increased with time as the amplitude increased as well see Fig.2.6a. At 640s the first crack observed and then the big crack occurred at 700s which indicated that the sample was almost solid as the liquid cannot crack (see the inset in Fig 2.6a). The polymerisation of the oil phase is exothermic reaction so the temperature increases as the viscosity increased and the polymerisation accelerated further (see Fig2.6b). Initially, the viscosity fluctuated with time until reached the kick off ( $t_K$ ) point where the viscosity increased rapidly. The pot life ( $t_p$ ) is defined as the time needed for doubling the initial viscosity (blue square). The gelling point defined by us when the time at  $\eta_a = 1000$  Pa s is the gelling time.

### **2.2.6 Mechanical properties and porosity determination**

The compressional mechanical testing is done according to the standard ASTM D1621 using cylindrical samples at a speed of compression of 1.2 mm/min. The instrument used is Mark-10 with a Series 5 load cell (2500 N). All measurements were performed at room temperature. Ten samples were measured for every single system. Typical graphs of stress versus strain for macroporous polymer produced at room temperature (redox initiation) and high temperature (thermo-initiation) are shown in Figs 2.8 and 2.9, respectively. The data obtained were analysed in Excel using a program (a macro) developed by us.

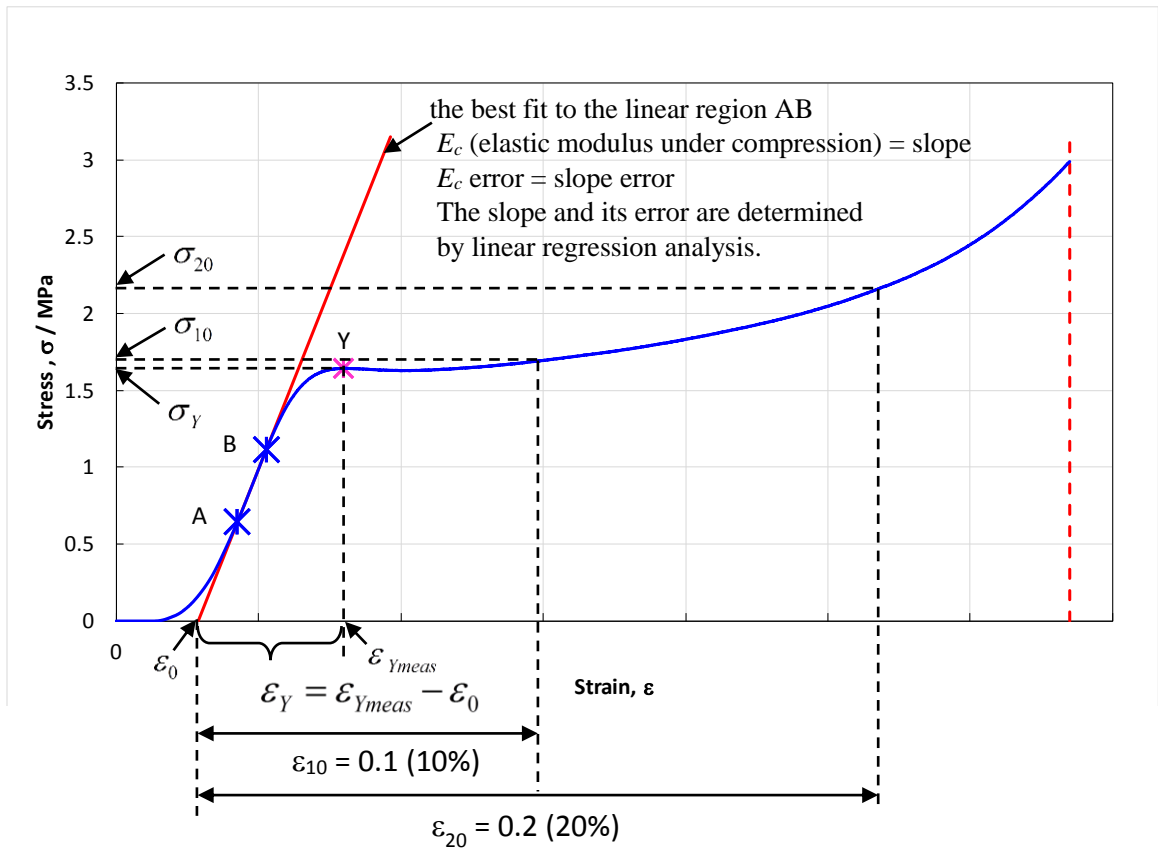


**Figure 2.7.** A typical stress versus strain curve for a rigid cellular plastics (foam).

The program finds the linear range AB (see Fig. 2.7). Then it fits a straight line and determines the slope ( $E_c$ ) and the x-intercept =  $\epsilon_0$ .  $\epsilon_0$  is used to correct the measured strains,  $\epsilon_{meas}$ , i.e. the corrected strain is equal to  $\epsilon_{meas} - \epsilon_0$ . If there is a real maximum on the stress-strain curve, the macro finds it. It corresponds to the Yield point at a maximum (point Y shown in purple on Fig. 2.7). The stress at that point is reported as “Yield Stress(max)”,  $\sigma_Y$ . The strain at point Y is corrected by  $\epsilon_0$  and reported as “Yield strain(max)”,  $\epsilon_Y$ , i.e.  $\epsilon_Y = \epsilon_{Ymeas} - \epsilon_0$ . The macro adds 0.1 or 0.2 to  $\epsilon_0$  and reports the “Stress(10% strain)”,  $\sigma_{10}$ , and “Stress(20% strain)”,  $\sigma_{20}$ . According to the ASTM Standard D 1621 – 00 “Standard Test Method for Compressive Properties of Rigid Cellular Plastics”, the compressive strength,  $\sigma_M$ , is equal to the stress at 10 % strain,  $\sigma_{10}$ , or to the Yield stress at the maximum,  $\sigma_Y$ , if the Yield strain at the maximum,  $\epsilon_Y$ , is smaller than 10 %. Therefore, the macro reports “Strength (10% strain)”,

$$\sigma_M = \left\{ \begin{array}{l} \sigma_{10}, \text{ if } \epsilon_Y > 0.1(10\%) \\ \sigma_Y, \text{ if } \epsilon_Y < 0.1(10\%) \end{array} \right\}.$$

The cross-sectional area, sample volume, density, porosity and their errors are calculated by eqns (2.2) -(2.10) shown below.

**Cross-sectional area,  $A$ , and its error,  $\Delta A$ :**

$$A = \frac{\pi D^2}{4} \quad (\text{circle with diameter } D) \quad (2.2)$$

$$\Delta A = A \sqrt{2(\Delta D/D)^2} \quad (2.3)$$

**Total volume,  $V$ , and its error,  $\Delta V$ :**

$$V = Ah \quad (2.4)$$

$$\Delta V = V \sqrt{(\Delta A/A)^2 + (\Delta h/h)^2} \quad (2.5)$$

where  $h$  is the height of the sample with cross-sectional area  $A$ ,  $\Delta h$  is the height error.

**Overall density,  $\rho$ , and its error,  $\Delta\rho$ :**

$$\rho = W/V \quad (2.6)$$

$$\Delta\rho = \rho \sqrt{(\Delta W/W)^2 + (\Delta V/V)^2} \quad (2.7)$$

where  $W$  and  $\Delta W$  are the weight of the porous sample and its error, respectively.

**Porosity,  $P$ , and its error,  $\Delta P$ :**

$$P(\%) = \frac{V_{pores}}{V} = \left(1 - \frac{\rho}{\rho_{env}}\right) \times 100 \quad (2.8)$$

$$\Delta P = P \sqrt{(\Delta\rho/\rho)^2 + (\Delta\rho_{env}/\rho_{env})^2} \quad (2.10)$$

where  $V_{pores}$  is the volume of pores,  $V$  is the total volume,  $\rho$  and  $\rho_{env}$  are the overall density of the porous material and the density of the solid envelope around the pores, respectively.

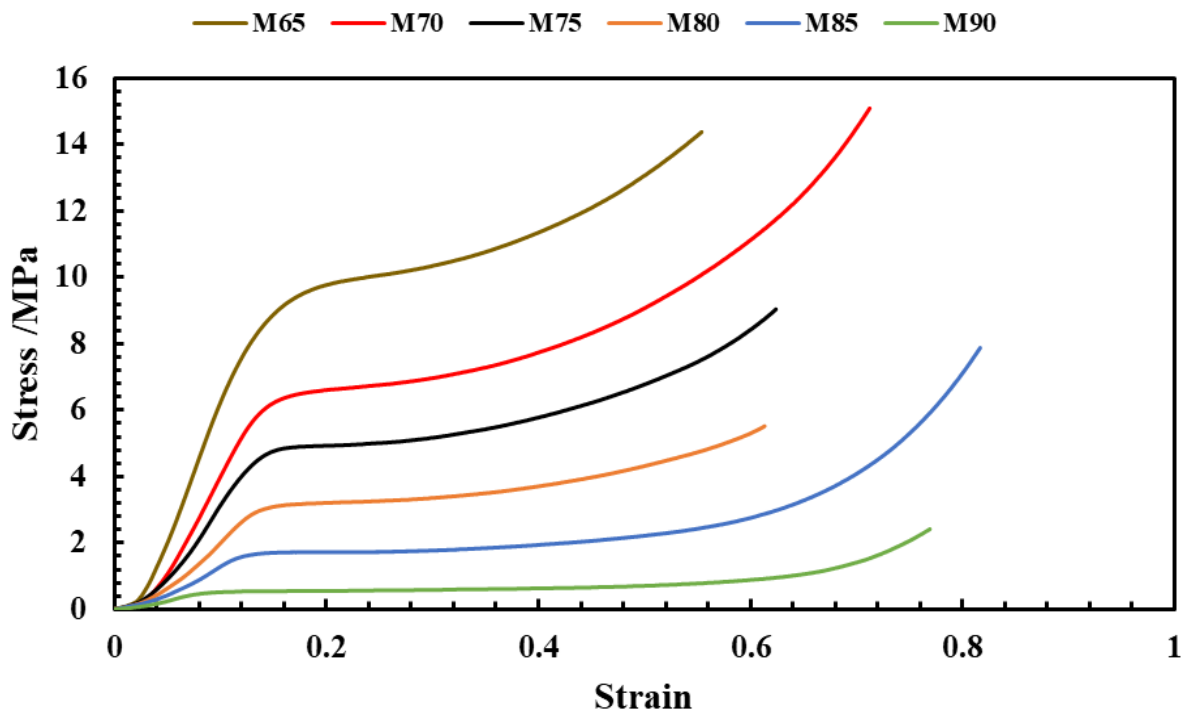


**Figure 2.8.** Typical stress versus strain graphs for macroporous polymer produced at room temperature. The percentage of the water phase in the emulsion template is varied from 65 vol.% (M65) to 90vol. % (M90).

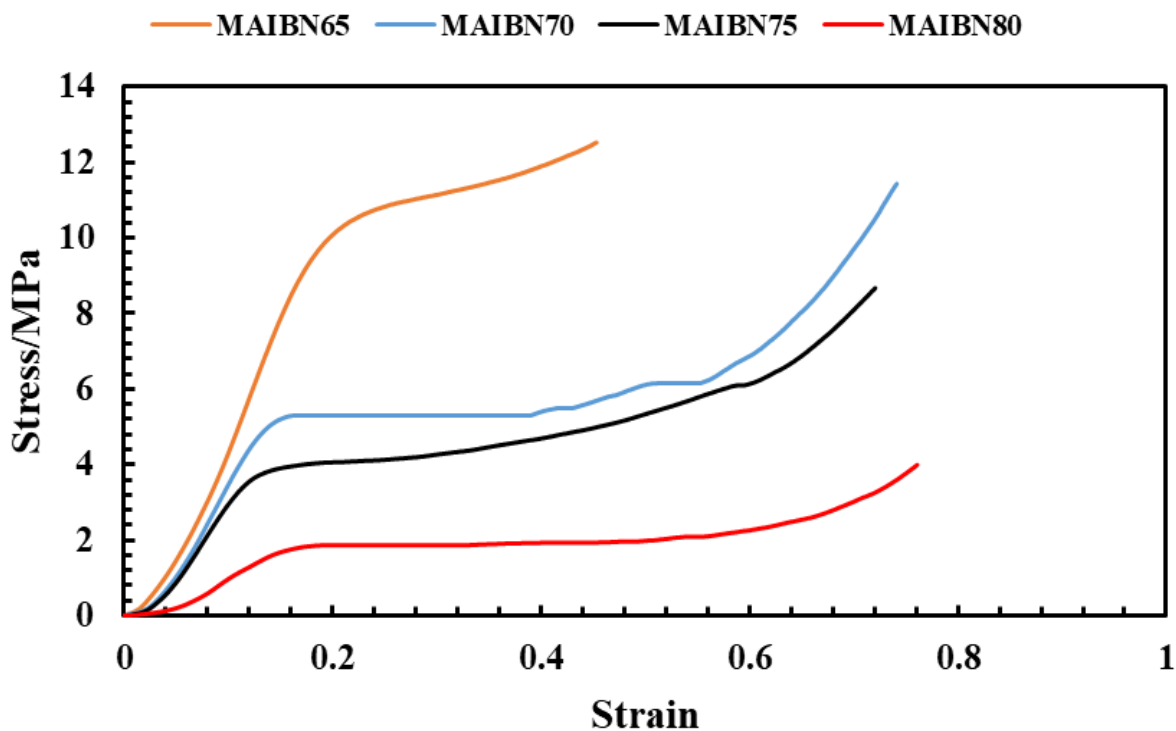


**Figure 2.9.** Typical stress versus strain curves for macroporous polymer produced at high temperature (70°C). The percentage of the water phase in the emulsion template is varied from 65 vol.% (MAIBN65) to 80vol. % (MAIBN80).

### 2.2.7 Voids and pore throat determination

SEM images of the fractured surface of macroporous polymer were taken to study the internal structure and used to measure the voids and pore throat size using the program Image j. The data obtained were analysed in Excel using a program (a macro) developed by us. The number of measurement for each sample,  $N_{tot}$ , was at least 400 for voids and pore throats. The data then plotted as cumulative voids and pore throat to extract D-Values (D10, D50 and D90) which are the intercepts for 10%, 50% and 90% of cumulative diameter. These D-values divided the diameter of voids and the pore throat into three values as D10 where 10% of diameter's values have less than this value .D50 where 50% of the values of diameter in the sample smaller than this value. D90 where 90% of the diameter values smaller than this value (See Fig.2.10.)

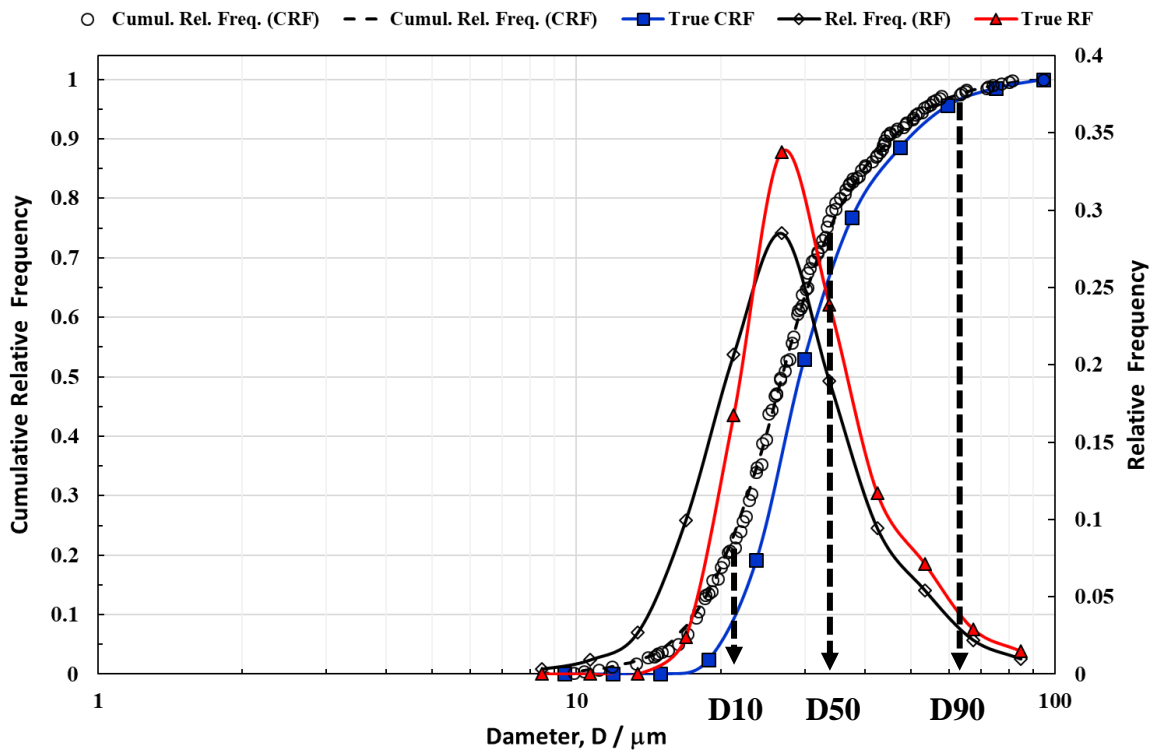


**Figure 2.10.** Typical graph for the cumulative relative frequency and the relative frequency versus the diameter ( $\mu\text{m}$ ). The sample is M903.

Frequency (F) is how many times this diameter repeated.

$$\text{Relative frequency (RF)} = \frac{F}{400} \quad (2.11)$$

where (F) is the frequency and 400 is the total number of measurements.

Cumulative frequency (CF) is obtained by adding the frequency as you go along.

$$\text{Cumulative relative frequency (CRF)} = \frac{\text{Cumulative frequency (CF)}}{400} \quad (2.12)$$

In Fig.2.10. There are True CRF and True RF present the corrected values of diameters of voids. During the sample fracture voids do not necessarily break at the equatorial level. It can be break in the middle or the top or the bottom of voids. The measured value and the equatorial diameter of voids can be correlated. This problems could be solved using the stereological analysis to determine the correct diameter for the voids.<sup>3 4</sup> The diameters of voids fall into different class with range sizes, it called the width bin which is 0.1 as  $\frac{D_{measured}}{D_{Max\ measured}} = 0.1$ . These class size each is given factor smaller than the previous and this factor is the same (e.g,  $10^{-0.1}$ ).  $D^*$  is the end of the class size.

$$\log_{10} D_1^* - \log_{10} D_2^* = 0.1 \quad (2.13)$$

Then, from these class the probability could be calculated using equation (2.14)

$$\alpha_i = \frac{1}{P_1} \left( \alpha_1 P_i - \sum_{j=1}^{i-2} \alpha_j + 1 P_{i-j} \right) \quad (2.14)$$

$\alpha_i$  is the actual probabilities of 2D observation,  $P_1$  is the probability (fraction) of all 2D cross-sections produced from the largest size in the class.

The diameter could be calculated using equation (2.15)

$$P(r_1 < r < r_2) = \frac{1}{R} \left( \sqrt{R^2 - r_1^2} - \sqrt{R^2 - r_2^2} \right) \quad (2.15)$$

Where P is the cross-section size probability,  $r_1$  and  $r_2$  are lower and upper limits of the class, respectively, R is the sphere radius

## 2.3 Methods used in the preparation of Janus particles

### 2.3.1 Cleaning of silica particles

The silica particles were cleaned as following, 10 g of silica particles dispersed in 30mL of ethanol and sonicate in ultrasonic bath (Grant Ultrasonic bath MXB6) for 10 minutes. Then, centrifuge it (Sorvall Biofuge Primo centrifuge) at 400 rpm for 15 min. After that, the ethanol replaced with fresh ethanol and repeated this step three times. Then, the particles washed with deionised water three times the same way as the ethanol step. The particles left to dry in the vacuum oven (Gallenhamp) at room temperature for overnight.

### 2.3.2 Amination of silica particles

The surface of the silica particles was treated with 3-aminopropyltriethoxysilane (APTES) to graft amino groups on the silica particles surface. 0.1g of silica particles were dispersed

in 10mL APTES solution (10vol.%). The solution was stirred with a magnetic stirrer for 2 hours. Then it was centrifuged at 4000 rpm for 20 minutes. The liquid was removed and replaced with deionised water. It was then centrifuged at 4000 rpm for 20 minutes. This was repeated 5-6 times to ensure complete remove of unreacted APTES.

### **2.3.3 Zeta potential measurements for silica particles**

The following procedure was replicated across all the different silica samples prepared (silica untreated, aminated silica and Janus particles). The zeta potential of silica particles was measured using a Zeta-sizer Nano ZS with a measurement range of 3.8nm – 100 microns. A stock suspension of particles was prepared by dispersing 1g of the silica particles in a 10 mL solution of NaCl ( $1 \times 10^{-3}$  M) prepared by mixing 0.01461g of NaCl powder in 250 mL de-ionized water. Samples were prepared by adding 10 mL of NaCl in a glass vile and adding 5-8 drops of the silica stock solution. The different samples were prepared to have pH values varying between 1 and 10. The pH is adjusted by adding HCl (1M, 0.25M and 0.1M), or NaOH (1M, 0.25M and 0.1M) to the sample.

### **2.3.4 Preparation of emulsions and investigation of their type and stability**

Different concentration of TTAB solution were made (0.01, 0.05, 0.1, 0.5, 1, 2, 3, 10 mM) to be used to adjust the hydrophobicity of silica particles. The water phase (70vol.%) was made of 4wt/vol.% silica particles dispersed in TTAB solution. The oil phase was made of 15vol.% EGDMA, 1wt/vol.% BPO all dissolved in IBMA. After that, 3 mL of the oil phase added to 7 mL of the suspension of silica particles and emulsifying using Ultra-Turrax homogeniser (T25, IKA) with an 18 mm head for 1:30 min at 11000 rpm. Then, the emulsion stability investigated up to 12 h. The emulsion type was determined by using the drop test.

### **2.3.5 Polymerisation of Pickering emulsions**

The polymerisation of emulsion was performed with two different homogeniser (Ultra-Turrax homogeniser and over-head stirrer)

The first method by using Ultra-Turrax. Different concentration of TTAB solution were made (0.01, 0.05, 0.1, 0.5, 1, 2, 3, 10 mM) to adjust the hydrophobicity of silica particles. The water phase (70vol.%) was consisted of 4wt/vol.% silica particles dispersed in TTAB solution. The oil phase made of 1wt/vol.% BPO, 15vol.% EGDMA, 1.19 vol.% DMPT all dissolved in IBMA. After that, quickly the oil phase added to the water phase and emulsifying using Ultra-Turrax homogeniser (T25, IKA) with an 18 mm head for 1:30 min at 11000 rpm. Then, the emulsion stirred using a magnetic stirrer bar for 2 h. After

that, the filtration step to obtain the polymer beads with filter paper (porous 5-8 $\mu$ m). Then, the polymer beads dried in the vacuum oven at room temperature for overnight.

The second method by using over-head stirrer. The water phase (70vol.%) was made of 4wt/vol.% silica particles dispersed in the TTAB solution. Then, the suspension of silica particles transferred to 500 mL three necks flask fitted with overhead stirrer and stirred at 700 rpm while the N<sub>2</sub> is running. The oil phase 9mL (1wt/vol.% BPO, 15vol.% EGDMA all dissolved in MMA) was added dropwise 4mL/min using the syringe pump. Once the oil phase added, the emulsion stirred for 10 min to ensure the formation of emulsion. Then, the accelerator DMPT (216 $\mu$ L) was added. The speed of stirring decreased from 700 rpm to 400 rpm. The stirring was continuing for 1 h. After that, the polymer beads collected by using filtration with filter paper (porous 5-8 $\mu$ m). Followed by drying in the vacuum oven at room temperature overnight.

### **2.3.6 Microscope images**

Samples taken from the emulsions were placed on a glass microscope slide with a dimple, covered with a cover slip and observed under a microscope (Microtec RM-1). The images were captured with a camera (QICAM Fast 1394, QImaging) using Image-Pro Plus software (MediaCybernetics) and stored on a computer.

### **2.4 Scanning electron microscope (SEM) images**

The sample was coated with 1 nm layer of gold by using a sputter coater. The SEM images were taken by a Scanning Electron Microscope (EVO 60, Carl Zeiss Ltd.). Some of the SEM images in chapter 5 were obtained by bench-top scanning electron microscope TM-100 (HITACHI).

### **2.5 References**

1. A. Pitto-Barry and N. P. E. Barry, *Polym. Chem.*, 2014, **5**, 3291-3297.
2. J. A. Tallmadge and C. Gutfinger, *Ind. Eng. Chem*, 1967, **59**, 18-34.
3. D. L. Sahagian and A. A. Proussevitch, *J. Volcanol. Geotherm. Res.*, 1998, **84**, 173-196.
4. H. E. Rose, *Sedimentology*, 1968, **10**, 293-309.

## CHAPTER 3

### Preparation of macroporous polymers from emulsion templates using redox-initiated polymerisation at room temperature

#### 3.1 Introduction

Macroporous materials have distinctive properties such as low densities, high porosities and lightweight. Due to their fascinating properties, macroporous polymers have been exploited and used in many areas such as catalyst supports,<sup>1, 2</sup> scaffolds for tissue engineering,<sup>3</sup> ion exchange<sup>4</sup> and separation media.<sup>5</sup> Various methods have been established for their preparation such as chemical or physical blowing or foaming,<sup>6, 7</sup> thermally induced phased separation<sup>8</sup> and emulsion templating. The most simple and versatile method to produce macroporous polymers is by emulsion templating as the internal emulsion phase can be easily removed and take the shape of its casting mould. Moreover, the flexibility of tuning the emulsion template is a remarkable advantage for controlling the properties of the materials produced. The macroporous polymeric materials made by this method can be casted to thin membranes,<sup>9</sup> porous monoliths<sup>10, 11</sup> or micrometre-sized beads<sup>12</sup> with open or closed cell structure. Due to its simplicity, the preparation of macroporous materials via emulsion templating attracted significant scientific interest in the last decade. Water-in-oil emulsion templates are commonly used for that purpose. The oil phase is made of a monomer, crosslinker, initiator and surfactant or particles while the water phase contains an electrolyte to enhance the emulsion stability. The polymerisation process of the external oil phase can affect the mechanical properties and morphology of the materials produced.<sup>13, 14</sup> To start the polymerisation of the oil phase, the initiator is decomposed by supplying heat or UV light to the system.<sup>15, 16</sup> A drawback of the thermal initiation is that the emulsion becomes unstable as the temperature rises, which limits the control over the emulsion template.<sup>17, 18</sup> The polymerisation at room temperature using UV light could help to maintain the emulsion stability, however, the sample has to be thin to allow the light penetration through it. Both approaches have been used for the preparation of porous polymers, but that required the oil phase to be purified to remove the inhibitors, inert atmosphere to be used for expelling the oxygen from the system and adding large amounts of electrolyte to the water phase to enhance the emulsion stability.<sup>17</sup> Those complications could be avoided if the polymerisation can be conducted quickly at room temperature. In this chapter we investigate if redox-initiated polymerisation could be used for that purpose.

The polymerisation of methyl methacrylate by redox-initiation using benzoyl peroxide-amine couples has been known since the 1950s and used in many applications such as bone cement,<sup>19</sup> dentistry<sup>20</sup> and other restorative processes. The polymerisation takes place at room temperature without the need for any external source of energy<sup>21</sup> which could be advantageous for the polymerisation of emulsion templates. Very recently, redox-initiation has been used for a rapid polymerisation of w/o HIPE templates prepared under nitrogen atmosphere from an aqueous solution of CaCl<sub>2</sub> as a water phase and purified dimethacrylates as an oil phase.<sup>22</sup>

In contrast to previous studies,<sup>22</sup> we focus our investigation on methyl methacrylate because it is inexpensive widely used monomer. In addition, poly(methyl methacrylate) (PMMA) has a moral mechanical properties and many practical applications such as bone cement, dentistry . In our study, we also use EGDMA as a crosslinker, benzoyl peroxide as an initiator, DMPT as an accelerator and Pluronic PEL-121 surfactant which is soluble in the oil phase and can stabilise w/o emulsions due to its low Hydrophilic-lipophilic balance (HLB) value.<sup>23</sup> Deionised water is used as a water phase of the w/o emulsions in our investigation. The percentage of the water phase in the emulsion template is varied from 65-90 vol%. The effect of surfactant and crosslinker concentrations on the mechanical properties and the morphology of the produced materials is also investigated.

### **3.2 Preparation of macroporous polymeric materials from water-in-oil emulsion templates with variable volume fraction of water**

The percentage of the water phase in the emulsion template was varied from 65 to 90 vol.% in two series of experiments. In the first series, the surfactant concentration in the oil phase was kept constant. Whereas, in the second study, the surfactant concentration in the oil was adjusted to maintain its concentration constant with respect to the total volume of the emulsion. The crosslinker (EGDMA) and initiator (BPO) were fixed at 15 vol.% and 1 wt/vol.% (as received), respectively, in both series of experiments.

#### **3.2.1 Porous polymers prepared at constant surfactant concentration in the oil phase**

Emulsion templates were prepared as described previously in section 2.2.1. The accelerator (DMPT) was added to the emulsion template and stirred for 4-5 min. The emulsion was transferred to the mould and left to polymerise at room temperature overnight. Deionised water was used as a water phase of the w/o emulsions at a volume fraction in the range 65-90 vol.%. The oil phase contained 1 wt/vol.% BPO (as received, mixed with 50 % dicyclohexyl phthalate for stabilisation), 15 vol.% EGDMA and 5

wt/vol.% PEL-121 surfactant, all dissolved in MMA. The amount of accelerator (DMPT) added to the emulsion to start the polymerisation was 12  $\mu\text{L}$  per 1 mL of oil phase (1.19 vol.% in the oil phase).

Images of the emulsion templates before polymerisation, after polymerisation and those of the materials produced are shown in Figs 3.1 – 3.6. The samples produced from templates with 65-80 vol.% water (see Fig.3.1-3.4) have a smooth surface without any visible defects. Those produced at 85-90 vol.% water (see Fig.3.5-3.6) have some flaws in their surfaces which indicates some partial destabilisation of the emulsions. The polymerisation of HIPEs containing more than 90 vol.% water was unsuccessful and the emulsion templates destabilised during the polymerisation. This could be attributed to the limited amount of surfactant which was unable to maintain the stability of such emulsions with large oil-water interfacial area.

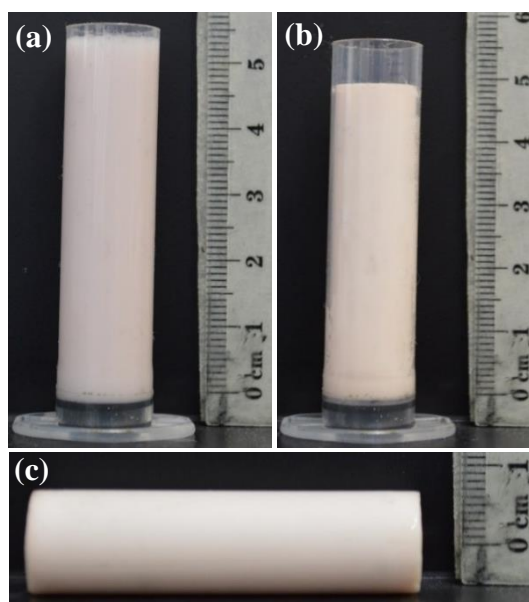


**Figure 3.1.** Images of the mould loaded with w/o emulsion template (a) before polymerisation and (b) after polymerisation at room temperature overnight. (c) An image of the solid material after demoulding. The emulsion template contains 65 vol.% internal phase of deionised water. The external oil phase is made of 15vol.% EGDMA, 5wt/vol.% PEL-121 surfactant, 1wt/vol.% of BPO and 1.19 vol.% DMPT, all dissolved in MMA.

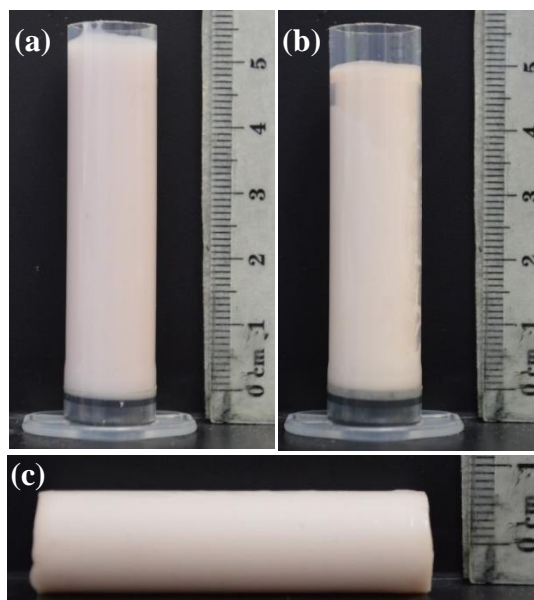


**Figure 3.2.** Images of the mould loaded with w/o emulsion template (a) before polymerisation and (b) after polymerisation at room temperature overnight. (c) An image of the solid material after demoulding. The emulsion template contains 70 vol.% internal phase of deionised water. The external oil phase is made of 15vol.% EGDMA, 5wt/vol.% PEL-121 surfactant, 1wt/vol.% of BPO and 1.19 vol.% DMPT, all dissolved in MMA.

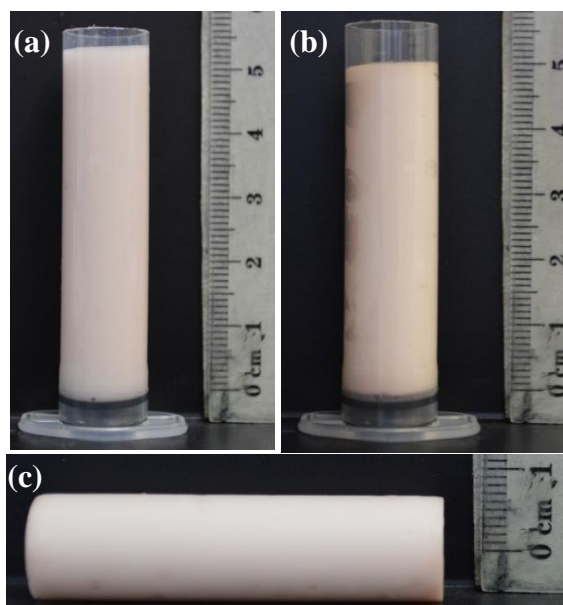


**Figure 3.3.** Images of the mould loaded with w/o emulsion template (a) before polymerisation and (b) after polymerisation at room temperature overnight. (c) An image of the solid material after demoulding. The emulsion template contains 75 vol.% internal phase of deionised water. The external oil phase is made of 15vol.% EGDMA, 5wt/vol.% PEL-121 surfactant, 1wt/vol.% of BPO and 1.19 vol.% DMPT, all dissolved in MMA.

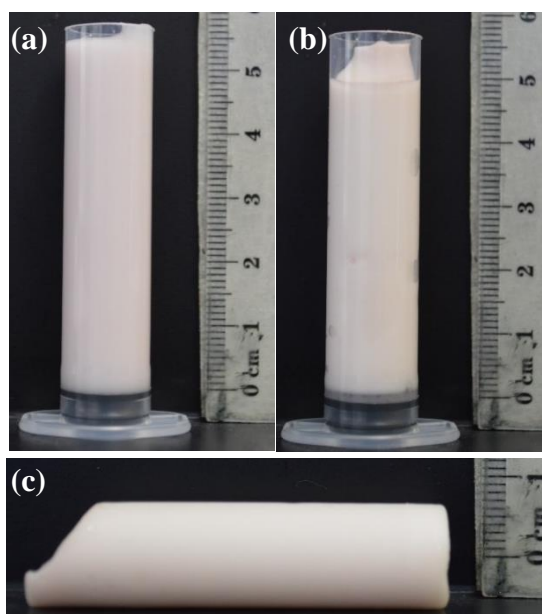


**Figure 3.4.** Images of the mould loaded with w/o emulsion template (a) before polymerisation and (b) after polymerisation at room temperature overnight. (c) An image of the solid material after demoulding. The emulsion template contains 80 vol.% internal phase of deionised water. The external oil phase is made of 15vol.% EGDMA, 5wt/vol.% PEL-121 surfactant, 1wt/vol.% of BPO and 1.19 vol.% DMPT, all dissolved in MMA.

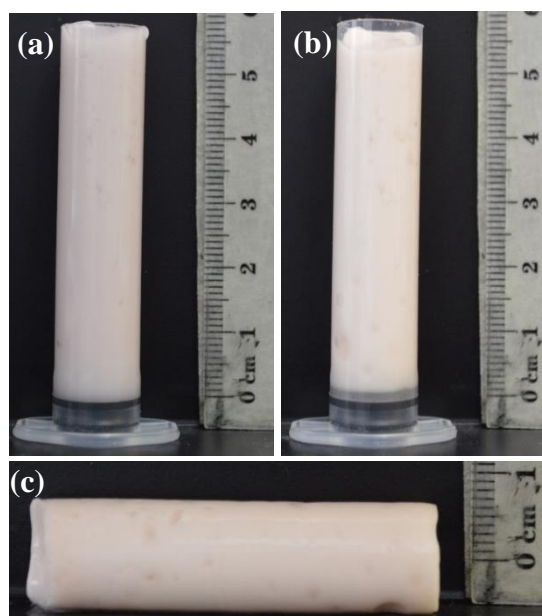


**Figure 3.5.** Images of the mould loaded with w/o emulsion template (a) before polymerisation and (b) after polymerisation at room temperature overnight. (c) An image of the solid material after demoulding. The emulsion template contains 85 vol.% internal phase of deionised water. The external oil phase is made of 15vol.% EGDMA, 5wt/vol.% PEL-121 surfactant, 1wt/vol.% of BPO and 1.19 vol.% DMPT, all dissolved in MMA.

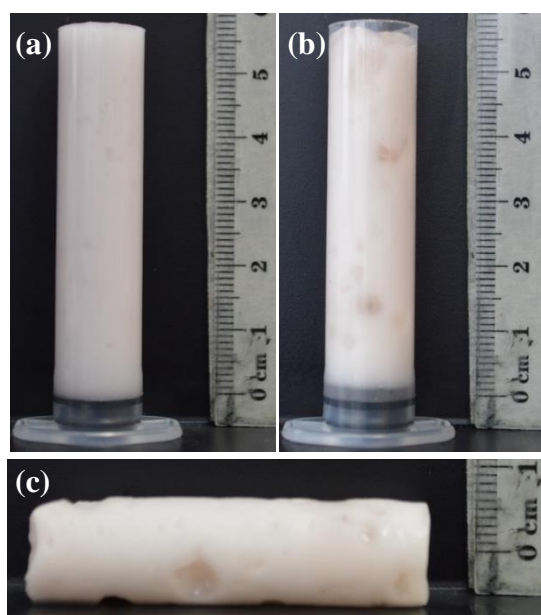


**Figure 3.6.** Images of the mould loaded with w/o emulsion template (a) before polymerisation and (b) after polymerisation at room temperature overnight. (c) An image of the solid material after demoulding. The emulsion template contains 90 vol.% internal phase of deionised water. The external oil phase is made of 15vol.% EGDMA, 5wt/vol.% PEL-121 surfactant, 1wt/vol.% of BPO and 1.19 vol.% DMPT, all dissolved in MMA.

The polymerised samples were purified by Soxhlet extraction with ethanol overnight to remove unreacted monomers, oligomers, uncrosslinked polymers and surfactant, then dried in air inside a fumed cupboard at room temperature for ~12 hours.

The morphology of polymeric materials produced at room temperature by redox-initiated polymerisation was studied by SEM imaging (Fig. 3.7). The materials have an open structure with voids connected via pore throats as can be seen from the SEM images. The void and pore throat sizes are polydisperse and the polymer surface seems very smooth for all samples. Interestingly, the materials at 65 and 70 vol.% water phase have open cell structure although the droplets occupy less than 74 % required for hexagonal close-packing of monodisperse spheres.<sup>18</sup> The explanation for the open structure observed could be that the emulsion droplets in those systems flocculated and touched each other thus allowing the pore throats to open during the polymerisation. It is observed that the number of pore throats per void increases with the increase of the water content in the emulsion template. The voids in the systems with 75 vol.% water or higher are almost spherical because the droplets of the emulsion template were polydisperse and the small droplets have been fit in between the bigger ones without significant deformations. As a result, the number of contacts between the droplets has increased with the increase of droplet volume fraction leading to the formation of more pore throats per void.

The void and pore throat diameters were measured as described in section 2.2.7 and the results are summarised in Tables 3.1 and 3.2 where DN0.1, DN0.5 and DN0.9 are the diameters at which 10%, 50% and 90% from the population of voids (or throats) do not exceed that diameter. For example, in the sample produced from a template with 65vol.% water, 10 % of voids have diameters  $\leq$  DN0.1 =  $6.5 \pm 0.6 \mu\text{m}$ , 50 % of voids have diameters  $\leq$  DN0.5 =  $9.0 \pm 0.5 \mu\text{m}$  and 90 % of voids have diameters  $\leq$  DN0.9 =  $13.8 \pm 1.3 \mu\text{m}$ . The Span =  $(\text{DN0.9} - \text{DN0.1})/\text{DN0.5}$  gives information for the polydispersity of diameters and is also shown in the tables. It is observed that the diameter of voids and pore throats increases as the percentage of the water phase is increased. Although the surfactant concentration in the oil phase is kept constant in these experiments, its concentration with respect to the total emulsion volume,  $C_{SE}$ , decreases with the increase of volume fraction of water (decrease of the oil volume fraction). As a result, the emulsifying power of the surfactant present also decreases thus making an emulsion template with bigger droplets and, consequently, a material with larger voids.<sup>13</sup> The pore throat diameters are 4-9 times smaller than the respective void diameters, but follow similar trends when plotted against  $C_{SE}$  (Fig. 3.8).

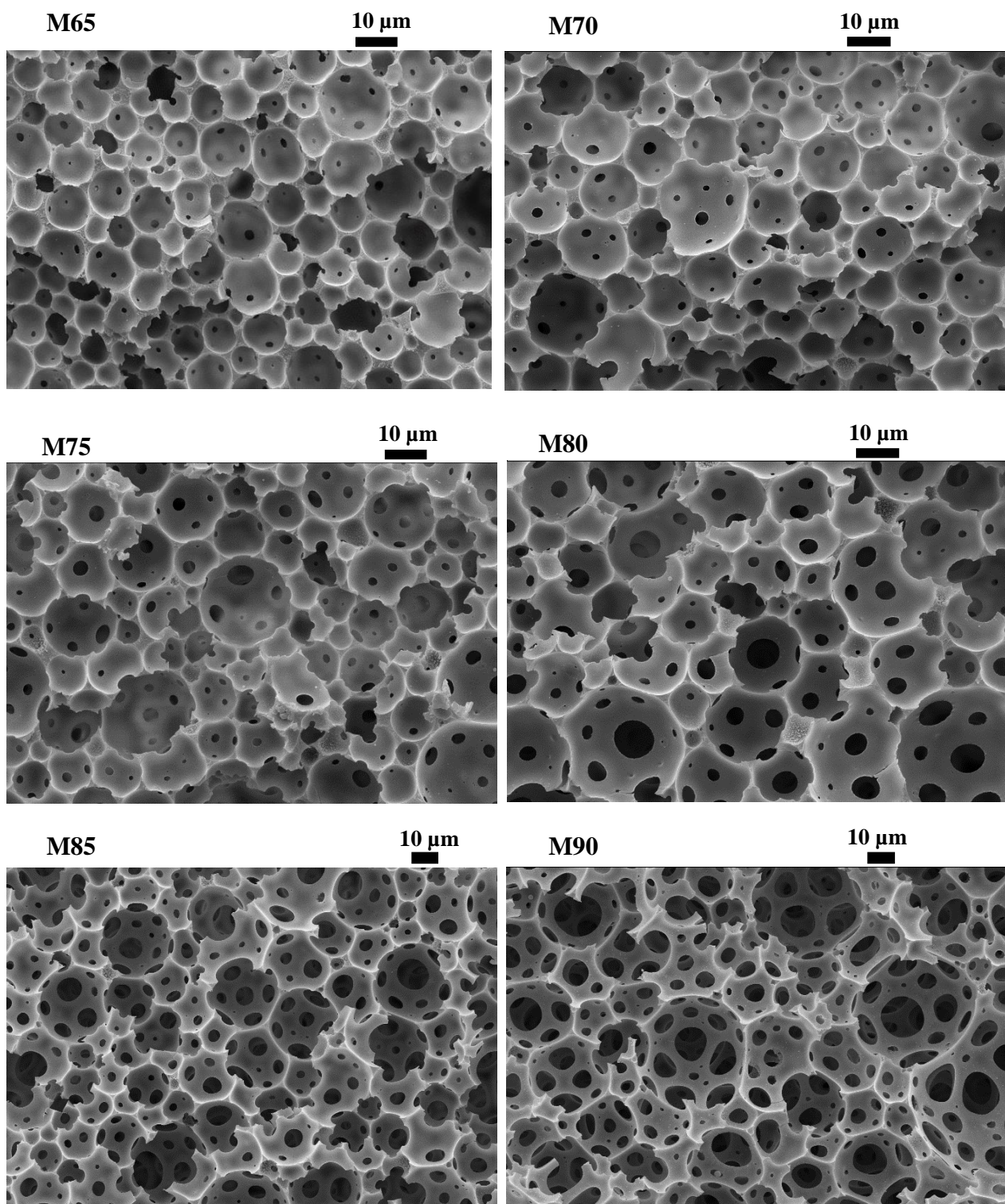


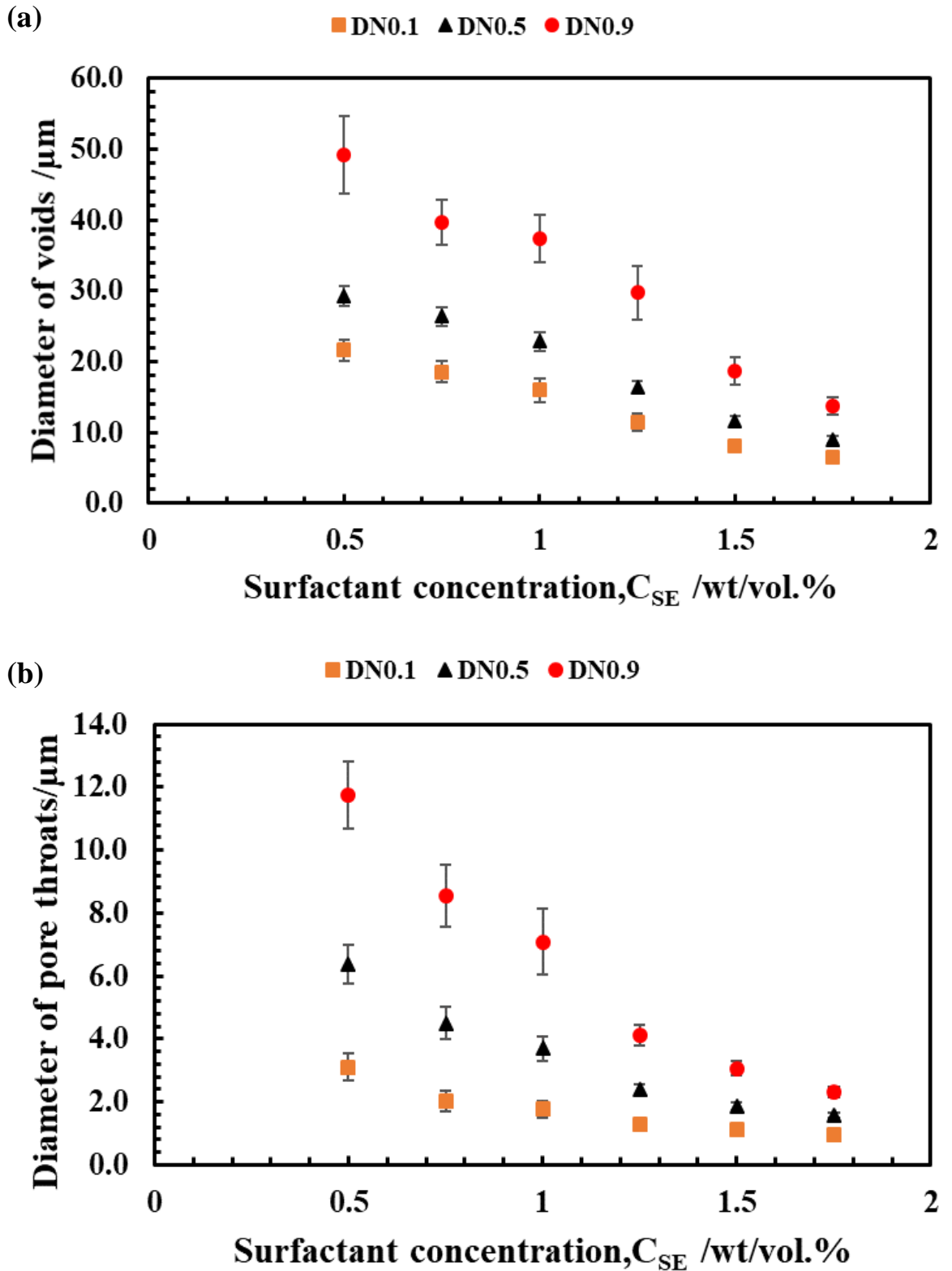
**Figure 3.7.** SEM images of macroporous polymeric materials produced from w/o emulsion templates with different volume fraction of the internal water phase from 65 vol.% (M65) to 90 vol.% (M90). The external oil phase contains 15vol.% of EGDMA, 1 wt/vol.% BPO, 1.19 vol.% DMPT and 5wt/vol.% PEL-121, all dissolved in MMA. The water phase is deionised water.

**Table 3.1.** Void diameters (DN0.1, DN0.5 and DN0.9) determined from SEM images of polymeric materials produced from w/o emulsion templates with varying volume fraction of water ( $\phi_w$ ). The external oil phase contains 15vol.% of EGDMA, 1 wt/vol.% BPO, 1.19 vol.% DMPT and 5wt/vol.% PEL-121, all dissolved in MMA. The water phase is deionised water.  $C_{SE}$  is the PEL-121 surfactant concentration with respect to the total volume of emulsion template.

Sample code	$\phi_w$ /vol.%	$C_{SE}$ /wt/vol.%	DN0.1/ $\mu\text{m}$	DN0.5/ $\mu\text{m}$	DN0.9/ $\mu\text{m}$	Span
<b>M65</b>	65	1.75	6.5 $\pm$ 0.6	9.0 $\pm$ 0.5	13.8 $\pm$ 1.3	0.8 $\pm$ 0.2
<b>M70</b>	70	1.50	8.1 $\pm$ 0.8	12.0 $\pm$ 0.7	18.7 $\pm$ 1.9	0.9 $\pm$ 0.2
<b>M75</b>	75	1.25	11.5 $\pm$ 1.2	16.0 $\pm$ 0.9	29.7 $\pm$ 3.8	1.1 $\pm$ 0.3
<b>M80</b>	80	1.00	16.0 $\pm$ 1.7	23.0 $\pm$ 1.3	37.4 $\pm$ 3.3	0.9 $\pm$ 0.2
<b>M85</b>	85	0.75	18.5 $\pm$ 1.5	26.0 $\pm$ 1.3	39.7 $\pm$ 3.1	0.8 $\pm$ 0.2
<b>M90</b>	90	0.50	21.7 $\pm$ 1.5	29.0 $\pm$ 1.5	49.2 $\pm$ 5.5	0.9 $\pm$ 0.3

**Table 3.2.** Pore throat diameters (DN0.1, DN0.5 and DN0.9) determined from SEM images of polymeric materials produced from w/o emulsion templates with varying volume fraction of water ( $\phi_w$ ). The external oil phase contains 15vol.% of EGDMA, 1 wt/vol.% BPO, 1.19 vol.% DMPT and 5wt/vol.% PEL-121, all dissolved in MMA. The water phase is deionised water.  $C_{SE}$  is the PEL-121 surfactant concentration with respect to the total volume of emulsion template.

Sample code	$\phi_w$ /vol.%	$C_{SE}$ / wt/vol.%	DN0.1/ $\mu\text{m}$	DN0.5/ $\mu\text{m}$	DN0.9/ $\mu\text{m}$	Span
<b>M65</b>	65	1.75	1.0 $\pm$ 0.1	1.6 $\pm$ 0.1	2.3 $\pm$ 0.2	0.9 $\pm$ 0.2
<b>M70</b>	70	1.50	1.1 $\pm$ 0.1	1.9 $\pm$ 0.1	3.1 $\pm$ 0.2	1.0 $\pm$ 0.2
<b>M75</b>	75	1.25	1.3 $\pm$ 0.2	2.4 $\pm$ 0.2	4.1 $\pm$ 0.3	1.2 $\pm$ 0.2
<b>M80</b>	80	1.00	1.8 $\pm$ 0.3	3.7 $\pm$ 0.4	7.1 $\pm$ 1.0	1.4 $\pm$ 0.4
<b>M85</b>	85	0.75	2.0 $\pm$ 0.3	4.5 $\pm$ 0.5	8.5 $\pm$ 1.0	1.4 $\pm$ 0.3
<b>M90</b>	90	0.50	3.1 $\pm$ 0.4	6.4 $\pm$ 0.6	11.8 $\pm$ 1.1	1.4 $\pm$ 0.3

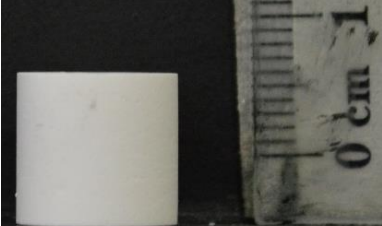


**Figure 3.8.** Diameter of voids (a) and pore throats (b) of porous materials versus PEL-121 surfactant concentration in the total volume of emulsion template,  $C_{SE}$ . For other details see Tables 3.1 and 3.2. DN0.1, DN0.5 and DN0.9 stand for 10%, 50% and 90% where the diameter's values have less than this value.

The mechanical properties of porous polymers produced were investigated by compression tests with Mark 10 instrument as described in section 2.2.6. Cylindrical specimens with height 10 mm were cut from the samples using a diamond disc cutter and dried in air for at least 24 hours before determining their porosity and performing mechanical tests. The calculation of elastic modulus, strength (at 10% strain) and porosity is described in section 2.2.4. The porosity and the density of the materials were obtained from the polymer matrix density and foam density (see section 2.2.6). Results obtained for porous samples produced by polymerisation of emulsion templates with increasing volume fraction of the internal water phase,  $\phi_w$ , are shown in Table 3.3. In the ideal case, the porosity should match the percentage of the water phase in the emulsion template. Our results show that the porosity of all samples is higher than the percentage of the water phase used in the template. The differences are not big and decrease with  $\phi_w$  from 5 % at  $\phi_w = 65$  vol.% to 3 % at  $\phi_w = 90$  vol.%. This discrepancy could be attributed to two factors: (i) the unconverted monomers and surfactant used have been extracted from the samples during its purification thus reducing the sample weight and (ii) the shrinkage of the polymer during polymerisation.<sup>24</sup>

Images of the specimens before and after the compression test are shown in Table 3.3. Except the sample with highest porosity, the materials were not brittle and did not fracture during the tests. The relationship between the mechanical properties and the morphology of porous solids is not fully understood yet.<sup>25</sup> However, the compressive behaviour of the porous polymers produced by us follows the general trends for open cell materials predicted by the model of Gibson and Ashby discussed in section 1.6 of chapter one.<sup>26</sup> As expected, the elastic modulus decreases with increasing the porosity of material from  $109.6 \pm 1.8$  MPa at 70 % porosity to  $14.4 \pm 0.4$  MPa at 93% porosity (see Table.3.4 and Fig 3.9 and 3.10). Similar then is observed for the strength of the samples which decreases by 93% as the porosity increases from 70 to 93 % (see Table 3.4 and Fig 3.11).

**Table 3.3.** Images of porous materials before and after the compression test. For the sample composition see Table 3.4.

Sample code	Before testing	After testing
M65		
M70		
M75		
M80		
M85		
M90		

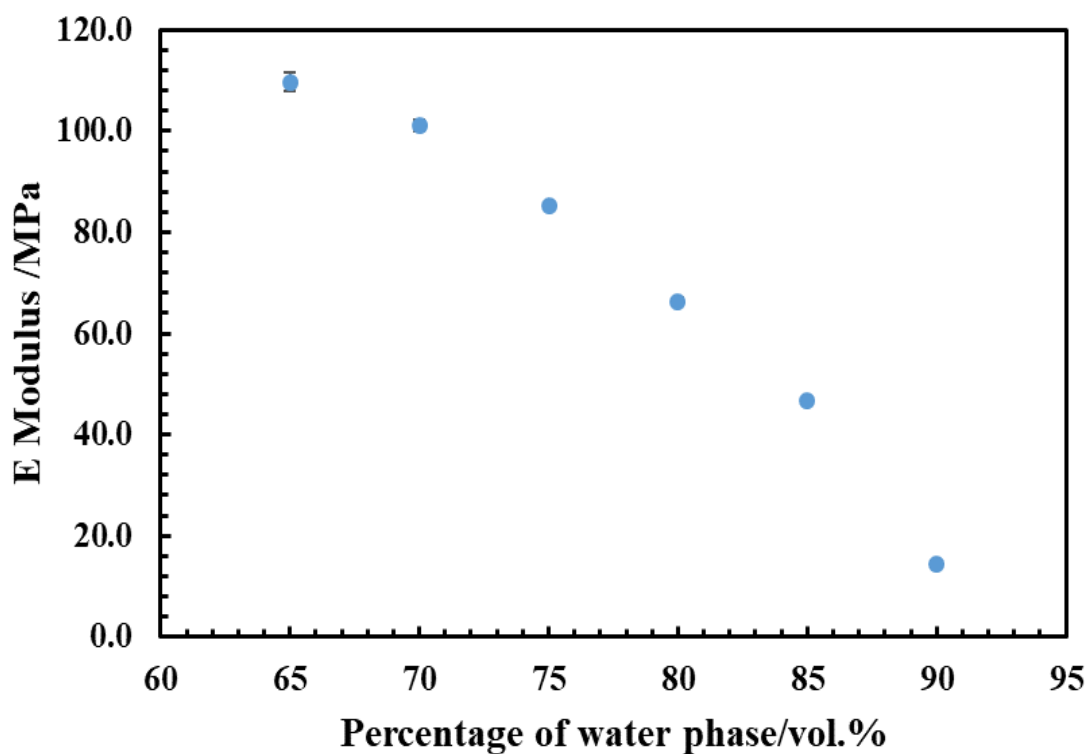


**Figure 3.9.** The elastic modulus versus the percentage of water phase for porous materials produced by redox-initiated polymerisation from emulsion templates with different volume fractions of the internal water phase and kept the surfactant concentration constant to the respect of the total volume of the emulsion (see Table 3.4).

**Table 3.4.** The density, porosity, elastic modulus and strength (at 10 % strain) of porous materials produced by redox-initiated polymerisation from emulsion templates with different volume fractions of the internal water phase,  $\phi_w$ . The external oil phase is made of 15vol.% EGDMA, 5wt/vol.% PEL-121 surfactant, 1wt/vol.% of BPO and 1.19 vol.% DMPT, all dissolved in MMA. The water phase is deionised water.

Sample code	$\phi_w$ /vol. %	Density /g/cm <sup>3</sup>	Porosity /%	Elastic Modulus /MPa	Strength /MPa
M65	65	0.357±0.004	70±2	109.6±1.8	8.71±0.20
M70	70	0.304±0.002	75±2	101.1±1.3	7.02±0.16
M75	75	0.249±0.001	79±2	85.3±0.3	5.05±0.02
M80	80	0.194±0.001	84±2	66.3±0.6	3.23±0.04
M85	85	0.144±0.003	88±2	46.8±0.6	1.83±0.06
M90	90	0.086±0.001	93±2	14.4±0.4	0.57±0.01

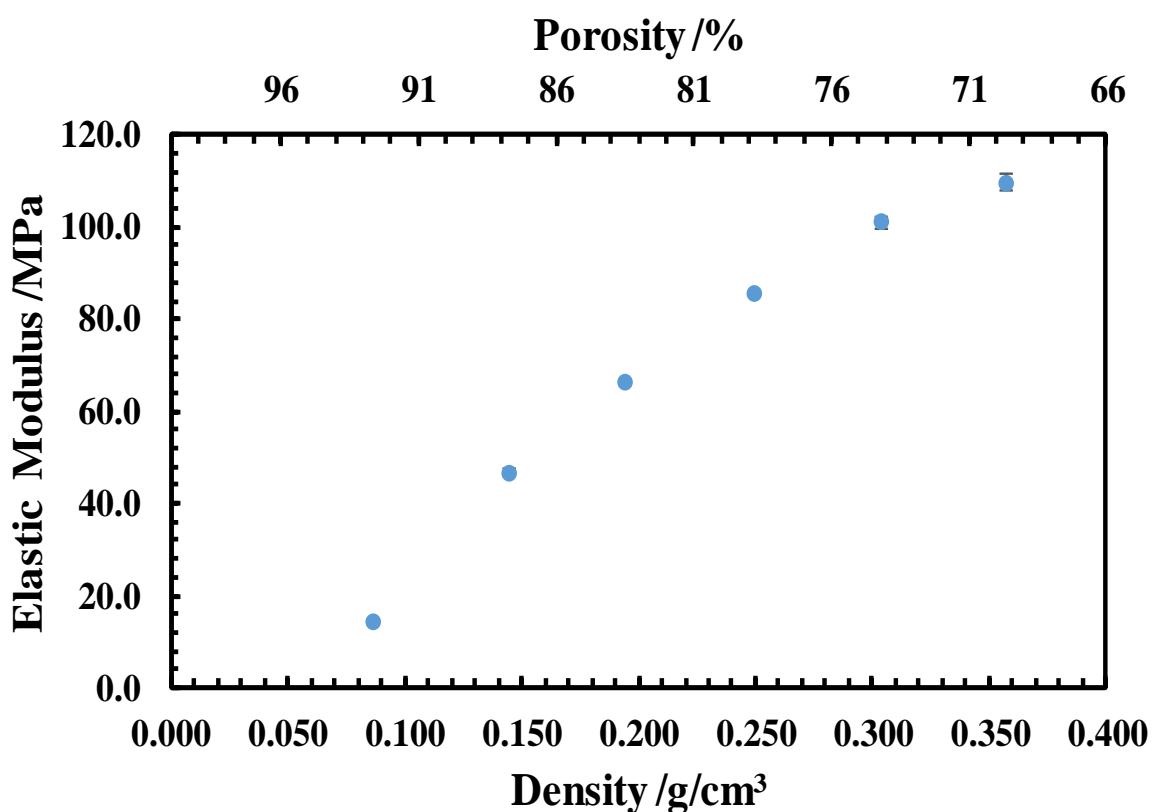


**Figure 3.10.** The elastic modulus versus density and porosity of porous materials produced by redox-initiated polymerisation from emulsion templates with different volume fractions of the internal water phase (see Table 3.4).

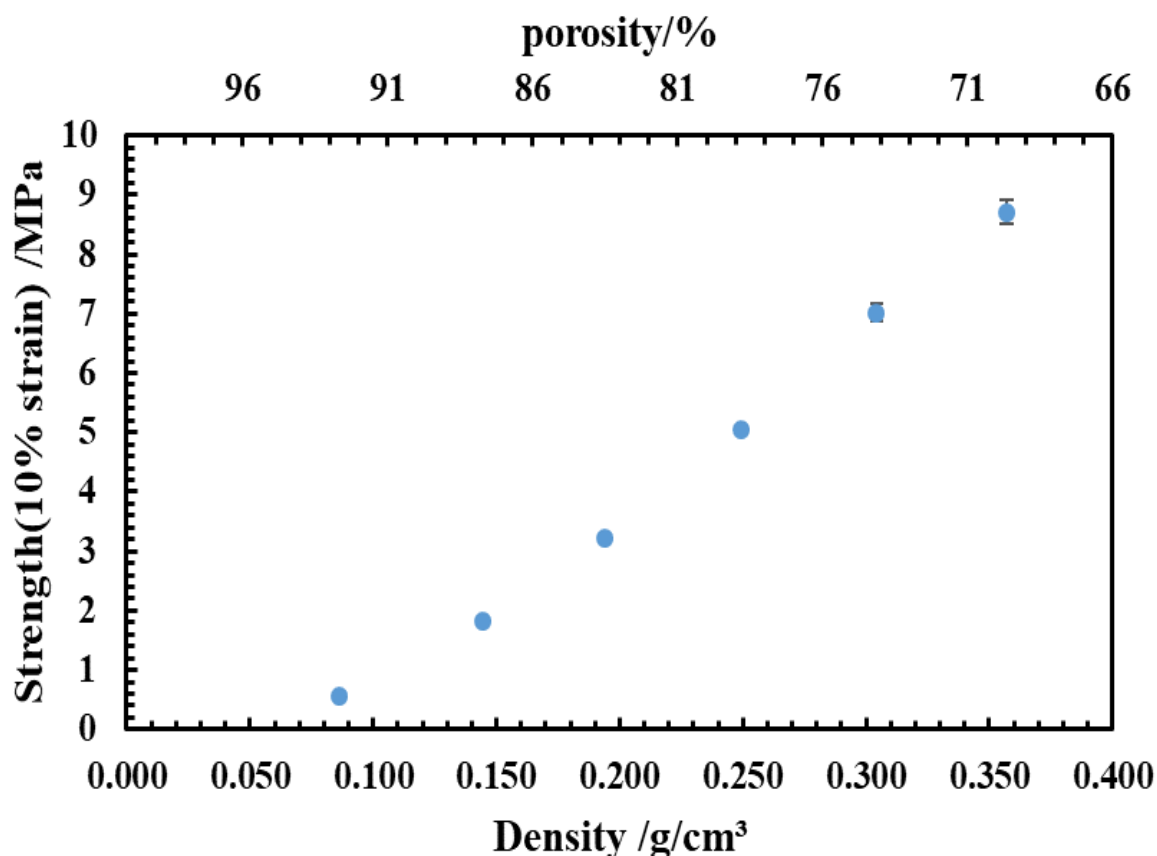


**Figure 3.11.** The strength (at 10% strain) versus density and porosity of porous materials produced by redox-initiated polymerisation from emulsion templates with different volume fractions of the internal water phase (see Table 3.4).

### 3.2.2 Macroporous polymers prepared at constant surfactant concentration in the emulsion template

In the previous section, the concentration of surfactant (PEL-121) was kept constant with respect to the oil phase. When the volume of the water phase increased in the system, the surfactant concentration decreased and lead to affect the structure and the properties of the materials. In addition, at high volume fraction of the water phase samples had some defect on their surfaces, suggested that the surfactant struggle to stabilise the emulsion. In order to understand the effect of water volume fraction on the structure and the properties, we conducted experiments by keeping the surfactant concentration constant with respect to the total volume of the emulsion. The emulsion template was prepared as decsribed in th section 2.2.1. The emulsion stability seems improved as samples produced without any defects across all the different percentage of the water phase (see Figs 3.12-3.17). At 90vol.% sample produced without any defects as the surface was smooth in comparison to previous sample (M903, Fig. 3.6). Therefore, keeping the surfactant

concentration constant with respect to the total volume of the emulsion template has helped to enhance the stability of the emulsion during the polymerisation.<sup>13</sup>

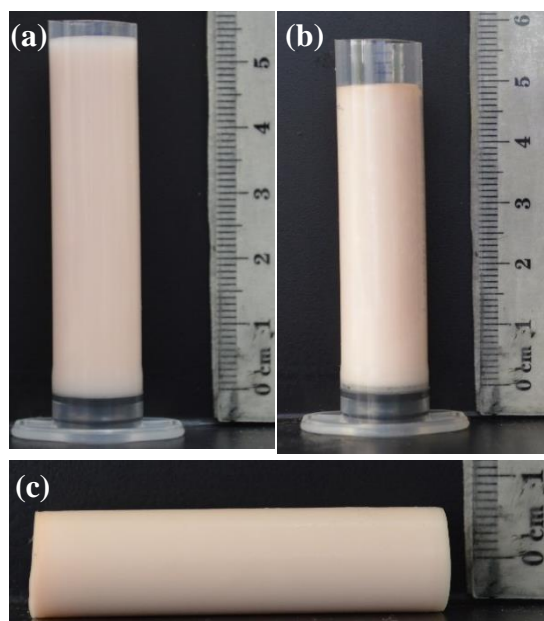


**Figure 3.12.** Images of the mould loaded with w/o emulsion template (a) before polymerisation and (b) after polymerisation at room temperature overnight. (c) An image of the solid material after demoulding. The emulsion template contains 65 vol.% internal phase of deionised water. The external oil phase is made of 15vol.% EGDMA, 5wt/vol.% PEL-121 surfactant, 1wt/vol.% of BPO and 1.19 vol.% DMPT all dissolved in MMA.

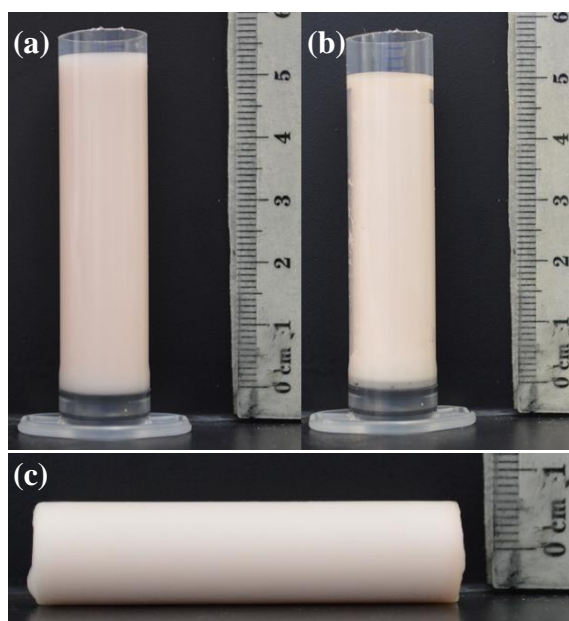


**Figure 3.13.** Images of the mould loaded with w/o emulsion template (a) before polymerisation and (b) after polymerisation at room temperature overnight. (c) An image of the solid material after demoulding. The emulsion template contains 70 vol.% internal phase of deionised water. The external oil phase is made of 15 vol.% EGDMA, 5.5 wt/vol.% PEL-121 surfactant, 1 wt/vol.% of BPO and 1.19 vol.% DMPT, all dissolved in MMA.

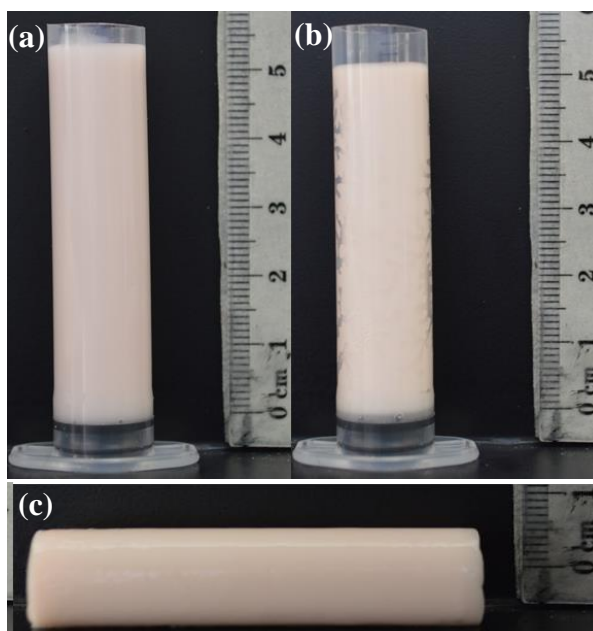


**Figure 3.14.** Images of the mould loaded with w/o emulsion template (a) before polymerisation and (b) after polymerisation at room temperature overnight. (c) An image of the solid material after demoulding. The emulsion template contains 75 vol.% internal phase of deionised water. The external oil phase is made of 15vol.% EGDMA, 7wt/vol.% PEL-121 surfactant, 1wt/vol.% of BPO and 1.19 vol.% DMPT all dissolved in MMA.

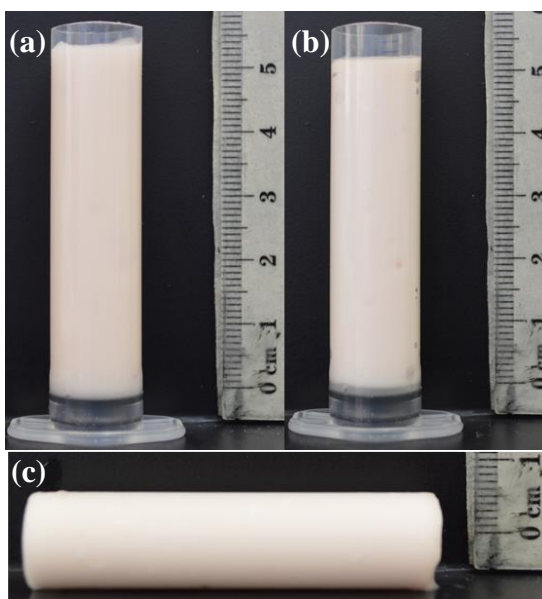


**Figure 3.15.** Images of the mould loaded with w/o emulsion template (a) before polymerisation and (b) after polymerisation at room temperature overnight. (c) An image of the solid material after demoulding. The emulsion template contains 80 vol.% internal phase of deionised water. The external oil phase is made of 15vol.% EGDMA, 8.8wt/vol.% PEL-121 surfactant, 1wt/vol.% of BPO and 1.19 vol.% DMPT all dissolved in MMA.

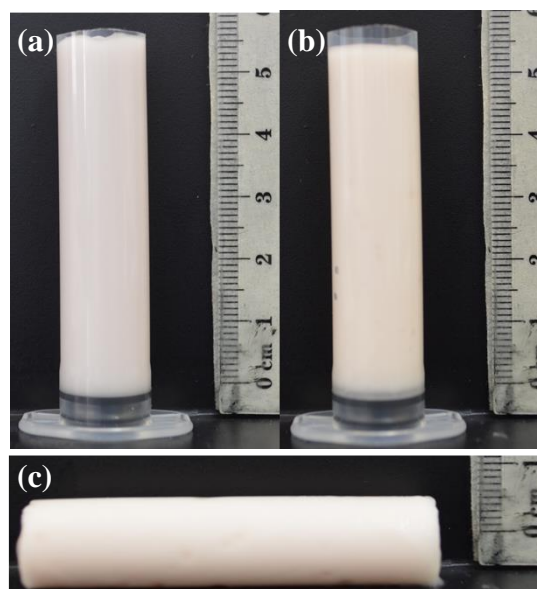


**Figure 3.16.** Images of the mould loaded with w/o emulsion template (a) before polymerisation and (b) after polymerisation at room temperature overnight. (c) An image of the solid material after demoulding. The emulsion template contains 85 vol.% internal phase of deionised water. The external oil phase is made of 15vol.% EGDMA, 11.7wt/vol.% PEL-121 surfactant, 1wt/vol.% of BPO and 1.19 vol.% DMPT all dissolved in MMA.

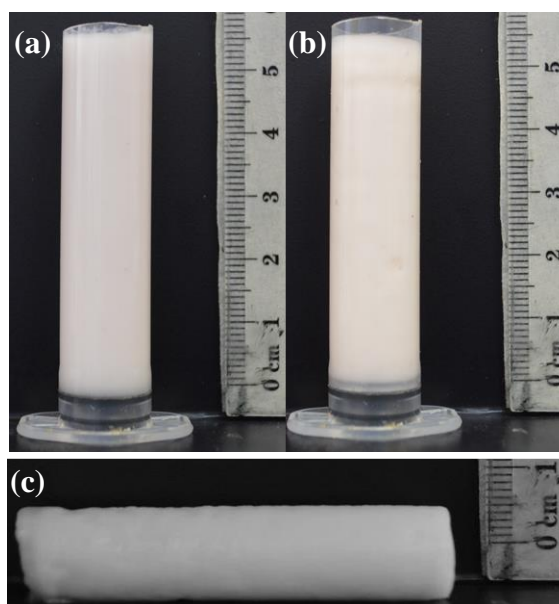


**Figure 3.17.** Images of the mould loaded with w/o emulsion template (a) before polymerisation and (b) after polymerisation at room temperature overnight. (c) An image of the solid material after demoulding. The emulsion template contains 90 vol.% internal phase of deionised water. The external oil phase is made of 15vol.% EGDMA, 17.5wt/vol.% PEL-121 surfactant, 1wt/vol.% of BPO and 1.19 vol.% DMPT all dissolved in MMA.

Similar to the previous series of experiment, the SEM images show an open structure across all samples (Fig.3.18). The diameter of voids also increases with the increase of the percentage of water. However, this increase is less pronounced (see Table.3.5 and Figs.3.19). The DN0.5 diameter of voids at 65 vol.% water is  $13.49 \pm 0.66 \mu\text{m}$  while that at 90vol.% is  $18.11 \pm 0.7 \mu\text{m}$ , an increase of 34% in comparison to 222% increased observed in the experiments at constant surfactant concentration in the oil phase. This could be attributed to the higher amount of surfactant in the emulsions with high volume fraction of water which lead to the formation of templates with smaller droplets and also enhanced the emulsion stability during the polymerisation.<sup>13,27</sup> The pore throat diameter DN0.5 increase is more pronounced, from  $1.49 \pm 0.10 \mu\text{m}$  at 65vol.% water to  $4.51 \pm 0.31 \mu\text{m}$  at 90vol.% water (see Table.3.6 and Figs.3.199) but smaller to that observed in the previous series of experiments (Table 3.2).

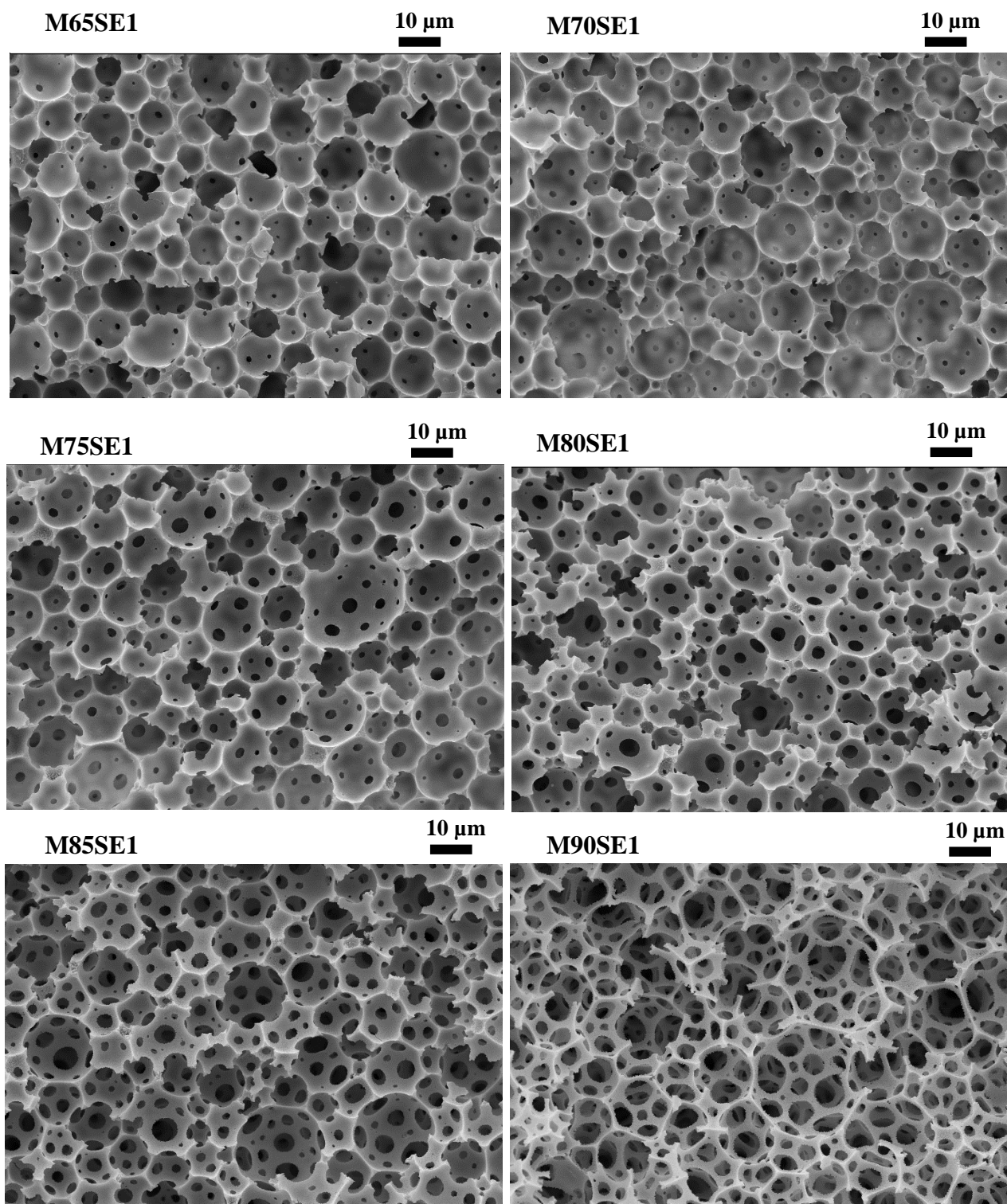


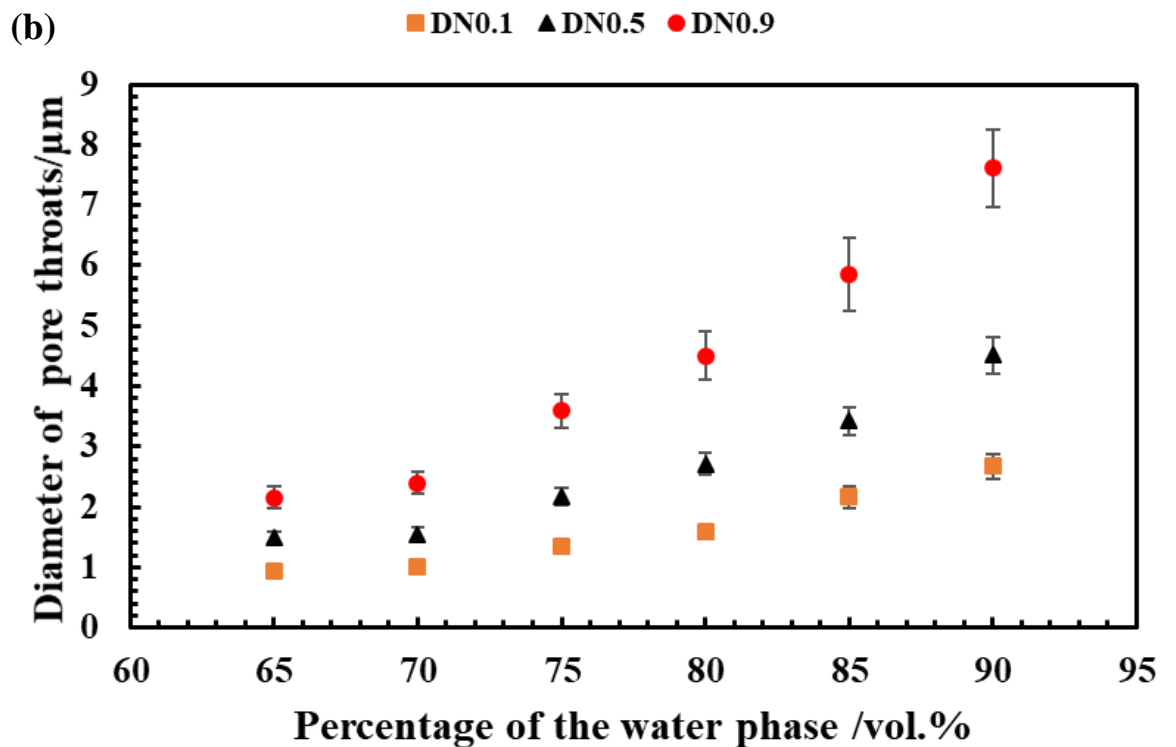
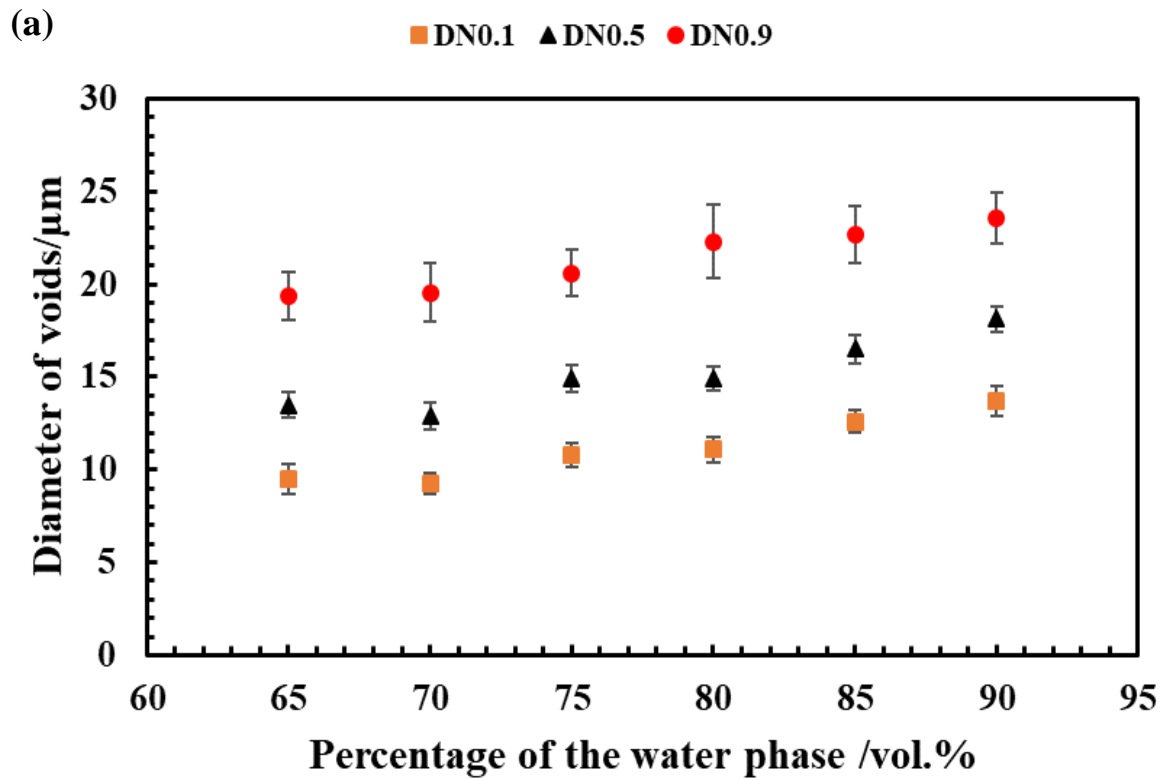
**Figure 3.18.** SEM images of macroporous polymeric materials produced from w/o emulsion templates with different volume fraction of the internal water phase from 65 vol.% (M65SE1) to 90 vol.% (M90SE1) and fixed surfactant concentration in respect to the total volume of the emulsion,  $C_{SE} = 1.75$  wt/vol.%. The external oil phase contains 15vol.% of EGDMA, 1 wt/vol.% of BPO, 1.19 vol.% DMPT and variable concentration of PEL-121 surfactant,  $C_{SO}$  (5 - 17.5 wt/vol.%), all dissolved in MMA. The water phase is deionised water.

**Table 3.5.** Void diameters (DN0.1, DN0.5 and DN0.9) determined from SEM images of polymeric materials produced from w/o emulsion templates with varying volume fraction of water ( $\phi_w$ ) at a constant surfactant concentration in the emulsion,  $C_{SE} = 1.75$  wt/vol.%. The external oil phase contains 15vol.% of EGDMA, 1 wt/vol.% BPO, 1.19 vol.% DMPT and variable PEL-121 surfactant concentration,  $C_{SO}$ , all dissolved in MMA. The water phase is deionised water.

Sample code	$\phi_w$ /vol. %	$C_{so}$ /wt/vol. %	DN0.1/ $\mu$ m	DN0.5/ $\mu$ m	DN0.9/ $\mu$ m	Span
M65SE1	65	5.0	9.49 $\pm$ 0.81	13.49 $\pm$ 0.66	19.36 $\pm$ 1.28	0.73 $\pm$ 0.16
M70SE1	70	5.5	9.26 $\pm$ 0.58	12.89 $\pm$ 0.69	19.54 $\pm$ 1.59	0.80 $\pm$ 0.17
M75SE1	75	7.0	10.79 $\pm$ 0.68	14.91 $\pm$ 0.75	20.61 $\pm$ 1.27	0.66 $\pm$ 0.14
M80SE1	80	8.8	11.08 $\pm$ 0.69	14.91 $\pm$ 0.62	22.30 $\pm$ 2.00	0.75 $\pm$ 0.18
M85SE1	85	11.7	12.59 $\pm$ 0.62	16.49 $\pm$ 0.75	22.67 $\pm$ 1.52	0.61 $\pm$ 0.13
M90SE1	90	17.5	13.72 $\pm$ 0.81	18.11 $\pm$ 0.70	23.59 $\pm$ 1.38	0.55 $\pm$ 0.12

**Table 3.6.** Pore throat diameters (DN0.1, DN0.5 and DN0.9) determined from SEM images of polymeric materials produced from w/o emulsion templates with varying volume fraction of water ( $\phi_w$ ) at a constant surfactant concentration in the emulsion,  $C_{SE} = 1.75$  wt/vol.%. The external oil phase contains 15vol.% of EGDMA, 1 wt/vol.% BPO, 1.19 vol.% DMPT and variable PEL-121 surfactant concentration,  $C_{SO}$ , all dissolved in MMA. The water phase is deionised water.

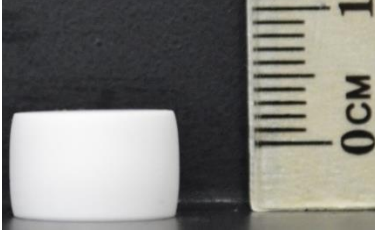
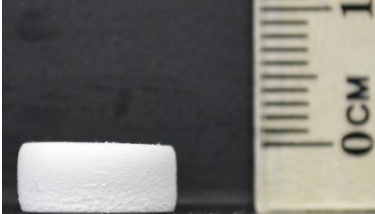
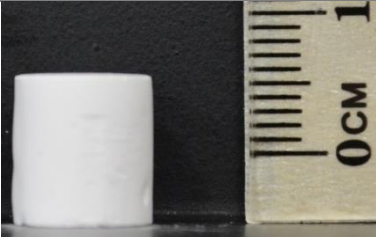
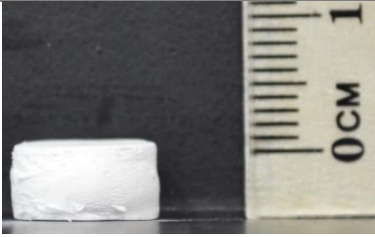
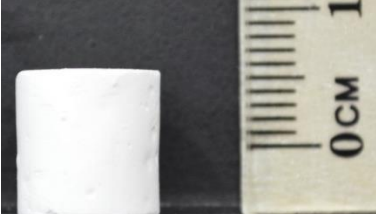
Sample code	$\phi_w$ /vol.%	$C_{so}$ / wt/vol.%	DN0.1/ $\mu$ m	DN0.5/ $\mu$ m	DN0.9/ $\mu$ m	Span
M65SE1	65	5	0.93 $\pm$ 0.10	1.49 $\pm$ 0.10	2.16 $\pm$ 0.18	0.82 $\pm$ 0.19
M70SE1	70	5.5	1.01 $\pm$ 0.09	1.55 $\pm$ 0.11	2.40 $\pm$ 0.18	0.90 $\pm$ 0.18
M75SE1	75	7	1.36 $\pm$ 0.12	2.17 $\pm$ 0.14	3.59 $\pm$ 0.29	1.03 $\pm$ 0.20
M80SE1	80	8.8	1.59 $\pm$ 0.11	2.71 $\pm$ 0.18	4.50 $\pm$ 0.40	1.08 $\pm$ 0.20
M85SE1	85	11.7	2.17 $\pm$ 0.18	3.42 $\pm$ 0.23	5.85 $\pm$ 0.61	1.08 $\pm$ 0.24
M90SE1	90	17.5	2.67 $\pm$ 0.21	4.51 $\pm$ 0.31	7.62 $\pm$ 0.64	1.10 $\pm$ 0.20



**Figure 3.19.** Diameter of voids (a) and pore throats (b) of porous materials versus the percentage of the water phase 65-90vol.% in the emulsion template. For other details see Tables 3.5 and 3.6. DN0.1, DN0.5 and DN0.9 stand for 10%, 50% and 90% where the diameter's value have less than this value.

The mechanical properties of samples produced were studied by compression tests at room temperature. Keeping the surfactant concentration constant with respect to the total volume of the emulsion template and varying the percentage of the water phase seemed to have a potential effect on improving the mechanical properties in comparison to the previous experiment in section (3.2.1) due to the emulsion template is more stable. The mechanical properties were as expected as it decreased with increasing the percentage of the water phase (see Table 3.7 and Fig.3.20). Images of samples before and after the compression test is in Table.3.7. The elastic modulus decreases with increasing the porosity (see Table.3.8, Fig.3.21). It decreased by 94% from  $113\pm 1.1$  MPa to  $6.7\pm 0.2$  MPa. The strength (10% strain) decreased by 97% (see Table.3.8, Fig.3.22). The porosity achieved up to 94%. Here the effect on the mechanical properties could be related to the volume fraction of the water phase as surfactant concentration constant in the total volume of the emulsion. The increase in the water fraction is produced materials with lighter density which could affect the mechanical properties. Another explanation for the reduction of the mechanical properties could be that the wall between the droplets becomes thinner as the water fraction increased. In other words, the amount of the surfactant increased in the systems because it is with respect to the total volume of the emulsion. This increase in the surfactant concentration in the oil phase resulting in thinning the wall between the droplets. As consequence, the materials produced becomes weaker as they rely on the compression test on their wall thickness.<sup>18, 26 27</sup>

**Table 3.7.** Images of porous materials before and after the compression test. For the sample composition see Table 3.8.

Sample code	Before testing	After testing
M65SE1		
M70SE1		
M75SE1		
M80SE1		
M85SE1		
M90SE1		

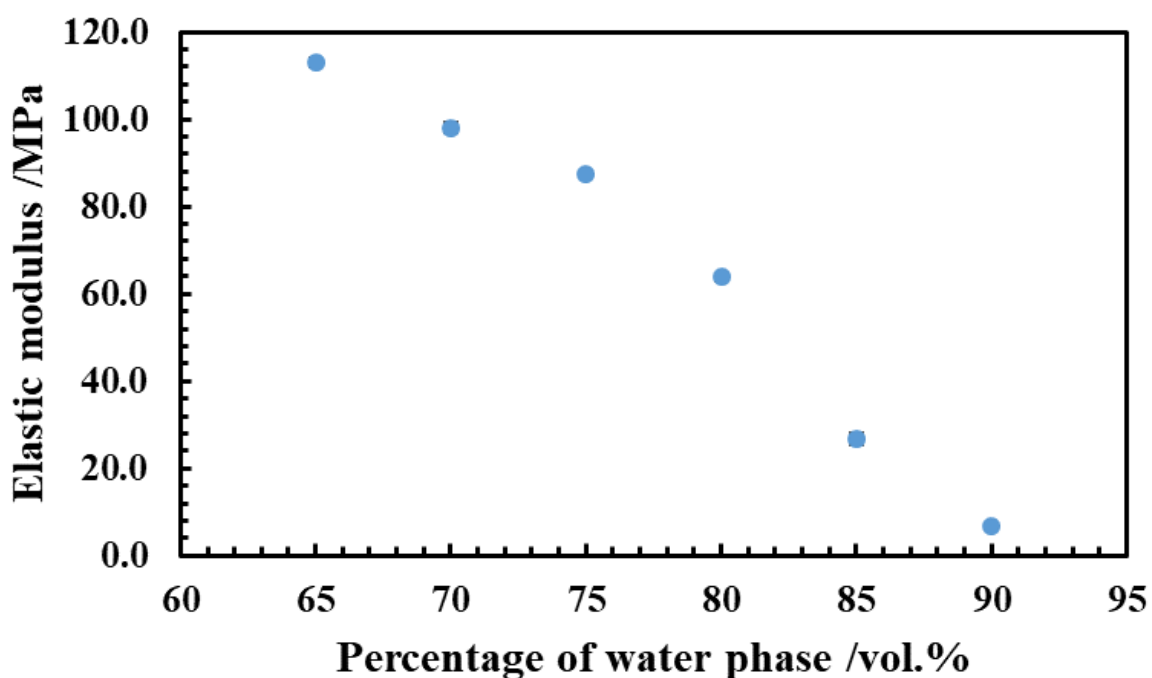


**Figure 3.20.** The elastic modulus versus the percentage of water phase for porous materials produced by redox-initiated polymerisation from emulsion templates with different volume fractions of the internal water phase and kept the surfactant concentration constant to the respect of the total volume of the emulsion (see Table 3.8).

**Table 3.8.** The density, porosity, elastic modulus and strength (at 10 % strain) of porous materials produced by redox-initiated polymerisation from emulsion templates with different volume fractions of the internal water phase,  $\phi_w$ . The external oil phase is made of 15vol.% EGDMA, varied in respect to the total volume of the emulsion 5-17.5wt/vol.% PEL-121 surfactant, 1wt/vol.% of BPO and 1.19 vol.% DMPT, all dissolved in MMA. The water phase is deionised water.

Sample code	$\phi_w$ /vol.%	Density /g/cm <sup>3</sup>	Porosity /%	Elastic Modulus /MPa	Strength /MPa
M65SE1	65	0.355±0.0014	70±2	113.0±1.1	9.04±0.13
M70SE1	70	0.298±0.0024	75±2	98.1±1.2	6.88±0.14
M75SE1	75	0.239±0.0002	80±2	87.5±0.5	4.91±0.04
M80SE1	80	0.191±0.0018	84±2	63.8±0.8	3.04±0.08
M85SE1	85	0.120±0.0029	90±2	26.8±1.4	0.98±0.05
M90SE1	90	0.071±0.0017	94±2	06.7±0.2	0.28±0.02

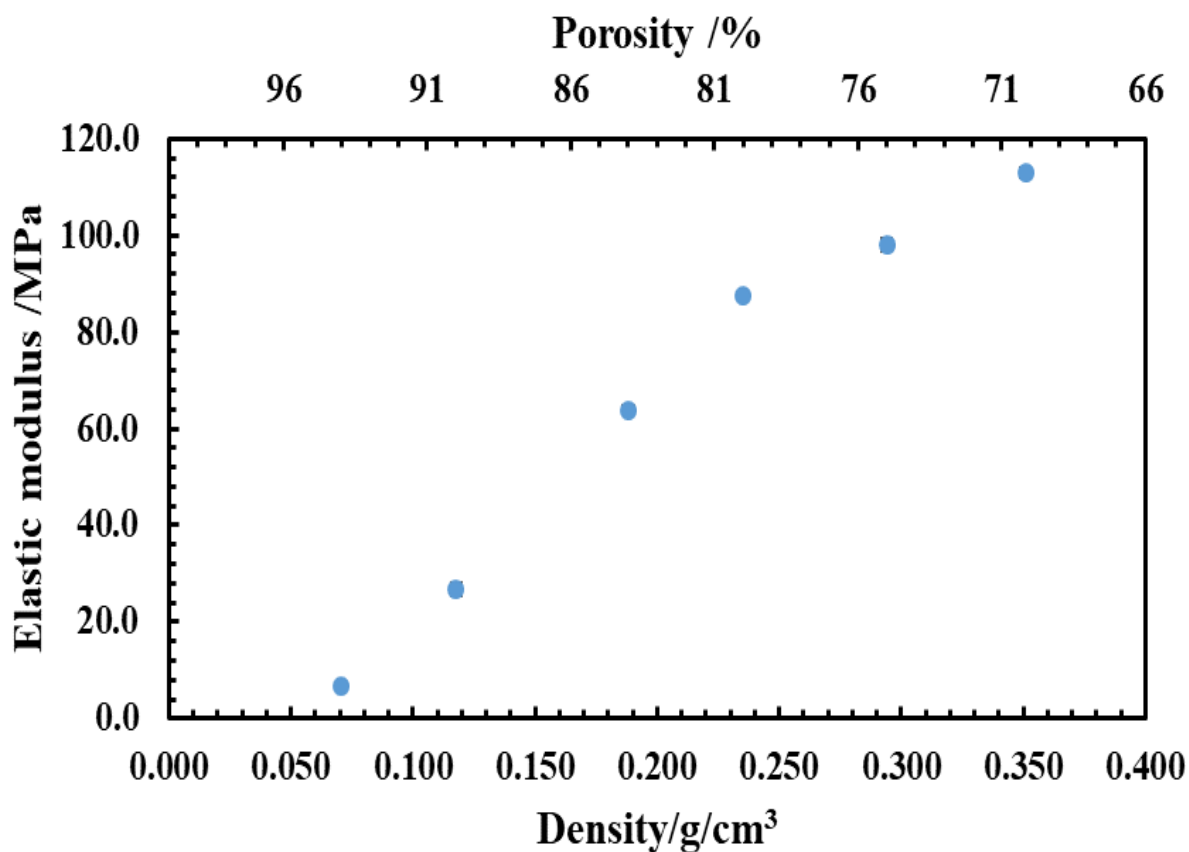


**Figure 3.21.** The elastic modulus versus density and porosity of porous materials produced by redox-initiated polymerisation from emulsion templates with different volume fractions of the internal water phase and kept the surfactant concentration constant to the respect of the total volume of the emulsion (see Table 3.8).

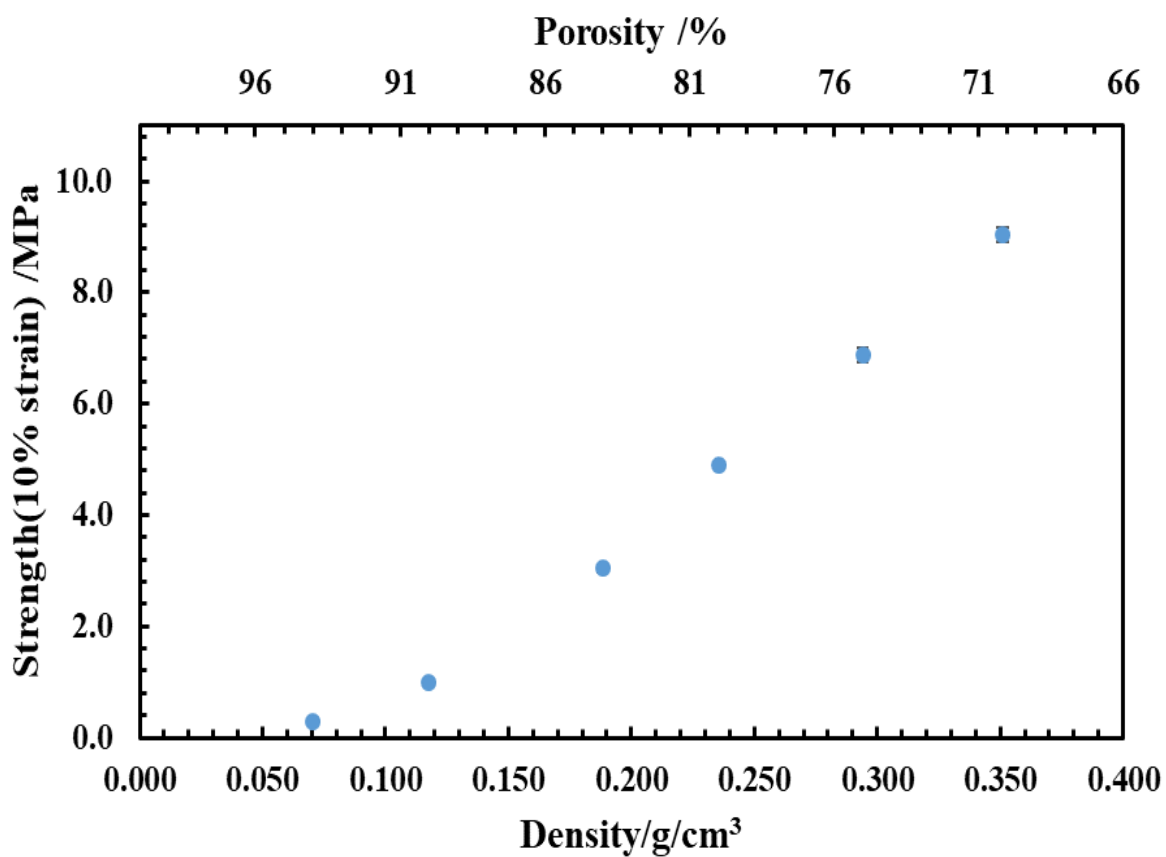


**Figure 3.22.** The strength (at 10% strain) versus density and porosity of porous materials produced by redox-initiated polymerisation from emulsion templates with different volume fractions of the internal water phase (see Table 3.8).

### **3.3 Effect of surfactant concentration on the properties of polyHIPEs at a fixed volume fraction of water in the emulsion template**

The stability of emulsion template is essential as it could influence the mechanical properties and the morphology of PolyHIPEs. The more control of the stability of HIPE could lead to tune the mechanical properties and the morphology. Studying the surfactant concentration to test how potentially this could affect the mechanical properties and the morphology of polyHIPEs. In this section, the surfactant (PEL-121) concentration varies from 0.4 to 10wt/vol.% with respect to the oil phase. The oil phase is made of 1wt/vol.% of BPO, 15vol.% of EGDMA, variable PEL-121 surfactant at concentrations from 0.4-10 wt/vol.% and 1.19 vol.% DMPT, all dissolved in MMA. The water phase is deionised at a fixed volume fraction of 80vol.%. The emulsion template made as described in section 2.2.1. The lowest concentration of surfactant achieved to produce polyHIPEs is 0.4wt/vol.% in respect to the oil phase. However, the samples at a low concentration of surfactant (PEL-121) 0.4, 0.5, 0.8wt/vol.% have some small holes in their surfaces. This suggests that the emulsion has been partially destabilised during the polymerisation as results of there were not enough surfactant in the system (see Figs.3.23-3.25). In addition, The samples were applicable for mechanical testing and any applications needed. Concentraion towrdes 10wt/vol.% improved the sample produced without any defects on their surfaces (see Fig.3.26-3.30). In the literature, usually for the preparation of macroporus polymers are required tremendous amount of surfactant 5-50vol.% whether the polymerisation at high temperature or room temperature (UV light). The vast amount of surfactant needed is to enhance the emulsion stability during the polymerisation.<sup>11, 17, 27, 28</sup> Whereas, in our systems, the lowest achieved was 0.4wt/vol.% of PEL-121 with respect to the oil phase. It suggested that the polymerisation at room temperature has less effect on the emulsion stability as there is no heat supplied to the system.

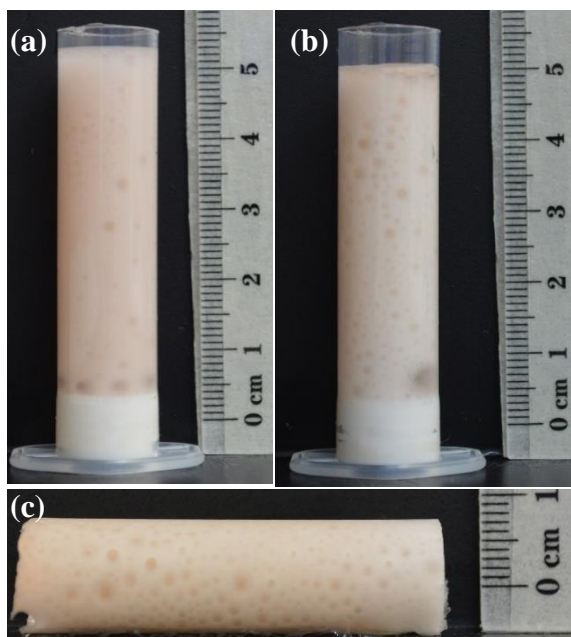


**Figure 3.23.** Images of the mould loaded with w/o emulsion template (a) before polymerisation and (b) after polymerisation at room temperature overnight. (c) An image of the solid material after demoulding. The emulsion template contains 80 vol.% internal phase of deionised water. The external oil phase is made of 15vol.% EGDMA, 0.4wt/vol.% PEL-121 surfactant, 1wt/vol.% of BPO and 1.19 vol.% DMPT all dissolved in MMA.

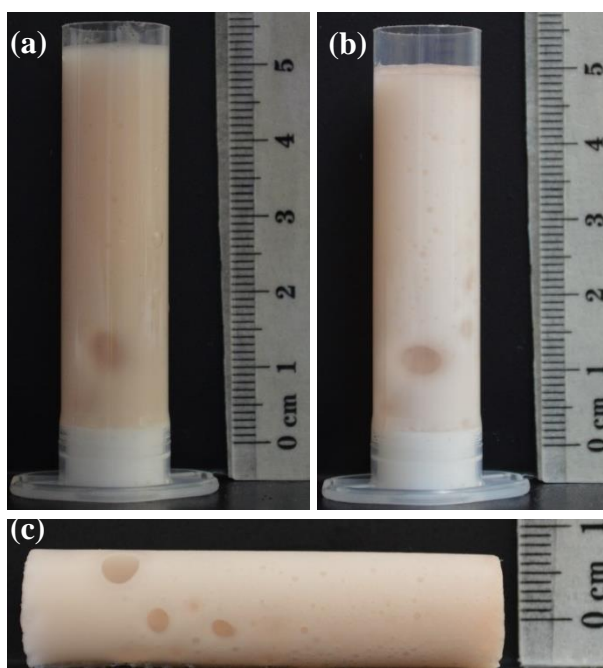


**Figure 3.24.** Images of the mould loaded with w/o emulsion template (a) before polymerisation and (b) after polymerisation at room temperature overnight. (c) An image of the solid material after demoulding. The emulsion template contains 80 vol.% internal phase of deionised water. The external oil phase is made of 15vol.% EGDMA, 0.5wt/vol.% PEL-121 surfactant, 1wt/vol.% of BPO and 1.19 vol.% DMPT all dissolved in MMA.

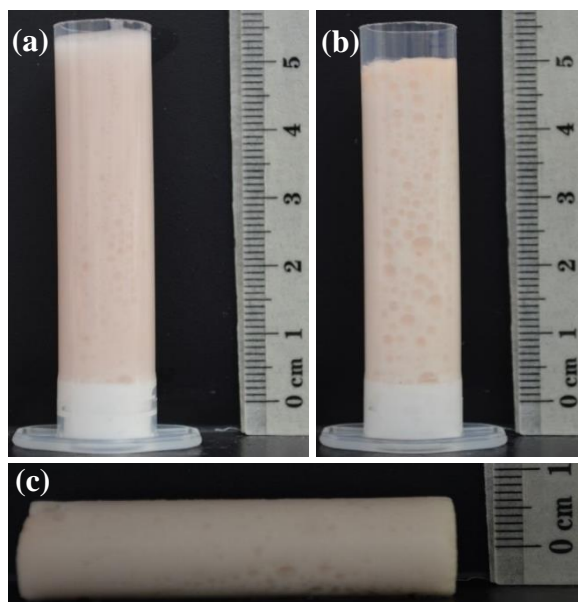


**Figure 3.25.** Images of the mould loaded with w/o emulsion template (a) before polymerisation and (b) after polymerisation at room temperature overnight. (c) An image of the solid material after demoulding. The emulsion template contains 80 vol.% internal phase of deionised water. The external oil phase is made of 15vol.% EGDMA, 0.8wt/vol.% PEL-121 surfactant, 1wt/vol.% of BPO and 1.19 vol.% DMPT all dissolved in MMA.

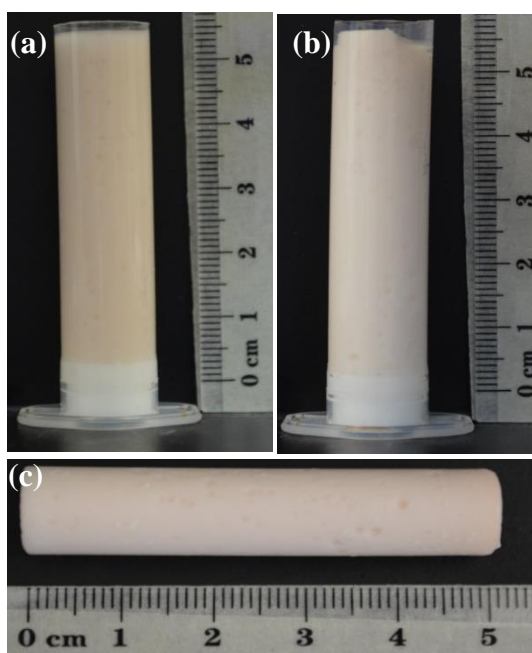


**Figure 3.26.** Images of the mould loaded with w/o emulsion template (a) before polymerisation and (b) after polymerisation at room temperature overnight. (c) An image of the solid material after demoulding. The emulsion template contains 80 vol.% internal phase of deionised water. The external oil phase is made of 15vol.% EGDMA, 1wt/vol.% PEL-121 surfactant, 1wt/vol.% of BPO and 1.19 vol.% DMPT all dissolved in MMA.

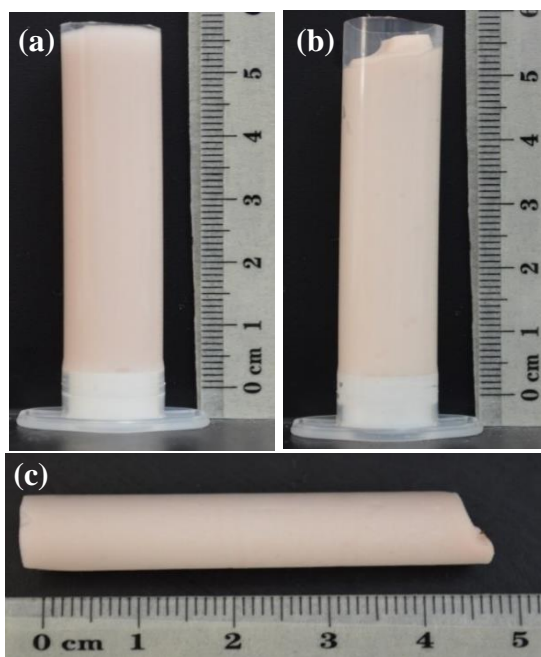


**Figure 3.27.** Images of the mould loaded with w/o emulsion template (a) before polymerisation and (b) after polymerisation at room temperature overnight. (c) An image of the solid material after demoulding. The emulsion template contains 80 vol.% internal phase of deionised water. The external oil phase is made of 15vol.% EGDMA, 3wt/vol.% PEL-121 surfactant, 1wt/vol.% of BPO and 1.19 vol.% DMPT all dissolved in MMA.

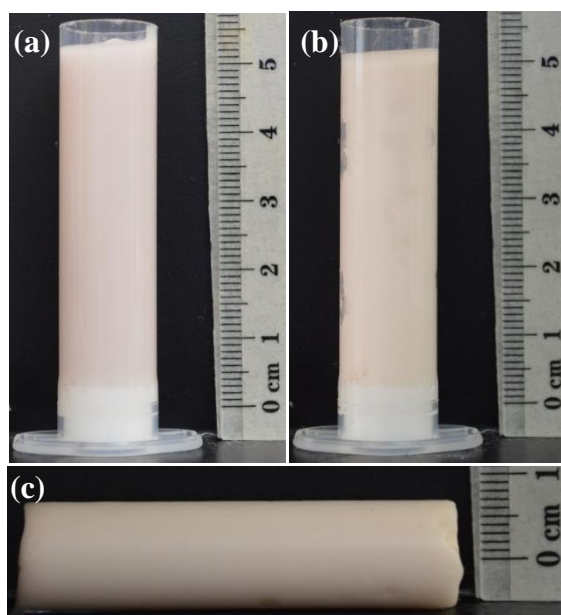


**Figure 3.28.** Images of the mould loaded with w/o emulsion template (a) before polymerisation and (b) after polymerisation at room temperature overnight. (c) An image of the solid material after demoulding. The emulsion template contains 80 vol.% internal phase of deionised water. The external oil phase is made of 15vol.% EGDMA, 5wt/vol.% PEL-121 surfactant, 1wt/vol.% of BPO and 1.19 vol.% DMPT all dissolved in MMA.

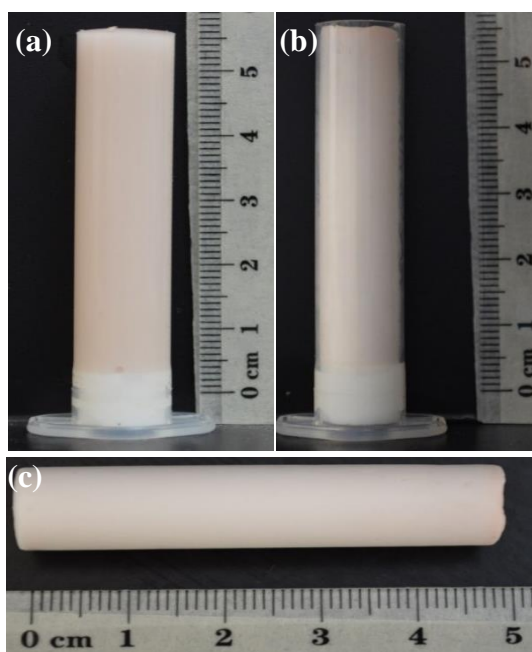


**Figure 3.29.** Images of the mould loaded with w/o emulsion template (a) before polymerisation and (b) after polymerisation at room temperature overnight. (c) An image of the solid material after demoulding. The emulsion template contains 80 vol.% internal phase of deionised water. The external oil phase is made of 15vol.% EGDMA, 8wt/vol.% PEL-121 surfactant, 1wt/vol.% of BPO and 1.19 vol.% DMPT all dissolved in MMA.

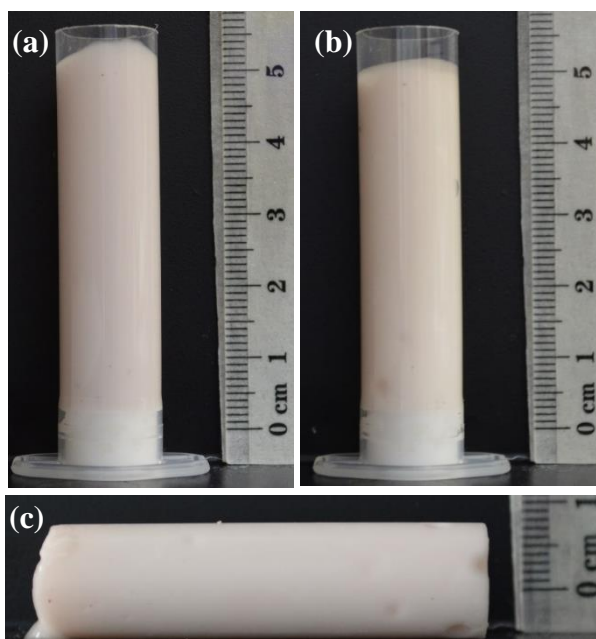


**Figure 3.30.** Images of the mould loaded with w/o emulsion template (a) before polymerisation and (b) after polymerisation at room temperature overnight. (c) An image of the solid material after demoulding. The emulsion template contains 80 vol.% internal phase of deionised water. The external oil phase is made of 15vol.% EGDMA, 10wt/vol.% PEL-121 surfactant, 1wt/vol.% of BPO and 1.19 vol.% DMPT all dissolved in MMA.

The surfactant concentration affects the morphology of macroporous polymers prepared at room temperature as can be seen in the SEM images (Figs.3.31 and 3.32). The diameter of voids and pore throats decreases as the surfactant concentration increases (see Table 3.9-3.10 and Fig.33). This is due the surfactant enhance the emulsion stability.<sup>13, 29</sup> The surfactant reduces the interfacial tension in the emulsion template to generate small droplets as concentration increases.<sup>30</sup> At the lowest concentration of surfactant (M80S0.4) the structure of macroporous polymers are not fully open structure as some of the voids are closed (see Fig.3.31 (M80S0.4)). Whereas, the rest of the samples have an open structure. The possible explanation for that is the void walls are thick resulting in preventing the formation of the pore throats.<sup>24</sup> The reason for the thickness of the wall is that the low surfactant concentration cannot thin the wall between the droplets.<sup>27</sup> The number of pore throats increased as the concentration of surfactant increased. The film between the droplets is thinning as the surfactant rises.<sup>13, 27</sup> As results the formation of pore throats occurred at the thinnest point of the film between the droplets.<sup>18, 29</sup> In addition, the droplets in substantial contact with each other as the water phase fixed at 80vol.%.

The pore throats diameter has slightly increased across the concentration of surfactant. The explanation for that the droplets are in much contact as the percentage of the water phase is 80vol.% in all the concentration. As a consequence, the diameter of the pore throats depends on the thickness of film between the droplets.<sup>27</sup>The increase in the surfactant concentration resulting in thinning the film between the droplets which allow the pore throats to open at the thinnest point. In another hand, the surfactant concentration significantly affects the diameter of the voids. The assumption for that could be related to the emulsion stability.<sup>13</sup>As at low concentration of surfactant the emulsion is less stable, and coalescences could take place. This instability of the emulsion during the polymerisation resulting in generating larger voids. Whereas, increasing the surfactant concentration leads to enhance the emulsion stability and create smaller droplets.<sup>13, 30</sup>

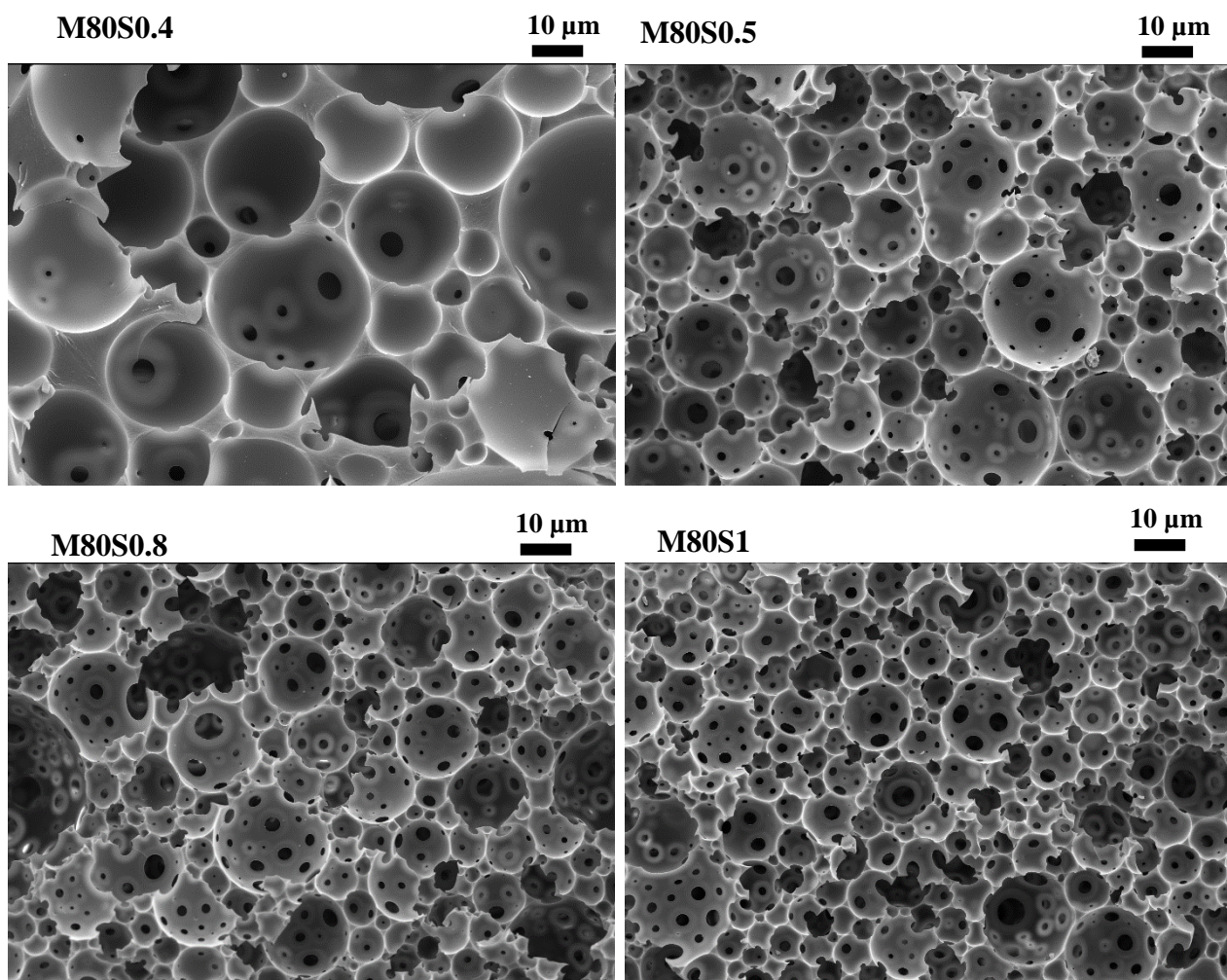


**Figure 3.31.** SEM images of macroporous polymeric materials produced from w/o emulsion templates with different concentration of PEI-121 and fixed water phase 80vol.%. The external oil phase contains 15vol.% of EGDMA, 1 wt/vol.% of BPO, 1.19 vol.% DMPT and varied 0.4-1wt/vol.% PEL-121, all dissolved in MMA. The water phase is deionised water.

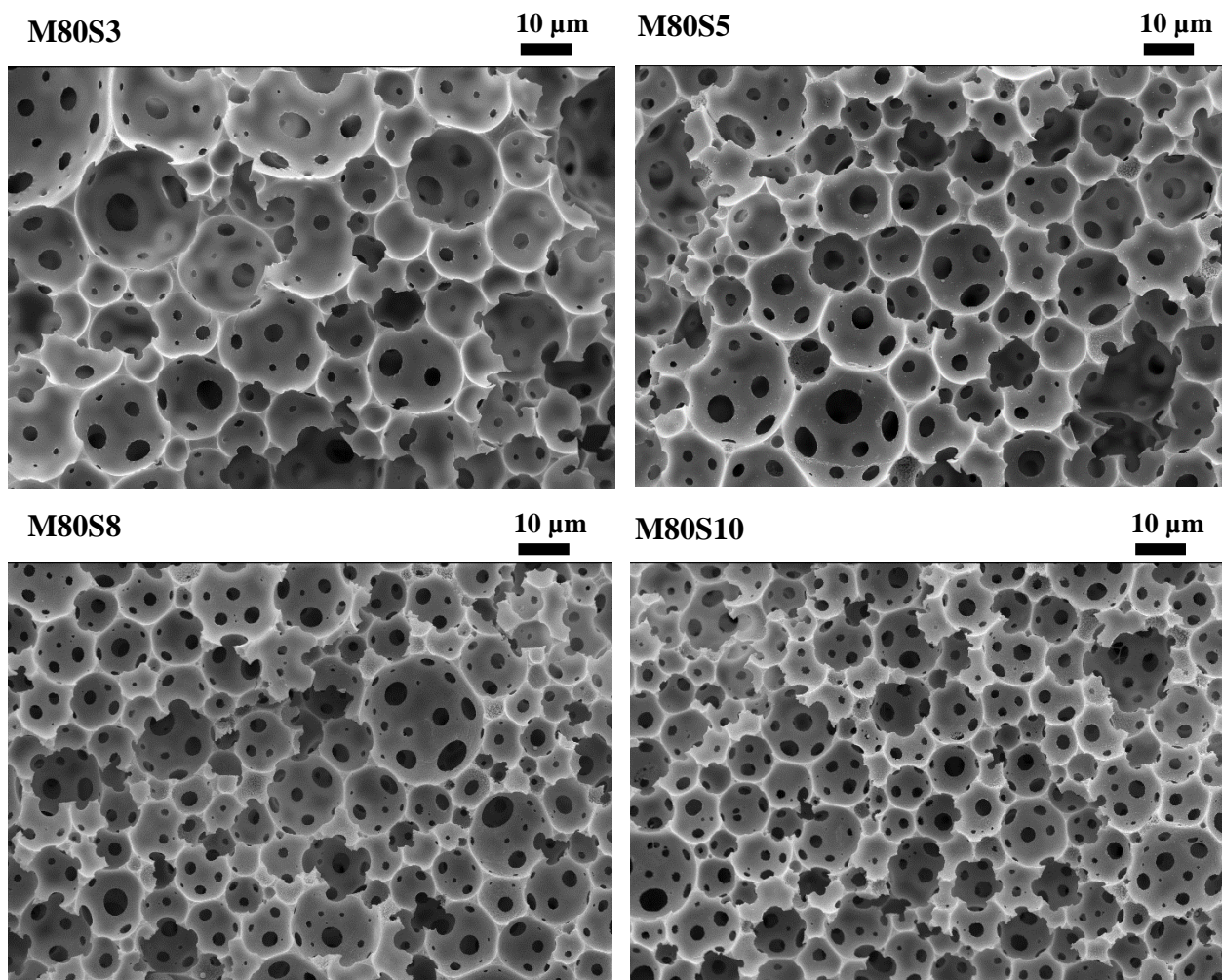


**Figure 3.32.** SEM images of macroporous polymeric materials produced from w/o emulsion templates with different concentration of PEI-121 and fixed water phase 80vol.%. The external oil phase contains 15vol.% of EGDMA, 1 wt/vol.% of BPO, 1.19 vol.% DMPT and varied 3-10wt/vol.% PEI-121, all dissolved in MMA. The water phase is deionised water.

**Table 3.9.** Void diameters (DN0.1, DN0.5 and DN0.9) determined from SEM images of polymeric materials produced from w/o emulsion templates with fixed volume fraction of water ( $\phi_w$ ) at 80vol.% and vary the surfactant concentration in respect to the oil phase,  $C_{SO} = 0.4-10$  wt/vol.%. The external oil phase contains 15vol.% of EGDMA, 1 wt/vol.% BPO, 1.19 vol.% DMPT and variable PEL-121 surfactant concentration,  $C_{SO}$ , all dissolved in MMA. The water phase is deionised water.

Sample code	$C_{SO}$ /wt/vol.%	DN0.1/ $\mu$ m	DN0.5/ $\mu$ m	DN0.9/ $\mu$ m	Span
<b>M80S0.4</b>	0.4	53.9 $\pm$ 4.6	88.7 $\pm$ 7.2	359.6 $\pm$ 189.1	3.5 $\pm$ 2.2
<b>M80S0.5</b>	0.5	21.6 $\pm$ 2.0	35.3 $\pm$ 3.3	93.0 $\pm$ 19.3	2.0 $\pm$ 0.6
<b>M80S0.8</b>	0.8	30.8 $\pm$ 2.4	46.0 $\pm$ 3.6	97.2 $\pm$ 14.2	1.4 $\pm$ 0.4
<b>M80S1</b>	1.0	23.8 $\pm$ 1.5	35.2 $\pm$ 2.6	73.4 $\pm$ 12.9	1.4 $\pm$ 0.4
<b>M80S3</b>	3.0	17.5 $\pm$ 1.4	24.7 $\pm$ 1.5	45.0 $\pm$ 7.4	1.1 $\pm$ 0.4
<b>M80S5</b>	5.0	13.7 $\pm$ 1.0	18.7 $\pm$ 1.0	28.6 $\pm$ 2.6	0.8 $\pm$ 13.7
<b>M80S8</b>	8.0	9.9 $\pm$ 0.8	13.5 $\pm$ 0.6	18.9 $\pm$ 1.2	0.7 $\pm$ 0.2
<b>M80S10</b>	10.0	8.1 $\pm$ 0.6	11.3 $\pm$ 0.6	16.91.2	0.8 $\pm$ 8.1

**Table 3.10.** Pore throats diameters (DN0.1, DN0.5 and DN0.9) determined from SEM images of polymeric materials produced from w/o emulsion templates with fixed volume fraction of water ( $\phi_w$ ) at 80vol.% and vary the surfactant concentration in respect to the oil phase,  $C_{SO} = 0.4-10$  wt/vol.%. The external oil phase contains 15vol.% of EGDMA, 1 wt/vol.% BPO, 1.19 vol.% DMPT and variable PEL-121 surfactant concentration,  $C_{SO}$ , all dissolved in MMA. The water phase is deionised water.

Sample code	$C_{SO}$ / wt/vol.%	DN0.1/ $\mu$ m	DN0.5/ $\mu$ m	DN0.9/ $\mu$ m	Span
<b>M80S0.4</b>	0.4	4.18 $\pm$ 0.37	7.38 $\pm$ 0.54	13.23 $\pm$ 2.02	1.23 $\pm$ 0.34
<b>M80S0.5</b>	0.5	1.73 $\pm$ 0.19	3.28 $\pm$ 0.26	7.14 $\pm$ 1.21	1.65 $\pm$ 0.45
<b>M80S0.8</b>	0.8	2.14 $\pm$ 0.23	4.32 $\pm$ 0.54	9.08 $\pm$ 1.21	1.61 $\pm$ 0.39
<b>M80S1</b>	1.0	2.19 $\pm$ 0.27	4.33 $\pm$ 0.39	7.91 $\pm$ 0.82	1.32 $\pm$ 0.28
<b>M80S3</b>	3.0	2.09 $\pm$ 0.24	3.78 $\pm$ 0.29	6.58 $\pm$ 0.72	1.19 $\pm$ 0.27
<b>M80S5</b>	5.0	2.01 $\pm$ 0.19	3.67 $\pm$ 0.26	6.19 $\pm$ 0.39	1.14 $\pm$ 0.18
<b>M80S8</b>	8.0	1.73 $\pm$ 0.19	3.28 $\pm$ 0.26	7.14 $\pm$ 1.21	1.65 $\pm$ 0.45
<b>M80S10</b>	10.0	1.56 $\pm$ 0.12	2.48 $\pm$ 0.17	4.12 $\pm$ 0.26	1.03 $\pm$ 0.17

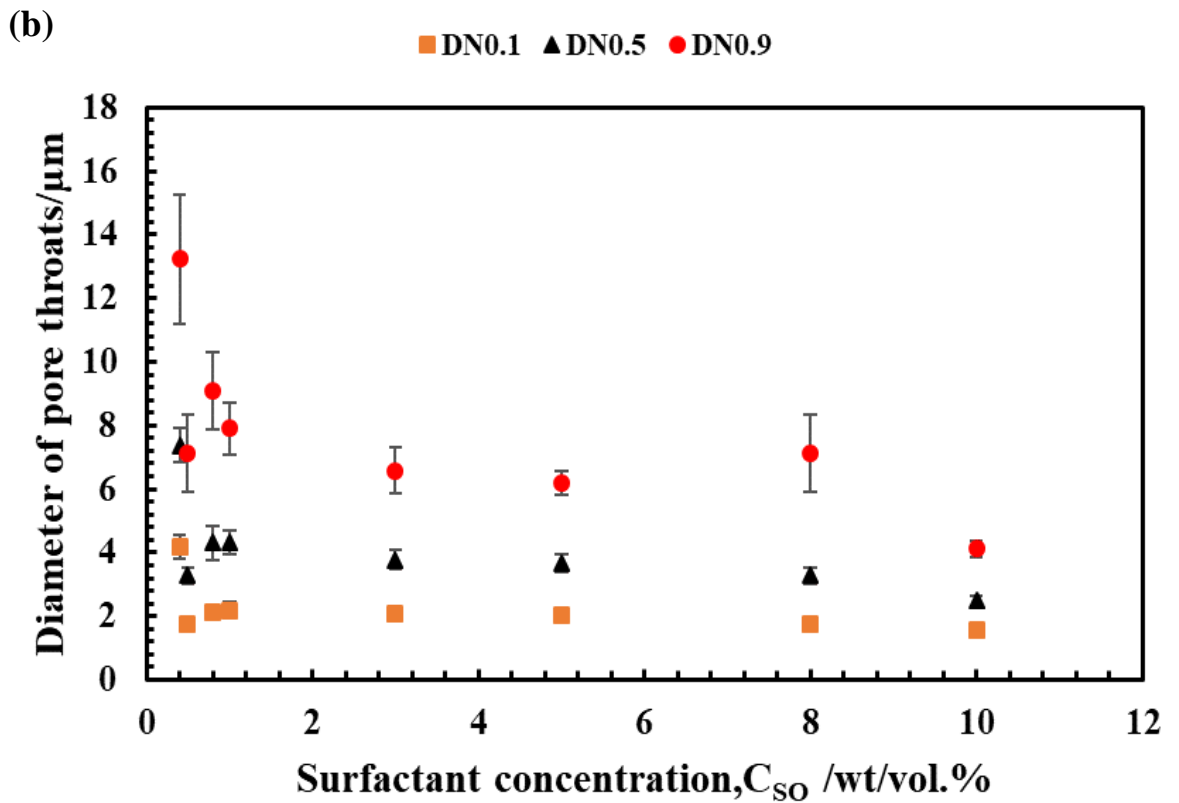
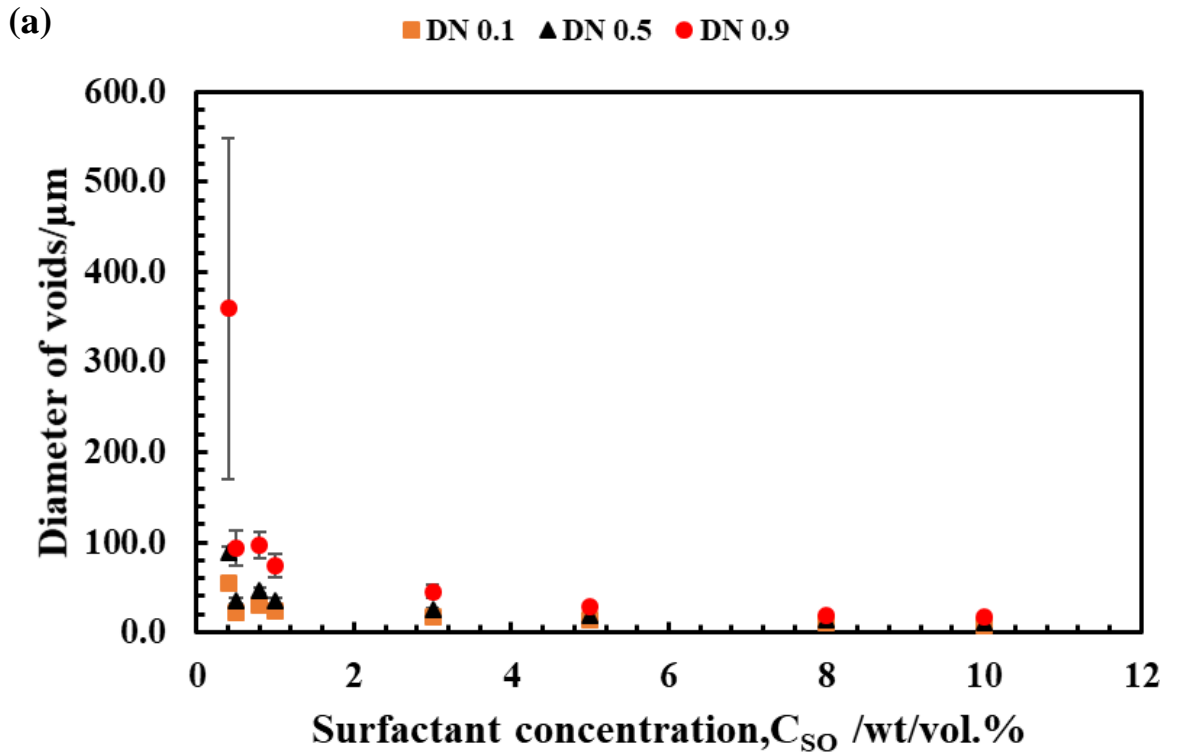


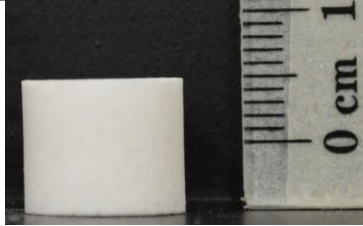
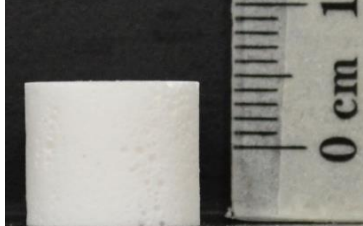
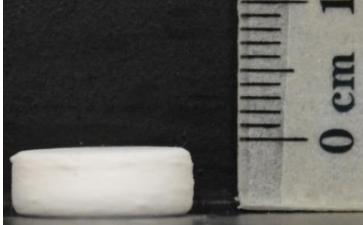
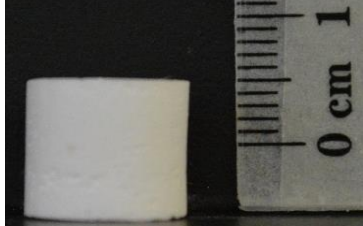
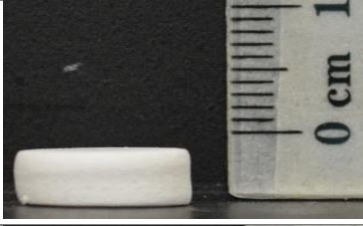
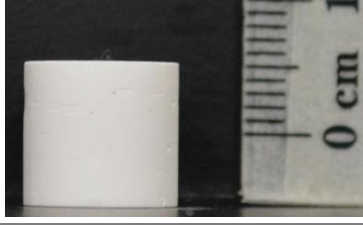
**Figure 3.33.** Diameter of voids (a) and pore throats (b) of porous materials versus PEL-121 surfactant concentration in respect to the oil phase,  $C_{SE}$ . For other details see Tables 3.9 and 3.10. DN0.1, DN0.5 and DN0.9 stand for 10%, 50% and 90% where the diameter's values have less than this value.

The surfactant (PEL-121) concentration affects the mechanical properties. The compression test was performed at room temperature. Images of the samples before and after compression test are shown in Tables 3.11 and 3.12. The elastic modulus and strength (at 10% strain) have an initial increase until reached maximum value at 1wt/vol.% and after that they decrease with the increase of the concentration of the surfactant (see Table 3.13, Fig.3.34). Bismarck's group has observed similar behaviour.<sup>31</sup> He explained that by the uniformity of the wall of the voids is vital for standing the load applied to macroporous materials. The number of the pore throats in the wall of the voids affect the mechanical properties.<sup>32</sup> In addition, the diameter of the voids and the pore throats affects the mechanical properties.

Initial increase of the mechanical properties as you increase the surfactant concentration. The surfactant concentration is very low (0.4-0.8wt/vol.%). As results, the emulsion becomes less stable and generate big voids during the polymerisation. These big voids have a thick wall as the interconnectivity between the droplets is low. In the compression test, the wall of the voids is quite brittle and crushed easily. The behaviour follows the elastic-brittle foam which shows brittle crushing as shown for the sample before and after the test in Table 3.11(see section 1.6 in chapter one).<sup>33</sup>

The highest elastic modulus and strength achieved in our study are at 1wt/vol.% of surfactant. According to Bismarck's group, such maximum could be explained by the fact that the system has reached the optimal balance between the small and large voids. This balance improves the load transfer mechanism under the compression test.<sup>31</sup> After this point, the mechanical properties decreased as the surfactant concentration increased. Williams has also found an optimal surfactant concentraion in his studies.<sup>13, 27</sup> At low surfactant concentration the quality of the foam product was poor. At a very high concentration of surfactant, the foam could not retain its shape and became like powder. The optimal concentration found was 20-50% with respect to the oil phase.<sup>27</sup> He explained the decrease in the mechanical properties with increasing of surfactant concentration in relation to the emulsion stability. The film between the droplets is thinning as the surfactant concentration increased. As results, the number of pore throats rose in the wall of the voids. The reason for that is the film between the droplets is thin, and there is enormous contact between the droplets so that the pore throats are formed. The wall of the voids cannot stand the load applied as the wall is thin and the number of pore throat is high. Thus the materials become weaker.

**Table 3.11.** Images of porous materials before and after the compression test. For the sample composition see Table 3.13.

Sample code	Before testing	After testing
M80S0.4		
M80S0.5		
M80S0.8		
M80S1		
M80S3		
M80S5		

**Table 3.12.** Images of porous materials before and after the compression test. For the sample composition see Table 3.13.

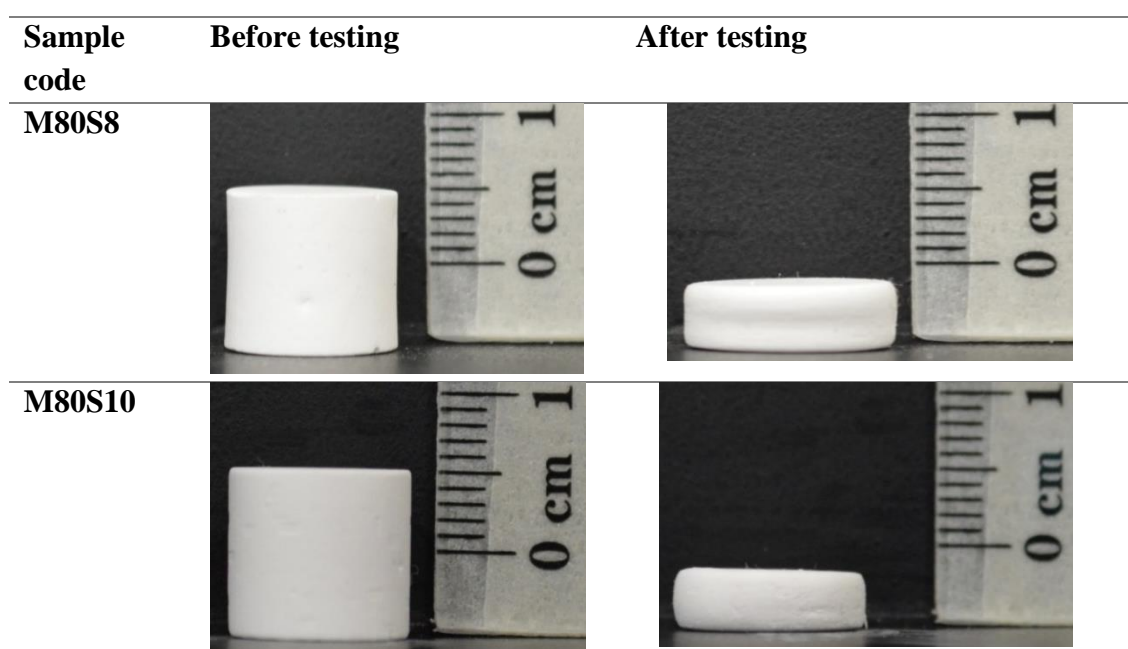


**Table 3.13.** The density, porosity, elastic modulus and strength (at 10 % strain) of porous materials produced by redox-initiated polymerisation from emulsion templates with fixed volume fractions of the internal water phase,  $\phi_w = 80\text{vol}\%$ . The external oil phase is made of 15vol.% EGDMA, variable surfactant concentration (PEL-121) in respect to the oil phase,  $C_{so} = 0.4\text{-}10\text{wt/vol.}\%$ , 1wt/vol.% of BPO and 1.19 vol.% DMPT, all dissolved in MMA. The water phase is deionised water.

Sample code	$C_{so}$ / wt/vol.%	Density /g/cm <sup>3</sup>	Porosity /%	Elastic Modulus /MPa	Strength /MPa
M80S0.4	0.4	0.202±0.002	83±2	58.4±1.6	3.31±0.14
M80S0.5	0.5	0.201±0.003	83±2	69.0±1.0	3.64±0.21
M80S0.8	0.8	0.200±0.002	83±2	73.2±0.8	3.87±0.08
M80S1	1.0	0.202±0.003	83±2	74.2±1.1	4.06±0.07
M80S3	3.0	0.197±0.001	84±2	71.2±0.5	3.46±0.04
M80S5	5.0	0.197±0.002	84±2	66.7±0.7	3.30±0.07
M80S8	8.0	0.192±0.001	84±2	64.0±1.0	3.06±0.04
M80S10	10.0	0.194±0.003	84±2	60.9±1.0	2.94±0.12

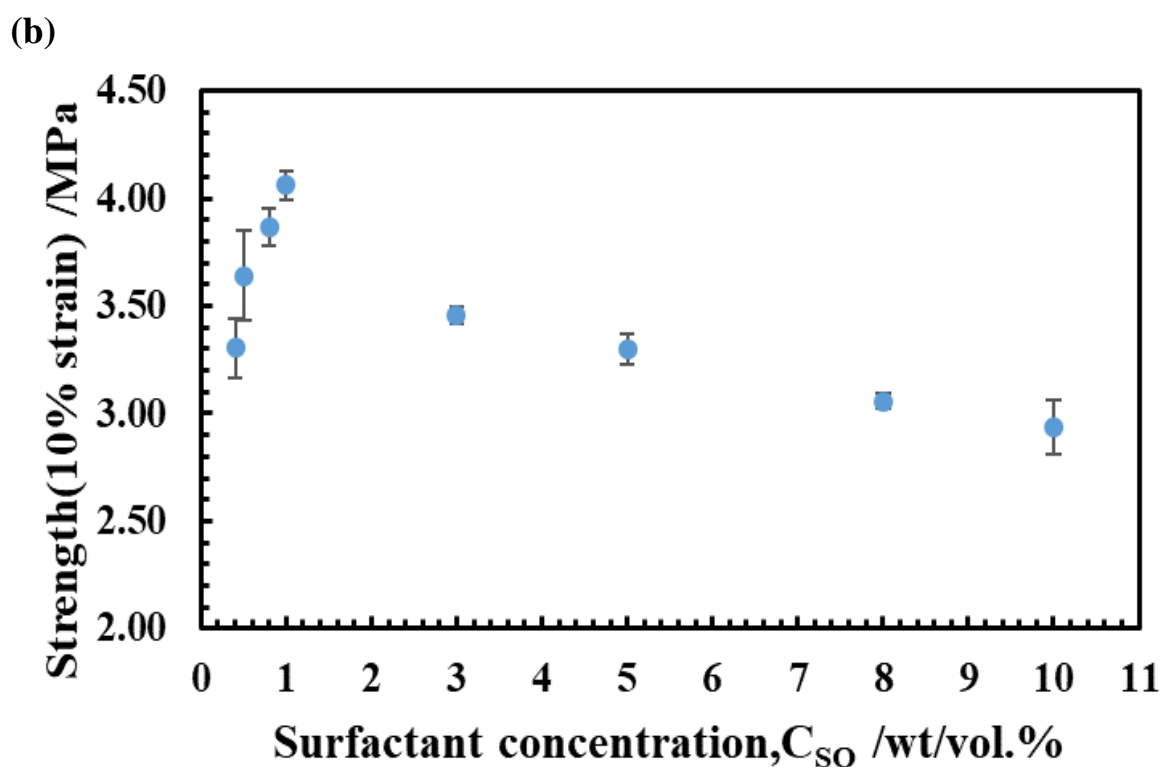
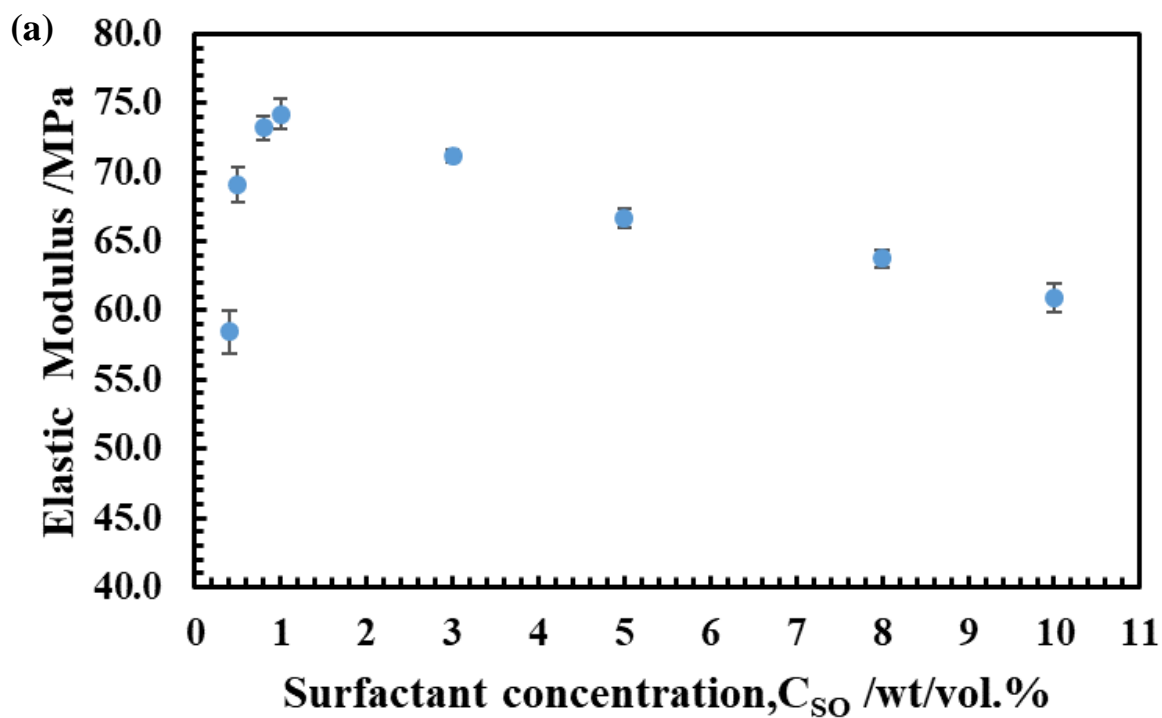


**Figure 3.34.** The elastic modulus (a) and the strength (10% strain) (b) versus the surfactant concentration in respect to the oil phase for porous materials produced by redox-initiated polymerisation from emulsion templates with different concentration of surfactant constant and fixed the water phase at 80vol.% in the emulsion template (see Table 3.13).

### 3.4 Effect of cross-linker concentration on the properties of polyHIPEs at a fixed volume fraction of water in the emulsion template

In the previous section, we studied the effect of surfactant concentration (PEL-121), so it would be interesting to see how varying the concentration of crosslinker (EGDMA) influence the mechanical properties and the morphology of polyHIPEs. The concentration of crosslinker (EGDMA) varied from 5-50vol.%. The oil phase made of 1wt/vol.% of BPO, 5wt/vol.% of PEL-121, EDMA (vary from 5-50vol.%) and 1.19vol.% DMPT all dissolved in MMA. The water phase (deionised water) fixed at 80vol.%. The emulsion template prepared as described in section 2.1.1. The samples produced in the range from 5-35vol.% were without any defects even after drying (see Figs.3.35-3.39). Whereas, the sample at 50vol.% cracks upon drying overnight (see Fig.3.40). This possible explanation for that is the polymer is highly crosslinked. After taken the sample out of Soxhlet extraction and during the drying the polymer shrank. Due to a high degree of crosslinker, the polymer shrinkage. As results, the polymer cracks during the drying process.<sup>17</sup>

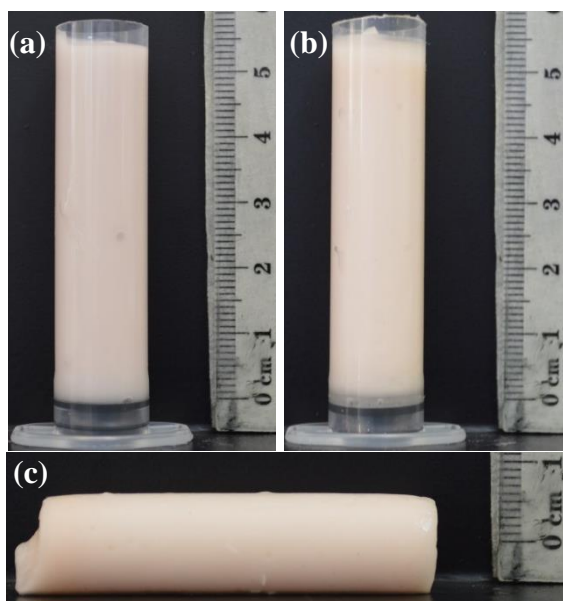


**Figure 3.35.** Images of the mould loaded with w/o emulsion template (a) before polymerisation and (b) after polymerisation at room temperature overnight. (c) An image of the solid material after demoulding. The emulsion template contains 80 vol.% internal phase of deionised water. The external oil phase is made of 5vol.% EGDMA, 5wt/vol.% PEL-121 surfactant, 1wt/vol.% of BPO and 1.19 vol.% DMPT all dissolved in MMA.

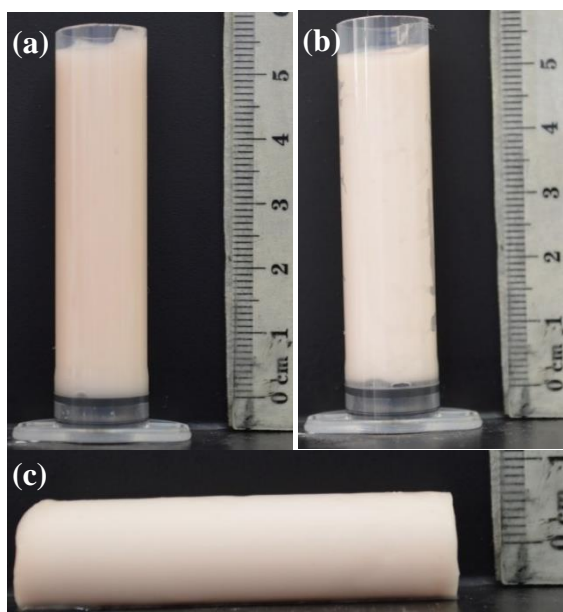


**Figure 3.36.** Images of the mould loaded with w/o emulsion template (a) before polymerisation and (b) after polymerisation at room temperature overnight. (c) An image of the solid material after demoulding. The emulsion template contains 80 vol.% internal phase of deionised water. The external oil phase is made of 10vol.% EGDMA, 5wt/vol.% PEL-121 surfactant, 1wt/vol.% of BPO and 1.19 vol.% DMPT all dissolved in MMA.

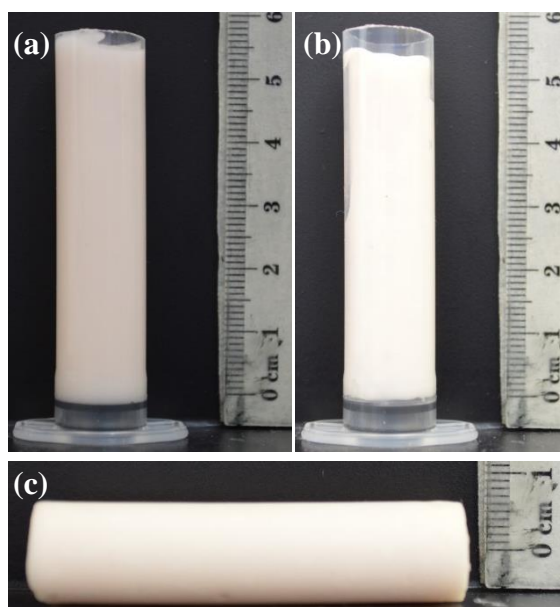


**Figure 3.37.** Images of the mould loaded with w/o emulsion template (a) before polymerisation and (b) after polymerisation at room temperature overnight. (c) An image of the solid material after demoulding. The emulsion template contains 80 vol.% internal phase of deionised water. The external oil phase is made of 15 vol.% EGDMA, 5wt/vol.% PEL-121 surfactant, 1wt/vol.% of BPO and 1.19 vol.% DMPT all dissolved in MMA.

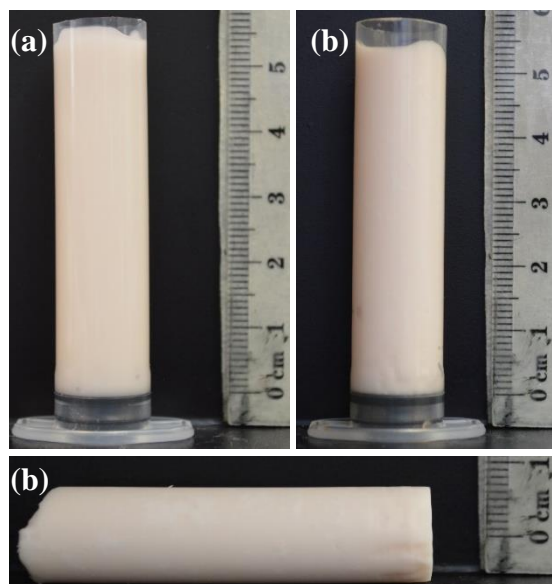


**Figure 3.38.** Images of the mould loaded with w/o emulsion template (a) before polymerisation and (b) after polymerisation at room temperature overnight. (c) An image of the solid material after demoulding. The emulsion template contains 80 vol.% internal phase of deionised water. The external oil phase is made of 30vol.% EGDMA, 5wt/vol.% PEL-121 surfactant, 1wt/vol.% of BPO and 1.19 vol.% DMPT all dissolved in MMA.

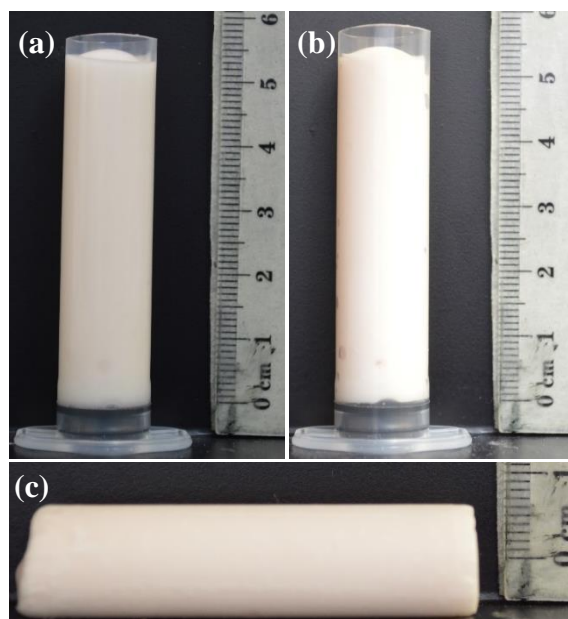


**Figure 3.39.** Images of the mould loaded with w/o emulsion template (a) before polymerisation and (b) after polymerisation at room temperature overnight. (c) An image of the solid material after demoulding. The emulsion template contains 80 vol.% internal phase of deionised water. The external oil phase is made of 35vol.% EGDMA, 5wt/vol.% PEL-121 surfactant, 1wt/vol.% of BPO and 1.19 vol.% DMPT all dissolved in MMA.



**Figure 3.40.** An images of the solid material after demoulding and drying at room temperature. The sample cracked during the drying process. The emulsion template contains 80 vol.% internal phase of deionised water. The external oil phase is made of 50vol.% EGDMA, 5wt/vol.% PEL-121 surfactant, 1wt/vol.% of BPO and 1.19 vol.% DMPT all dissolved in MMA.

The morphology of PolyHIPEs with varying the crosslinker (EGDMA) concentration in the oil phase was studied with SEM imaging (see Fig.3.41).The voids are connected with pore throats (open structure) as can be seen from the SEM images. The diameter of voids and pore throats decreased with rising the concentration of crosslinker (EGDMA) see Table 3.14-3.15 and Fig.3.42. The diameter of voids at 5vol% EGDMA is  $DN_{0.5} = 18.9 \pm 1.2 \mu\text{m}$ ) but dropped to  $14.2 \pm 0.7 \mu\text{m}$  at 50vol% EGDMA. Whereas, the pore throats at 5vol% EGDMA is ( $DN_{0.5} = 4.2 \pm 0.2 \mu\text{m}$ ) decreased to ( $DN_{0.5} = 2.5 \pm 0.2 \mu\text{m}$ ) at 50vol% EGDMA. The emulsion stability could explain the decrease in the diameters of voids and pore throats. Williams studied the effect of the crosslinker concentration in the diameter of the void for the system styrene/DVB. The diameter of the voids dropped from  $15 \mu\text{m}$  to  $6 \mu\text{m}$ . It was hypothesised that the decreases in the diameter of the voids were related to the decrease in the internal phase droplets diameter in the HIPE. The increases of DVB increases the emulsion stability and generate small droplets due to the difference in the interfacial tension between the monomer and the crosslinker.<sup>17</sup> However, in our system not only the emulsion stability increased, but the rate of polymerisation also increased as the crosslinker concentration increased as well.<sup>34</sup> This increased in the rate of polymerisation could help the emulsion stability. The process of coalescence reduced greatly due to the fast polymerisation as well as Ostwald ripening. As a result, the droplets diameter of the internal phase would be similar to the diameter of the void. The decrease of the pore throats diameter could be related to the diameter of the internal phase droplets of the HIPE. As the droplets diameter of the internal phase decreased, the area of contact between the droplets reduced.

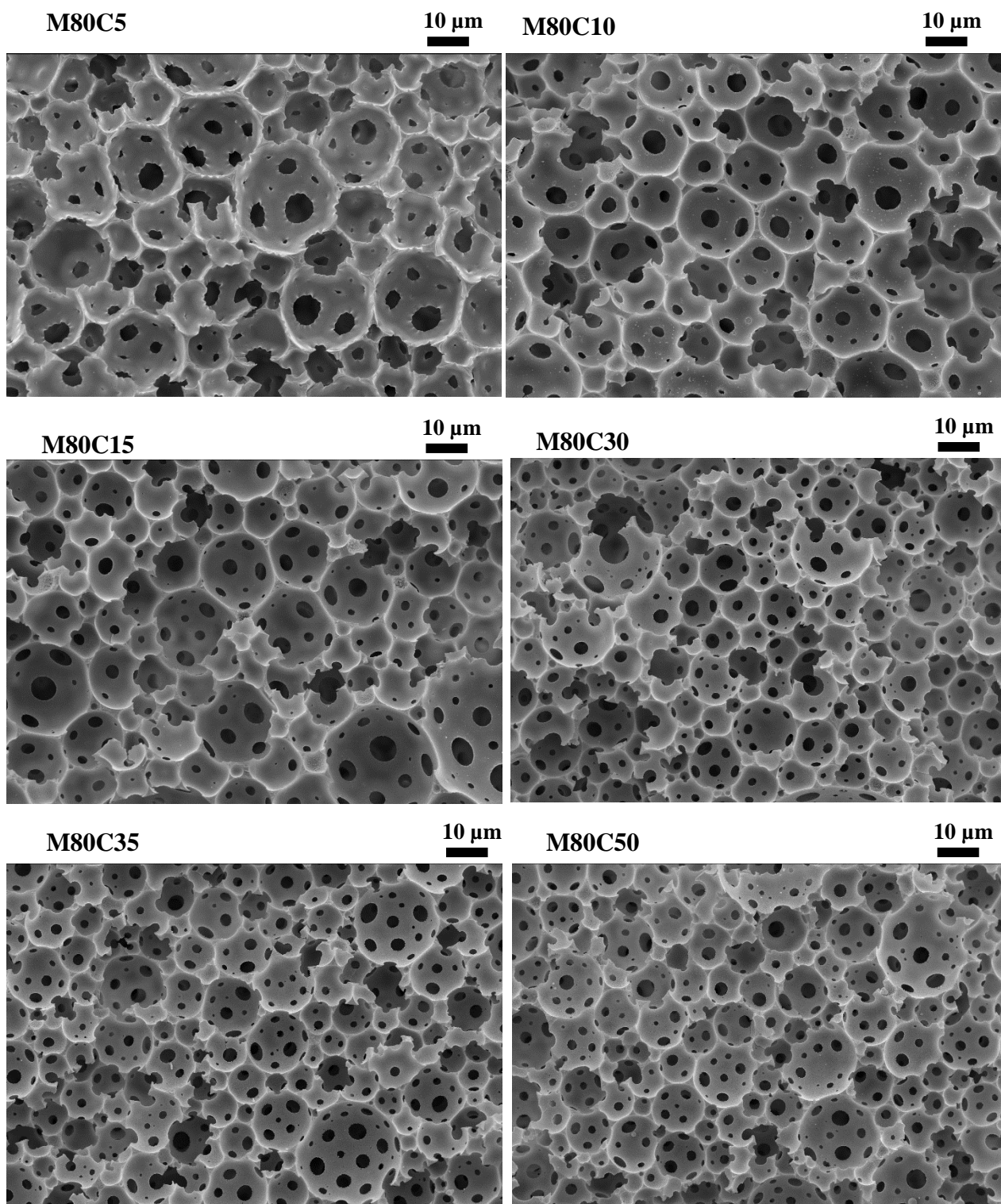


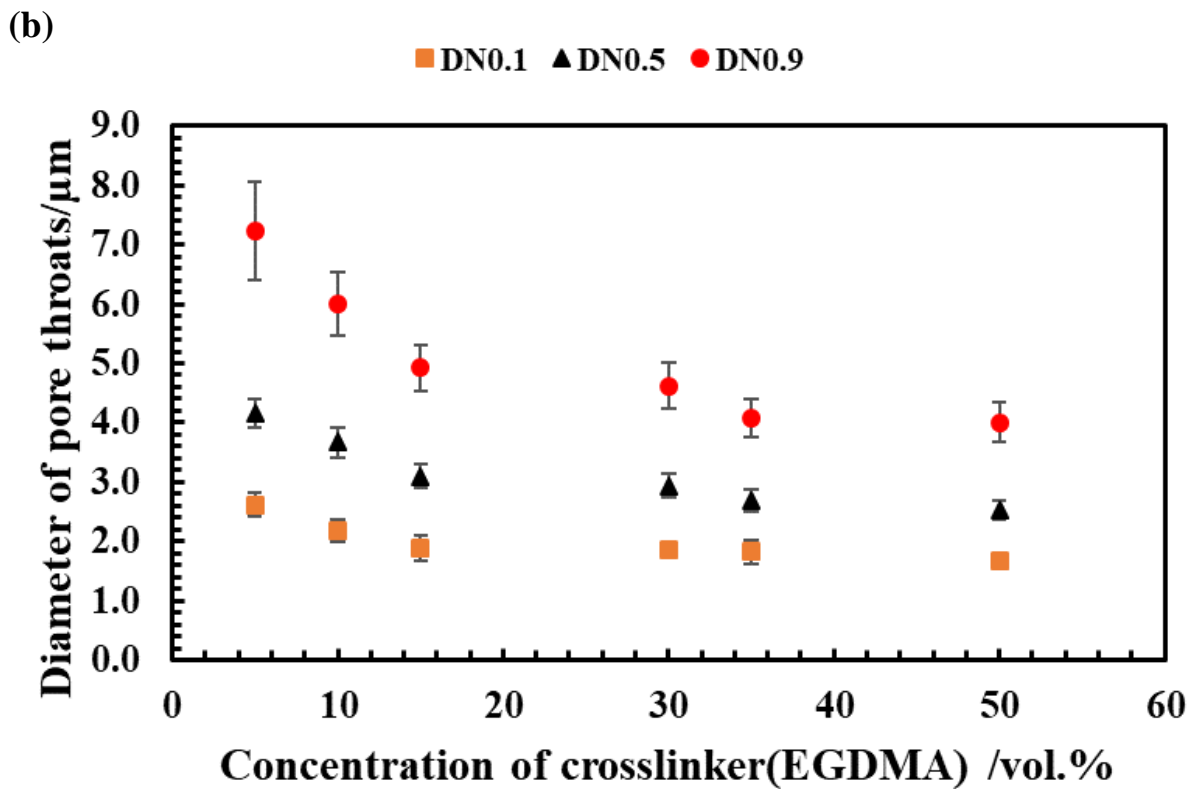
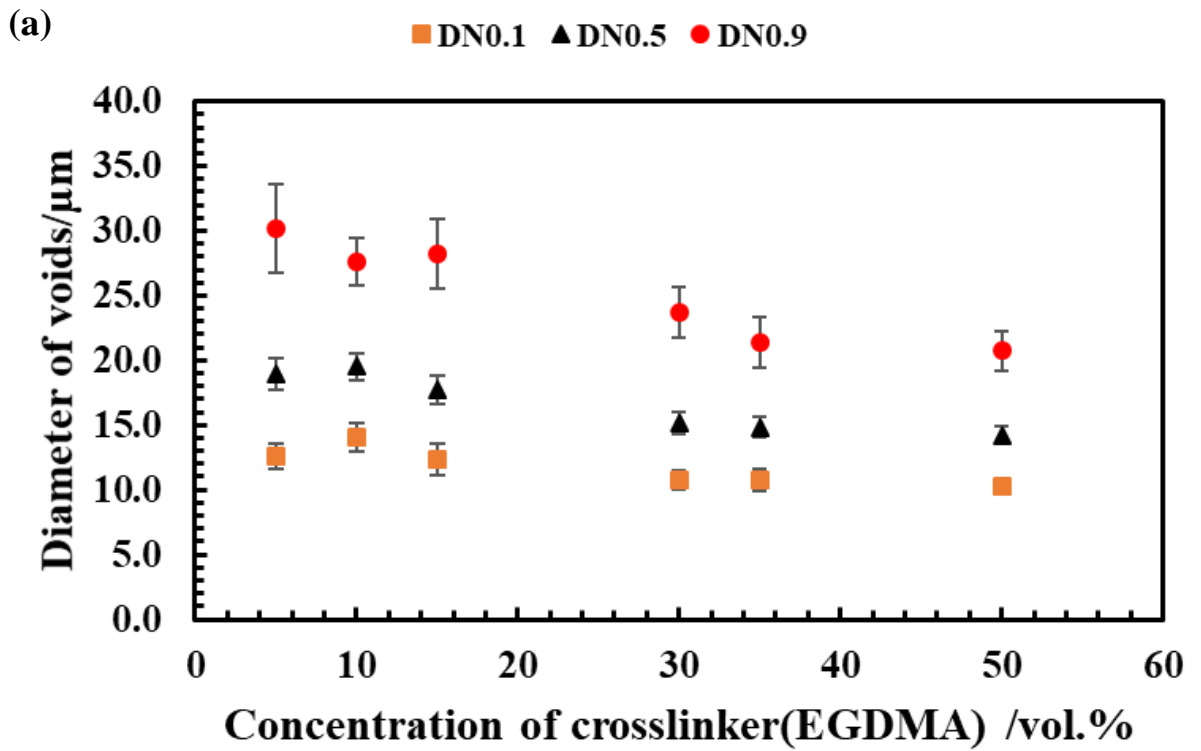
**Figure 3.41.** SEM images of macroporous polymeric materials produced from w/o emulsion templates with different crosslinker concentration (EGDMA) and fixed water phase at 80vol.%. The external oil phase contains varied 5-50 vol.% of EGDMA, 1 wt/vol.% of BPO, 1.19 vol.% DMPT and 5wt/vol.% PEL-121, all dissolved in MMA. The water phase is deionised water.

**Table 3.14.** Void diameters (DN0.1, DN0.5 and DN0.9) determined from SEM images of polymeric materials produced from w/o emulsion templates with fixed volume fraction of water ( $\phi_w$ ) at 80vol.% and vary the crosslinker concentration in respect to the oil phase 5-50vol.%. The external oil phase contains variable concentration of crosslinker (EGMDA) 5-50 vol.%, 1 wt/vol.% BPO, 1.19 vol.% DMPT and 5wt/vol.% PEL-121, all dissolved in MMA. The water phase is deionised water.

Sample code	EGDMA / vol.%	DN0.1/ $\mu\text{m}$	DN0.5/ $\mu\text{m}$	DN0.9/ $\mu\text{m}$	Span
<b>M80C5</b>	5	12.60 $\pm$ 0.94	18.94 $\pm$ 1.23	30.20 $\pm$ 3.41	0.93 $\pm$ 0.24
<b>M80C10</b>	10	14.70 $\pm$ 1.11	19.50 $\pm$ 1.04	27.66 $\pm$ 1.85	0.70 $\pm$ 0.16
<b>M80C15</b>	15	12.37 $\pm$ 1.24	17.69 $\pm$ 1.12	28.22 $\pm$ 2.67	0.90 $\pm$ 0.23
<b>M80C30</b>	30	10.73 $\pm$ 0.72	15.14 $\pm$ 0.81	23.74 $\pm$ 1.93	0.86 $\pm$ 0.18
<b>M80C35</b>	35	10.74 $\pm$ 0.84	14.83 $\pm$ 0.78	21.37 $\pm$ 1.99	0.72 $\pm$ 0.19
<b>M80C50</b>	50	10.31 $\pm$ 0.60	14.23 $\pm$ 0.66	20.72 $\pm$ 1.54	0.73 $\pm$ 0.15

**Table 3.15.** Void diameters (DN0.1, DN0.5 and DN0.9) determined from SEM images of polymeric materials produced from w/o emulsion templates with fixed volume fraction of water ( $\phi_w$ ) at 80vol.% and vary the crosslinker concentration in respect to the oil phase 5-50vol.%. The external oil phase contains variable concentration of crosslinker (EGMDA) 5-50 vol.%, 1 wt/vol.% BPO, 1.19 vol.% DMPT and 5wt/vol.% PEL-121, all dissolved in MMA. The water phase is deionised water.

Sample code	EGDMA / vol.%	DN0.1/ $\mu\text{m}$	DN0.5/ $\mu\text{m}$	DN0.9/ $\mu\text{m}$	Span
<b>M80C5</b>	5	2.62 $\pm$ 0.20	4.16 $\pm$ 0.24	7.23 $\pm$ 0.83	1.11 $\pm$ 0.26
<b>M80C10</b>	10	2.17 $\pm$ 0.19	3.67 $\pm$ 0.25	6.00 $\pm$ 0.54	1.04 $\pm$ 0.21
<b>M80C15</b>	15	1.88 $\pm$ 0.21	3.10 $\pm$ 0.21	4.93 $\pm$ 0.39	0.98 $\pm$ 0.20
<b>M80C30</b>	30	1.87 $\pm$ 0.13	2.93 $\pm$ 0.20	4.62 $\pm$ 0.39	0.94 $\pm$ 0.19
<b>M80C35</b>	35	1.82 $\pm$ 0.19	2.69 $\pm$ 0.18	4.08 $\pm$ 0.32	0.84 $\pm$ 0.20
<b>M80C50</b>	50	1.66 $\pm$ 0.13	2.53 $\pm$ 0.16	4.01 $\pm$ 0.34	0.93 $\pm$ 0.19

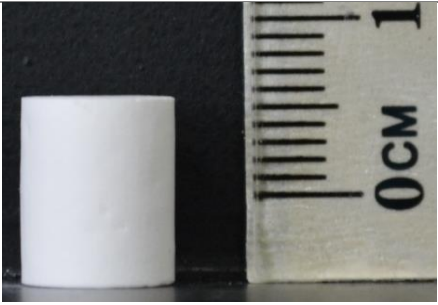
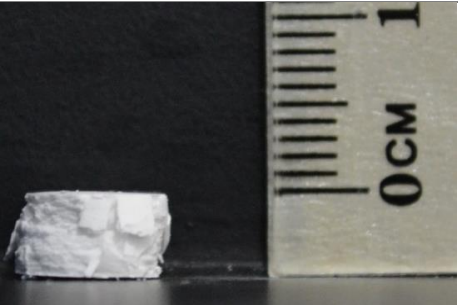
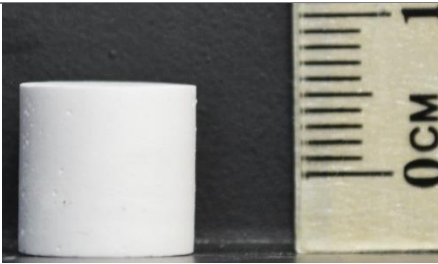
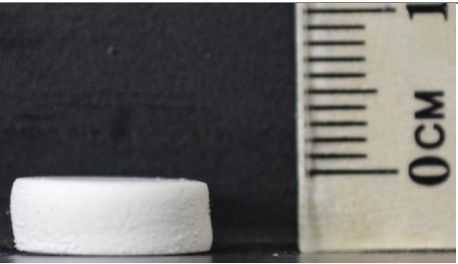
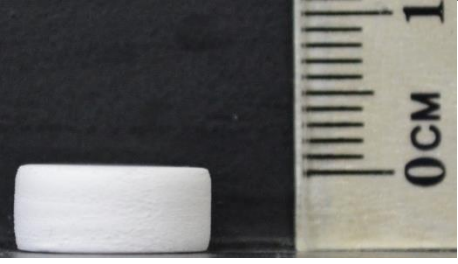
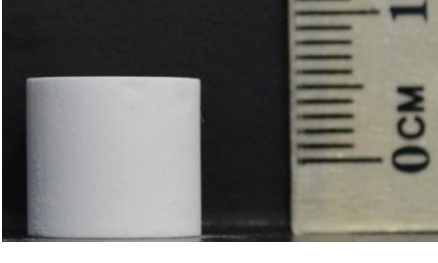
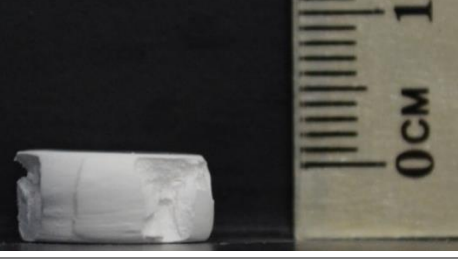


**Figure 3.42.** Diameter of voids (a) and pore throats (b) of porous materials versus crosslinker concentration (EGDMA). For other details see Tables 3.14 and 3.15. DN0.1, DN0.5 and DN0.9 stand for 10%, 50% and 90% where the diameter's values have less than this value.

The crosslinker (EGDMA) concentration has influenced the mechanical properties. The compression test performed at room temperature. Images of the samples before and after the compression test (See Table 3.16). The mechanical properties of macroporous polymeric materials decreases as the concentration of crosslinker (EGDMA) increases (see Tables 3.17 and Figs.3.43-3.44).The sample at the lowest (M80C5) and the highest (M80C35) concentration of crosslinker cracks from the sides during the compression test (see Table 3.16). This cracks on the sides of the samples indicate that the ratio between the monomer and the crosslinker is important. The ratio has to be adjusted to produce the desired materials. The elastic modulus decreased by 56%, and the strength (10% strain) fell by 38% as the concentration of crosslinker rose. This decrease in the mechanical properties was due to (EGDMA) replacing the monomer (MMA) as the concentration increases. It is true that the degree of crosslinking increases as the crosslinker concentration increases. However, at high concentration of crosslinker, not all EGDMA serves as a crosslinker due to not all the double bound can react. Thus this affects the backbone of the polymer regarding stiffness and brittleness.<sup>35</sup> Interestingly, Bismarck used EGDMA as crosslinker to reduce the brittleness of the materials.<sup>28, 32</sup>

The curing time of this study of varying the concentration of crosslinker (EGDMA) at fixed volume fraction of the water phase (80vol.%) was studied. The increase of EGDMA decreased the curing time drastically as at 5 and 30vol.% the curing time is 6544 and 762 s respectively (see Table 3.18). The EGDMA increase the rate of polymerisation because it has similar reactive group to the monomer (MMA). The mechanical properties in the range from 10-35vol.% of EGDMA have quite close values. In contrast, the curing time is varied at 10vol.% = 2064s and 35vol.% = 762s. The advantage here is that the curing time can be tuned for the same mechanical properties of porous polymeric materials for any desire applications needed.

**Table 3.16.** Images of porous materials before and after the compression test. For the sample composition see Table 3.17.

Sample code	Before testing	After testing
M80C5		
M80C10		
M80C15		
M80C30		
M80C35		

**Table 3.17.** The density, porosity, elastic modulus and strength (at 10 % strain) of porous materials produced by redox-initiated polymerisation from emulsion templates with fixed volume fractions of the internal water phase,  $\phi_w = 80\text{vol}\%$ . The external oil phase is made of varied 5-35 vol.% EGDMA, 5wt/vol.% PEL-121 surfactant, 1wt/vol.% of BPO and 1.19 vol.% DMPT, all dissolved in MMA. The water phase is deionised water.

Sample code	EGDMA / vol.%	Density /g/cm <sup>3</sup>	Porosity /%	Elastic Modulus /MPa	Strength /MPa
M80C5	5	0.241±0.002	80±2	97.6±2.8	4.54±0.12
M80C10	10	0.204±0.002	83±2	70.9±3.6	3.63±0.05
M80C15	15	0.200±0.001	83±2	69.8±0.5	3.37±0.05
M80C30	30	0.195±0.001	84±2	62.8±1.0	3.23±0.06
M80C35	35	0.199±0.002	83±2	62.5±0.8	3.29±0.09

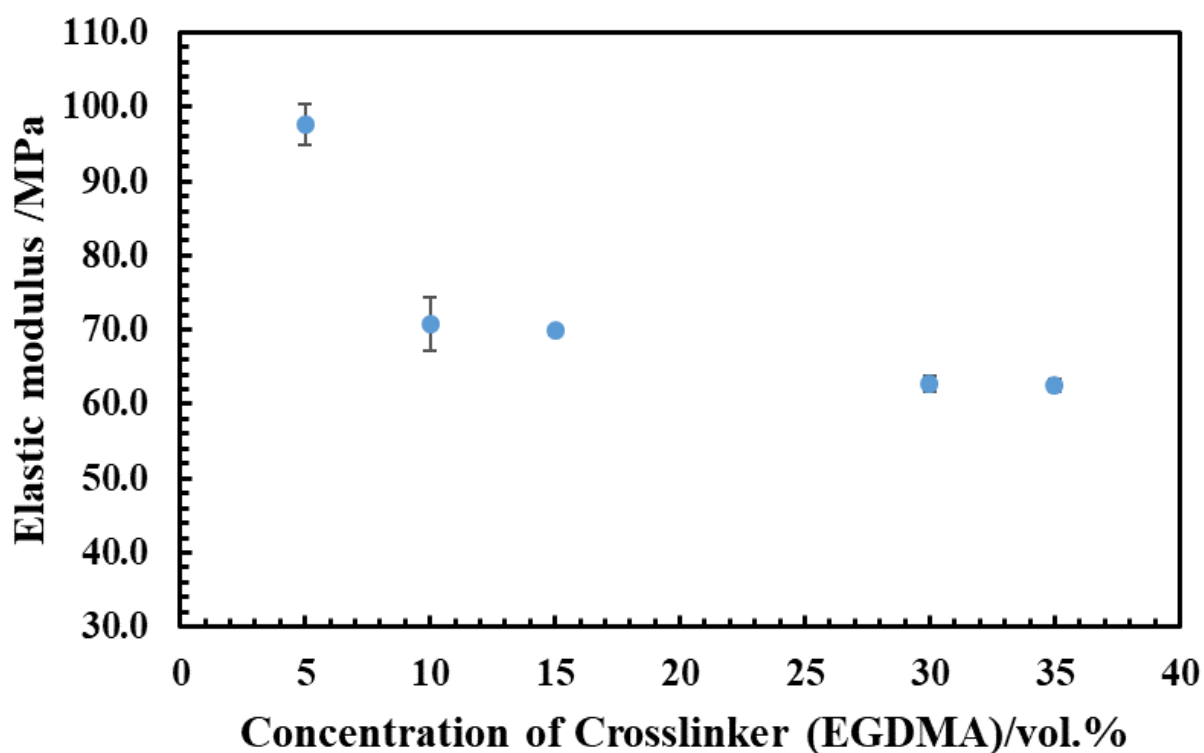


**Figure 3.43.** The elastic modulus versus crosslinker concentration (EGDMA) of porous materials produced by redox-initiated polymerisation from emulsion templates with fixed percentage of the water phase at 80vol.% (see Table 3.17).

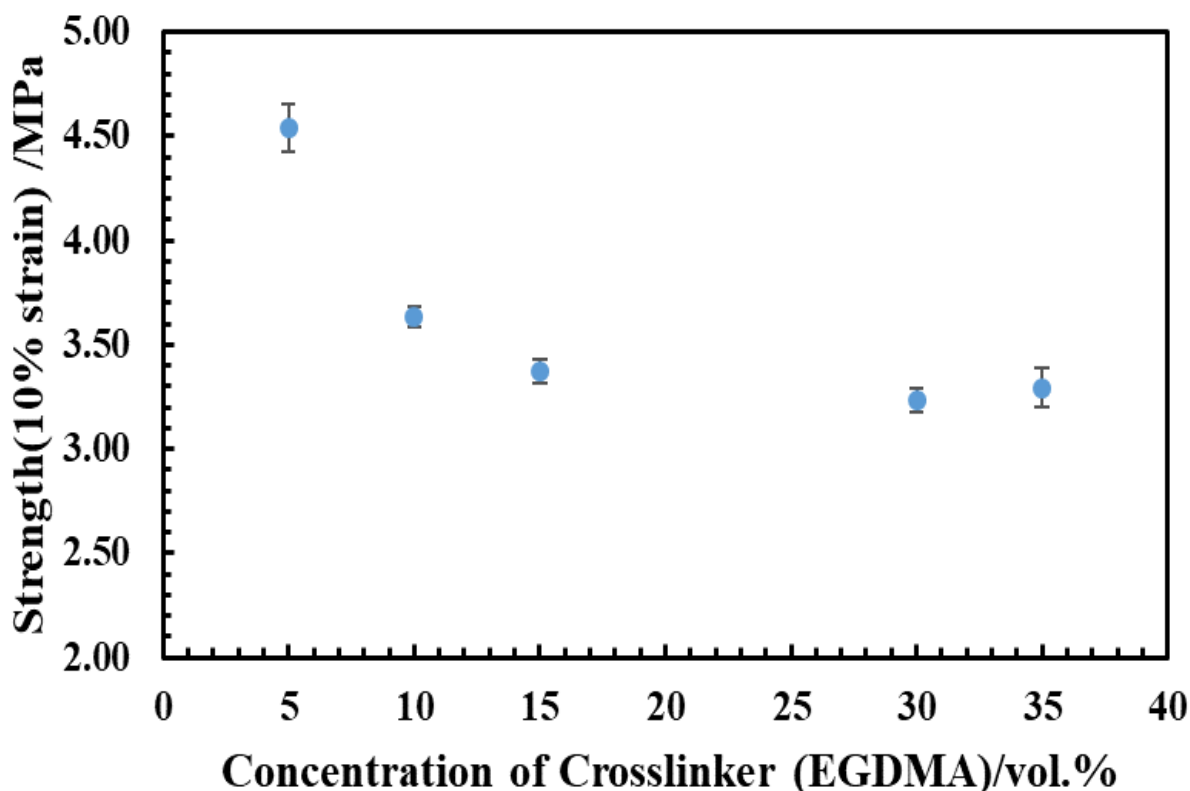


**Figure 3.44.** The strength (at 10% strain) versus crosslinker concentration (EGDMA) of porous materials produced by redox-initiated polymerisation from emulsion templates with fixed percentage of the water phase at 80vol.% (see Table 3.17).

**Table 3.18.** The ‘kick off’ time,  $t_k$ , pot life,  $t_p$ , gelling time,  $t_{gel}$  and maximum temperature,  $T_{max}$  determined during the polymerisation of w/o emulsion templates with fixed volume fraction of water ( $\phi_w = 80\text{vol.}\%$ ) and variable crosslinker concentration (EGDMA) (5-35vol.%) by oscillating probe experiments (see section 2.2.5). The external oil phase contains variable 5-35 vol.% of EGDMA, 1 wt/vol.% BPO, 1.19 vol.% DMPT and 5wt/vol.% PEL-121, all dissolved in MMA. The water phase is deionised water.

Sample code	$\phi_w/\text{vol.}\%$	$t_k/\text{s}$	$t_p/\text{s}$	$t_{gel}/\text{s}$	$T_{max}/\text{ }^\circ\text{C}$
M80C5	5	1430	1715	6544	26
M80C10	10	952	1162	2064	30
M80C15	15	961	1077	1596	33
M80C30	30	604	669	909	33
M80C35	35	540	589	762	33

### 3.5 Applications of macroporous materials produced at room temperature

The polymerisation of the emulsion template without any tedious preparation (purification of the oil phase, N<sub>2</sub> atmosphere, calcium chloride in the water phase .etc) could open a new area of exploiting the macroporous materials applications in the field. One of the remarkable element of our method is that there is no need for any external source of energy (heat or UV light) and the polymerisation occurs at room temperature. In addition, the emulsion template can take any shape of its casting mould. To show the versatility and flexibility of our system we choose different monomer. Benzyl methacrylate (BMA) was selected for this experiment.

The curing time is an important parameter for practical applications. Therefore, the curing dynamics during the polymerisation of w/o emulsion templates by redox-initiation with BPO-DMPT was investigated as described in section 2.2.5. The results for emulsion templates with variable water volume fraction at a fixed concentration of PEL-121 surfactant in the oil phase are summarised in Table 3.19.

**Table 3.19.** The ‘kick off’ time,  $t_k$ , pot life,  $t_p$ , gelling time,  $t_{gel}$  and maximum temperature,  $T_{max}$  determined during the polymerisation of w/o emulsion templates with varying volume fraction of water ( $\phi_w$ ) by oscillating probe experiments (see section 2.2.5). The external oil phase contains 15vol.% of EGDMA, 1 wt/vol.% BPO, 1.19 vol.% DMPT and 5wt/vol.% PEL-121, all dissolved in MMA (samples M65-M90) or benzyl methacrylate (sample B80). The water phase is deionised water.

Sample code	$\phi_w$ /vol.%	$t_k$ / s	$t_p$ /s	$t_{gel}$ / s	$T_{max}$ / °C
M65	65	726	675	1185	39
M70	70	820	862	1622	37
M75	75	901	958	1518	35
M80	80	961	1077	1596	33
M85	85	964	1304	1894	29
M90	90	987	1348	2088	26
B80*	80	156	204	324	26

\*The used the two emulsions method one has the initiator and the other one accelerator, whereas, the rest the accelerator was added directly to the emulsion.

The curing time increases as the water fraction increases in the system for samples (M65-M90). The presence of the water in the system absorb the heat produce from the reaction and slow down the rate of polymerisation. The maximum temperature decreased from 39 to 26°C as the volume fraction of the water phase increased (see Table 3.19). For faster polymerisation benzyl methacrylate was used for the preparation of the filter and the curing time was 324 s and the maximum temperature is 26 °C.

In this demonstration experiment, the aim is to make a filter *in situ* in water. Since the emulsion is in the form of liquid and can take the shape of its casting mould. There will not be any difficulty to make macroporous polymers in any place with any shape. By adjusting the curing time of polymerisation, the emulsion would have enough time to reach the aimed place to form macroporous polymers before polymerised. The emulsion will be inserted in the tube to polymerise in the water. Then, the macroporous polymer formed “filter” will be tested by passing coloured water through it. As it can be seen in the Fig.3.45 a, the set up for the experiment consists of a syringe attached to a syringe pump, a tube connected between the syringe and the conical shape and beaker filled with water. The tubes and the syringe are filled with water. Two emulsions were prepared, Emulsion one is made of 20vol.% oil phase (2wt/vol.% of BPO, 15vol.% of EGDMA, 5wt/vol.% of PEL-121 all dissolved in BMA) and 80vol% water phase (deionised water). Whereas, emulsion two is made of 20vol% (15vol.% of EGDMA, 5wt/vol.% of PEL-121 and 480µL of DMPT all dissolved in BMA) and 80vol.% water phase (deionised water). The reason for making two emulsions is to keep the main component for the rapid polymerisation separated: the initiator (BPO) and the accelerator (DMPT). Therefore, they can be used in the field at any point of use by mixing them in a 1:1 ratio.

In Fig.3.45, a schematic representation is shown which demonstrates the process of making a filter *in situ* (in water). The first step is mixing of the two emulsions in a 1:1 volume ratio. Then, the plastic conical shaped tube was immersed in this mixture. 0.5 mL was withdrawn (at a rate of 4mL/min) from the mixture of the two emulsions into the plastic tube and then this was placed in a beaker of water. The HIPE took around 15-20 min to polymerise in the water. In Fig. 3.45 and 3.46, the process of making the filter is presented. After the polymerisation was completed, ink was introduced into the water for better visualisation when the water passes through the filter. The coloured water was sucked through the filter by the syringe pump (at a rate of 4 mL/min). The coloured water passed through the filter as can be seen from the images. After that, the filter was dried in the fume cupboard at room temperature overnight. The filter was visualised with SEM to know the structure of the bottom surface, sides and the inner structure (see Fig.3.47). The structure was found to be an open porous network. The pores are open at the interface between the water and the polymer and are connected by pore throats that allow the water to pass through quickly.

The simplicity of making a filter *in situ* in water was demonstrated. The experiment shows the ability to make a filter in the field with any desired shape, porosity, mechanical properties and morphology.

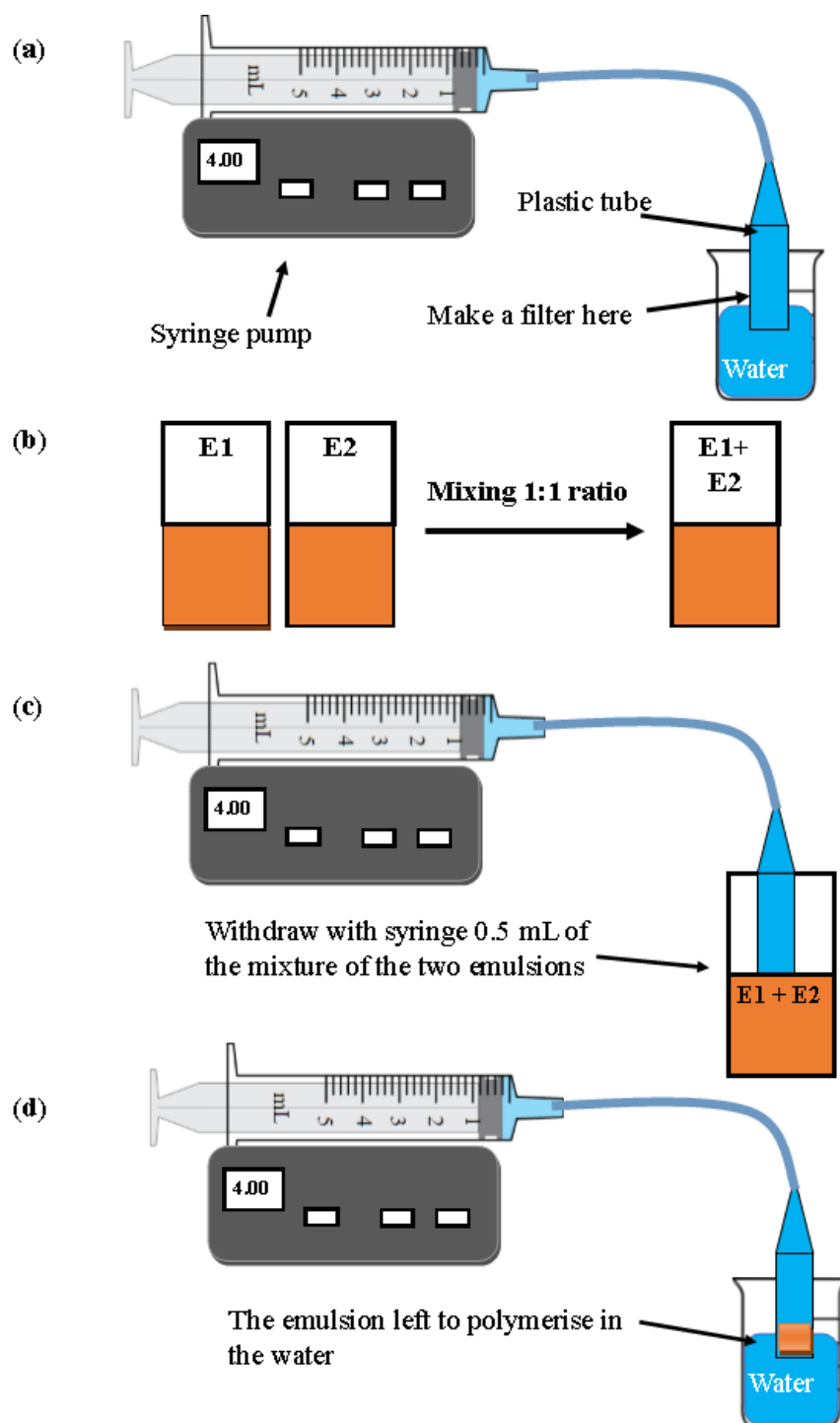


**Figure 3.45.** Schematic representation of the set up for making filter *in situ* in water. (a) The set up for making the filter and the place where the filter be made. (b) The two emulsions, emulsion 1(E1) has BPO as the initiator and emulsion 2 (E2) has DMPT as the accelerator, then mixing the two emulsion in 1:1 ratio. (c) Suck with syringe 0.5 mL of the mixture of the two emulsions to make the filter. (d) The emulsion left to polymerise in the water for about 15-20 minutes.

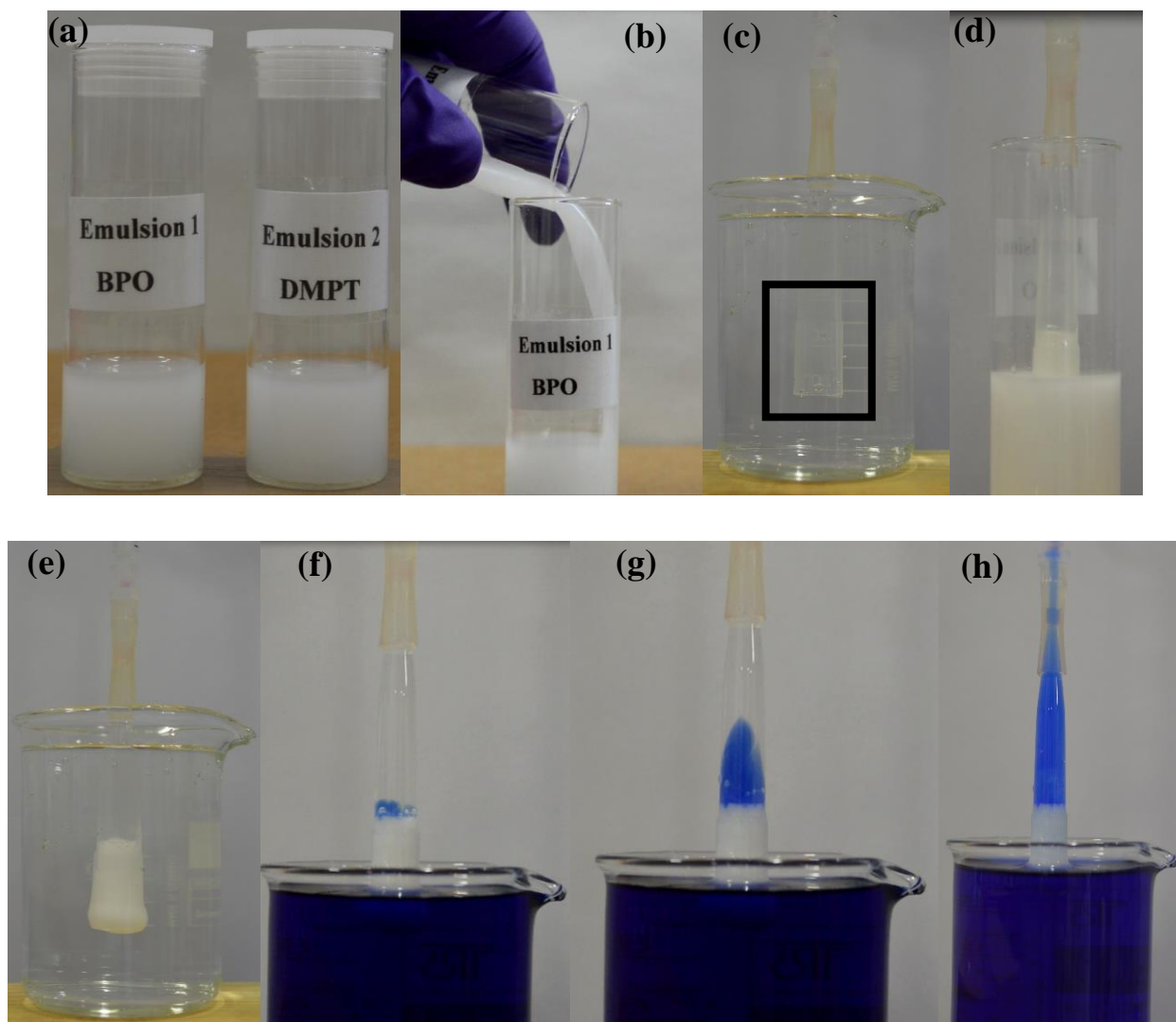


**Figure 3.46.** Pictures presented the process of making filter in situ in water. **(a)** The two emulsions, emulsion 1 has BPO as an initiator and emulsion 2 has DMPT as an accelerator. **(b)** Mixing the two emulsion in ratio 1:1. **(c)** The tube immersed in water and the place of making the filter. **(d)** Sucking 0.5 mL of the mixture of the two emulsion to make the filter in the tube. **(e)** Immersed the tube in water filled with the emulsion to let polymerise for 15-20 min. **(f)** The ink was introduced to colour the water and start sucking through the filter. **(g&h)** the coloured water passes through the filter.

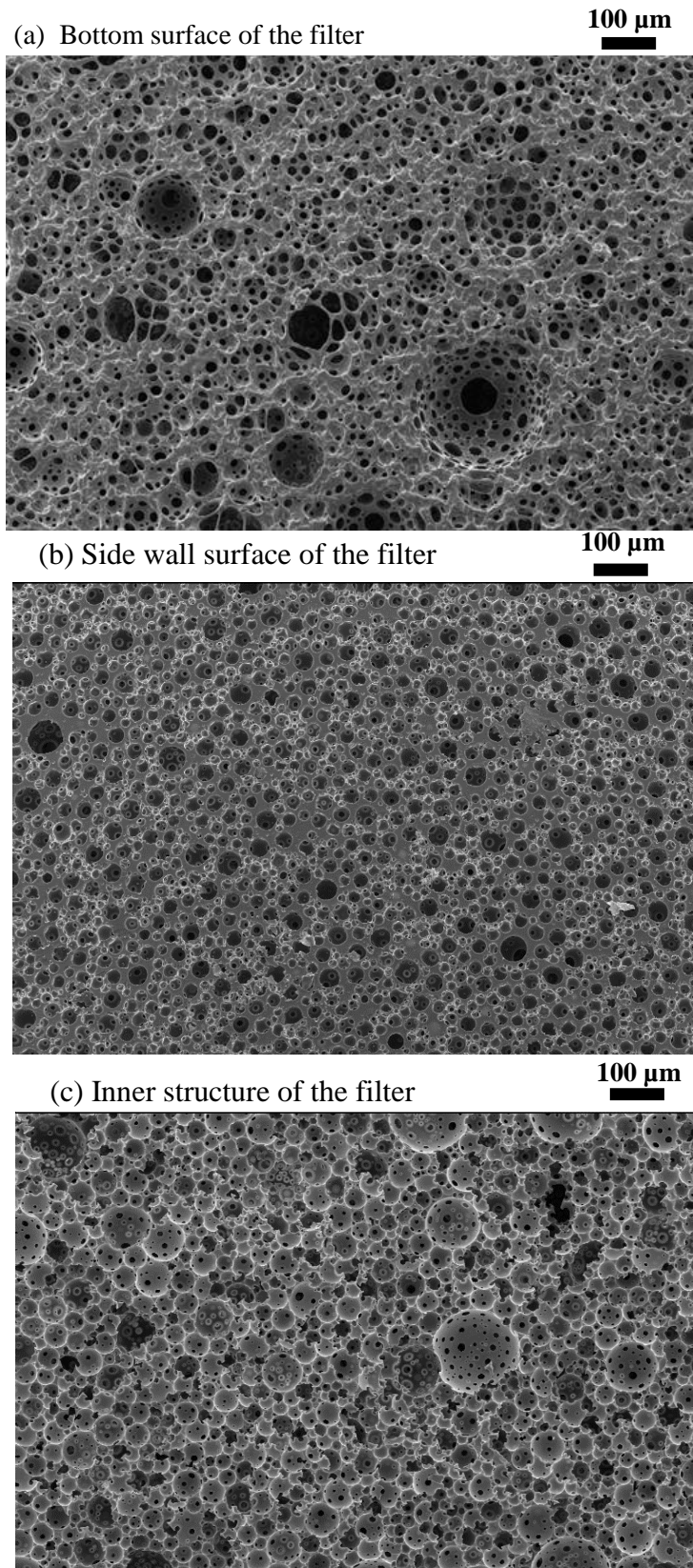


**Figure 3.47.** SEM images of macroporous polymeric materials (filter) produced from w/o emulsion templates. The external oil phase contains 5 vol.% of EGDMA, 1 wt/vol.% of BPO, 1.19 vol.% DMPT and 5wt/vol.% PEL-121, all dissolved in BMA. The water phase is 80vol.% deionised water.

Our results show that. The use of two emulsions to keep the initiator (BPO) and the accelerator (DMPT) separated until the demand to be used by mixing them in 1:1 ratio. The two emulsions can be stored safely for months at reduced temperature as the main components for the rapid polymerisation separated. Therefore, the two emulsions safely can be handled and used in the field at the point of use. For such applications, the emulsion templates should be stable for a considerable amount of time before their use. The Ostwald ripening could change the droplet size distribution in such emulsions during storage. To investigate if such changes are important, we have measured the droplet size distribution over time in two emulsion templates, one prepared with deionised water and another with 0.12 M CaCl<sub>2</sub> solution as a water phase. The results are shown in Figs 3.48 – 3.49 and tables 3.20 and 3.21. The measurement of the droplets size started 2 hours after emulsification of the emulsions. The initial droplets diameters for emulsion without CaCl<sub>2</sub> in the water phase (DN0.5 = 26.19 ± 1.41 μm) is bigger than the other emulsion (DN0.5 = 11.34 ± 0.80 μm). With time the emulsion with CaCl<sub>2</sub> in the water phase showed greater stability in comparison to the other one. The droplets diameter (DN0.5) for emulsion with CaCl<sub>2</sub> in the water phase with time increased by 27%, whereas, the other emulsion by 258%. The presence of electrolyte in the water phase definitely help to maintain the emulsion stability for longer time and slow down the process of Ostwald ripening.

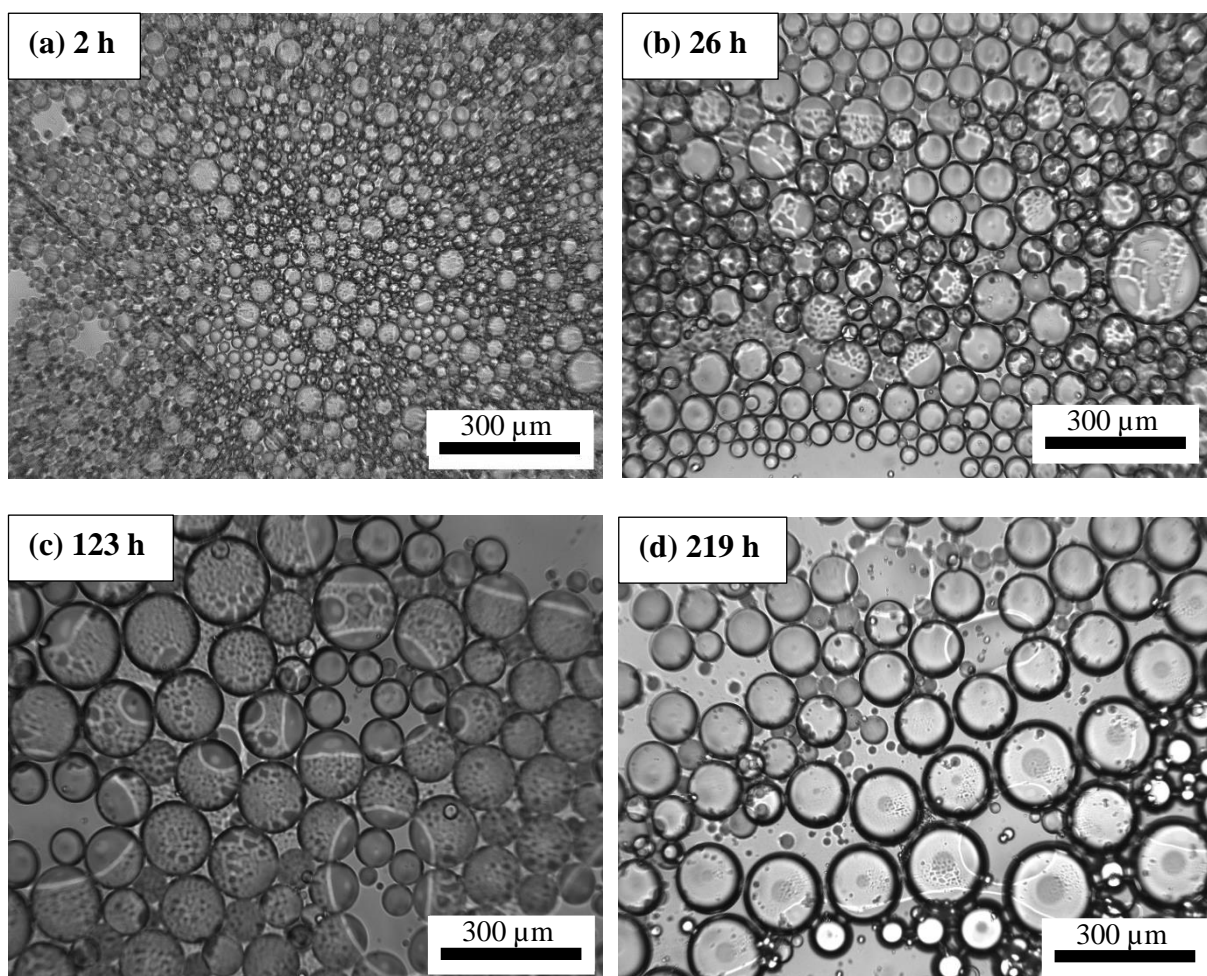


**Figure 3.48.** Microscopic images for emulsion investigated with time. The emulsion made of 20vol.% oil phase (15vol.% of EGDMA and 5wt/vol.% of PEI-121 all dissolved in MMA) and the water phase fraction is 80vol.% (deionised water). The images was taken after diluted the emulsion with the oil phase.

**Table 3.20.** The emulsion droplets diameters (DN0.1, DN0.5 and DN0.9) determined from microscopic images of emulsion prepared from w/o emulsion with volume fraction of water phase ( $\phi_w$ ) at 80vol.%. The external oil phase contains 15vol.% of EGDMA and 5wt/vol.% of PEI-121 all dissolved in MMA. The water phase is deionised water.

Time/h	DN0.1/ $\mu\text{m}$	DN0.5/ $\mu\text{m}$	DN0.9/ $\mu\text{m}$	Span
2	16.10 $\pm$ 1.57	26.19 $\pm$ 1.41	39.21 $\pm$ 2.36	0.88 $\pm$ 0.16
26	34.86 $\pm$ 2.95	55.7 $\pm$ 3.00	80.91 $\pm$ 3.69	0.83 $\pm$ 0.13
123	47.12 $\pm$ 7.22	90.57 $\pm$ 5.74	144.47 $\pm$ 8.77	1.07 $\pm$ 0.19
219	48.92 $\pm$ 5.3	93.77 $\pm$ 8.82	174.01 $\pm$ 18.87	1.33 $\pm$ 0.29

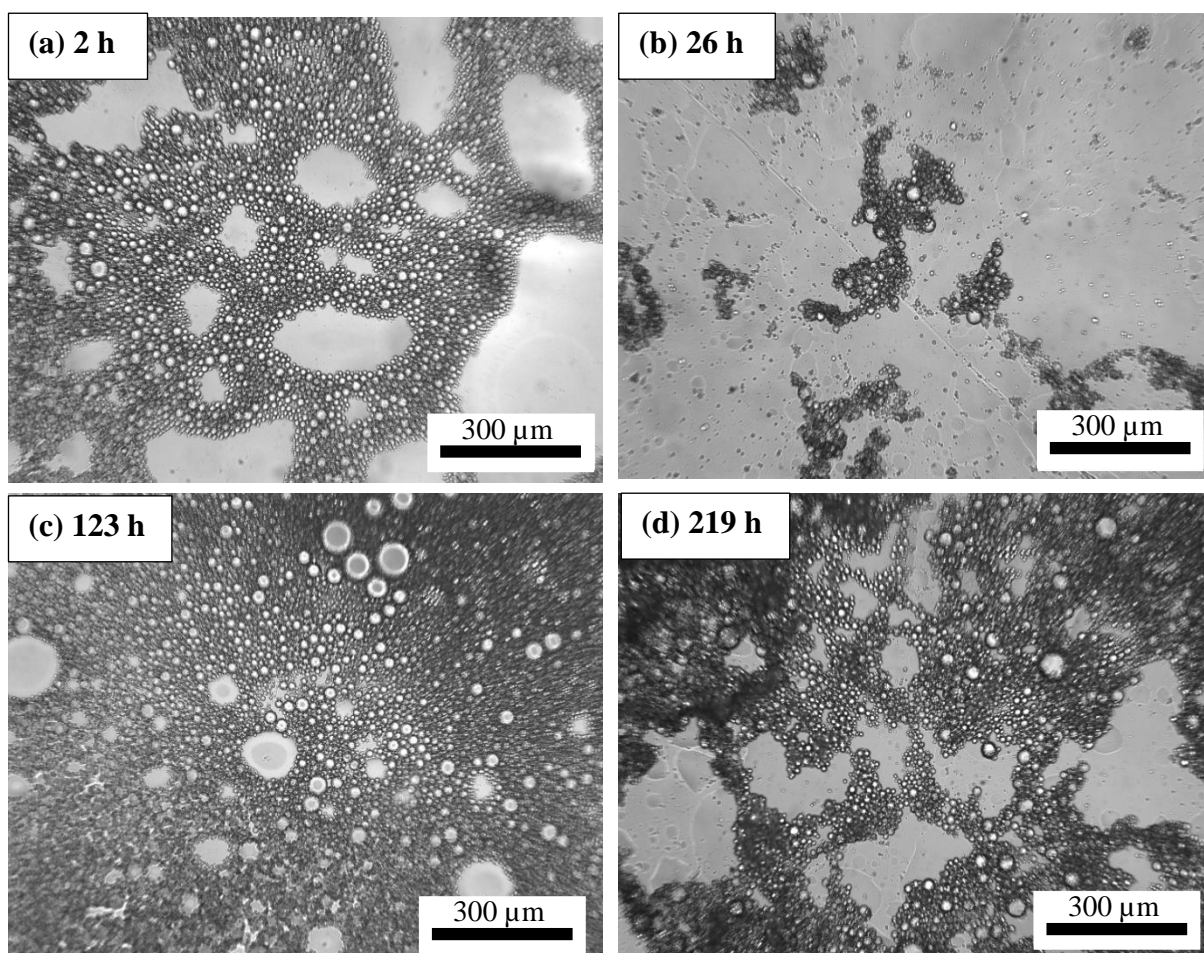


**Figure 3.49.** Microscopic images for emulsion investigated with time. The emulsions made of 20vol.% oil phase (15vol.% of EGDMA and 5wt/vol.% of PEI-121 all dissolved in MMA) and the water phase fraction is 80vol.% (0.12 M  $\text{CaCl}_2$  dissolved water). The images was taken after diluted the emulsion with the oil phase.

**Table 3.21.** The emulsion droplets diameters (DN0.1, DN0.5 and DN0.9) determined from microscopic images of emulsion prepared from w/o emulsion with volume fraction of water phase ( $\phi_w$ ) at 80vol.%. The external oil phase contains 15vol.% of EGDMA and 5wt/vol.% of PEI-121 all dissolved in MMA. The water phase contains 0.12 M  $\text{CaCl}_2$ .

Time/h	DN0.1/ $\mu\text{m}$	DN0.5/ $\mu\text{m}$	DN0.9/ $\mu\text{m}$	Span
2	8.03±0.65	11.34±0.80	16.16±1.19	0.72±0.17
26	10.2±0.65	13.82±0.76	19.62±4.09	0.68±0.35
123	9.3±0.96	14.19±1.05	21.41±2.21	0.85±0.23
219	9.03±1.00	14.36±1.14	23.37±3.98	1.00±0.36

### 3.6 Conclusions

Macroporous polymers were prepared from w/o emulsion templates by redox-initiated polymerisation at room temperature. The oil phase was consisted of MMA as the monomer, EGDMA as the crosslinker, PEL-121 as the surfactant, BPO as the initiator and DMPT as the accelerator. The water phase was deionised. There were 4 series of experiments performed using the redox-initiation system. The effect of the volume fraction of the water phase on the mechanical properties and morphology was studied by keeping the surfactant concentration with respect to the oil phase and then in separate study to the total volume of the emulsion. After that, the water fraction was fixed at 80vol.% and vary the surfactant or crosslinker concentration with respect to the oil phase. Application of porous polymeric materials was demonstrated. The curing dynamic and the droplets sizes distribution of the emulsion template with time were studied.

The water volume fraction in the emulsion template has affected the mechanical properties and the morphology of the materials produced. Porosity of up to 93% was achieved. The elastic modulus and strength of the materials decreased with the increase of porosity. Whereas, the diameter of voids and pore throats increase as the water fraction increased.

Keeping the surfactant concentration constant with respect to the total volume of the emulsion helped to improve the emulsion stability. It was found that, the mechanical properties of samples prepared at high fraction of the water phase were improved. The diameter of voids and pore throats increased as the water fraction increased.

It was observed that changing the surfactant concentration with respect to the oil phase at fixed water fraction (80vol.%) strongly affected the properties of the materials produced. The elastic modulus and compressional strength passed through a maximum at 1wt/vol.% of PEL-121 surfactant present in the oil phase. One can conclude that the optimal surfactant concentration in the studied system is 1wt/vol.% at which the highest elastic modulus and strength have been determined. The morphology has been hugely affected by varying the surfactant concentration. The voids and pore throats diameters decreased drastically with the surfactant concentration: DN0.5 of the voids from  $88.7 \pm 7.2 \mu\text{m}$  to  $11.3 \pm 0.6 \mu\text{m}$  and that of the pore throats from  $7.38 \pm 0.54 \mu\text{m}$  to  $2.48 \pm 0.17 \mu\text{m}$ .

The crosslinker concentration (EGDMA) at fixed water fraction (80vol.%) was studied. The elastic modulus and strength decreased with increasing the crosslinker concentration (EGDMA). The elastic modulus decreased from  $97.6 \pm 2.8 \text{ MPa}$  to  $62.5 \pm 0.8 \text{ MPa}$ , while the strength dropped from  $3.31 \pm 0.14 \text{ MPa}$  to  $2.94 \pm 0.12 \text{ MPa}$  when the EGDMA

concentration was changed from 5 vol.% to 35 vol.%. The diameter of voids and pore throats also decreased with the crosslinker concentration. We can control the curing time by increase of decrease the concentration of crosslinker as it decreased from 6544s to 762s with increasing the concentration of crosslinker.

Possible application of macroporous polymer in the field was demonstrated by making filter in situ in water. It was found that the curing time decreased as the fraction of the water increased in emulsion template. The curing time of system using benzyl methacrylate as the monomer was faster than those using MMA as the monomer. For that reason benzyl methacrylate used in the demonstration experiment. The filter was successfully made and tested as the coloured water passed through the filter. The droplets size distribution of the emulsion template was studied for two emulsions to observe the changes over time on the emulsion stability in case of the emulsion need to be stored for period of time before use. The two emulsions, one has an electrolyte ( $\text{CaCl}_2$ ) and the other deionised water. It was detected that the droplets size of the emulsion with electrolyte was smaller than the emulsion with deionised water. Our results showed that the Ostwald ripening progress faster in the absence of the electrolyte in the water phase.

The demonstration provided a remarkable advantage of how porous polymeric materials made via emulsion template can be used in the filed as it can take the shape of its casting mould. In addition, by using the redox-initiation method there is no need for any source of energy to be supplied to the systems. As a result, it can produce any sample with any thickness desired without concerned about how the initiator can be decomposed to initiate the polymerisation. The presence of electrolyte in the water phase could help to maintain the emulsion template for sufficient time before use.

### 3.7 References

1. S. Kovacic, K. Jerabek, P. Krajnc and C. Slugovc, *Polym. Chem.*, 2012, **3**, 325-328.
2. H. Deleuze, B. Maillard and O. Mondain-Monval, *Bioorg Med. Chem. Lett.*, 2002, **12**, 1877-1880.
3. R. Owen, C. Sherborne, T. Paterson, N. H. Green, G. C. Reilly and F. Claeysens, *J. Mech. Behav. Biomed. Mater.*, 2016, **54**, 159-172.
4. M. Tebboth, A. Kogelbauer and A. Bismarck, *Ind. Eng. Chem. Res.*, 2015, **54**, 5974-5981.
5. P. Krajnc, N. Leber, D. Štefanec, S. Kontrec and A. Podgornik, *J. Chromatogr A*, 2005, **1065**, 69-73.
6. K.-Y. Lee, L. L. C. Wong, J. J. Blaker, J. M. Hodgkinson and A. Bismarck, *Green Chem.*, 2011, **13**, 3117-3123.
7. F. Schüler, D. Schamel, A. Salonen, W. Drenckhan, M. D. Gilchrist and C. Stubenrauch, *Angew. Chem., Int. Ed.*, 2012, **51**, 2213-2217.
8. Y. S. Nam, J. J. Yoon and T. G. Park, *J. Biomed Mater. Res.*, 2000, **53**, 1-7.
9. C. Zhao, E. Danish, N. R. Cameron and R. Katakya, *J. Mater. Chem.*, 2007, **17**, 2446-2453.
10. F. Carn, A. Colin, M.-F. Achard, H. Deleuze, E. Sellier, M. Birot and R. Backov, *J. Mater. Chem.*, 2004, **14**, 1370-1376.
11. S. Jerenec, M. Šimić, A. Savnik, A. Podgornik, M. Kolar, M. Turnšek and P. Krajnc, *React. Funct. Polym.*, 2014, **78**, 32-37.
12. H. Zhang, G. C. Hardy, M. J. Rosseinsky and A. I. Cooper, *Adv. Mater.*, 2003, **15**, 78-81.
13. J. M. Williams, *Langmuir.*, 1991, **7**, 1370-1377.
14. A. Quell, B. de Bergolis, W. Drenckhan and C. Stubenrauch, *Macromolecules*, 2016, **49**, 5059-5067.
15. S. Huš and P. Krajnc, *Polymer*, 2014, **55**, 4420-4424.
16. N. Cameron, D. Sherrington, L. Albiston and D. Gregory, *Colloid Polym. Sci.*, 1996, **274**, 592-595.
17. J. M. Williams, A. J. Gray and M. H. Wilkerson, *Langmuir*, 1990, **6**, 437-444.
18. N. R. Cameron and D. C. Sherrington, in *Biopolymers Liquid Crystalline Polymers Phase Emulsion*, Springer Berlin Heidelberg, Berlin, Heidelberg, 1996, pp. 163-214.

19. B. VAZQUEZ , S. DEB and W. BONFIELD *J. Mater. Sci. Mater. Med.*, 1997, **8**, 455-460.
20. I. E. Ruyter, K. Ekstrand and N. Björk, *Dent. Mater.*, 1986, **2**, 6-9.
21. A. Zoller, D. Gigmes and Y. Guillauneuf, *Polym. Chem.*, 2015, **6**, 5719-5727.
22. R. S. Moglia, M. Whitely, P. Dhavalikar, J. Robinson, H. Pearce, M. Brooks, M. Stuebben, N. Cordner and E. Cosgriff-Hernandez, *Biomacromolecules*, 2014, **15**, 2870-2878.
23. A. Pitto-Barry and N. P. E. Barry, *Polym. Chem.*, 2014, **5**, 3291-3297.
24. R. Wu, A. Menner and A. Bismarck, *Polymer*, 2013, **54**, 5511-5517.
25. J. M. Williams, J. J. Bartos and M. H. Wilkerson, *J. Mater. Sci.*, 1990, **25**, 5134-5141.
26. L. J. Gibson and M. F. Ashby, *Cellular solids: structure and properties*, Cambridge university press, 1999.
27. J. M. Williams and D. A. Wroblewski, *Langmuir*, 1988, **4**, 656-662.
28. A. Menner, R. Verdejo, M. Shaffer and A. Bismarck, *Langmuir*, 2007, **23**, 2398-2403.
29. N. R. Cameron, *Polymer*, 2005, **46**, 1439-1449.
30. B. P. Binks, *Modern aspects of emulsion science*, Royal Society of Chemistry, Cambridge, 1998.
31. L. L. Wong, P. M. Baiz Villafranca, A. Menner and A. Bismarck, *Langmuir*, 2013, **29**, 5952-5961.
32. L. L. C. Wong, V. O. Ikem, A. Menner and A. Bismarck, *Macromol. Rapid Commun.*, 2011, **32**, 1563-1568.
33. G. Lorna, and M, Ashby, *Cellular Solids: Structure and Properties*, Cambridge University Press, Cambridge, 2nd edn., 1997.
34. U. S. Ramelow and S. Pingili, *Polymers*, 2010, **2**, 265-285.
35. S. Livshin and M. S. Silverstein, *Macromolecules*, 2008, **41**, 3930-3938.

## CHAPTER 4

### Porous polymeric materials produced by thermo-initiated polymerisation of emulsion templates at elevated temperature

In the previous chapter, porous polymeric materials were produced at room temperature using the redox-initiated system (BPO with DMPT). In this chapter, the preparation of porous polymeric materials via traditional methods of thermal initiation at elevated temperature is investigated in order to compare their mechanical properties and morphology to those prepared by redox-initiation at room temperature.

#### 4.1. Introduction

The preparation of porous polymeric materials from w/o emulsion templates using thermo-initiated polymerisation has been widely used for many years.<sup>1</sup> Most of the initiators used decay in the temperature range from 40 to 100 °C. Initiators which decompose at a temperature more than 100°C could not be used, because the water phase of the emulsion template would boil and evaporate. The most widely studied system is styrene with DVB as a crosslinker where the emulsion template has been polymerised at high temperature in the presence of a thermo-initiator.<sup>1-3</sup> The most common thermo-initiator used for making porous polymeric materials by emulsion templating is AIBN added to the oil phase. Williams studied water-in-styrene/DVB emulsion systems polymerised at high temperature by using the AIBN thermo-initiator.<sup>1</sup> He investigated the influence of the surfactant and the monomer concentration on the morphology of the materials produced. In his study, the opening of the pores was related to the surfactant concentration in the systems and to the oil phase fraction. He also studied the effects of electrolyte in the aqueous phase, crosslinker and initiator concentrations, and found that the concentration of electrolyte had strong effect on the morphology of the porous materials produced.<sup>4,5</sup> Significant decrease of the void size have been observed with an increase of the electrolyte concentration, suggesting for a decrease of the interfacial tension.<sup>4</sup> The electrolyte also reduces the water solubility in the oil phase, thus suppressing the Ostwald ripening and preventing the formation of larger droplets.<sup>1,6</sup> Calcium chloride is often used electrolyte, but potassium sulphate<sup>7</sup> and sodium chloride<sup>8</sup> have also been used. The thermo-initiated polymerisation requires high temperatures which are detrimental for the emulsion templates. Therefore, a large amount of surfactant in the oil phase (5-40vol.%)<sup>1,9</sup> has to be used in order to enhance the emulsion stability during the polymerisation. In addition, measures to facilitate the polymerisation have also be taken. These include the purification of the oil phase to remove the inhibitors, expelling

the oxygen (a potent inhibitor) by purging the oil phase with N<sub>2</sub> gas, degassing the aqueous phase and preparation of the emulsion template under N<sub>2</sub> atmosphere to prevent the oxygen from entering the system and inhibit the polymerisation.<sup>3, 4, 10, 11</sup>

In this study, our aim is to prepare porous polymeric materials in a traditional way using thermo-initiator at elevated temperature (70°C) in order to compare their mechanical properties and morphology to those synthesised by redox-initiation at room temperature (see Chapter 3) . Ideally, the same initiator (BPO) should be used in the comparison. Therefore, thermo-initiated polymerisation using BPO is investigated first. Then the AIBN is investigated and the properties of the porous materials compared to those produced by BPO/DMPT initiation at room temperature.

#### **4.2. Preparation of porous polymeric materials using BPO as thermo-initiator**

It is known that BPO can decompose in the temperature range 70-100°C<sup>12, 13</sup> and therefore should be able to initiate the polymerisation. In this study, BPO added to the oil the phase of the w/o emulsion template is used as thermo-initiator. Polymerisation experiments at 70 and 80°C have been performed. The oil phase has the same composition as in the redox-initiated polymerisation experiments (15 vol.% EGDMA crosslinker, 5 wt/vol.% PEL-121 surfactant, 1 wt/vol.% or 3.5 wt/vol.% BPO, all dissolved in MMA) but in the absence of the DMPT accelerator. The emulsion in all the experiment performed with BPO at high temperature consisted of 80vol.% Water phase (0.12 M of CaCl<sub>2</sub>) and 20vol.% oil phase ( 5wt/vol.% of PEL-121, 15vol.% of EGDMA, 1 or 3.5 wt/vol.% of BPO all dissolved in MMA). The water phase contained calcium chloride to enhance the emulsion stability at high temperature.

Experiments with w/o emulsion templates containing 80 vol.% internal water phase were conducted following the procedure for preparation of porous polymeric materials at high temperature described in section 2.2. The preparation was found to be very challenging since the emulsions destabilised during heating in the oven at 70 °C. All attempts to speed up the polymerisation by removing the inhibitors from the oil phase, adding 0.12 M CaCl<sub>2</sub> in the water phase and using nitrogen atmosphere did not produce porous materials with the desired properties. Partial success was achieved by using degassed aqueous phase (in addition to all previous measures) and conducting the polymerisation at 80 °C (Fig. 4.1). To conclude, using BPO as a thermo-initiator to produce porous polymeric materials from the system studied is complicated and challenging. Despite all the attempts to achieve faster polymerisation, the emulsion destabilised in the oven. The only sample of

reasonable quality produced with a degassed water phase at 80°C has big holes on its surface and is not suitable for practical applications (Fig. 4.1).

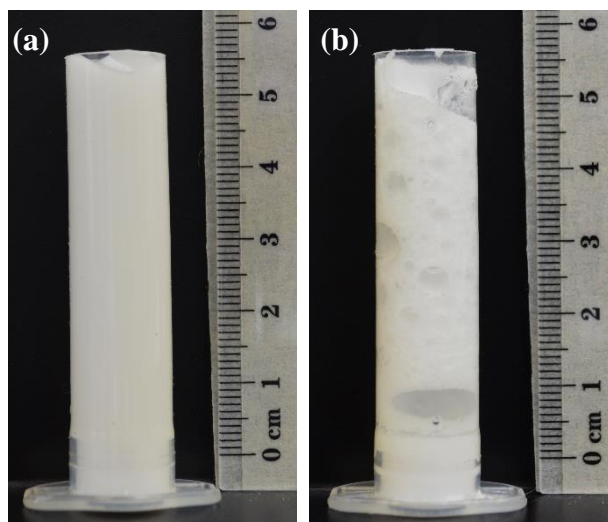


**Figure 4.1.** Images of the mould loaded with w/o emulsion template (a) before entering the oven and (b) after 1.5 hours in the oven at 80°C. The emulsion template contains 80 vol.% degassed internal water phase (0.12 M CaCl<sub>2</sub>). The external oil phase is made of 15 vol.% EGDMA, 5 wt/vol.% PEL-121 surfactant, 3.5 wt/vol.% of BPO, all dissolved in MMA.

### 4.3. Preparation of porous polymeric materials using AIBN as thermo-initiator

Since the use of BPO as thermo-initiator failed to produce porous polymeric materials (see previous section), we decided to use AIBN which is commonly used as a thermo-initiator in the preparation of porous materials from emulsion templates.<sup>9, 14-16</sup> The preparation of porous polymeric materials at high temperature is described in section (2.2.2). The emulsion is made of the oil phase (1.6 wt/vol.% of AIBN, 15vol.% of EGDMA, 5wt/vol.% of PEL-121 all dissolved in MMA) and the water phase (0.12 M CaCl<sub>2</sub>). The MMA and EGDMA are purified by passing three times via basic alumina to remove the inhibitors. The emulsion is made under the N<sub>2</sub> atmosphere, and the water phase degassed. Once the emulsion is formed, it is poured into a mould and left in the oven at 70°C to polymerise overnight. Then, the sample produced is purified by Soxhlet extraction to remove unconverted monomer and surfactant used.

The percentage of the water phase in the w/o emulsion templates is varied from 65-80vol.% in these experiments. Initially, a syringe mould was used to obtain porous polymeric materials with perfect cylindrical shape. Materials of good quality were obtained from emulsions with 65 and 70vol.% water phase (see Figs.4.2 and 4.3). However, at 75 and 80vol.% the sample produced has big holes on its surface and not suitable for mechanical testing. A possible explanation for this is that the syringe mould

is not well-sealed which allows the oxygen to enter the system and reduce the rate of polymerisation resulting in the partial destabilisation of emulsion (see Fig.4.4 and 4.5). To test this hypothesis, centrifuge tubes (15mL) which could be appropriately sealed were used as moulds. We found that the polymerisation has successfully occurred in the centrifuge tube producing samples with better quality (see Fig.4.6 and 4.7). However, when the percentage of water was increased to 85vol.%, the sample produced has large holes in its surface as shown in Fig.4.8. The results suggested that the emulsion partially destabilised in the oven due to the limited amount of surfactant which was not able to stabilise the emulsion at high temperature.<sup>17</sup>

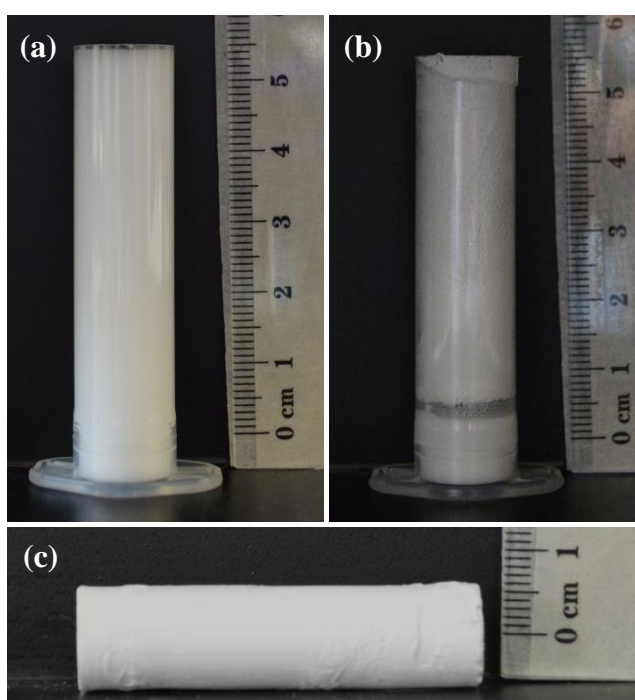


**Figure 4.2.** Images of the mould loaded with w/o emulsion template (a) before polymerisation and (b) after polymerisation in the oven at 70°C overnight. (c) An image of the solid material after demoulding. The emulsion template contains 65 vol.% internal water phase (0.12 M of CaCl<sub>2</sub>). The external oil phase is made of 15vol.% EGDMA, 5wt/vol.% PEL-121 surfactant, 1.6wt/vol.% of AIBN all dissolved in MMA.

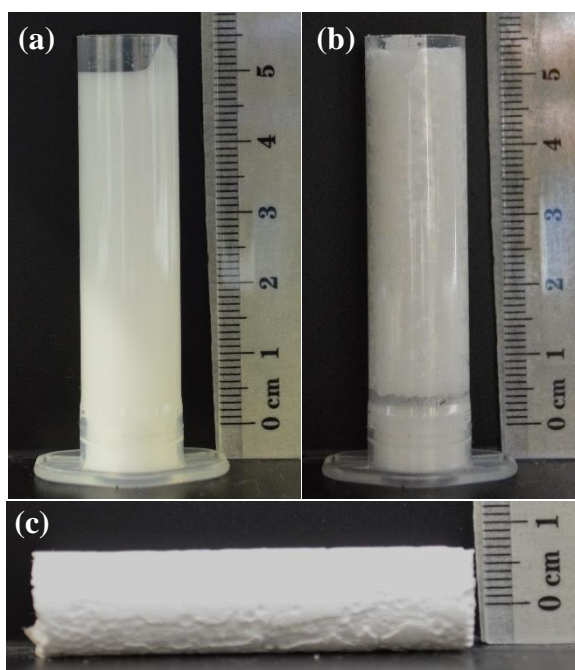


**Figure 4.3.** Images of the mould loaded with w/o emulsion template (a) before polymerisation and (b) after polymerisation in the oven at 70°C overnight. (c) An image of the solid material after demoulding. The emulsion template contains 70 vol.% internal water phase (0.12 M of  $\text{CaCl}_2$ ). The external oil phase is made of 15vol.% EGDMA, 5wt/vol.% PEL-121 surfactant, 1.6wt/vol.% of AIBN all dissolved in MMA.

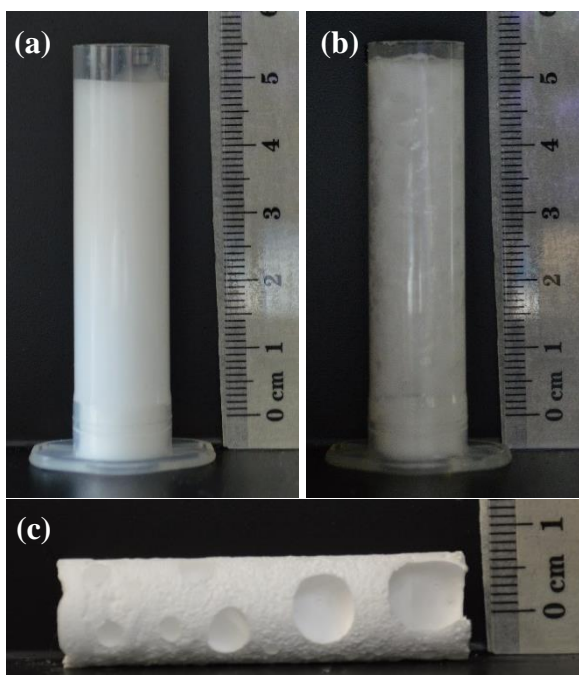


**Figure 4.4.** Images of the mould loaded with w/o emulsion template (a) before polymerisation and (b) after polymerisation in the oven at 70°C overnight. (c) An image of the solid material after demoulding. The emulsion template contains 75 vol.% internal water phase (0.12 M of  $\text{CaCl}_2$ ). The external oil phase is made of 15vol.% EGDMA, 5wt/vol.% PEL-121 surfactant, 1.6wt/vol.% of AIBN all dissolved in MMA.

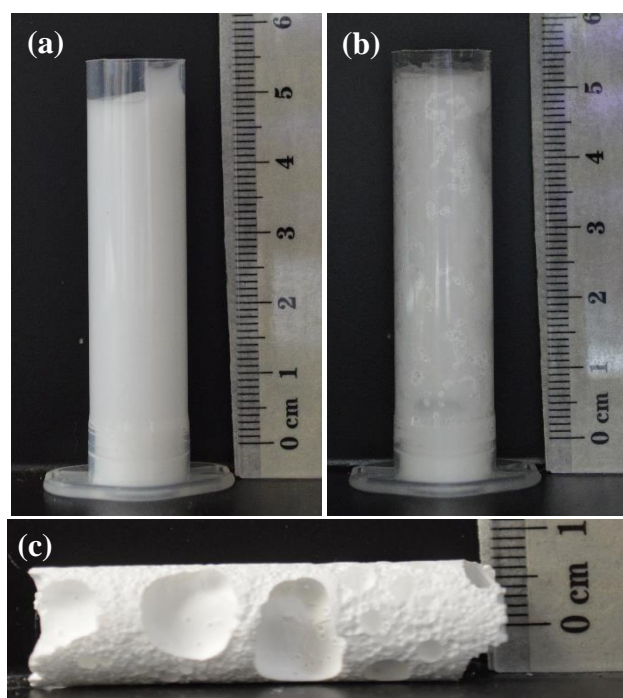


**Figure 4.5.** Images of the mould loaded with w/o emulsion template (a) before polymerisation and (b) after polymerisation in the oven at 70°C overnight. (c) An image of the solid material after demoulding. The emulsion template contains 80 vol.% internal water phase (0.12 M of  $\text{CaCl}_2$ ). The external oil phase is made of 15vol.% EGDMA, 5wt/vol.% PEL-121 surfactant, 1.6wt/vol.% of AIBN all dissolved in MMA.

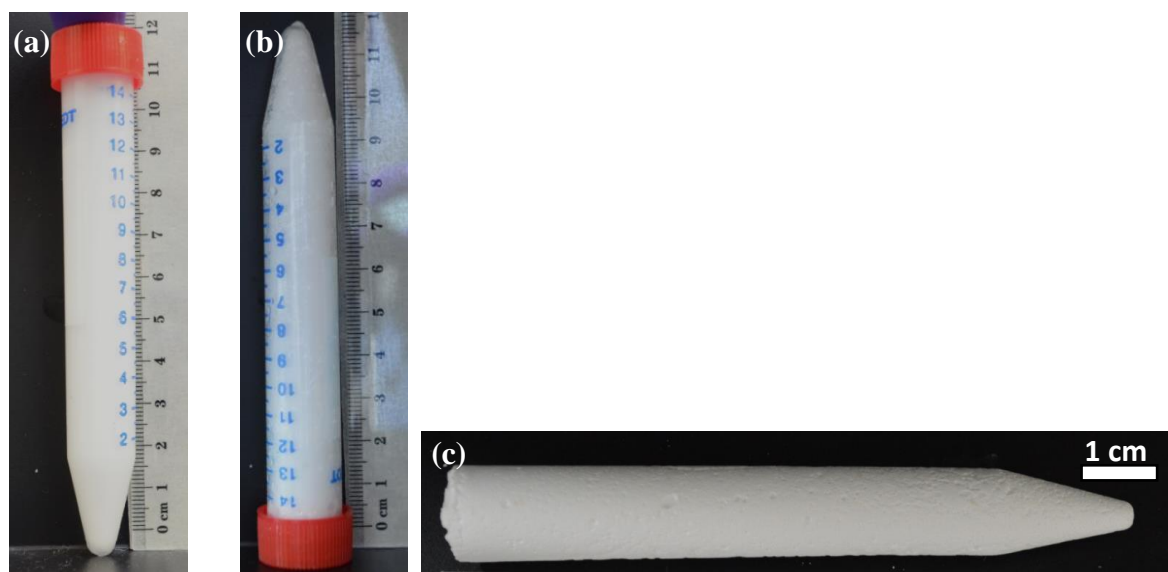


**Figure 4.6.** Images of the mould loaded with w/o emulsion template (a) before polymerisation and (b) after polymerisation in the oven at 70°C overnight. (c) An image of the solid material after demoulding. The emulsion template contains 75 vol.% internal water phase (0.12 M of  $\text{CaCl}_2$ ). The external oil phase is made of 15vol.% EGDMA, 5wt/vol.% PEL-121 surfactant, 1.6wt/vol.% of AIBN all dissolved in MMA.



**Figure 4.7.** Appearance of porous polymeric materials after demoulding. The emulsion template contains 80 vol.% internal water phase (0.12 M of  $\text{CaCl}_2$ ). The external oil phase is made of 15vol.% EGDMA, 5wt/vol.% PEL-121 surfactant, 1.6wt/vol.% of AIBN all dissolved in MMA.



**Figure 4.8.** Appearance of porous polymeric materials after demoulding. The emulsion template contains 85 vol.% internal water phase (0.12 M of  $\text{CaCl}_2$ ). The external oil phase is made of 15vol.% EGDMA, 5wt/vol.% PEL-121 surfactant, 1.6wt/vol.% of AIBN all dissolved in MMA.

The morphology of porous polymeric materials produced at high temperature was studied via the SEM imaging. As can be seen in Fig.4.9 the materials have an open pore structure of voids connected via pore throats. As the percentage of the water phase increases in the emulsion template, the number of the pore throats increases. An explanation for the increase in the number of pore throats in the walls of the voids is that at a low percentage of the water phase 65 - 70vol.%, the water droplets are not in very close contact. As the amount of the water phase in the emulsion increases above the limit of hexagonal close packing for monodisperse droplets (74%), there will be increased contact between the droplets which leads to the opening of pore throats upon polymerisation of the continuous phase and drying of the material.<sup>18</sup> Another reason could be that at low water fractions, the thickness of the wall between the droplets hinders the formation of the pore throats at low percentage of the water phase.<sup>16</sup> Whereas, at 75 and 80vol.%, the droplets are in close contact which allows the pore throats to open at the thinnest point of the film between droplets. The diameter of voids and pore throats increases with increasing the percentage of the water phase in the system (see Figs.4.10 and Table 4.1 - 4.2). The reason is that as the concentration of the surfactant decreased in the systems, the emulsion becomes less stable which affected the diameter of voids and pore throats.<sup>1, 16</sup> The diameter of the voids were decreased from (DN0.5)  $12.9 \pm 0.6 \mu\text{m}$  to  $16.5 \pm 1.0 \mu\text{m}$ . In addition, the diameter of pore throats were decreased from (DN0.5)  $1.7 \pm 0.2 \mu\text{m}$  to  $2.7 \pm 0.2 \mu\text{m}$

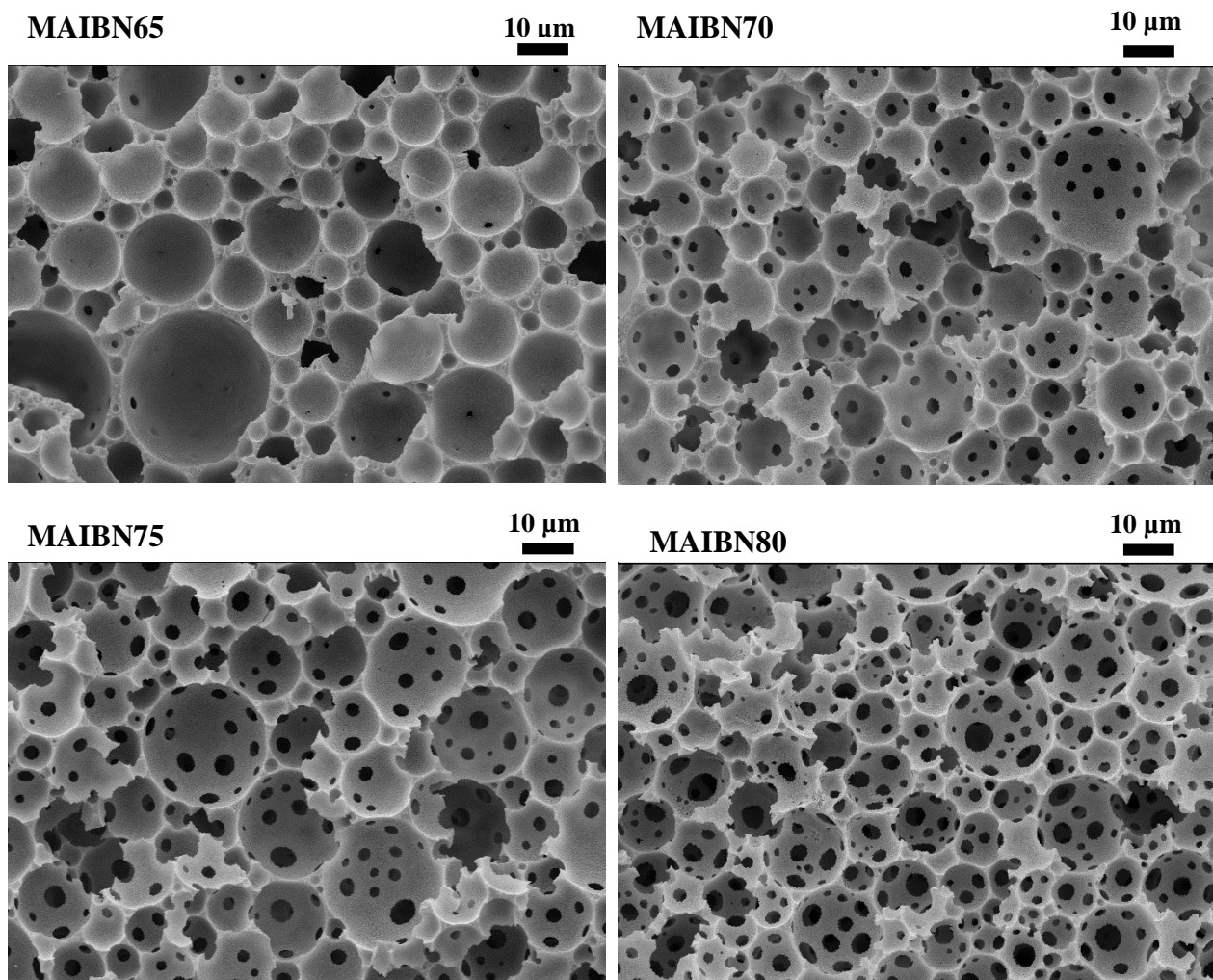


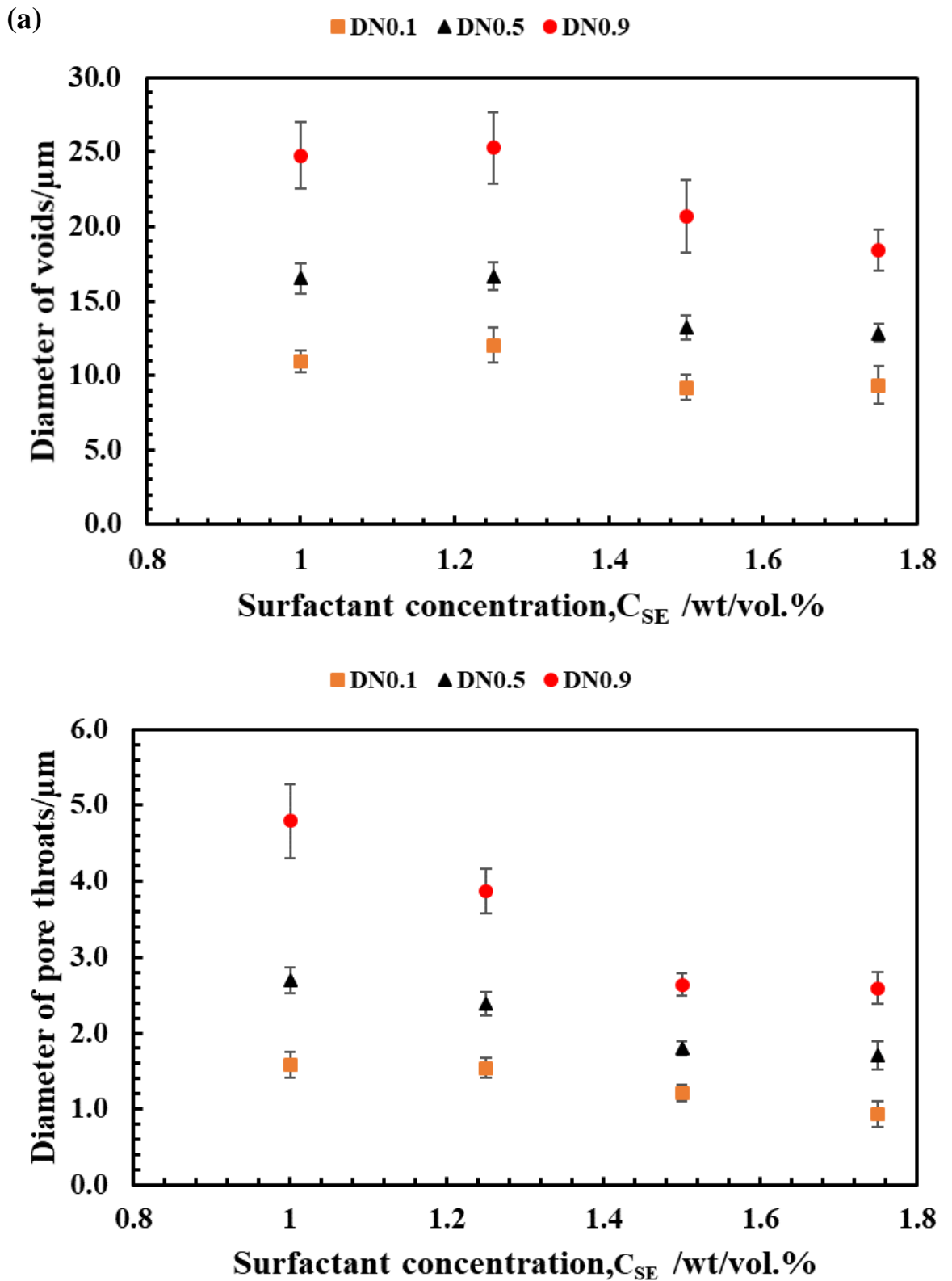
**Figure 4.9.** SEM images of macroporous polymeric materials produced from w/o emulsion templates with different volume fraction of the internal water phase from 65 vol.% (MAIBN65) to 80 vol.% (MAIBN80) at 70°C. The external oil phase contains 15vol.% of EGDMA, 1.6 wt/vol.% AIBN and 5wt/vol.% PEL-121, all dissolved in MMA. The water phase is deionised water. The water phase contained (0.12 M of  $\text{CaCl}_2$ ).

**Table 4.1.** Void diameters (DN0.1, DN0.5 and DN0.9) determined from SEM images of polymeric materials produced from w/o emulsion templates with varying volume fraction of water ( $\phi_w$ ). The external oil phase contains 15vol.% of EGDMA, 1.6 wt/vol.% AIBN and 5wt/vol.% PEL-121, all dissolved in MMA. The water phase is solution 0.12 M of  $\text{CaCl}_2$ .  $C_{SE}$  is the PEL-121 surfactant concentration with respect to the total volume of emulsion template.

Sample code	$\phi_w$ /vol. %	$C_{SE}$ /wt/vol. %	DN0.1/ $\mu\text{m}$	DN0.5/ $\mu\text{m}$	DN0.9/ $\mu\text{m}$	Span
<b>MAIBN65</b>	65	1.75	9.3 $\pm$ 1.3	12.9 $\pm$ 0.6	18.4 $\pm$ 1.4	0.7 $\pm$ 0.2
<b>MABIN70</b>	70	1.50	9.2 $\pm$ 0.9	13.2 $\pm$ 0.8	20.7 $\pm$ 2.4	0.9 $\pm$ 0.3
<b>MAIBN75</b>	75	1.25	12.0 $\pm$ 1.2	16.7 $\pm$ 0.9	25.3 $\pm$ 2.4	0.8 $\pm$ 0.2
<b>MAIBN80</b>	80	1.00	11.0 $\pm$ 0.8	16.5 $\pm$ 1.0	24.8 $\pm$ 2.2	0.8 $\pm$ 0.2

**Table 4.2.** Pore throats diameters (DN0.1, DN0.5 and DN0.9) determined from SEM images of polymeric materials produced from w/o emulsion templates with varying volume fraction of water ( $\phi_w$ ). The external oil phase contains 15vol.% of EGDMA, 1.6 wt/vol.% AIBN and 5wt/vol.% PEL-121, all dissolved in MMA. The water phase is solution 0.12 M of  $\text{CaCl}_2$ .  $C_{SE}$  is the PEL-121 surfactant concentration with respect to the total volume of emulsion template.

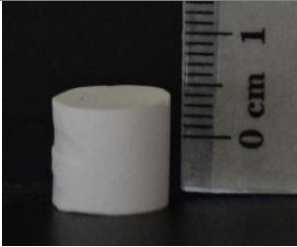
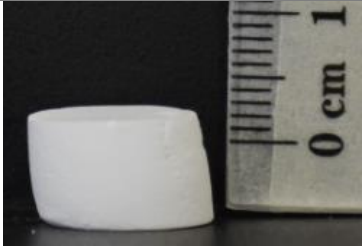
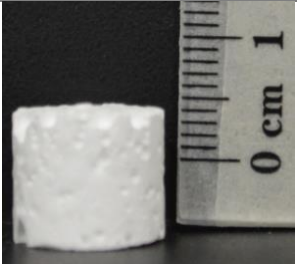
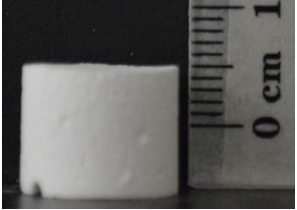
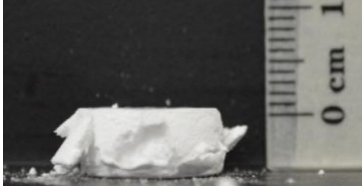
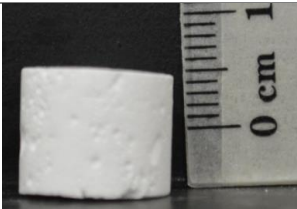
Sample code	$\phi_w$ /vol. %	$C_{SE}$ / wt/vol. %	DN0.1/ $\mu\text{m}$	DN0.5/ $\mu\text{m}$	DN0.9/ $\mu\text{m}$	Span
<b>MAIBN65</b>	65	1.75	0.9 $\pm$ 0.2	1.7 $\pm$ 0.2	2.6 $\pm$ 0.2	1.0 $\pm$ 0.3
<b>MABIN70</b>	70	1.50	1.2 $\pm$ 0.1	1.8 $\pm$ 0.1	2.6 $\pm$ 0.2	0.8 $\pm$ 0.2
<b>MAIBN75</b>	75	1.25	1.5 $\pm$ 0.1	2.4 $\pm$ 0.2	3.9 $\pm$ 0.3	1.0 $\pm$ 0.2
<b>MAIBN80</b>	80	1.00	1.6 $\pm$ 0.2	2.7 $\pm$ 0.2	4.8 $\pm$ 0.5	1.2 $\pm$ 0.3



**Figure 4.10.** Diameter of voids (a) and pore throats (b) of porous materials versus PEL-121 surfactant concentration in the total volume of emulsion template,  $C_{SE}$ . For other details see Tables 4.1 and 4.2. DN0.1, DN0.5 and DN0.9 stand for 10%, 50% and 90% where the diameter's values have less than this value.

The mechanical properties of porous polymeric materials produced at high temperature were tested with compression tests as described in section 2.2.4. Images of samples before and after the compression test can be seen in Table 4.3. The behaviour of the materials under the compression test is different from those materials produced at room temperature. The materials were brittle and crushed under the compression test. This behaviour under the compression test follows the elastic brittle foam (see chapter one, section 1.6). Thus, the mechanical properties are related to the density of the materials. The amount of the oil phase decreases in the emulsion template with increasing water fraction which results in a lower foam density.<sup>4</sup> The density at 65vol.% water phase is  $0.34\pm 0.01$  g/cm<sup>3</sup> and 80vol.% the water phase is  $0.14\pm 0.01$  g/cm<sup>3</sup> see Table 4.5. The porosity increases as the percentage of the water phase increase in the system to reach 88%. This explanation for the percentage of porosity is bigger than the percentage of the water phase in the emulsion template was explained in chapter three (section 3.2.1). The elastic modulus and strength (at 10% strain) decrease as the porosity increases in the system (see Table.4.4 and Figs.4.11 - 4.12). The elastic modulus decreases from  $75\pm 10$  MPa at 72 % porosity to  $25\pm 4$  MPa at 88% porosity. The strength (at 10% strain) decreased by 76% in the same porosity range. In the SEM images Fig.4.9 the number of the pore throats in the wall of the voids increased with increasing the water fraction in the system. This increase in the number of pore throats affected the mechanical properties of the materials.

**Table 4.3.** Images of porous polymeric materials produced at high temperature. Before and after the compression test.

Sample code	Before testing	After testing
MAIBN65		
MAIBN70		
MAIBN75		
MAIBN80		

**Table 4.4.** The density, porosity, elastic modulus and strength (at 10 % strain) of porous materials produced by redox-initiated polymerisation from emulsion templates with different volume fractions of the internal water phase,  $\phi_w$ . The external oil phase contains 15vol.% of EGDMA, 1.6 wt/vol.% AIBN and 5wt/vol.% PEL-121, all dissolved in MMA. The water phase is solution of 0.12 M of  $\text{CaCl}_2$ .

Sample code	$\phi_w$ /vol.%	Density /g/cm <sup>3</sup>	Porosity /%	Elastic Modulus /MPa	Strength /MPa
MAIBN65	65	0.339±0.010	72±2	75±10	7.2±0.7
MABIN70	70	0.264±0.009	78±2	53±3	4.8±0.2
MAIBN75	75	0.211±0.001	82±2	41±9	3.5±0.4
MAIBN80	80	0.137±0.007	88±1	26±4	1.7±0.1

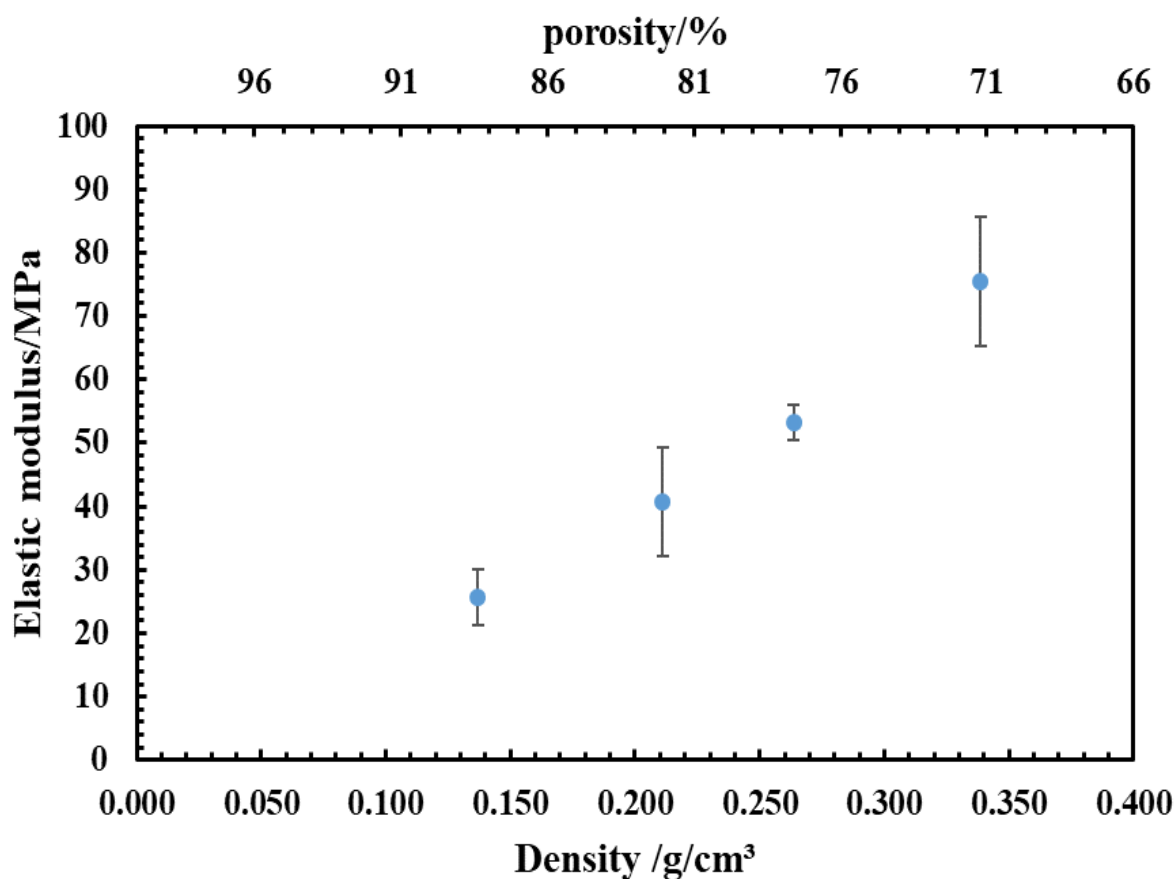


**Figure 4.11.** The elastic modulus versus density and porosity of porous materials produced by redox-initiated polymerisation from emulsion templates with different volume fractions of the internal water phase (see Table 4.4).

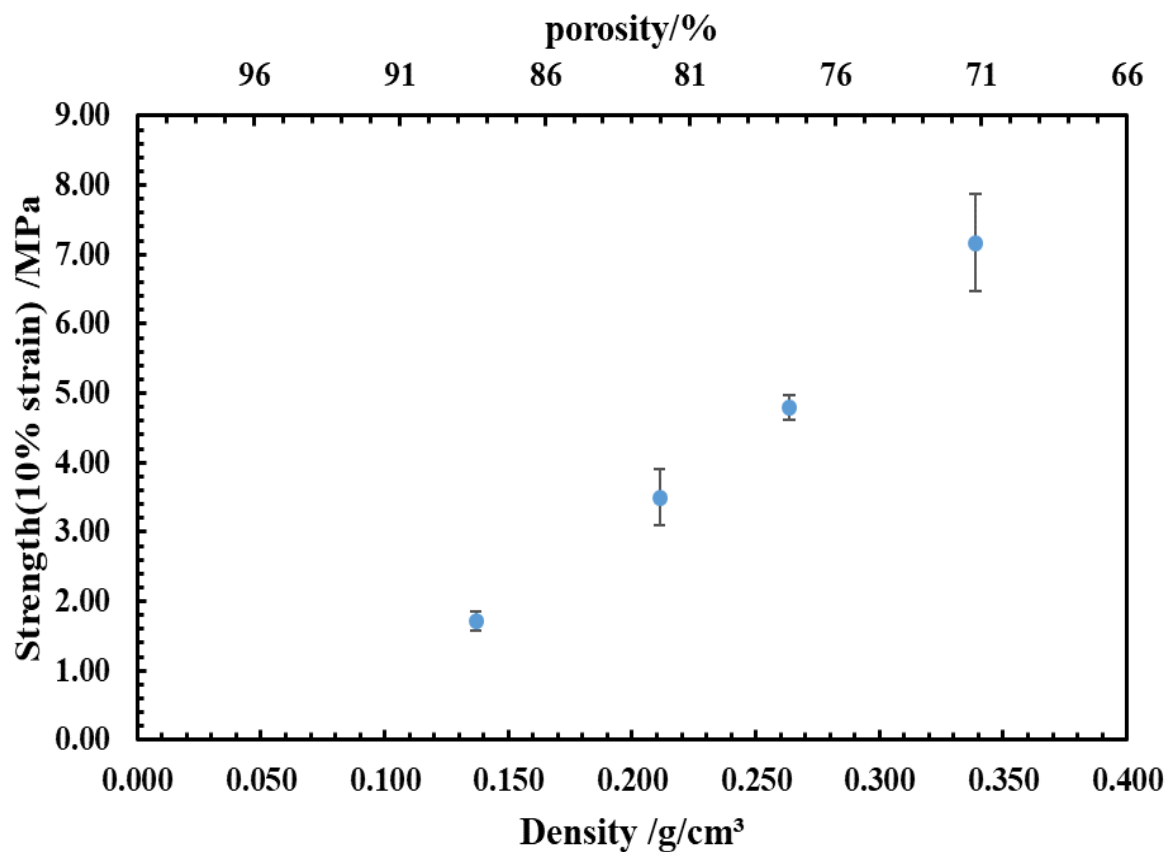


**Figure 4.12.** The strength (at 10% strain) versus density and porosity of porous materials produced by redox-initiated polymerisation from emulsion templates with different volume fractions of the internal water phase (see Table 4.4).

#### 4.4. Comparison of porous polymeric materials produced at room temperature to those produced at high temperature

Our results show that the way the porous polymeric materials have been prepared via emulsion templating is important for the mechanical properties and the morphology. In chapter three, porous polymeric materials were prepared using the redox-initiated systems to polymerise the oil phase at room temperature. Whereas, in this chapter porous polymeric materials are prepared with the traditional method using AIBN as thermo-initiator. The composition of the oil phase in both systems is the same except for the initiator (MMA as a monomer, EGDMA as crosslinker and PEL-121 as a surfactant). It is interesting to compare these methods and the properties of the materials produced by them.

The preparation method of porous polymeric materials is much simpler using the redox-initiation system in comparison to the thermo-initiation system as can be seen in Table 4.5. The preparation steps reduced from 5 steps to one step. The preparation method using the redox initiation system requires only mixing the two phases. There is no need for any prior step of preparation or any external source of energy and all chemicals are used as received. On the other hand, the preparation method using the thermo-initiation system required tedious steps of preparation (purification of the oil phase, degas the water phase, N<sub>2</sub> atmosphere and add electrolyte to the water phase) and it is much more time consuming. The method using redox-initiation system is a straightforward method in comparison to those using a thermo-initiation system.

**Table 4.5.** Comparison of the preparation steps for making porous polymeric materials via emulsion templating using redox-initiated or thermo-initiated polymerisation.

<b>Steps of preparation</b>	<b>Redox-initiated polymerisation</b>	<b>Thermo-initiated polymerisation</b>
<b>1- Purification of the oil phase</b>	NO	YES
<b>2- Using N<sub>2</sub> atmosphere</b>	NO	YES
<b>3- Adding electrolyte to the water phase</b>	NO	YES
<b>4- Degassing the water phase</b>	NO	YES
<b>5- Emulsification</b>	YES	YES
<b>6- Heating at high temperature</b>	NO	YES

The mechanical properties of porous polymeric materials produced by redox-initiated polymerisation at room temperature are better in comparison to those produced by thermo-initiated polymerisation at high temperature as shown in Figs.4.13 and 4.14. The behaviour of the materials produced at high temperature under compression testing was an initial compression followed by fracturing due to its brittle nature whereas the macroporous polymers prepared at room temperature simply compressed. The elastic modulus at 65vol.% water phase for porous polymeric materials at room temperature was  $109\pm 1.8$  MPa whereas for those produced at high temperature it was  $75\pm 10$  MPa. The elastic modulus at 80vol.% water phase for porous materials produced at room temperature was  $66.3\pm 0.6$  MPa compared to those prepared at high temperature which was significantly lower at  $26\pm 4$  MPa. The strength (10% strain) at 65vol.% water phase for porous materials produced at room temperature was  $8.7\pm 0.20$  MPa and the ones produced at high temperature were  $7.2\pm 0.7$  MPa. Furthermore, at 80vol.% water phase for porous polymeric materials at room temperature is  $3.23\pm 0.04$ MPa and high temperature is  $1.7\pm 0.1$  MPa. The porosity of porous polymeric materials produced at room temperature achieved up 93% in comparison to those at the high temperature reached 88%. The results suggested that the difference in the mechanical properties could be related to the emulsion stability as at room temperature the emulsion is more stable in comparison to high temperature.<sup>4, 17</sup> The type of the initiator could affect the mechanical properties of porous polymeric materials and the way of the oil phase polymerised as demonstrated by Bismarck.<sup>16</sup>

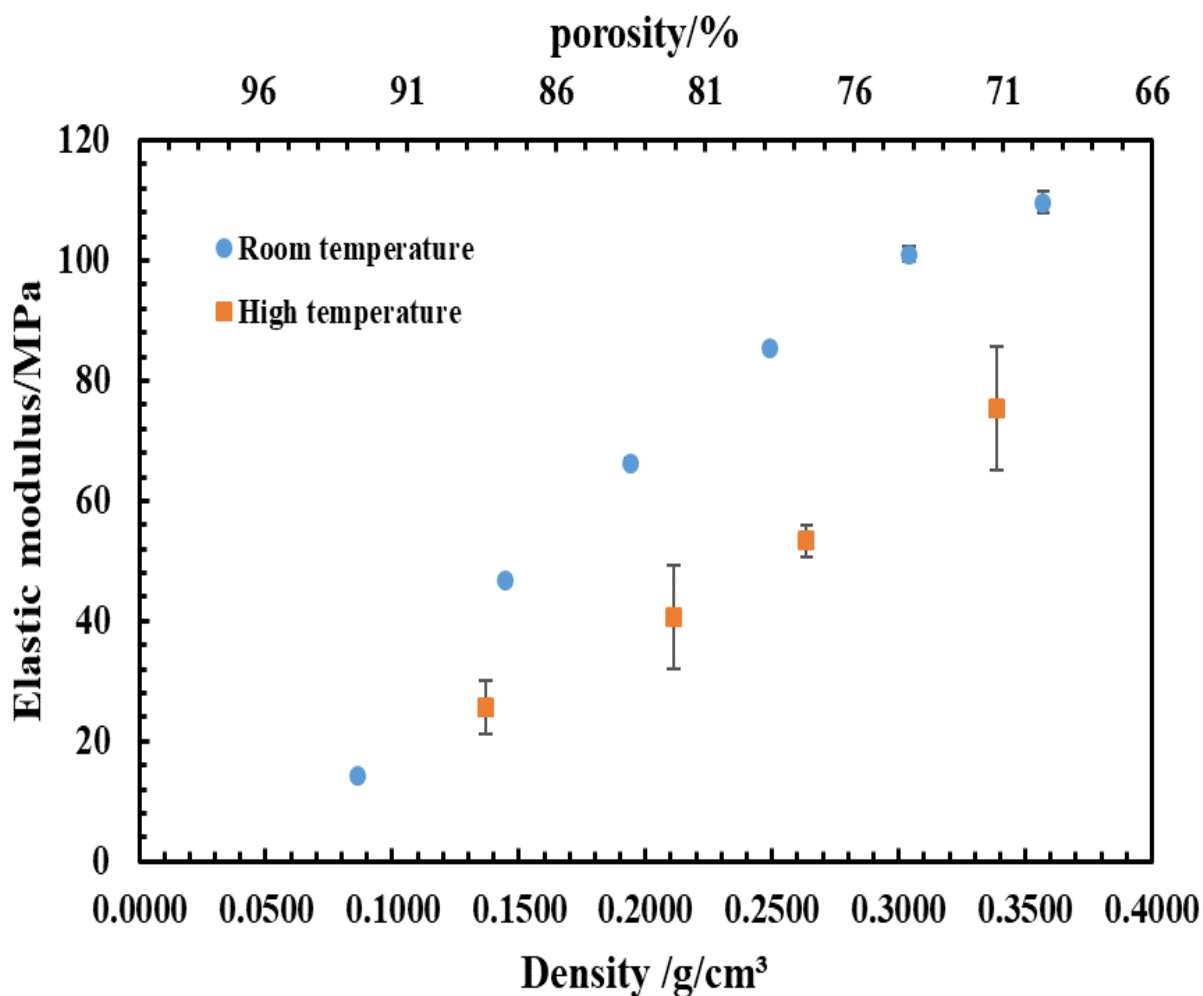


**Figure 4.13.** Elastic modulus versus density and porosity of porous polymeric materials were produced at room temperature and high temperature 70°C via w/o emulsion template. Room temperature, the emulsion made of the external oil phase contains 15vol.% of EGDMA, 1 wt/vol.% BPO, 1.19 vol.% DMPT and 5wt/vol.% PEL-121, all dissolved in MMA. The water phase is deionised water. High temperature, the emulsion made of the external oil phase contains 15vol.% of EGDMA, 1.6 wt/vol.% AIBN and 5wt/vol.% PEL-121, all dissolved in MMA The water phase contained (0.12 M of CaCl<sub>2</sub>).

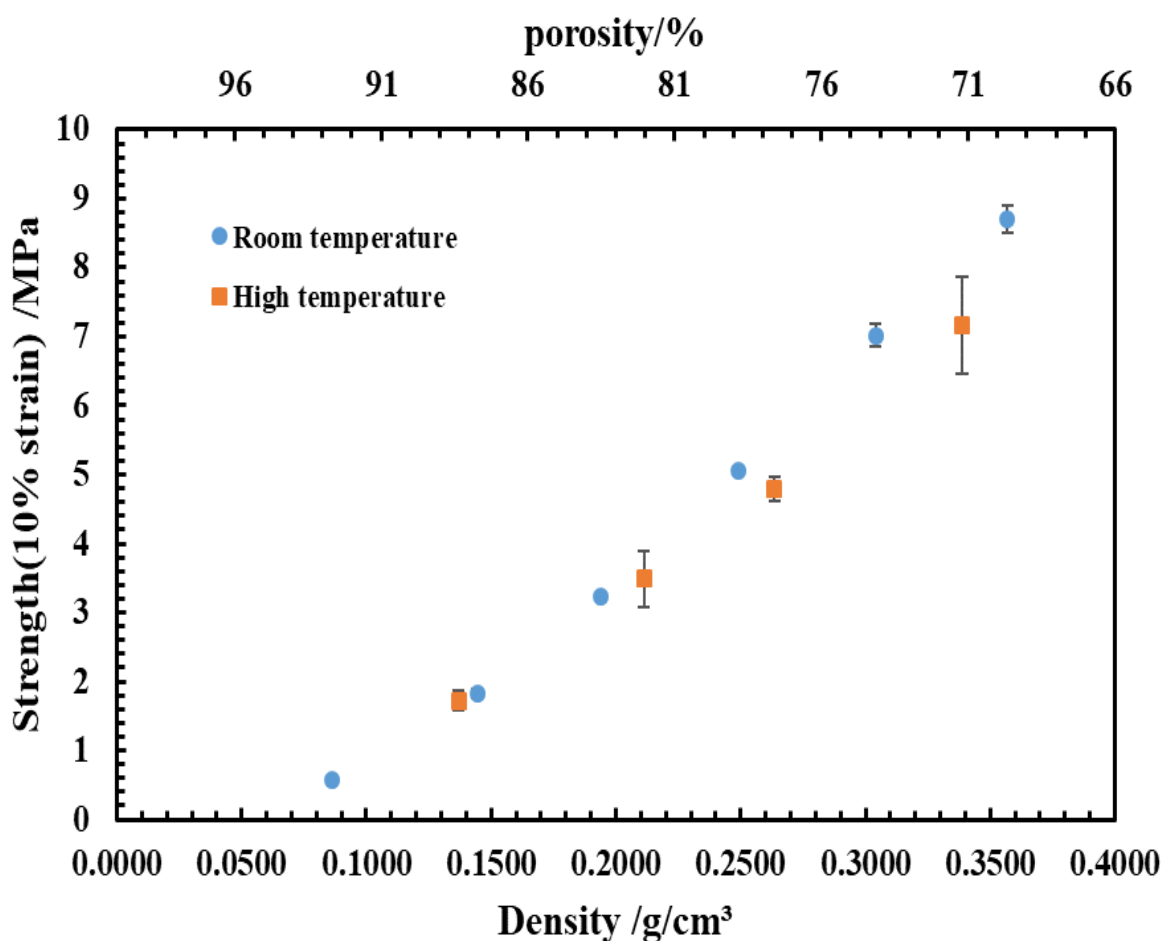


**Figure 4.14.** Strength (10% strain) versus density and porosity of polyHIPEs materials were produced at room temperature and high temperature 70°C via w/o emulsion template. Room temperature, the emulsion made of the external oil phase contains 15vol.% of EGDMA, 1 wt/vol.% BPO, 1.19 vol.% DMPT and 5wt/vol.% PEL-121, all dissolved in MMA. The water phase is deionised water. High temperature, the emulsion made of the external oil phase contains 15vol.% of EGDMA, 1.6 wt/vol.% AIBN and 5wt/vol.% PEL-121, all dissolved in MMA. The water phase contained (0.12 M of CaCl<sub>2</sub>).

The morphology of porous polymeric materials at room temperature is different from those at high temperature. Except both systems have an open structure. The first observation from the SEM images, the nature of the surface is different as shown in Fig.15. The surface seems smooth for porous polymeric materials produced at room temperature. Whereas, the surface for porous materials produced at high temperature has some grains. This differences in the nature of the surface could be related to the type of the initiator or the rate of polymerisation.<sup>16</sup> The grains of the surface could affect the mechanical properties, as there might be some regions weaker than the others. Thus, the mechanical properties of macroporous polymers produced at high temperature are weaker than those are produced at room temperature. The porous polymeric materials produced

at room temperature has a wide range of diameter ( $DN_{0.5} = 9 \pm 0.5$  to  $29 \pm 1.5 \mu\text{m}$ ) see Fig.4.16. Whereas, for the porous polymeric materials produced at high temperature the  $DN_{0.5}$  diameter of the voids varies in the range from  $12.9 \pm 0.6$  to  $16.5 \pm 1 \mu\text{m}$  (see Fig.4.16). This could be explained by the fact that the emulsion stability is higher at room temperature which allows the increases of the water phase to reach 90vol.%.<sup>1</sup> The diameter of pore throats is at room temperature ( $DN_{0.5} = 1.6 \pm 0.6$  to  $6.4 \pm 0.6 \mu\text{m}$ ) whereas at high temperature ( $DN_{0.5} = 1.7 \pm 0.2$  to  $2.7 \pm 0.2 \mu\text{m}$ ). The pore throats here are slightly affected by the type of the initiator and the type of the polymerisation. For example, at 65vol.% the diameter of pore throats  $DN_{0.5}$  is  $1.6 \pm 0.6 \mu\text{m}$  for room temperature, and the high-temperature  $DN_{0.5}$  is  $1.7 \pm 0.2 \mu\text{m}$ . In addition, at 80vol.%  $DN_{0.5}$  is  $3.7 \pm 0.4 \mu\text{m}$  at room temperature, and the high-temperature  $DN_{0.5}$  is  $2.7 \pm 0.2$ . At low percentage of the water phase, the effect of the type of polymerisation is not pronounced due to the system did not reach close-packing structure.<sup>18</sup> Whereas at 80vol.% the system achieved that and the diameter of pore throats increased by 37% for porous polymeric materials at high temperature. This suggests that the emulsion stability and the type of polymerisation play a key role.<sup>4, 16</sup>

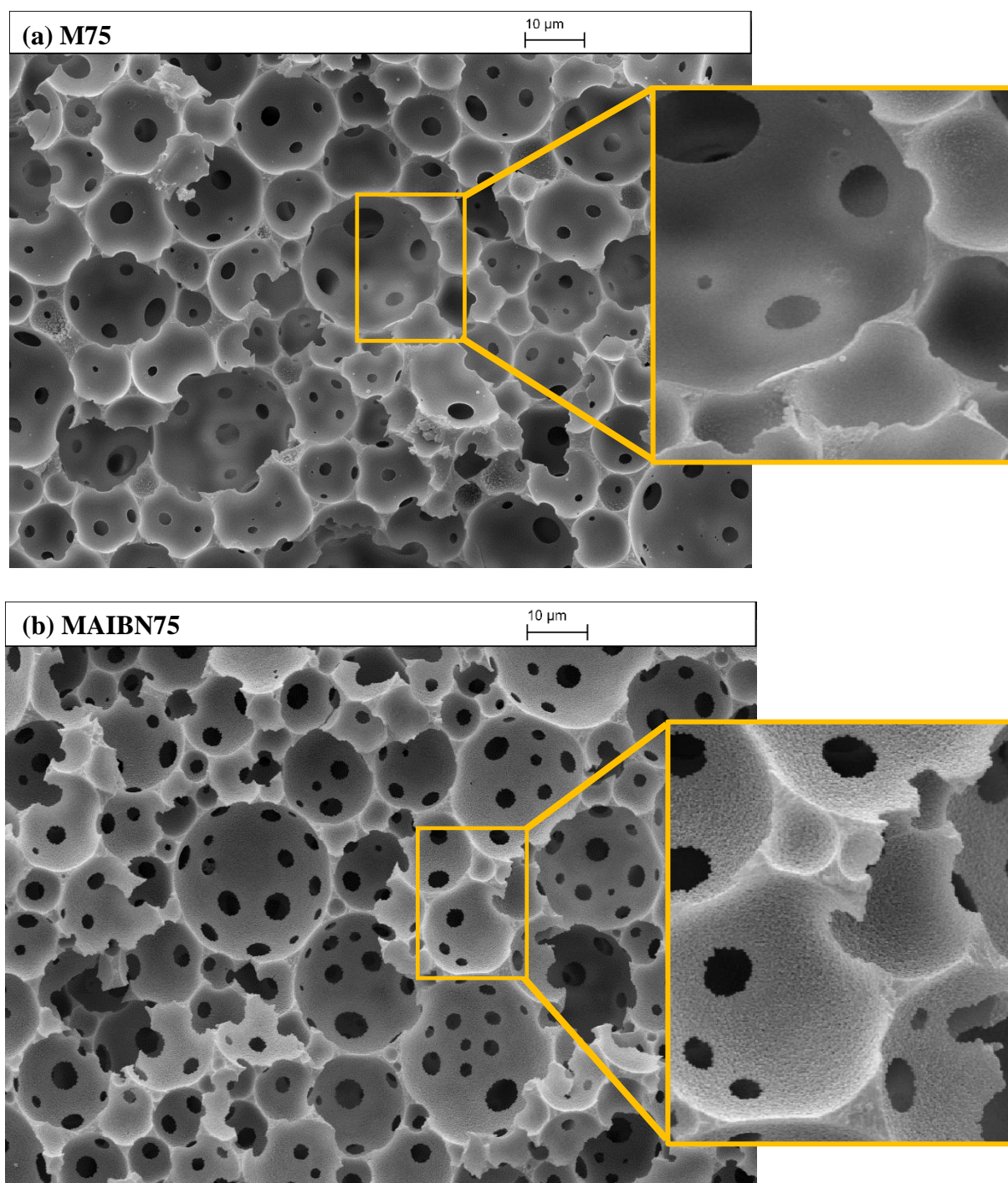


**Figure 4.15.** SEM images of microporous polymeric materials produced from w/o emulsion templates with different polymerisation method. (a) The emulsion template polymerised at room temperature, the emulsion made of the external oil phase contains 15vol.% of EGDMA, 1 wt/vol.% BPO, 1.19 vol.% DMPT and 5wt/vol.% PEL-121, all dissolved in MMA. The water phase is deionised water. (b) The emulsion template polymerised at 70°C, the emulsion made of the external oil phase contains 15vol.% of EGDMA, 1.6 wt/vol.% AIBN and 5wt/vol.% PEL-121, all dissolved in MMA. The water phase contained 0.12 M CaCl<sub>2</sub>

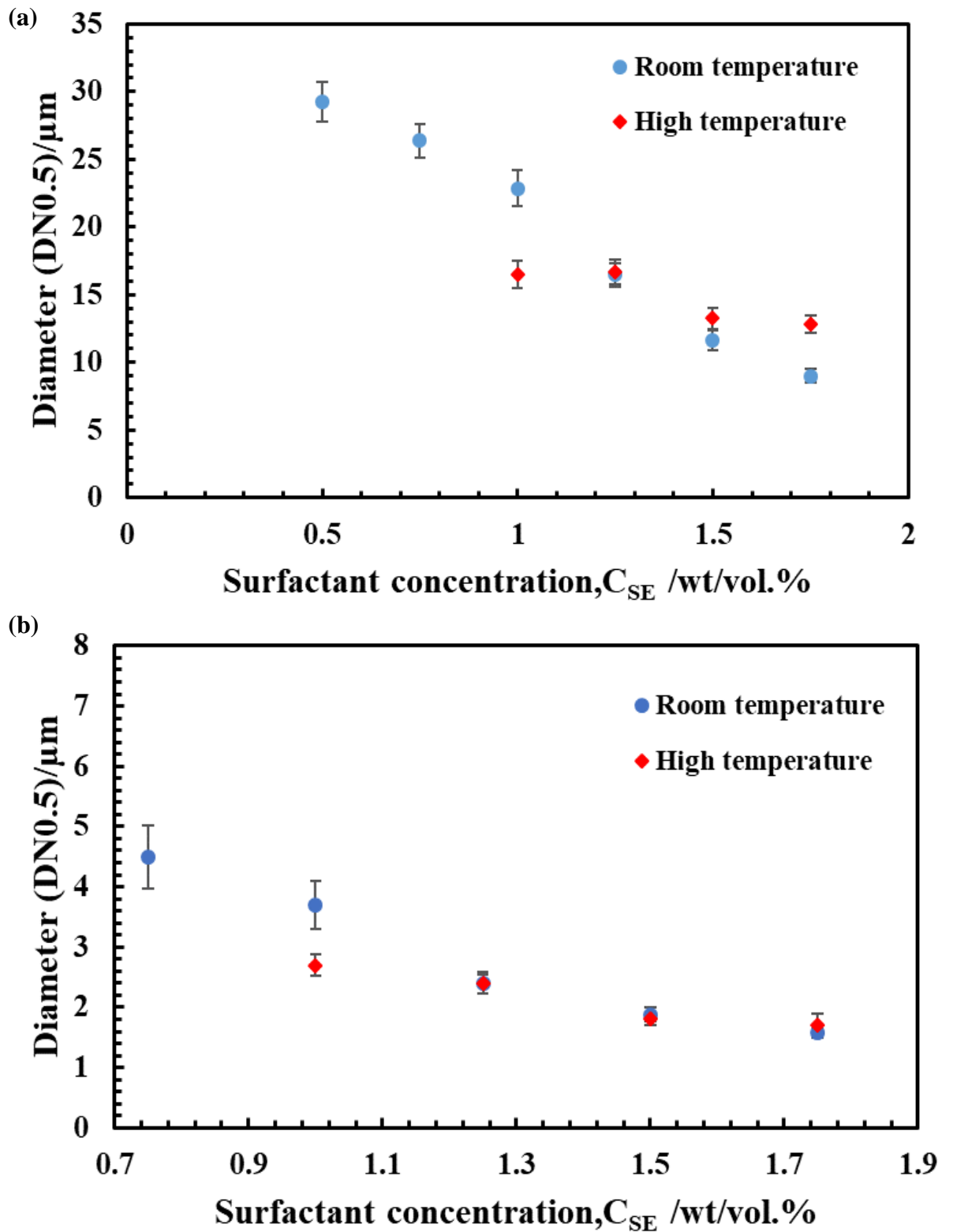


**Figure 4.16.** Diameter of voids (a) and pore throats (b) (DN0.5) of porous materials versus PEL-121 surfactant concentration in the total volume of emulsion template,  $C_{SE}$ .

#### 4.5. Conclusions

Porous polymeric materials have been prepared at high temperature by thermo-initiated polymerisation. The oil phase was made of MMA as the monomer, EGDMA as the crosslinker, PEL-121 as the surfactant and BPO as the initiator. BPO was used as a thermo-initiator to produce porous polymeric materials. It was found that the emulsions destabilised in the oven during the polymerisation. Different conditions and parameters were changed to achieve faster polymerisation and enhance the emulsion stability. Unfortunately, all the attempts failed to produce porous materials. Then, BPO was replaced by the AIBN thermo-initiator which is commonly used for the preparation of porous polymeric materials via emulsion templating. The polymerisation was successful and porous materials were obtained. The percentage of the water phase in the emulsion template was varied from 65-85vol.%. After polymerisation of the continuous phase and drying of the macroporous polymer, compression tests were performed to study the mechanical properties of the porous materials that were obtained. It has been found that the materials produced are brittle and fractured under compression. The highest porosity achieved was 88%. The materials have an open structure across all the percentage of the water phase. The diameter of voids and pore throats increased as the percentage of the water phase in the system was raised.

The samples produced with the thermo-initiation method were compared to those produced with the redox-initiation method. The preparation of porous polymeric materials using the redox-initiation is simpler and less time consuming in comparison to those using the thermo-initiation system. With redox-initiation method there is no need for any prior purification of the oil phase, degas the water phase, N<sub>2</sub> atmosphere and add electrolyte to the water phase. The redox-initiation method is less expensive as there is no need for any external source of energy or chemicals for purification. The preparation method at room temperature using the redox-initiation was able to produce materials with higher fraction of the water phase up to 90vol% whereas the thermo-initiation method could only go up to 80vol%. The materials produced at room temperature using the redox-initiation exhibited higher elastic modulus and strength in comparison to those at high temperature using the thermo-initiation. The morphology of both system have an open structure. The diameter of voids and pore throats in porous polymeric materials prepared at room temperature were broader range than those at high temperature.

#### 4.6. References

1. J. M. Williams, *Langmuir*, 1991, **7**, 1370-1377.
2. N. Cameron, D. Sherrington, L. Albiston and D. Gregory, *Colloid Polym. Sci.*, 1996, **274**, 592-595.
3. L. L. Wong, P. M. Baiz Villafranca, A. Menner and A. Bismarck, *Langmuir*, 2013, **29**, 5952-5961.
4. J. M. Williams, A. J. Gray and M. H. Wilkerson, *Langmuir*, 1990, **6**, 437-444.
5. J. M. Williams and D. A. Wroblewski, *Langmuir*, 1988, **4**, 656-662.
6. A. L. Márquez, A. Medrano, L. A. Panizzolo and J. R. Wagner, *J. Colloid Interface. Sci.*, 2010, **341**, 101-108.
7. M. G. Schwab, I. Senkovska, M. Rose, N. Klein, M. Koch, J. Pahnke, G. Jonschker, B. Schmitz, M. Hirscher and S. Kaskel, *Soft Matter.*, 2009, **5**, 1055-1059.
8. M.-T. Grosse, M. Lamotte, M. Birot and H. Deleuze, *J. Polym. Sci., Part A: Polym. Chem.*, 2008, **46**, 21-32.
9. N. R. Cameron, *Polymer*, 2005, **46**, 1439-1449.
10. S. Jerenec, M. Šimić, A. Savnik, A. Podgornik, M. Kolar, M. Turnšek and P. Krajnc, *React. Funct. Polym.*, 2014, **78**, 32-37.
11. R. S. Moglia, M. Whitely, P. Dhavalikar, J. Robinson, H. Pearce, M. Brooks, M. Stuebben, N. Cordner and E. Cosgriff-Hernandez, *Biomacromolecules*, 2014, **15**, 2870-2878.
12. C. G. Swain, L. J. Schaad and A. J. Kresge, *J. Am Chem Soc.*, 1958, **80**, 5313-5319.
13. K. C. Berger, P. C. Deb and G. Meyerhoff, *Macromolecules*, 1977, **10**, 1075-1080.
14. S. S. Manley, N. Graeber, Z. Grof, A. Menner, G. F. Hewitt, F. Stepanek and A. Bismarck, *Soft Matter*, 2009, **5**, 4780-4787.
15. A. Menner, and Alexander Bismarck, *Macromol. Symp.*, 2006, **424**, 19-24.
16. R. Wu, A. Menner and A. Bismarck, *Polymer*, 2013, **54**, 5511-5517.
17. B. P. Binks and A. Rocher, *J. Colloid Interface Sci.*, 2009, **335**, 94-104.
18. N. R. Cameron and D. C. Sherrington, in *Biopolymers Liquid Crystalline Polymers Phase Emulsion*, Springer Berlin Heidelberg, Berlin, Heidelberg, 1996, pp. 163-214.

## CHAPTER 5

### Preparation of Janus particles using polymerised particle-stabilised emulsions

#### 5.1 Introduction

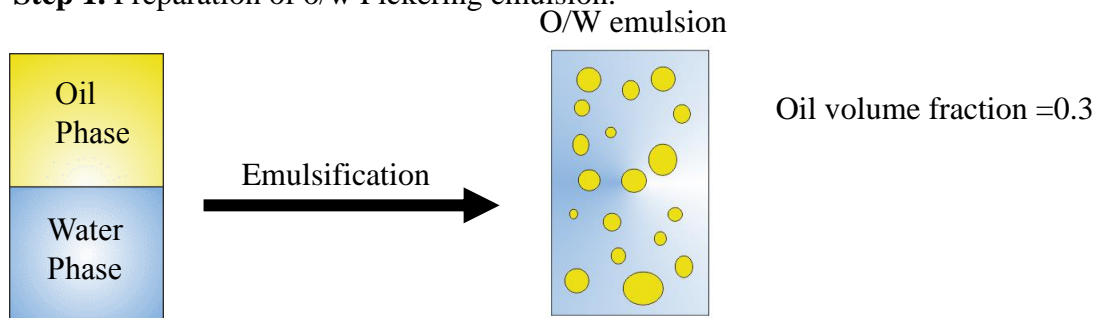
The surface of Janus particles have two different regions with distinct physical and chemical properties.<sup>1</sup> The Janus particle properties, such as functionality, polarity and electric/magnetic properties, could be tuned thus allowing them to be used in many applications, such as emulsion stabilisers,<sup>2</sup> smart materials<sup>3, 4</sup> and building blocks.<sup>5, 6</sup> During the past decade, different methods have been developed for the production of Janus particles for various desired applications. However, the production of Janus particles on a large scale is still one of the biggest challenges in this field. For example, the microfluidic technique for making Janus particles has the disadvantage of producing a limited yield or requiring a complicated procedure for the modification of the surface of the Janus particles.<sup>7, 8</sup> Moreover, industrial applications require methods which are simple, cost-efficient and capable of producing Janus particles on a large scale, while controlling the Janus balance (the ratio between the surface areas with different properties). Most of the existing methods for fabricating Janus particles have very limited yields which hamper their practical applications (see section 1.7 of chapter 1). Using particle-stabilised (Pickering) emulsions as a masking tool for making Janus particles is the only feasible approach which can produce large amounts of such particles. This approach has been applied with some success by using molten wax as a droplet phase in emulsions.<sup>9, 10</sup> However, the poor adhesion of particles to the solidified droplets and their limited thermal and chemical resistance are amongst its significant drawbacks.

The aim of this study is to develop an experimental procedure for making Janus particles using polymerised particle-stabilised emulsions which could be easily scaled up for producing large amounts of particles. In chapter 3, we demonstrated that methacrylate monomers can be easily polymerised at room temperature by redox-initiation using the BPO-DMPT couple. Here, we apply similar approach to polymerise the internal droplet phase of o/w particle-stabilised emulsions. The steps involved in our approach for the preparation of Janus particles are illustrated in Fig. 5.1. The first step is to make an oil-in-water (O/W) emulsion stabilised by silica particles. The oil phase of the emulsion contains methacrylate monomers (isobutyl methacrylate (IBMA) or MMA), a crosslinker (1,6-hexanediol diacrylate (HDDA) or EGDMA) and the BPO initiator. The water phase is an aqueous dispersion of silica particles in a TTAB solution with concentration up to

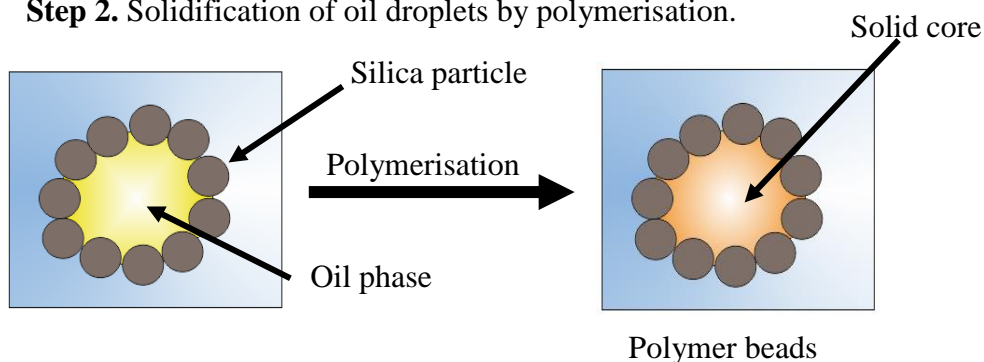
10 mM. The tetradecyltrimethylammonium bromide (TTAB) cationic surfactant is used to promote the particle attachment to the oil droplet surface by increasing their hydrophobicity. In step 2, the polymerisation of the oil droplets occurs in the presence of the DMPT accelerator. After the polymerisation is completed, the polymer beads are collected by filtration in step 3. This is followed by chemical modification of the exposed particle surface protruding outside the polymer bead (step 4). The final step 5 is to release the Janus particles made at step 4 by dissolving or swelling the polymer beads.

In the present study, we started by studying the stability of Pickering emulsions. Bare silica particles were treated with different concentrations of surfactant (TTAB) to tune the hydrophobicity and to enable the stabilisation of O/W emulsions. The volume fraction of the oil phase was 0.3, and the water phase consisted of 4 wt/vol.% of silica particles dispersed in TTAB solution (0–10 mM).

**Step 1.** Preparation of o/w Pickering emulsion.

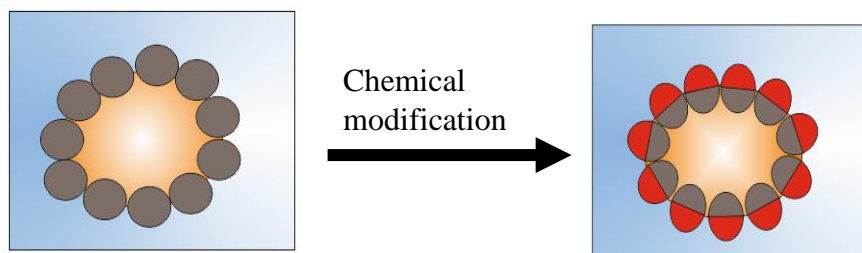


**Step 2.** Solidification of oil droplets by polymerisation.



**Step 3.** Isolation of polymer beads from the continuous phase by filtration.

**Step 4.** Chemical modification of the outer particle surface.



**Step 5.** Release of the Janus particles by dissolution or swelling of the polymer beads in appropriate solvents.

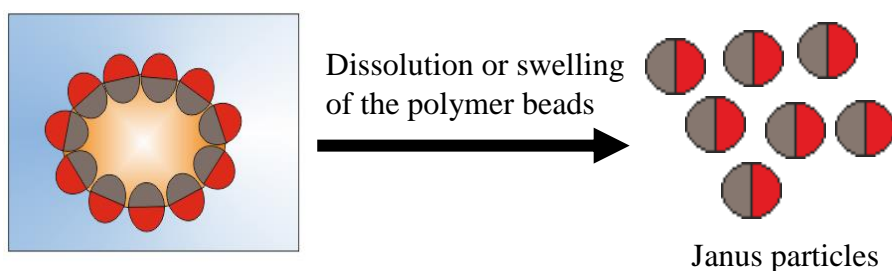


**Figure 5.1** Schematic representation of the procedure used in our study for the preparation of Janus particles using polymerised Pickering emulsions.

## 5.2 Small scale experiments with Pickering emulsions prepared by high speed homogenisation

The method we followed to produce Janus particles is illustrated in Fig. 5.2. Firstly, making o/w emulsion stabilised by silica particle. The silica particles were dispersed in TTAB solution to tune the hydrophobicity. Then, the oil phase was prepared separately to initiate the polymerisation before the emulsification step and consisted of the monomer, crosslinker, BPO and DMPT. Once the oil phase is ready, it added to the water phase and homogenised using Ultra-Turrax homogeniser at 11000 rpm for 90 s. After that, the emulsion was stirred at room temperature with a magnetic stirrer for 2 hours to make sure that the droplets have polymerised.

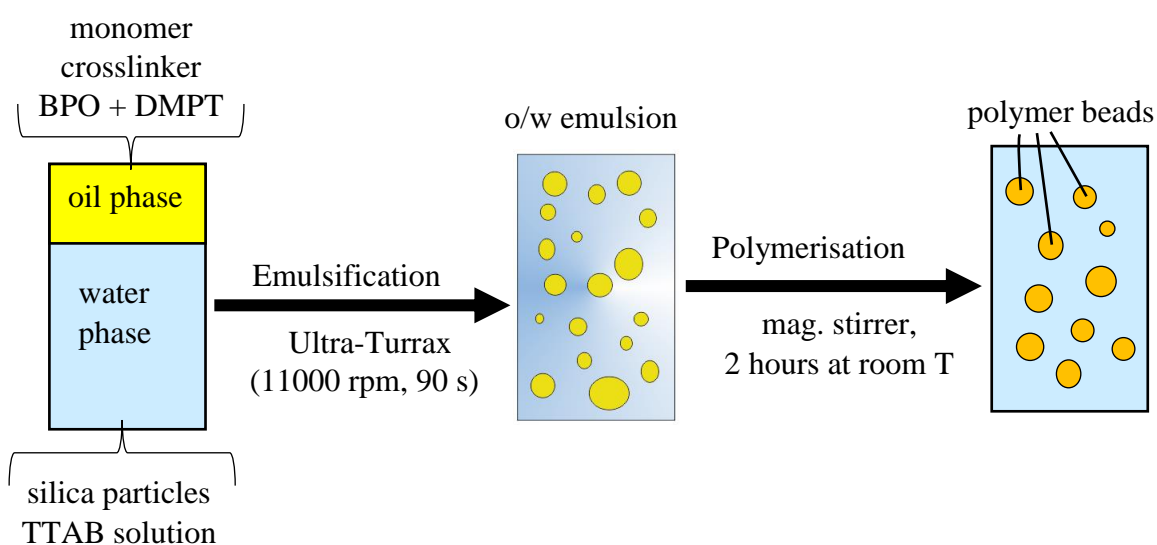


**Figure 5.2.** Diagram of the preparation and polymerisation of Pickering emulsions in the small scale experiments for making Janus particles.

The method we selected for the production of Janus particles required that the silica particles have the ability to stabilise o/w emulsions. For this reason, the emulsion stability was studied. The silica particles were hydrophilic as received from the supplier. A cationic surfactant tetradecyltrimethylammonium bromide (TTAB) was used to tune the hydrophobicity of the silica particles, in order for us to be able to control the properties of the Janus particles produced. The critical micelles concentration (CMC) for the cationic surfactant was around 3.5 mM.<sup>11</sup> The surfactant concentration varied from 0 to 10 mM. The concentration of the silica particles was fixed at 4 wt/vol.%. The volume fraction of the oil phase in the emulsions was 0.3. The emulsion was constituted as follows: 4 wt/vol.% of silica particles dispersed in 7 mL of TTAB solution and stirred with a magnetic stirrer bar for 1 h. Then, 3mL of the oil phase was added and homogenised by Ultra-Turrax at

11,000 rpm for 90 s. The emulsion stability was studied by taking images at different times.

IBMA monomer was selected as the main component of the oil phase of the emulsions in these experiments. HDDA or EGDMA were used as crosslinkers at a concentration of 15 vol.% in the oil phase. There were three experiments conducted for studying the emulsion stability and the production of Janus particles. The first system, the emulsion was made of oil phase 30vol.% (IBMA as the monomer, HDDA as the crosslinker, BPO as the initiator) and water phase (4wt/vol.% silica particles (2  $\mu\text{m}$  diameter) dispersed in TTAB solution). The second system, the emulsion consisted of oil phase 30vol.% (IBMA as the monomer, EGDMA as the crosslinker, BPO as the initiator) and water phase (4wt/vol.% silica particles (1 $\mu\text{m}$  diameter) dispersed in TTAB solution). The third system, the emulsion consisted of oil phase 30vol.% (IBMA as the monomer, EGDMA as the crosslinker, BPO as the initiator) and water phase (4wt/vol.% silica particles (0.1 $\mu\text{m}$  diameter) dispersed in TTAB solution).

### **5.2.1 Type and stability of emulsions**

Images of the vessels with the emulsions of IBMA-HDDA system stabilised by 2  $\mu\text{m}$  silica particles are shown in Fig.5.3. The emulsions at TTAB concentrations in the range 0–0.05 mM seemed not to be capable of maintaining their stability against creaming and coalescence. The cream layer of concentrated emulsion on the top of the water phase appeared just 10 min after emulsification. The height of the cream layer decreased with time. There was a transparent layer of water at the bottom of the vessel, as can be seen in Fig 5.3. In the emulsions at TTAB concentrations in the range 0.1–1 mM, their stability increased with increasing surfactant concentration. The cream layer was noticed after 1 h at 0.1 mM only. After 12 h, the water layer became visible and at 1 mM, the water layer looked turbid. In the emulsion at 2–10 mM, the stability improved further. Noticeably, during the emulsification, a lot of foam and overflow from the vessel were produced. This production of foam can be seen on the images, as the volume of the emulsions reduced with time. The cream layer was delayed and appeared after 12 h, which indicated a high stability of the emulsions against creaming. Emulsion were stable for up 12 hours. The drop tests confirmed that in all cases O/W emulsions were formed. Microscopic images of the IBMA-HDDA emulsions taken at two different magnifications are shown in Figures 5.4–5.6. The size of the emulsion droplets decreased with increasing surfactant concentration in the system. This decrease in size is due to a reduction in interfacial tension caused by the surfactant<sup>12</sup> that helped for smaller droplets to be generated. At a high concentration of surfactant, in particular close to the critical micelle concentration

(CMC, 3 mM), the diameter of some emulsion droplets is smaller than that of the silica particles (2  $\mu\text{m}$ ). This suggests that at least some of the oil droplets are stabilised by the surfactant only. The Pickering emulsion at high TTAB concentrations is turned into an emulsion stabilised by surfactant alone, owing to the highly competitive adsorption between the surfactant and particles at the interface. As a result, the surfactants molecules have replaced the particles at the oil-water interface.<sup>13</sup>

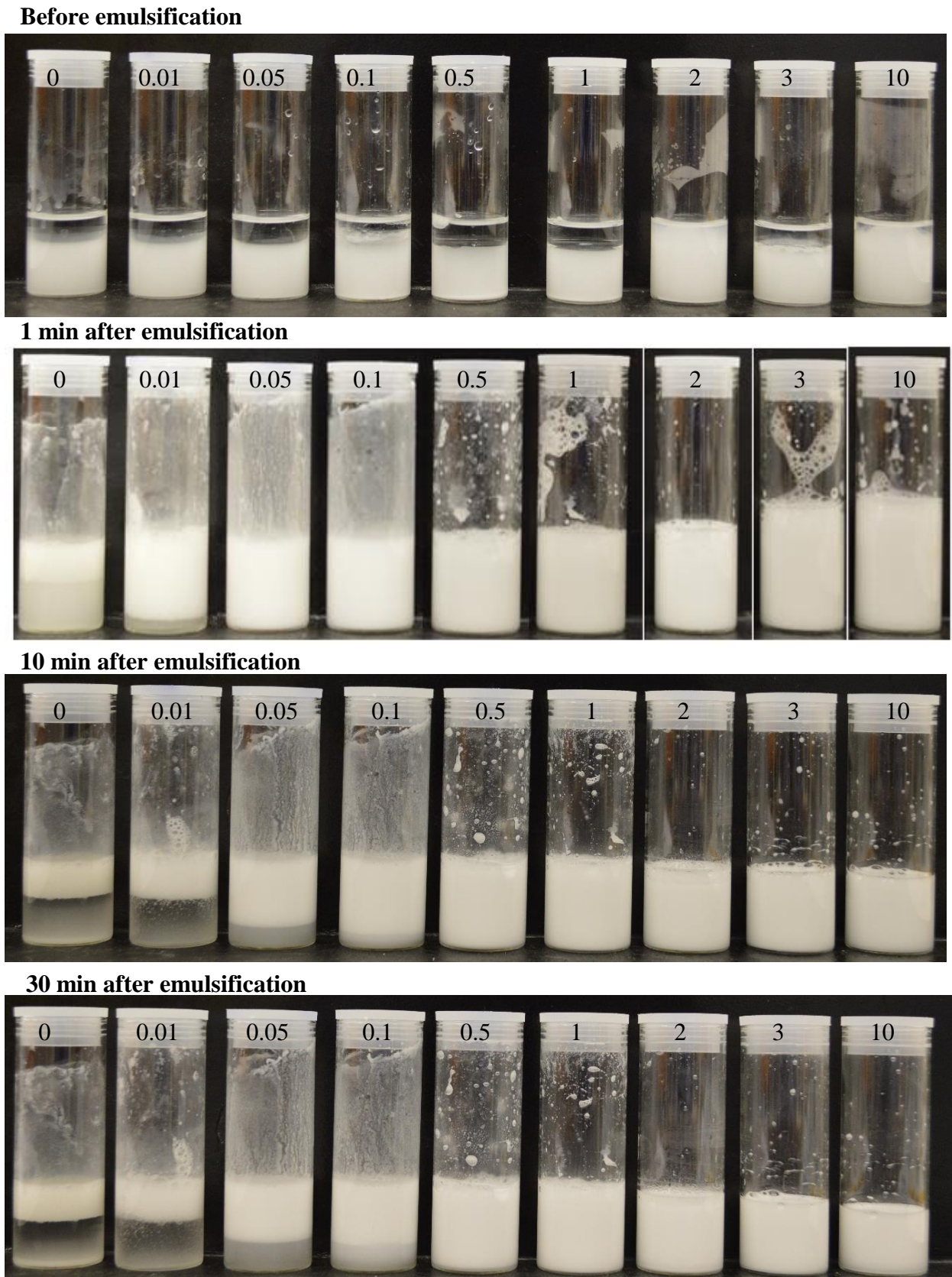


**Figure 5.3.** Appearance of vessels containing emulsions of IBMA and aqueous suspensions of 2  $\mu\text{m}$  silica particles in TTAB solutions at concentrations shown in mM, at different times after emulsification. The system with oil volume fraction  $\phi_o=0.3$  was homogenised by an Ultra-Turrax homogeniser (18 mm head) at 11,000 rpm for 90 sec. The oil phase was composed of 1wt/vol.% BPO and 15vol.% HDDA, all dissolved in IBMA. The water phase contained 4 wt/vol.% silica particles.

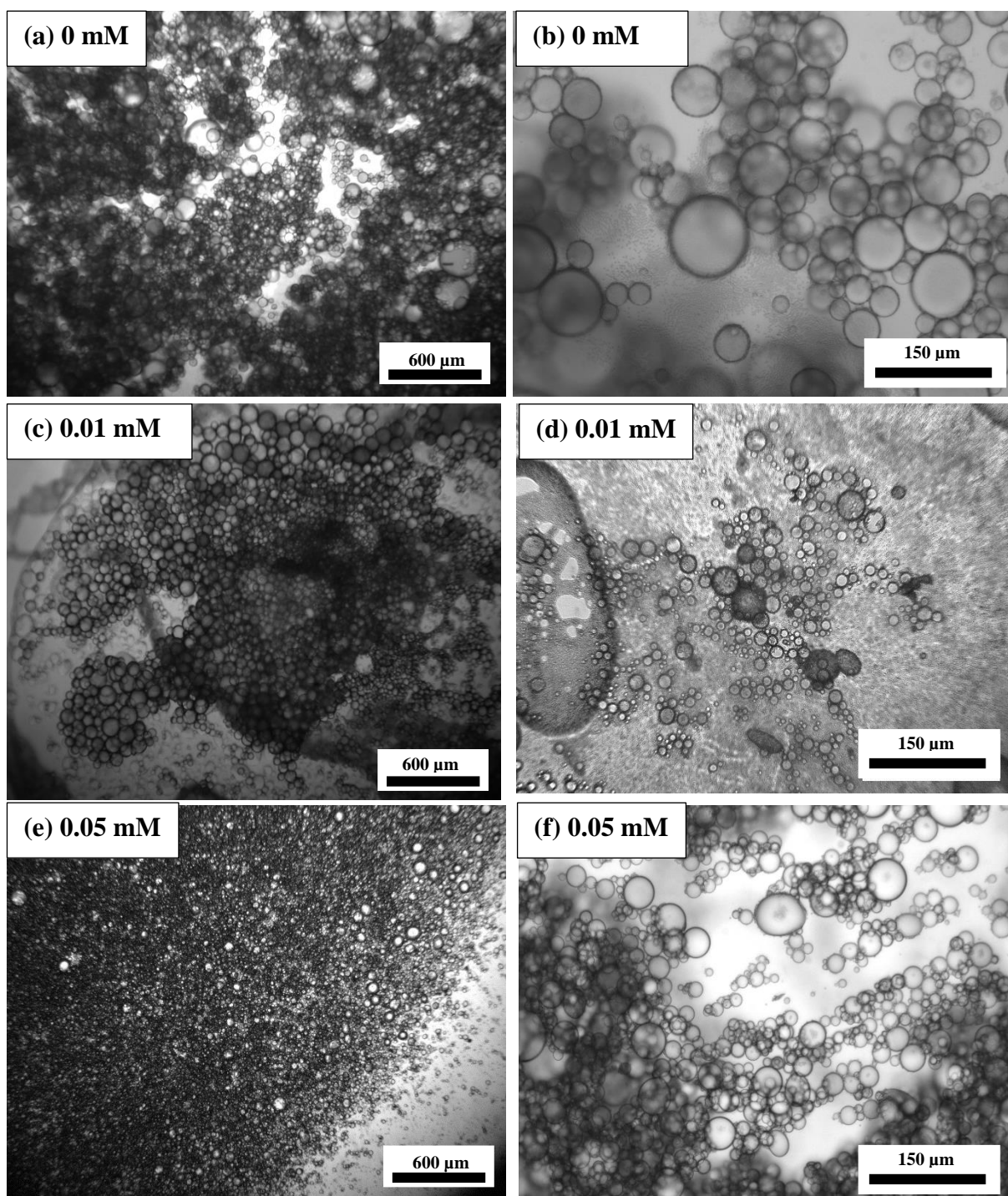


**Figure 5.4.** Microscopic images of emulsions stabilised by 2  $\mu\text{m}$  silica particles in the presence of TTAB at concentrations shown, taken at two different magnifications shortly after the emulsification by using an Ultra-Turrax homogeniser (18 mm head) at 11,000 rpm for 90 s. The silica particles were dispersed in aqueous TTAB solutions and stirred for 2 h before use. The oil phase (3mL) was composed of 1wt/vol.% BPO and 15vol.% HDDA, all dissolved in IBMA. The water phase (7 mL) contained 4 wt/vol.% silica particles.

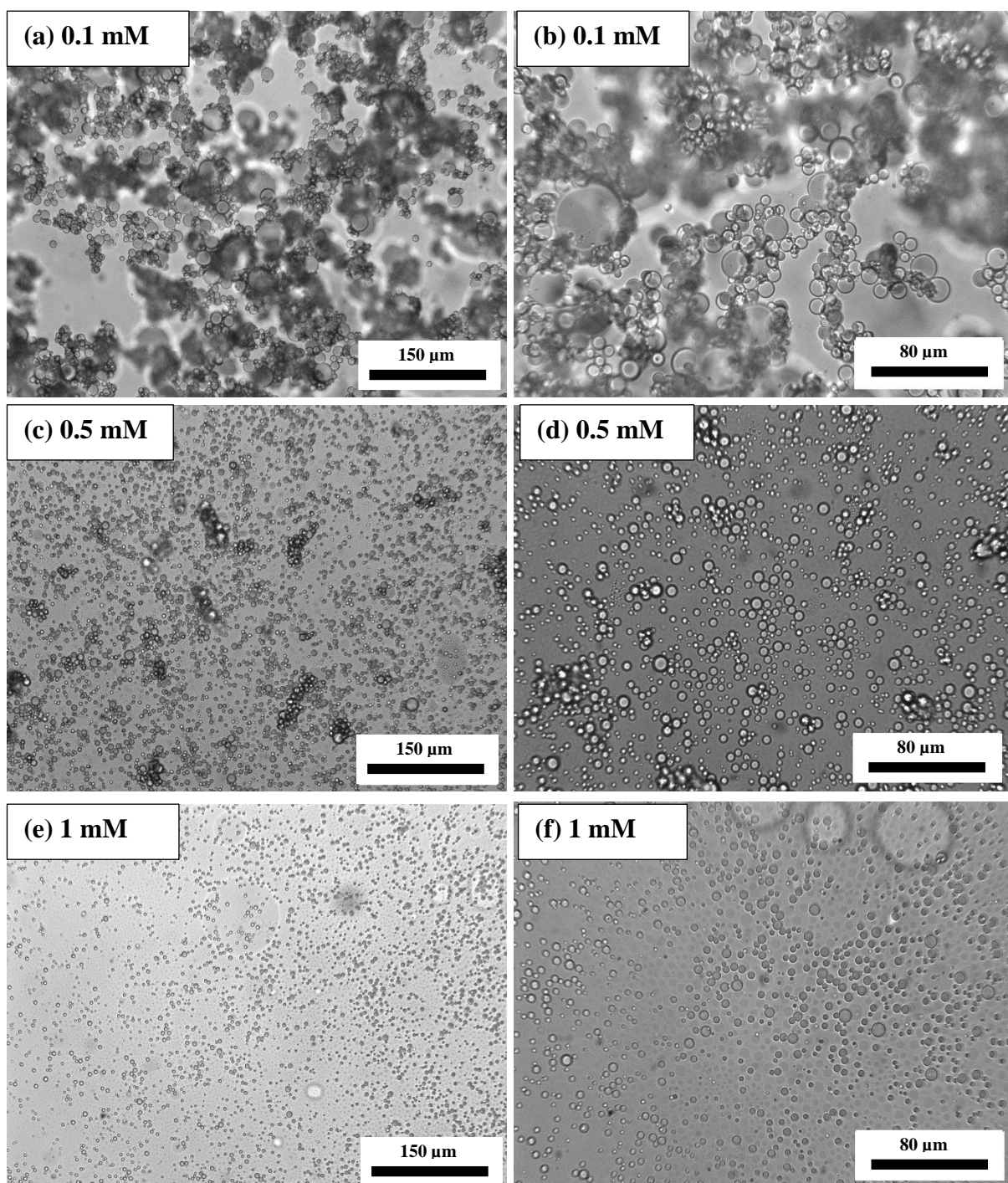


**Figure 5.5.** Microscopic images of emulsions stabilised by 2  $\mu\text{m}$  silica particles in the presence of TTAB at concentrations shown, taken at two different magnifications shortly after the emulsification by using an Ultra-Turrax homogeniser (18 mm head) at 11,000 rpm for 90 s. The experimental conditions are the same as in Fig. 5.4 except the TTAB concentrations.

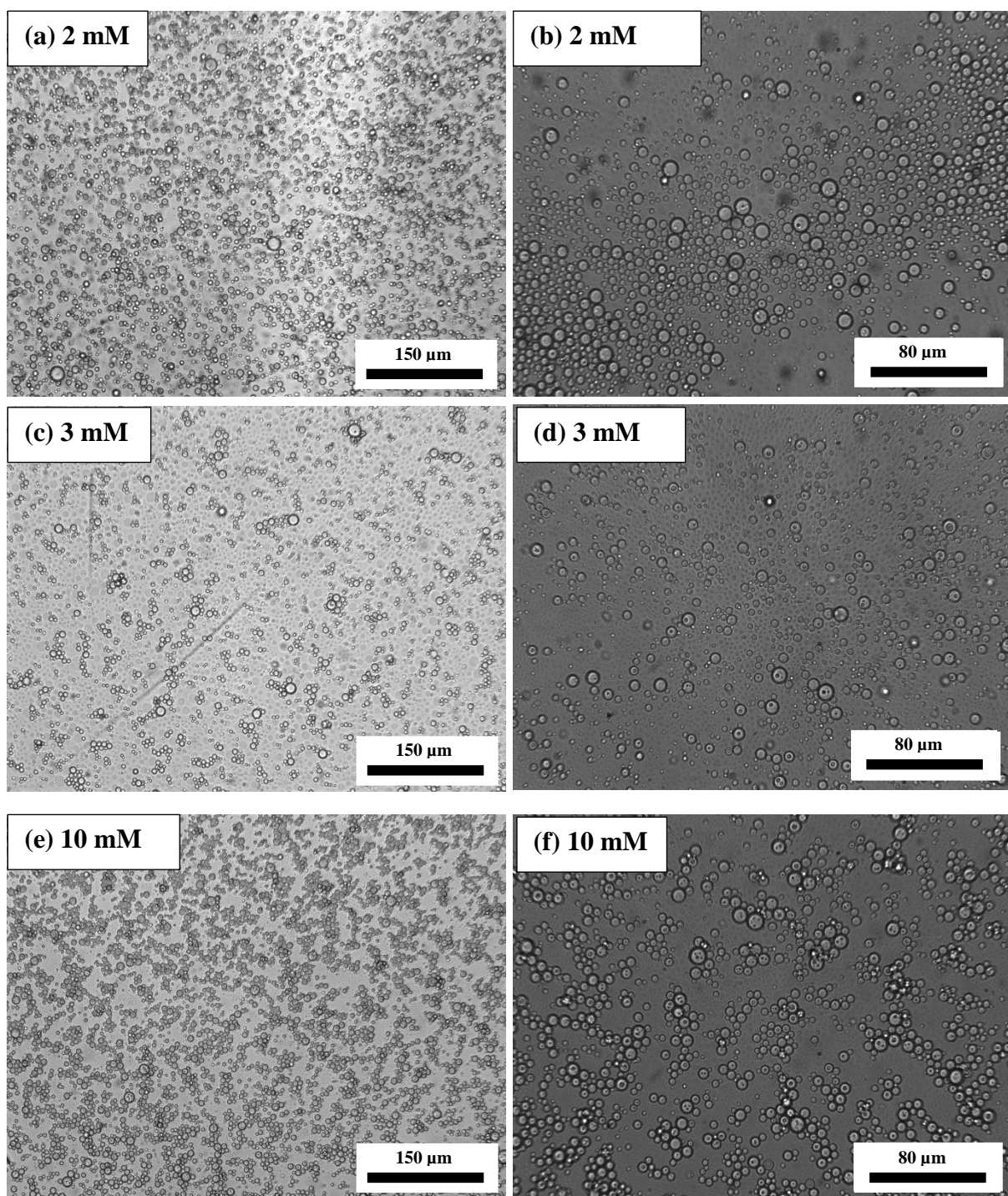


**Figure 5.6.** Microscopic images of emulsions stabilised by 2  $\mu\text{m}$  silica particles in the presence of TTAB at concentrations shown, taken at two different magnifications shortly after the emulsification by using an Ultra-Turrax homogeniser (18 mm head) at 11,000 rpm for 90 s. The experimental conditions are the same as in Fig. 5.4 except the TTAB concentrations.

Images of the vessels with emulsions stabilised by 1  $\mu\text{m}$  silica particles for the IBMA-EGDMA system are shown in Fig. 5.7. The images show that in the emulsions at TTAB concentration in the range 0–0.1 mM, the creaming layer appeared 1 min after the emulsification. Emulsions were not stable against creaming. The water layer became clear after 12 h (see Fig. 5.8). The emulsion at 0.5 mM TTAB was stable against coalescence and creaming and lasted up to 12 h (see Figs 5.7 and 5.8). The emulsion at 1 mM TTAB was of O/W type (confirmed by drop tests) but very unstable. An oil layer at the top of the emulsion appeared just 1 min after emulsification (see Figs 5.7 and 5.8). The emulsions at 2–3 mM TTAB showed highest stability against creaming up to 2 h. Coalescence in those emulsions was not observed even 12 h after emulsification (see Fig 5.8.). One should note that the emulsion at 10 mM TTAB foamed and overflowed the vessel during emulsification. Therefore, the volume of the emulsion was lower than that of the original system before emulsification. The drop tests showed that all emulsions were of an O/W type. Microscopic images of emulsions are shown in Figures 5.9–5.11. The size of the droplets decreased with increasing surfactant concentration.

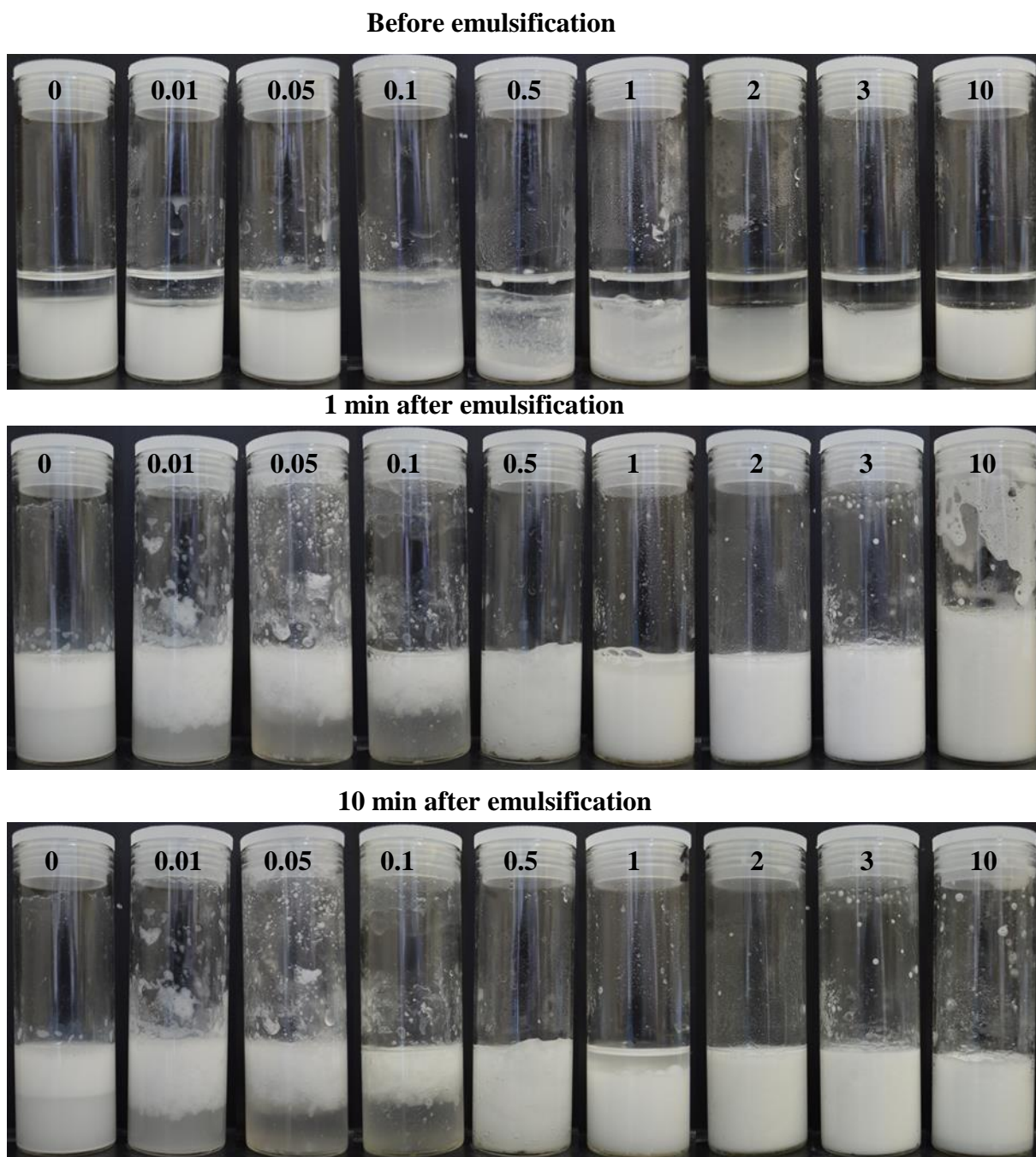
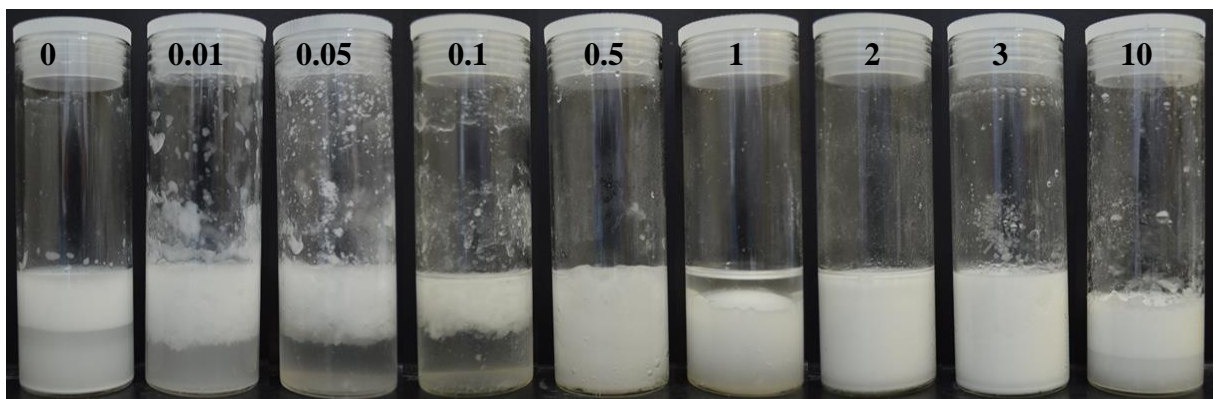


**Figure 5.7.** Appearance of vessels containing emulsions of IBMA-EGDMA and 1  $\mu\text{m}$  silica particles dispersed in aqueous TTAB solutions at concentrations shown in mM, at different times after emulsification. The system with oil volume fraction  $\phi_o=0.3$  was homogenised by an Ultra-Turrax homogeniser (18 mm head) at 11,000 rpm for 90 sec. The oil phase was composed of 1wt/vol.% BPO and 15vol.% EGDMA, all dissolved in IBMA. The water phase contained 4 wt/vol.% silica particles.

30 min after emulsification



2 h after emulsification



12 h after emulsification



**Figure 5.8.** Appearance of vessels containing emulsions of IBMA-EGDMA and 1  $\mu\text{m}$  silica particles dispersed in aqueous TTAB solutions at concentrations shown in mM, at different times after emulsification. The system with oil volume fraction  $\phi_o=0.3$  was homogenised by an Ultra-Turrax homogeniser (18 mm head) at 11,000 rpm for 90 sec. The oil phase was composed of 1wt/vol.% BPO and 15vol.% EGDMA, all dissolved in IBMA. The water phase contained 4 wt/vol.% silica particles.

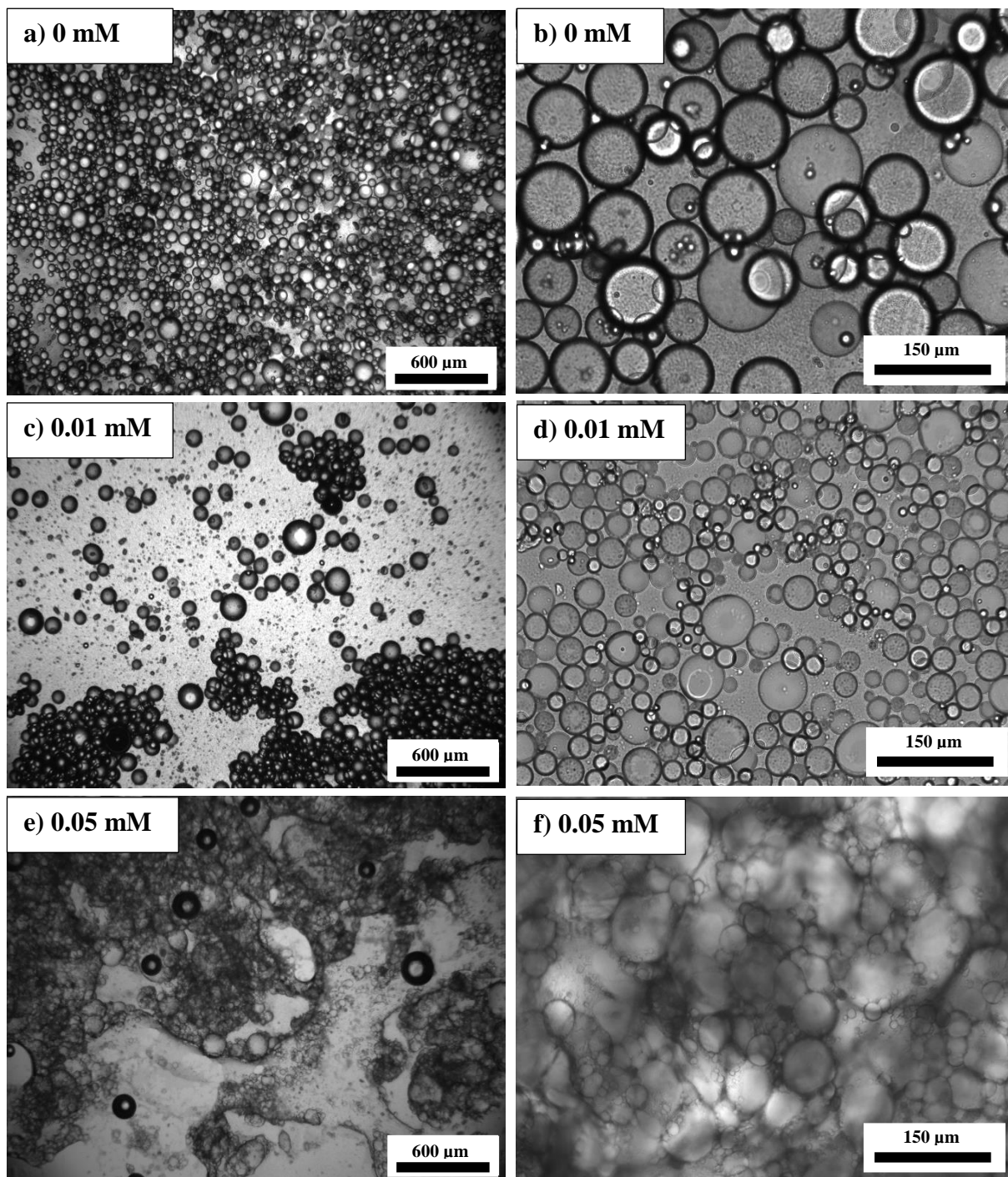


**Figure 5.9.** Microscopic images of IBMA-EGDMA emulsions stabilised by 1  $\mu\text{m}$  silica particles in the presence of TTAB at concentrations shown, taken at two different magnifications shortly after the emulsification by using an Ultra-Turrax homogeniser (18 mm head) at 11,000 rpm for 90 s. The silica particles were dispersed in aqueous TTAB solutions and stirred for 2 h before use. The oil phase (3mL) was composed of 1wt/vol.% BPO and 15vol.% EGDMA, all dissolved in IBMA. The water phase (7 mL) contained 4wt/vol.% silica particles.

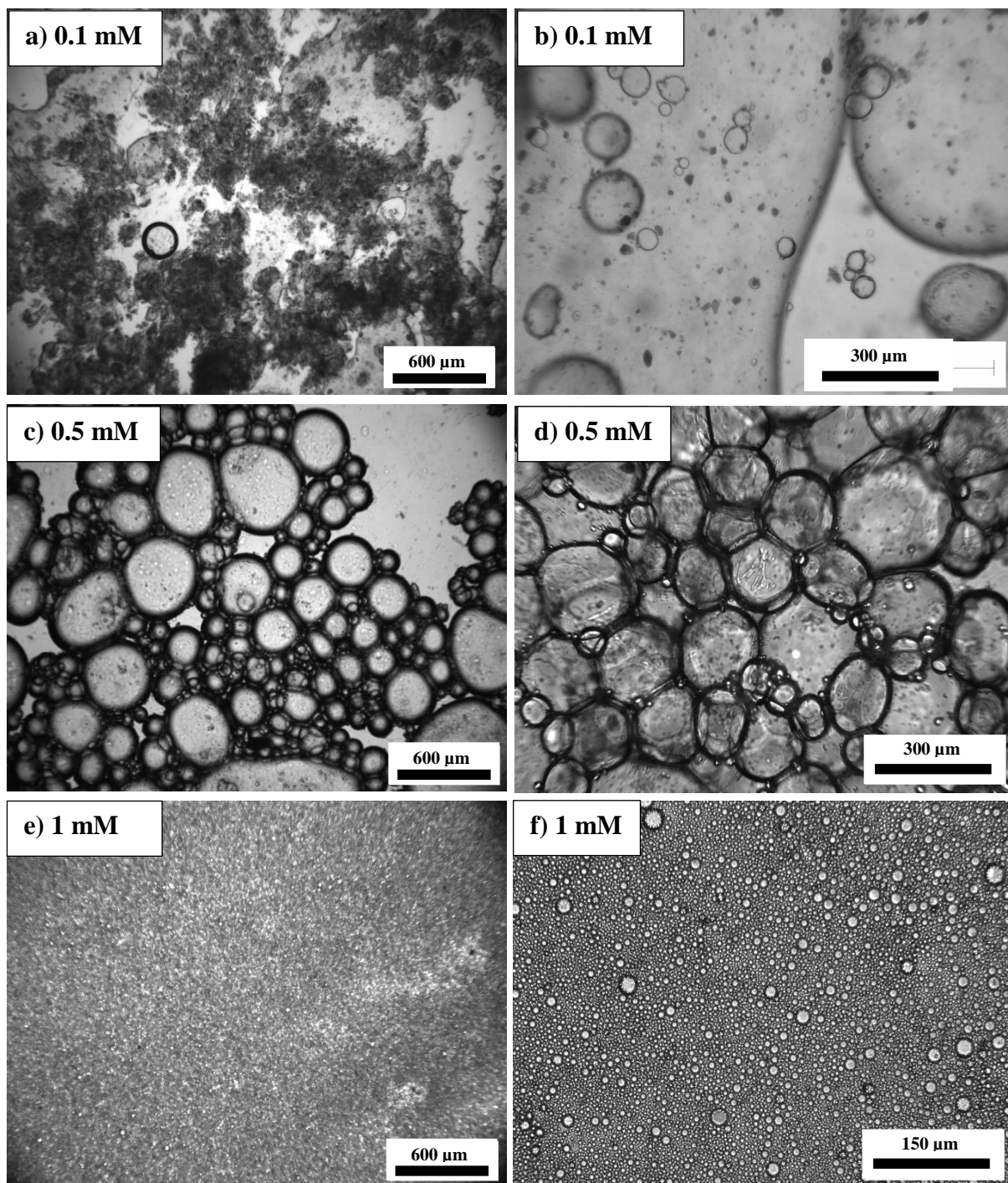


**Figure 5.10.** Microscopic images of IBMA-EGDMA emulsions stabilised by 1  $\mu\text{m}$  silica particles in the presence of TTAB at concentrations shown, taken at two different magnifications shortly after the emulsification by using an Ultra-Turrax homogeniser (head 18 mm) at 11,000 rpm for 90 s. The experimental conditions are the same as in Fig. 5.9 except the TTAB concentrations.

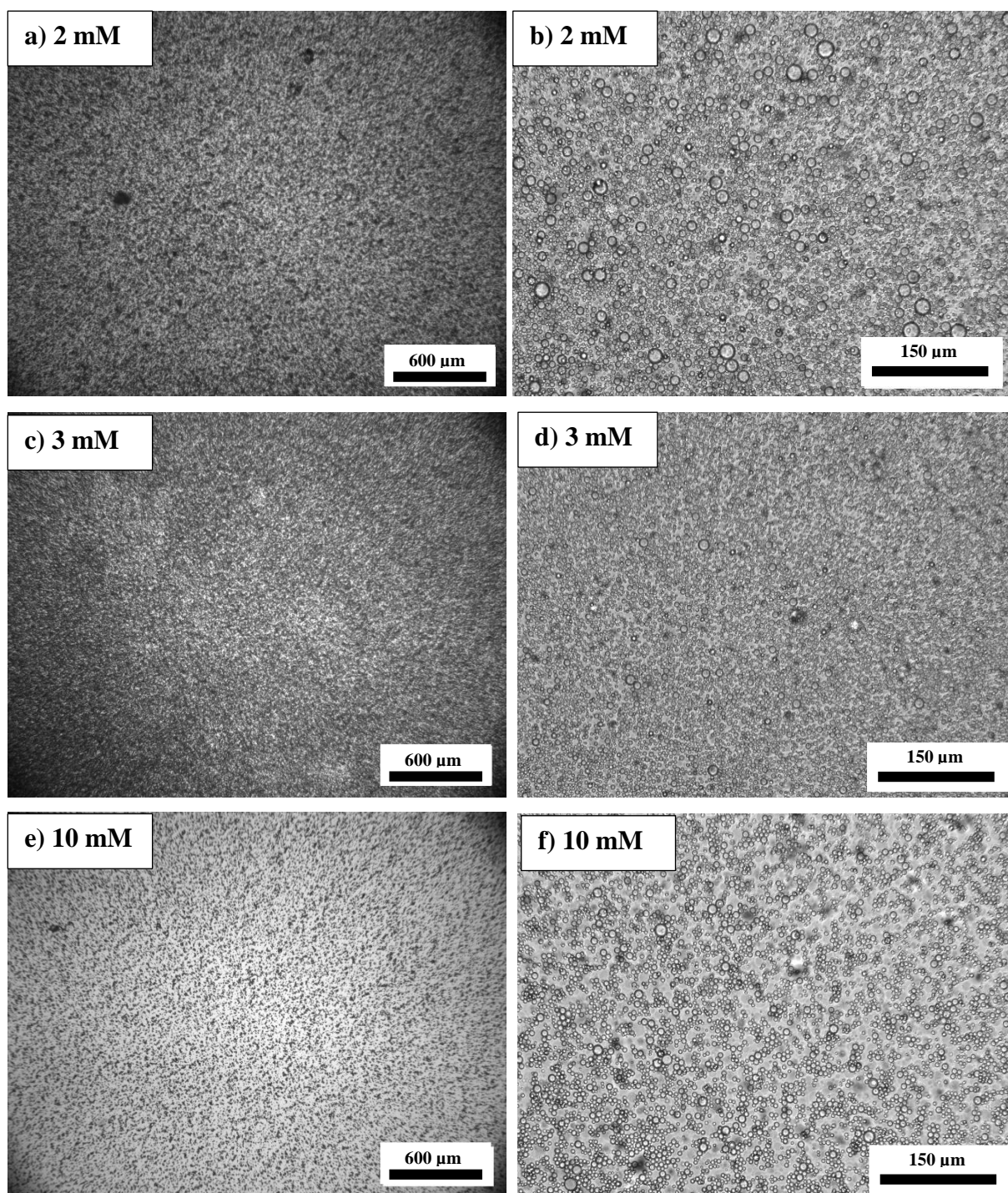


**Figure 5.11.** Microscopic images of IBMA-EGDMA emulsions stabilised by 1  $\mu\text{m}$  silica particles in the presence of TTAB at concentrations shown, taken at two different magnifications shortly after the emulsification by using an Ultra-Turrax homogeniser (head 18 mm) at 11,000 rpm for 90 s. The experimental conditions are the same as in Fig. 5.9 except the TTAB concentrations.

The emulsion stability of IBMA-EGDMA emulsions stabilised with silica particles (0.1  $\mu\text{m}$  diameter). The type of the emulsion was O/W emulsion confirmed by the drop test. At lower surfactant concentration the creaming was faster than those with high concentration. Emulsions were stable against coalescence for up to 12 hours. The

behaviour of the emulsion stability was similar to those stabilised with silica particles (1  $\mu\text{m}$  diameter).

### 5.2.2 Polymerisation of the Pickering emulsions

Images of polymerised emulsions were stirred with a magnetic stirrer bar for 2 h (see Fig. 5.12). The polymer beads were then collected using vacuum filtration with filter paper (pore size range 5–8  $\mu\text{m}$ ), as shown in Fig. 5.13. The emulsion was stabilised with a mixture of surfactant (0–10 mM) and silica particles. Three different sizes of silica particles were used (2  $\mu\text{m}$ , 1  $\mu\text{m}$ , and 0.1  $\mu\text{m}$  diameter). The cross-linker HDDA was used with silica particles (2  $\mu\text{m}$  diameter) and EGDMA with silica particles (1 and 0.1  $\mu\text{m}$  diameter).

Images of the vessels of the Pickering emulsions after polymerisation are shown in Fig. 5.12. In most cases, the polymerisation at room temperature was successful. The oil droplets become solid polymers and sediment as shown in the images. In Fig. 5.12 a and b, the polymer beads were obtained in the range 0–0.1 mM of TTAB and then further increase in surfactant concentration, the production was flaky polymers or bulk polymers. In Fig. 5.12c, the range of surfactant was explored from 0–0.5 mM of TTAB, the polymerisation was successful and the production was polymer beads except for 0.3 and 0.5 mM of TTAB where the bulk polymers or small pieces obtained see Fig. 5.14. The surfactant concentration affected the polymerisation, in some cases inhibiting it. The polymer beads were obtained in the range of surfactant concentration 0–0.1 mM. A further increase in surfactant concentration, to 0.5–2 mM, produced a bulk of polymer or small pieces of polymers, as shown in Fig. 5.13. Therefore, the system reached CMC at 3 mM and went beyond that level up to 10 mM, at which point polymerisation utterly failed and nothing was obtained after filtration. This behaviour was observed with all the polymerisation performed using different sizes of silica particles. A possible explanation is that there was interference between the surfactant and the polymerisation. In particular, at high surfactant concentration, polymerisation could not occur, and the outcome of the filtration step was liquid, which could be a clear indication that the polymerisation was inhibited. The effect of surfactant and silica particles on the rate of polymerisation has been studied.<sup>14</sup> It has been suggested that surfactants could slow down the rate of polymerisation and the surfactant with silica particles could block the generation of free radicals.<sup>14</sup> The reaction between the free silanol group and the free radical are most likely to inhibit the polymerisation. In addition, the lack of production of polymer beads at a higher concentration of surfactant could be related to the stability of the emulsion. Therefore, an optimal surfactant concentration is needed to obtain the silica particles

attached to the polymer beads (0–0.1 mM). An excess of surfactant in the system could replace the particles at the interface, and the emulsion would be less stable during the polymerisation.<sup>13</sup> The emulsion started destabilising at 0.5 mM and continued with increasing surfactant concentration, whereas, at a low surfactant concentration of 0.01–0.1 mM, there was possibly no excess of surfactant and all of it was used to adjust the hydrophobicity of silica particles. As a result, polymer beads were obtained.

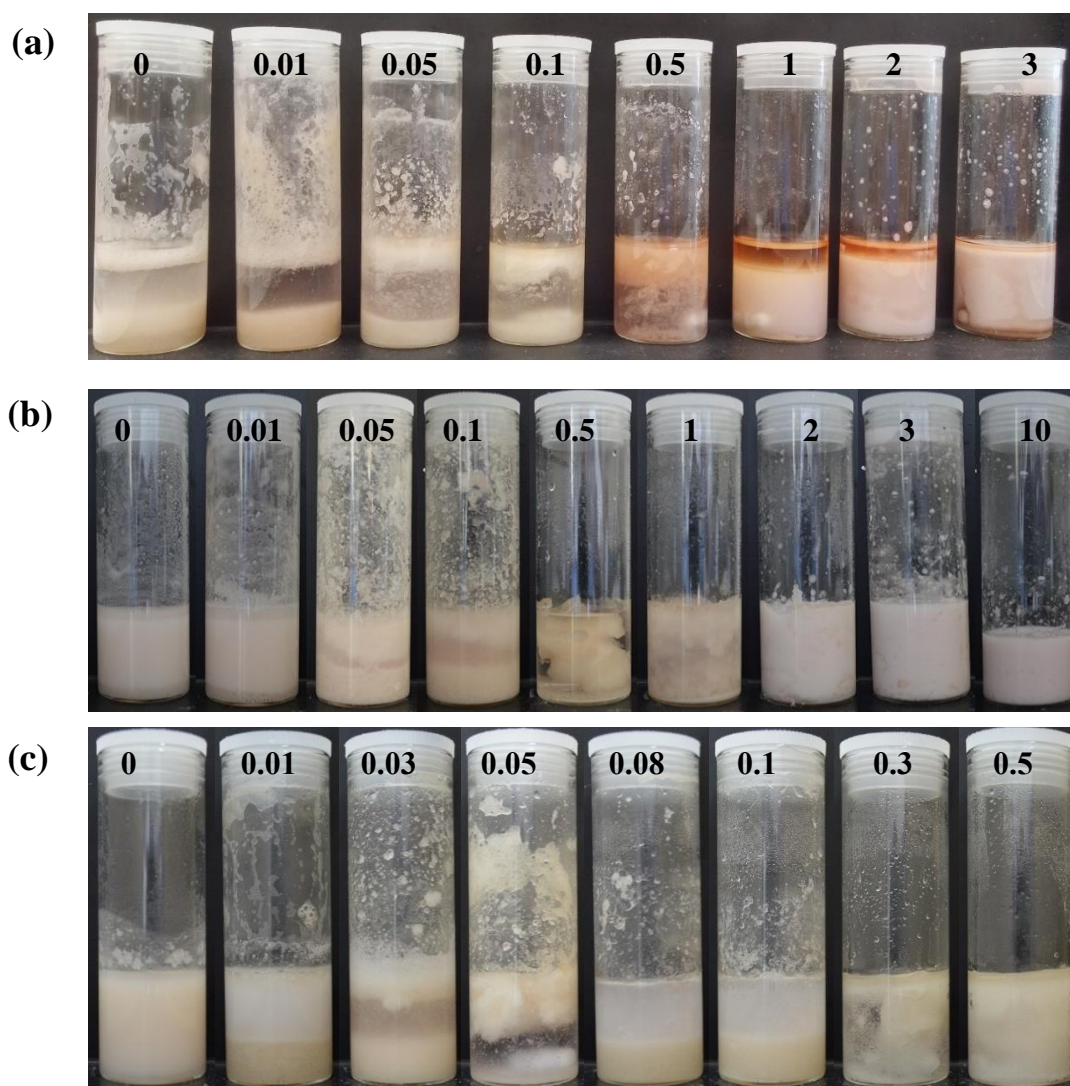


**Figure 5.12.** Appearance of vessels containing polymerised emulsions at concentrations in mM, shown after 2 hours of emulsification and stirring with magnetic stirrer bar. The system with oil volume fraction  $\phi_o=0.3$  was homogenised by an Ultra-Turrax homogeniser (18 mm head) at 11,000 rpm for 90 sec. (a) the oil phase consisted of 1 wt/vol.% of BPO and 15vol.% of HDDA, 1.19 vol.% DMPT all dissolved in IBMA. The water phase (4wt/vol.% silica particles (2 $\mu$ m diameter) dispersed in TTAB solution). The oil phase was composed of 1wt/vol.% BPO and 15vol.% EGDMA, 1.19vol.% DMPT all dissolved in IBMA and the water phase made of 4wt/vol.% of silica particles, (b) 1  $\mu$ m diameter and (c) 0.1  $\mu$ m diameter.

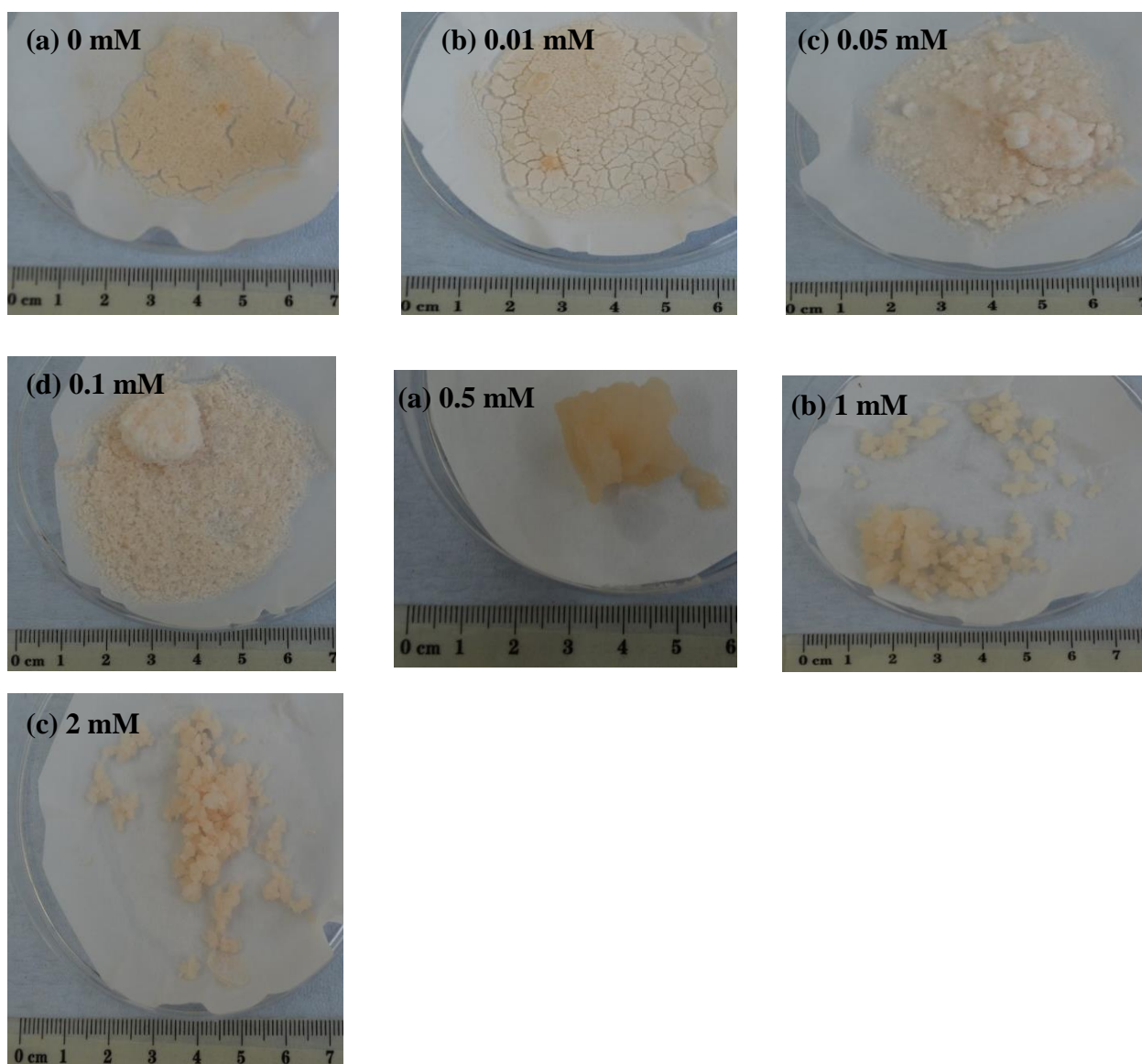


**Figure 5.13.** Polymer beads after drying in the vacuum oven at room temperature overnight. The emulsion consisted of oil phase 3 mL (1wt/vol.% of BPO, 15vol% of EGDMA, 1.19vol.% DMPT, all dissolved in IBMA), and the water phase consisted of 4wt/vol.% silica particles (1  $\mu\text{m}$  diameter) dispersed in 7 mL of TTAB solution.

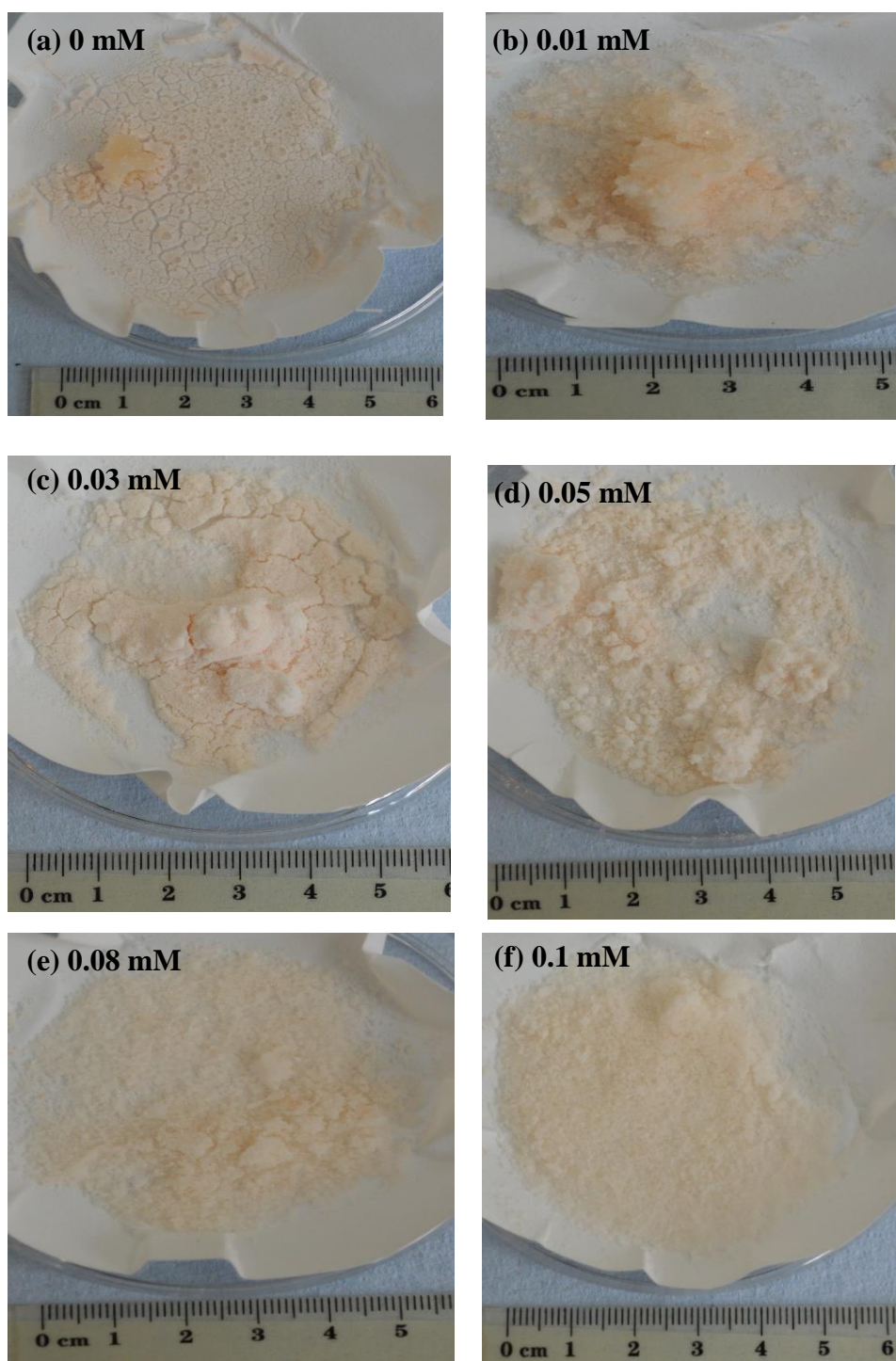


**Figure 5.14.** Polymer beads after drying in the vacuum oven at room temperature overnight. The emulsion consisted of oil phase 3 mL (1wt/vol.% of BPO, 15vol.% of EGDMA and 1.19vol.% DMPT, all dissolved in IBMA), and the water phase consisted of 4wt/vol.% silica particles (0.1  $\mu\text{m}$  diameter) dispersed in 7 mL of TTAB solution.

The SEM images of the system stabilised with silica particles (1  $\mu\text{m}$  diameter) are presented in Figs 5.16 and 5.17. The particles achieved complete coverage of the polymer beads at 0 and 0.01 mM of TTAB solution. However, the coverage was not a monolayer, and there was some aggregation of particles. At 0.05 mM, the particles almost covered the polymer beads. Some particles formed a multilayer and others were detached from the polymer beads. At 0.1 mM, the particles covered the polymer beads poorly and were not attached firmly. There were some particles left on the polymer beads after polymerisation, as there was some concavity on the surface of the beads. There was also some aggregation of the particles. To obtain monolayer coverage, the polymer beads were washed with pH=10 in order to charge the particles and make them repel one another see Fig.5.15, in order to remove the multilayer and SEM images were taken see Figs.5.18 and 5.19. At 0 mM, the washing succeeded in making the coverage almost monolayer. A few particles remained attached as a second layer but these were not significant. At 0.01–0.1 mM, some of the particles left the polymer beads as a result of washing. The monolayer coverage improved but some remaining particles aggregated and formed the second layer. At 0 mM of surfactant, washing helped remove the multilayer. However, on the rest of the samples, some silica particles were still left on the polymer beads and there was an aggregation of particles.

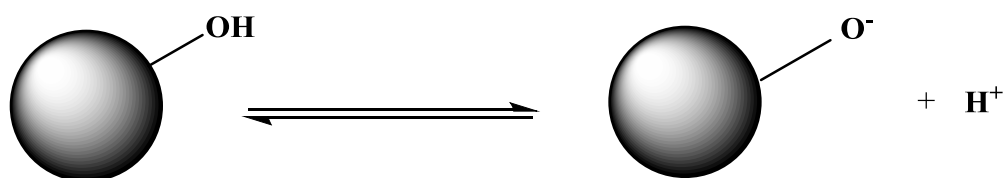


**Figure 5.15.** Schematic representation for the silica particles at pH=10. The hydroxyl group ionised.

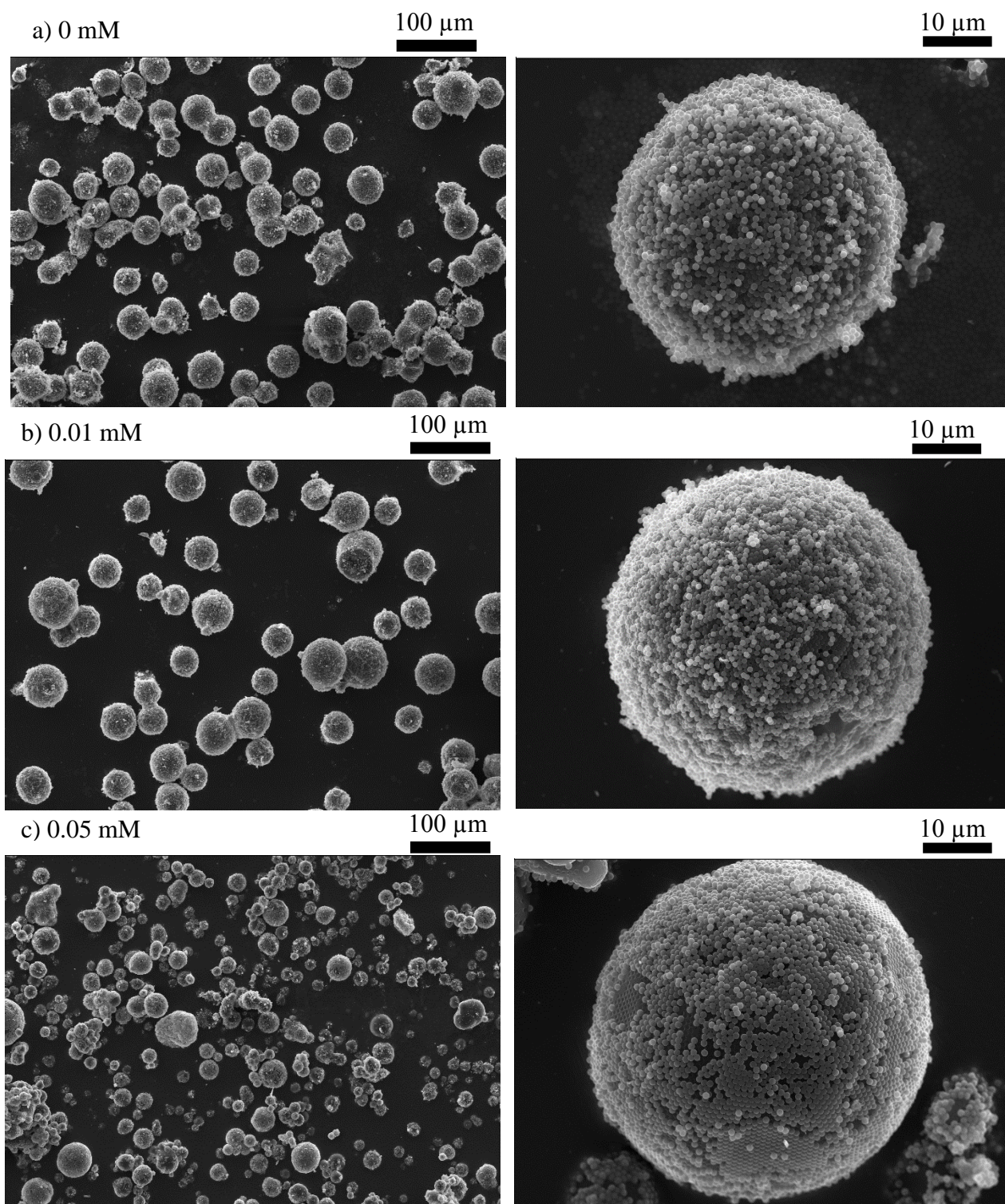


**Figure 5.16.** SEM images of silica particles (1 μm diameter) attached to polymer beads produced after the polymerisation of IBMA-EGDMA emulsions. Emulsions consisted of 30vol.% oil phase (1wt/vol.% BPO, 15vol.% EGDMA and 1.19vol.% DMPT, all dissolved in IBMA) and 70vol.% water phase (4wt/vol.% silica particles dispersed in TTAB solutions at concentrations 0, 0.01, 0.05 mM).

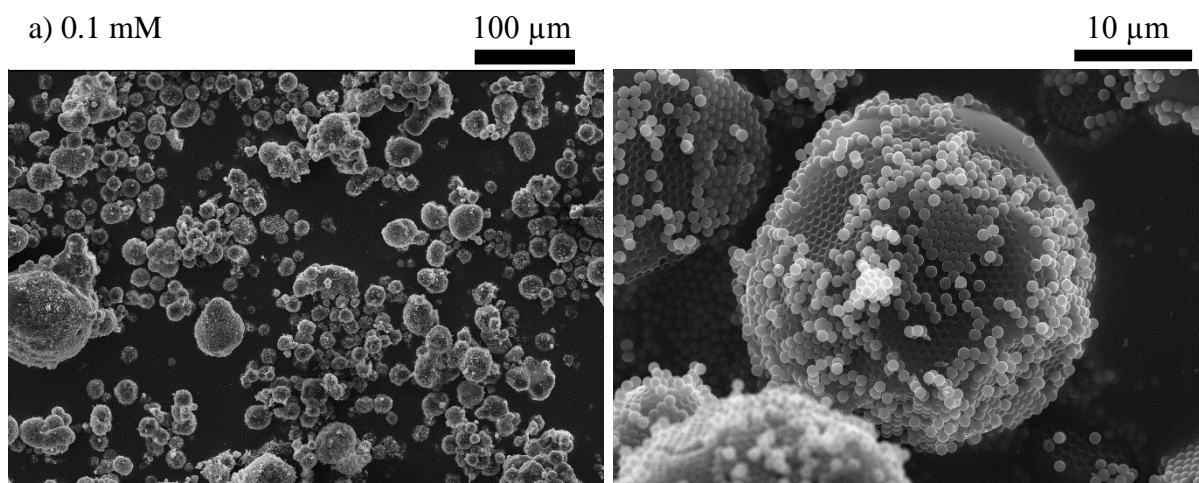


**Figure 5.17.** SEM images of silica particles (1  $\mu\text{m}$  diameter) attached to polymer beads produced after the polymerisation of IBMA-EGDMA emulsions. Emulsions consisted of 30vol.% oil phase (1wt/vol.% BPO, 15vol.% EGDMA and 1.19vol.% DMPT, all dissolved in IBMA) and 70vol.% water phase (4wt/vol.% silica particles dispersed in TTAB solutions at concentrations 0.1 mM).

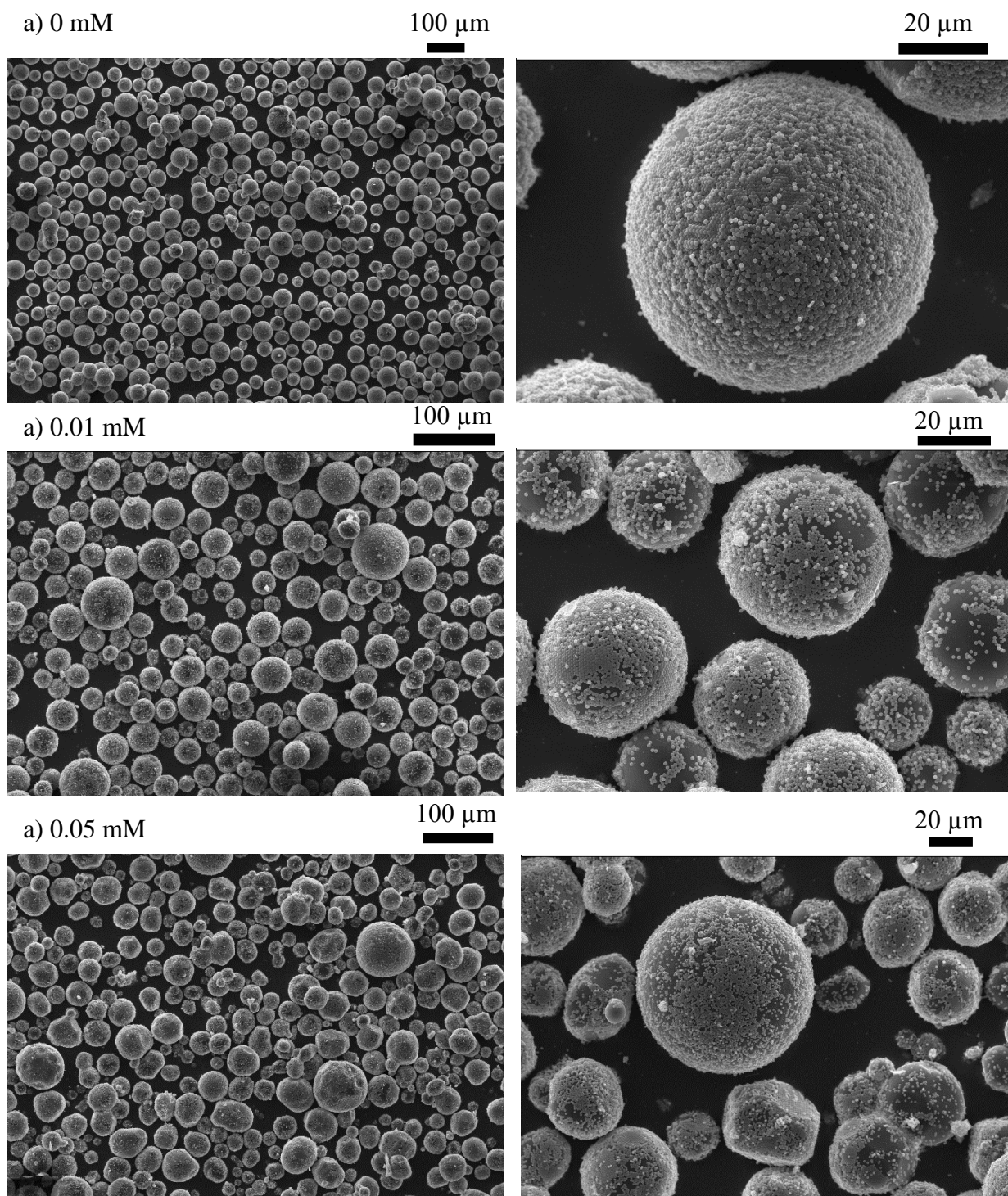


**Figure 5.18.** SEM images of silica particles (1 μm diameter) attached to polymer beads produced after the polymerisation of IBMA-EGDMA emulsions. Emulsions consisted of 30vol.% oil phase (1wt/vol.% BPO, 15vol.% EGDMA and 1.19vol.% DMPT, all dissolved in IBMA) and 70vol.% water phase (4wt/vol.% silica particles dispersed in TTAB solutions at concentrations 0, 0.01, 0.05 mM). The SEM images were taken after washing the polymer beads with water pH=10 for 30 min and gentle shaking.

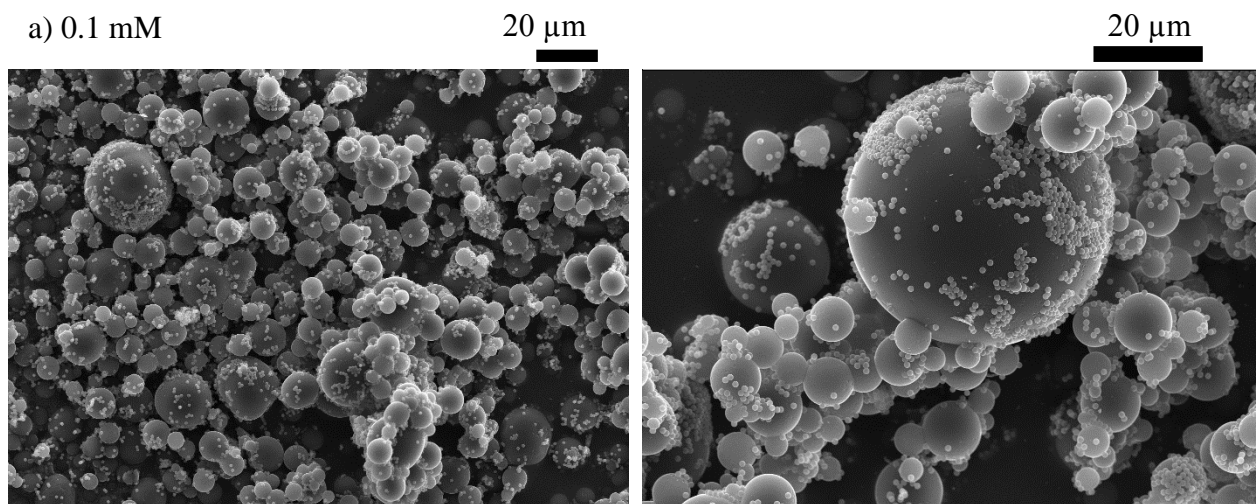


**Figure 5.19.** SEM images of silica particles (1  $\mu\text{m}$  diameter) attached to polymer beads produced after the polymerisation of IBMA-EGDMA emulsions. Emulsions consisted of 30vol.% oil phase (1wt/vol.% BPO, 15vol.% EGDMA and 1.19vol.% DMPT, all dissolved in IBMA) and 70vol.% water phase (4wt/vol.% silica particles dispersed in TTAB solutions at concentrations 0.1 mM). The SEM images were taken after washing the polymer beads with water pH=10 for 30 min and gentle shaking.

### 5.2.3 Release of silica particles from polymerised emulsion droplets

The silica particles attached to the polymer beads successfully, as shown previously. Our method of releasing the particles from the polymer beads was to use an ultrasonic probe. Optimisation was achieved by emulsifying with Ultra-Turrax and using silica particles of 2  $\mu\text{m}$  diameter. This size of particle was chosen in order to allow us to observe it with our bench top SEM. As discussed, polymer beads were successfully produced in the range of 0–0.1 mM TTAB. The emulsion consisted of 30vol.% oil. The oil phase consisted of 1wt/vol.% of BPO and 15vol.% of HDDA, 1.19vol.% DMPT all dissolved in IBMA. The polymer beads were dispersed in deionised water and sonicated with an ultrasonic probe for 1 min and for 10 min. The SEM images presented in Figs 2.20-2.23 show that sonication for 10 min was sufficient to release the particles from the polymer beads. The images also show that the particles are more readily released by increasing the surfactant concentration. However, some particles remained firmly attached to the polymer beads. The angle of the immersion of the silica particles in the polymer measured from the SEM images is illustrated in Fig 5.24. This depth increased with increasing surfactant concentration (see Table 5.1).

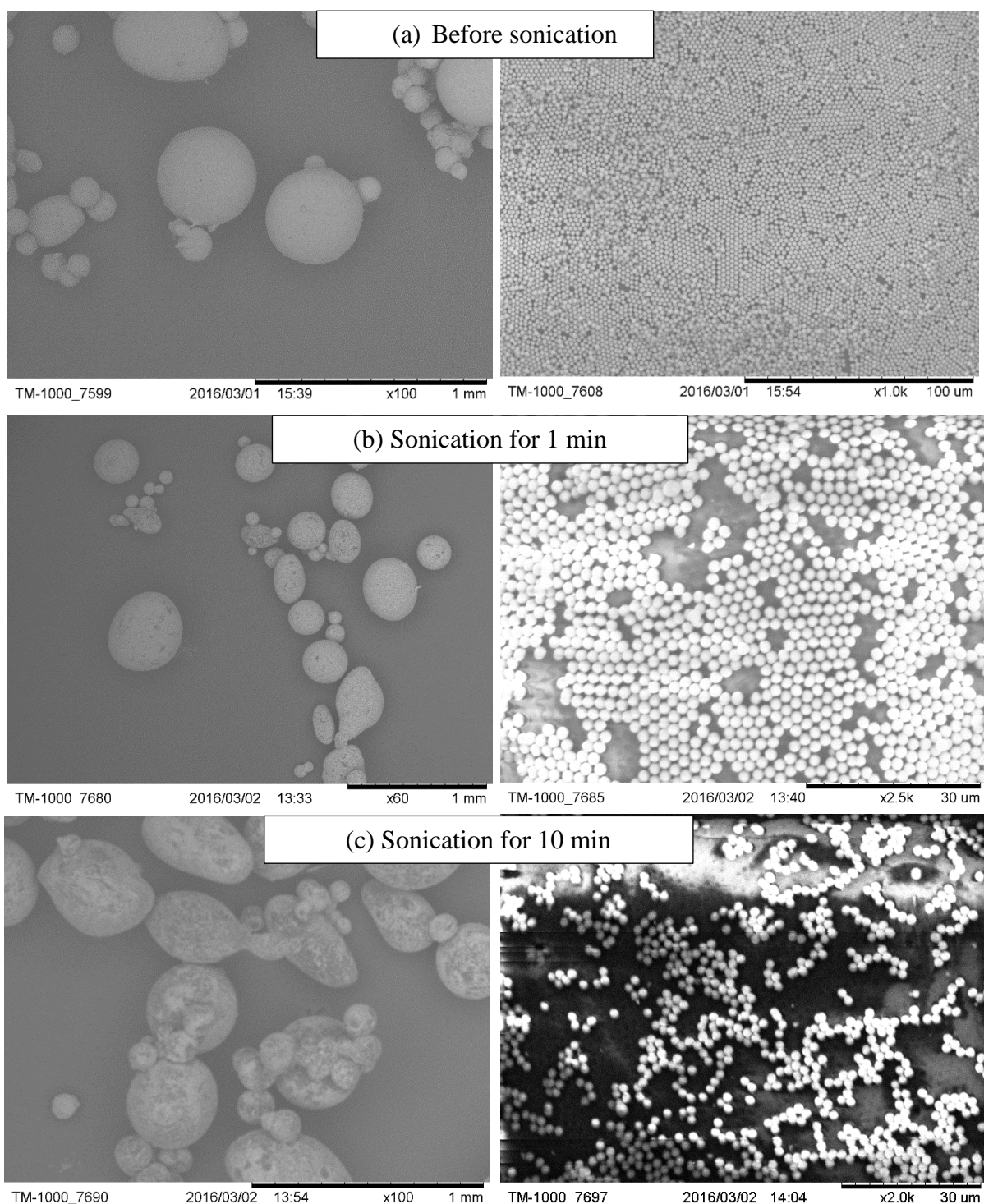


**Figure 5.20.** SEM images of silica particles ( $2\mu\text{m}$  diameter) attached to polyIBMA cross-linked with HDDA. a) Silica particles attached to polymer beads after the polymerisation of a Pickering emulsion stabilised by 4 wt/vol.% silica particles in deionised water (0 mM TTAB). b) The polymer beads were dispersed in deionised water and sonicated with an ultrasonic probe for 1 min at 40% amplitude. c) The polymer beads were dispersed in deionised water and sonicated with an ultrasonic probe for 10 min at 40% amplitude.

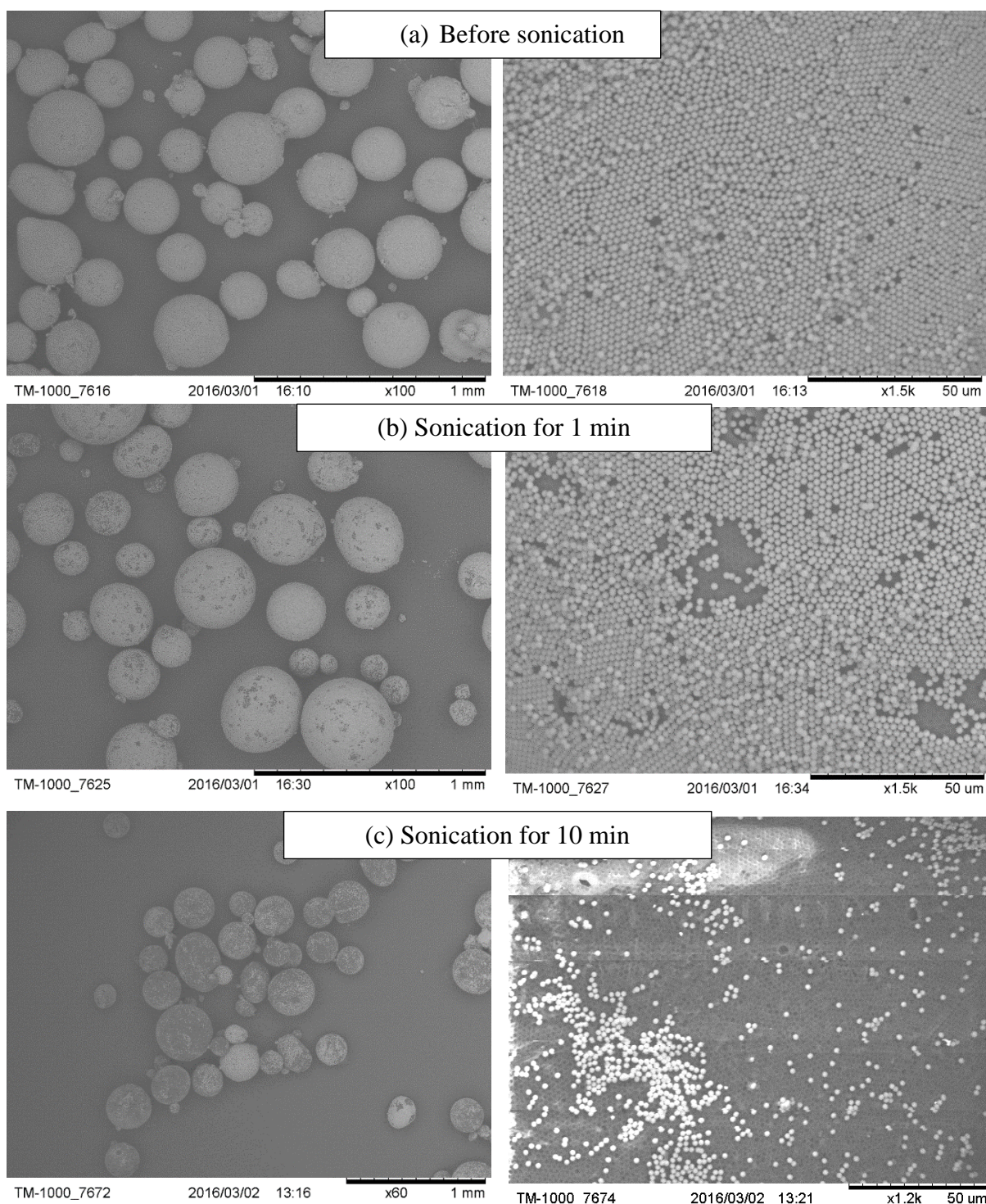


**Figure 5.21.** SEM images of silica particles (2 $\mu$ m diameter) attached to polyIBMA cross-linked with HDDA. a) Silica particles attached to polymer beads after the polymerisation of a Pickering emulsion stabilised by 4 wt/vol.% silica particles dispersed in 0.01 mM TTAB aqueous solution. b) The polymer beads were dispersed in deionised water and sonicated with an ultrasonic probe for 1 min at 40% amplitude. c) The polymer beads were dispersed in deionised water and sonicated with an ultrasonic probe for 10 min at 40% amplitude.

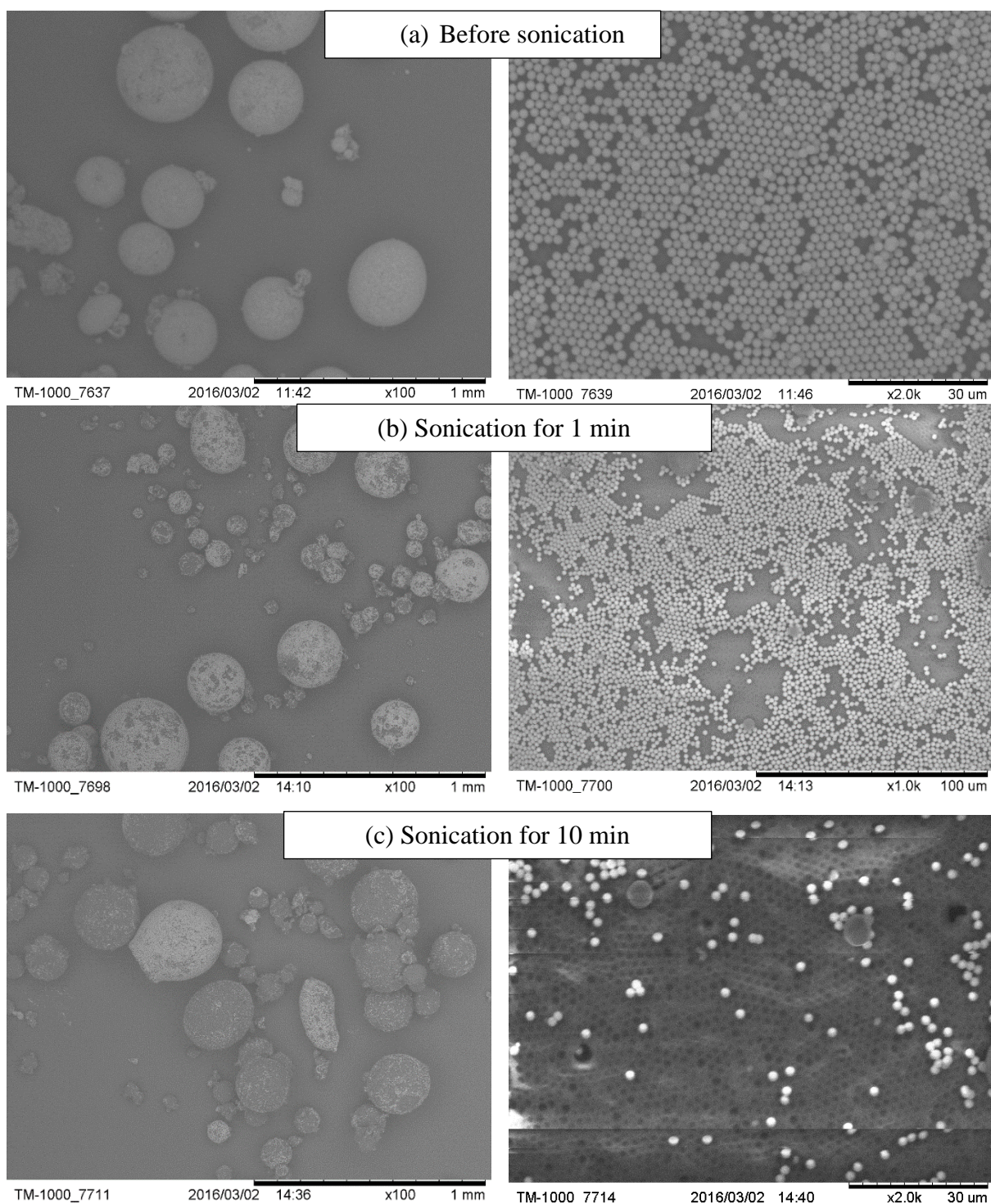


**Figure 5.22.** SEM images of silica particles (2 $\mu$ m diameter) attached to polyIBMA cross-linked with HDDA. a) Silica particles attached to polymer beads after the polymerisation of a Pickering emulsion stabilised by 4 wt/vol.% silica particles dispersed in 0.05 mM TTAB aqueous solution. b) The polymer beads were dispersed in deionised water and sonicated with an ultrasonic probe for 1 min at 40% amplitude. c) The polymer beads were dispersed in deionised water and sonicated with an ultrasonic probe for 10 min at 40% amplitude.

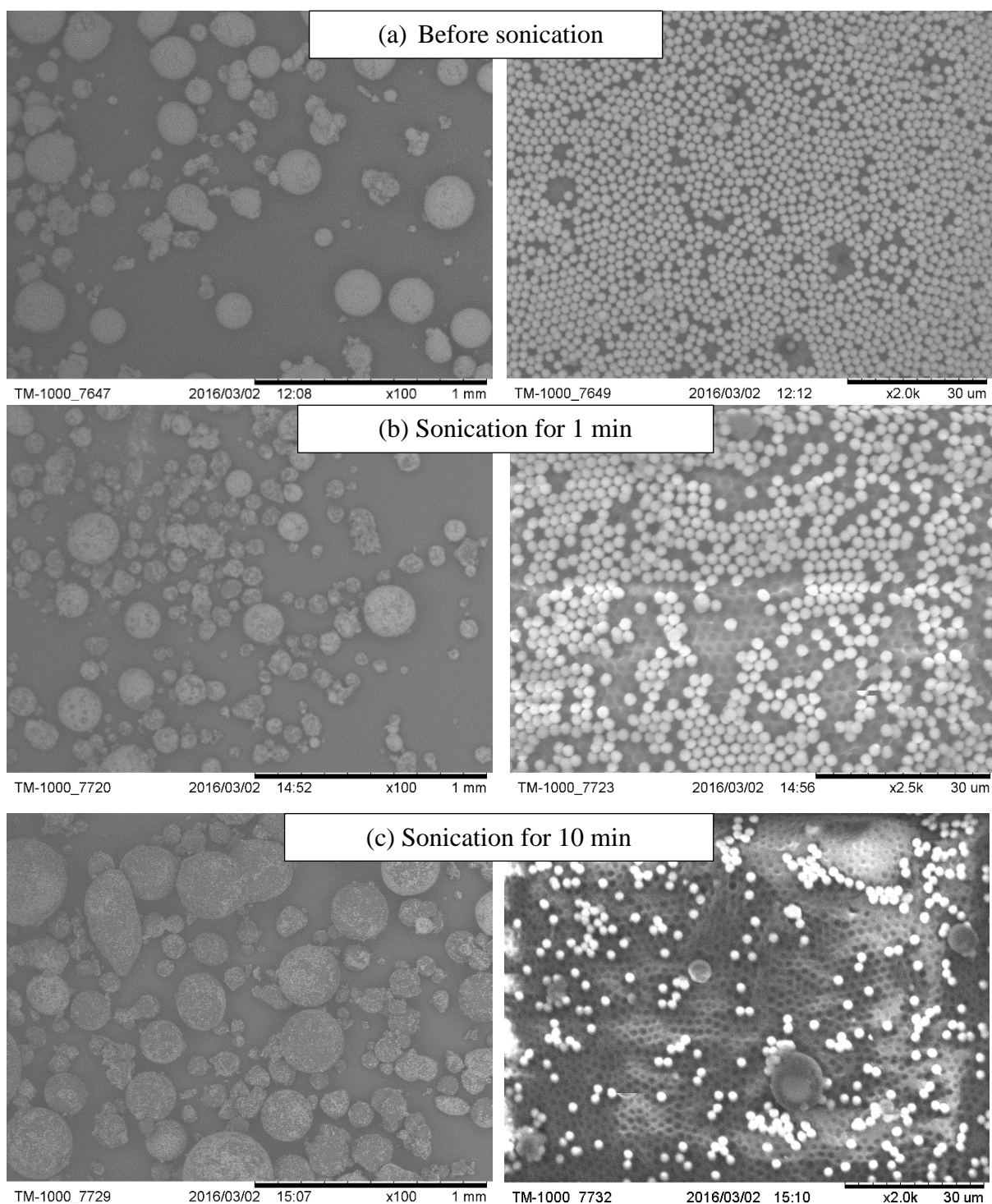


**Figure 2.23.** SEM images of silica particles (2 $\mu$ m diameter) attached to polyIBMA cross-linked with HDDA. a) Silica particles attached to polymer beads after the polymerisation of a Pickering emulsion stabilised by 4 wt/vol.% silica particles dispersed in 0.1 mM TTAB aqueous solution. b) The polymer beads were dispersed in deionised water and sonicated with an ultrasonic probe for 1 min at 40% amplitude. c) The polymer beads were dispersed in deionised water and sonicated with an ultrasonic probe for 10 min at 40% amplitude.

### 5.2.4 Particle immersion in the polymer and ‘Janus balance’

The immersion of particles in the polymer bead was estimated from the dents left after occasional detachment of some particles from the polymer bead surface (Fig. 5.24) The particle and dent diameters ( $d$  and  $d_c$ , respectively) were measured from the SEM images and used to calculate the angle of immersion,  $\theta$ , by the formula  $\sin\theta = d_c/d$ . Then the ‘Janus balance’ defined as the ratio between the external (exposed) area of the particle,  $A_{ex}$ , and the area immersed in the polymer,  $A_{im}$ , was calculated by the equation

$$\frac{A_{ex}}{A_{im}} = \frac{1+\cos\theta}{1-\cos\theta} \quad (5.1)$$

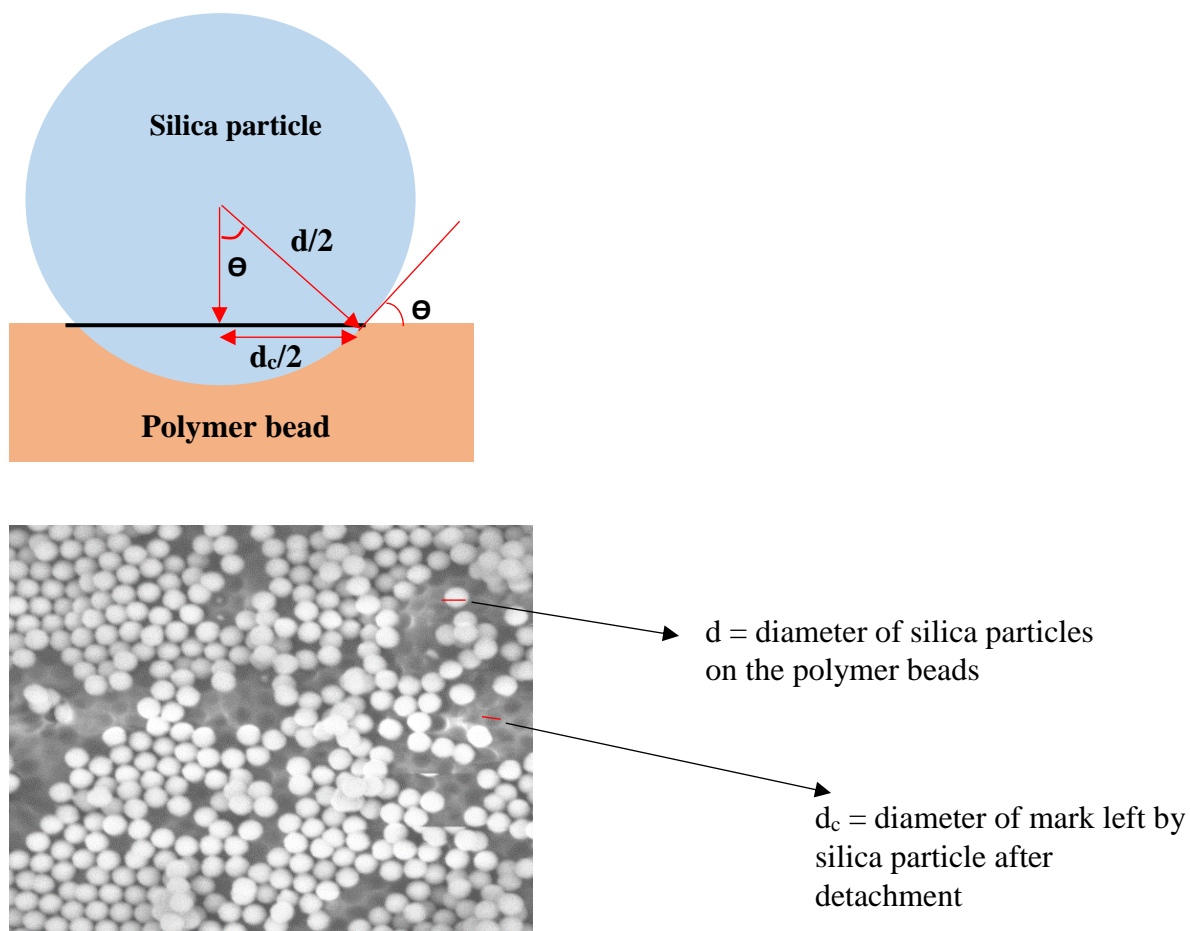


**Figure 2.24.** Schematic diagram is showing calculation of the immersion angle on the polymer beads;  $d_c$  and  $d$  were identified to estimate the depth of immersion on the polymer beads. The SEM image shows the cavity measured from the image as  $d_c$  and the diameter of silica particles as  $d$  in the image.

**Table 5.1.** Estimated angle of particle immersion in the polymer bead and the ‘Janus balance’ defined as  $A_{ex}/A_{im}$  (see eq. 5.1) at different TTAB surfactant concentrations for the system IBMA-HDDA. The particle diameter is  $2\mu\text{m}$ .

TTAB concentration / mM	Average estimated immersion angle / °	$A_{ex}/A_{im}$
0	$43 \pm 8$	$6.4 \pm 2.8$
0.01	$45 \pm 7$	$5.8 \pm 2.1$
0.05	$54 \pm 9$	$3.9 \pm 1.6$
0.10	$53 \pm 8$	$4.0 \pm 1.5$

The results showed that the sonication of the polymer beads for 10 min in deionised water was sufficient to release the particles from the polymer beads. The immersion angle of silica particles varied from  $43^\circ$  to  $53^\circ$  according to the concentration of TTAB. Janus balance decreased with increasing the surfactant concentration from 6.4 to 4. The results of immersion angle and Janus balance suggest that the surfactant helped the silica particles to immerse deeper in the polymer as the surfactant increased.

The release of silica particles from the polymer beads was optimised. The best sonication time was found to be 10 min. The quantity of particles obtained was very small and not enough for further experiment.

### 5.3 Scaling-up the process of Janus particle preparation

The previous section described emulsification done by the Ultra-Turrax method when the total volume of emulsion was 10 mL. Here, the emulsification was done by an overhead stirrer, and the monomer was changed to MMA. This was done in an attempt to produce a larger quantity of polymer beads and increase the quantity of silica particles obtained. An apparent weakness of our approach is that after releasing the Janus particles from the polymer beads, those polymer beads would be considered as waste. However, we changed the monomer from IBMA to MMA to take advantage of the polymer beads left after releasing Janus particles. PolyMMA is harder and could be used as filter to other polymeric materials. PolyMMA has more applications than polyIBMA. The oil phase was made up of 1wt/vol.% of BPO and 15vol.% of EGDMA, 1.19vol.% DMPT all dissolved in MMA. The silica particles ( $1\mu\text{m}$  diameter) 4wt/vol.% were dispersed in 21 mL of 0.01 mM TTAB solution and stirred for 1 hour. Then, the suspension was transferred to a three-neck flask fitted with an overhead stirrer and stirred at 700 rpm. In the Fig.5.25, it shows the experiment of making Janus particles with large scale. The oil phase was added drop-wise using the syringe pump at 4mL/min. The emulsion was stirred

for 10 min at that speed. Next, the accelerator (DMPT) was added and the speed reduced to 400 rpm. The  $N_2$  was running during the experiment to speed up the polymerisation by replacing the oxygen in the system. The polymer beads were filtrated by vacuum filtration using filter paper (porous 5–8  $\mu\text{m}$ ) (see Fig.5.26). The coverage of silica particles on the polymer beads was improved, as shown in the SEM images in Fig.5.27. The multilayer was less present in comparison to the previous method. There are some polymer beads fully covered with particles and other partially covered.

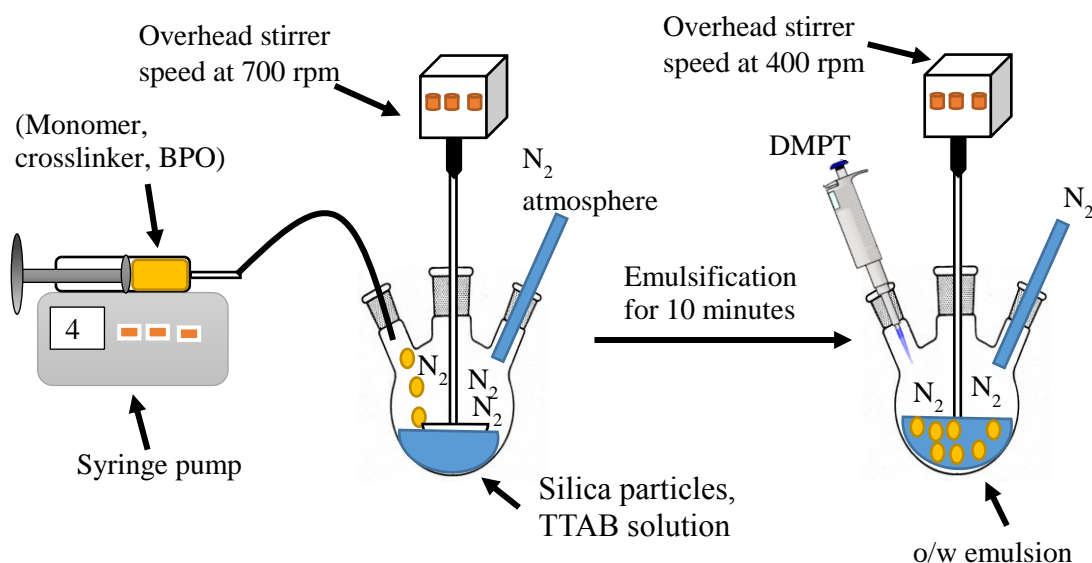


**Figure 5.25.** Diagram of the preparation and polymerisation of Pickering emulsions in the large scale experiments for making Janus particles.



**Figure 5.26.** Polymer beads after drying in the vacuum oven at room temperature overnight. The emulsion was made up of oil phase 9 mL( 1wt/vol.% of BPO, 15vol.% of EGDMA and 1.19vol.% of DMPT all dissolved in MMA) and the water phase was made up of 4wt/vol.% silica particles (1  $\mu\text{m}$  diameter) dispersed in 21 mL of TTAB solution.

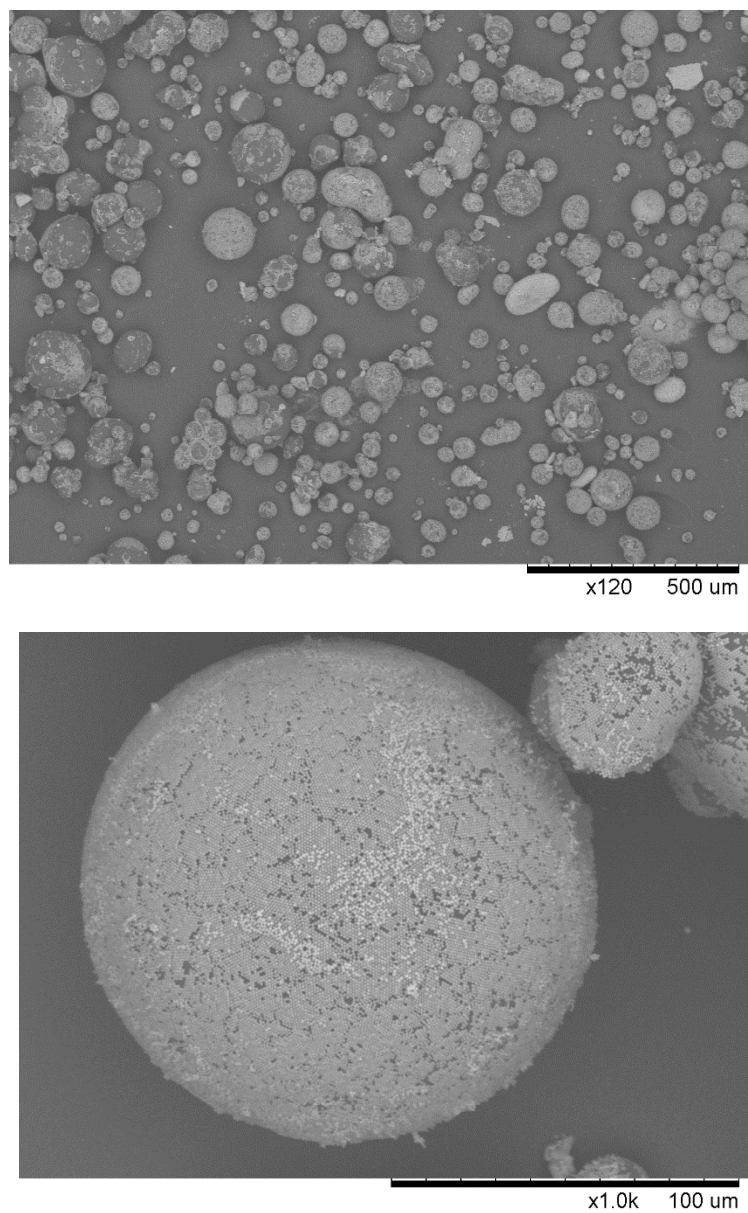


**Figure 5.27.** SEM images of silica particles (1  $\mu\text{m}$  diameter) attached to polymer beads produced by emulsion polymerisation. Emulsions were made up of 30vol.% oil phase (1wt/vol.% of BPO and 15vol.% EGDMA, 1.19vol.% DMPT, dissolved in MMA) and 70vol.% water phase (4wt/vol.% silica particles dispersed in TTAB solution 0.01 mM). These polymer beads were obtained with emulsification using an overhead stirrer.

After obtaining the polymer beads and treated the exposed surface of silica particles with APTES to graft amino group, the polymer beads dispersed in deionised water and sonicated with ultrasonic probe for 10 min to release the Janus particles. Most of the particle left the polymer beads. However, there were some particles still did not detach from the polymer beads as shown in the SEM images Fig.5.28. The immersion angle of particles was measured from the SEM images  $\theta=31\pm4$ .

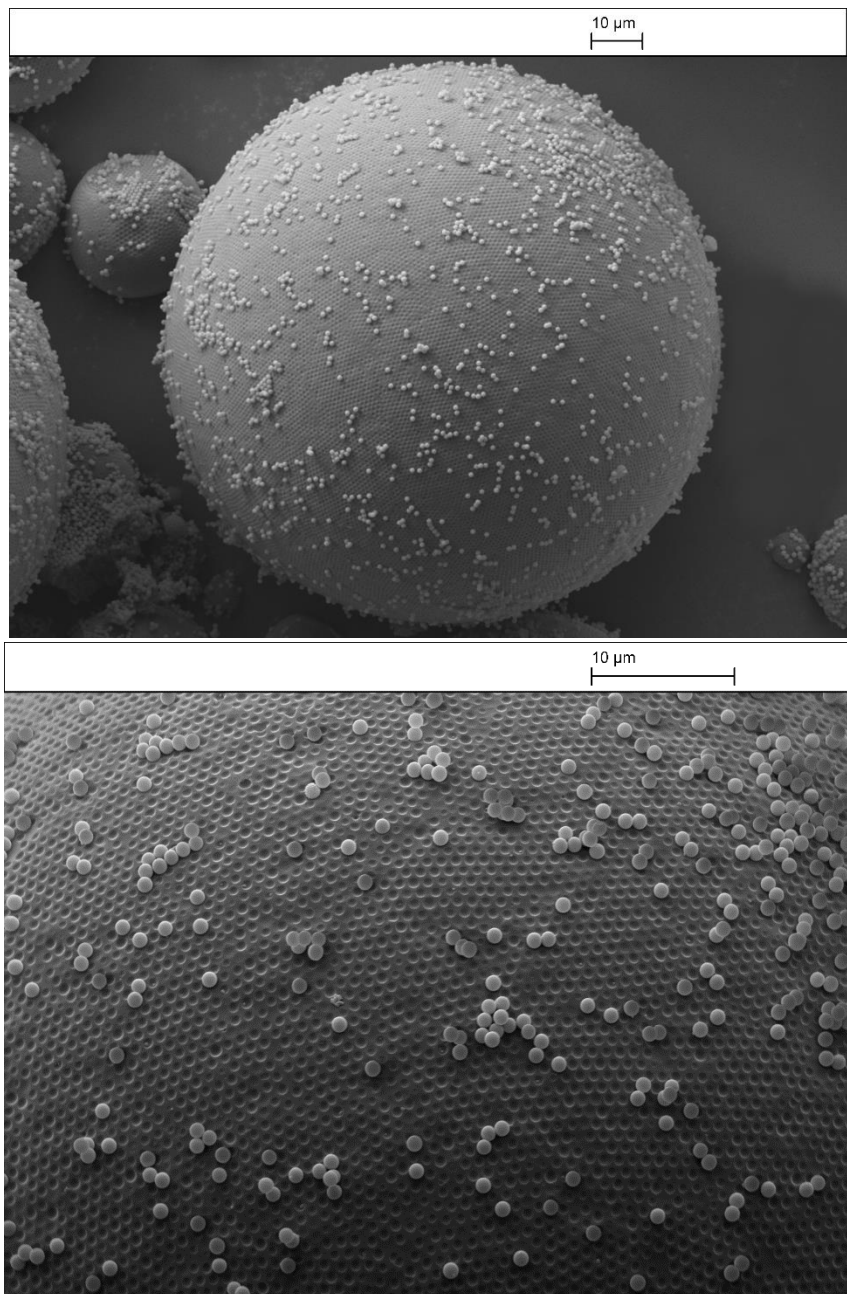


**Figure 5.28.** SEM images of silica particles attached to polyMMA cross-linked with EGDMA. The polymer beads were sonicated for 15 minutes to detach the silica particles from the polymer beads. The method of emulsification was with overhead stirrer. The emulsion made of oil phase (9mL) 1 wt/vol.% BPO, 15vol.% EGDMA, 1.19vol.% DMPT all dissolved in MMA. The water phase (21 mL) made of 4 wt/vol.% of silica particles (1μm diameter) dispersed in 0.01 mM TTAB solution.

The amount of silica particles obtained from emulsification with an overhead stirrer was 0.2 g, which was enough to perform additional experiments. The initial quantity of silica particles in the system was 0.84 g and the quantity obtained 0.2 g. The overhead stirrer needed to be further optimised to improve the production of the yield.

Zeta potential is used as a tool to confirm the production of Janus particles. Emulsification with an overhead stirrer helped to obtain Janus particles. After the polymerisation of the Pickering emulsion, the collected polymer beads were washed with pH=10 to remove the excess particles. Then, the exposed surface of the silica particles was treated with APTES to graft the amino group. After that, the polymer beads were sonicated with an ultrasonic probe to remove the Janus particles. The zeta potential for Janus particles was measured, as shown in Fig.5.29. The zeta potential of clean and aminated silica particles (1  $\mu\text{m}$  diameter) was measured as well, because we expected that the zeta potential of the particles would register approximately midway between the clean and aminated silica particles. The isoelectric point of the bare silica particle was at pH=3 and for the aminated particle around pH=8. It was found that the isoelectric point of Janus particles fitted perfectly between the clean and aminated silica particles at around pH=6. The immersion depth of Janus particles seemed to be less than 90°. As in Fig.5.29, the values of zeta potential were closer to the aminated silica particles than to the clean particles. This indicated that the silica particles have more amino groups than hydroxyl groups. The zeta potential measurement suggest that the production of Janus particles was successful.

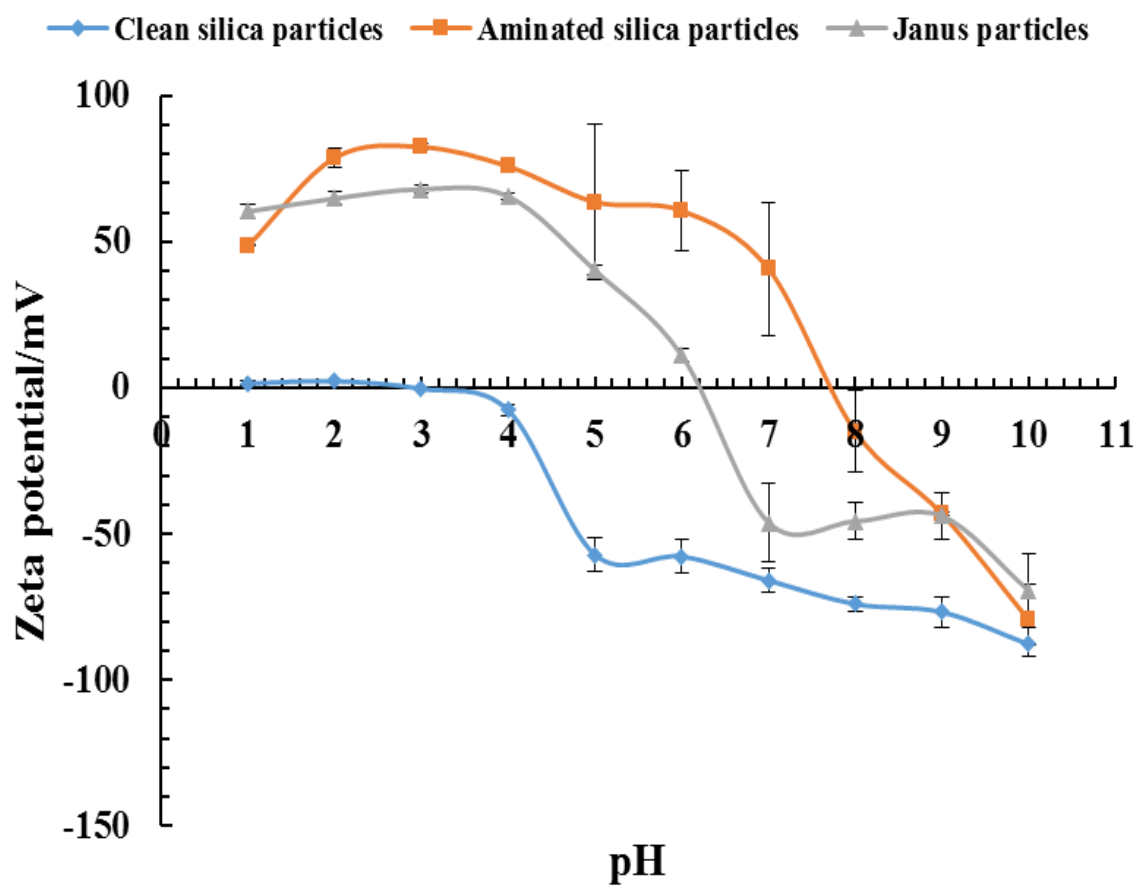


**Figure 5.29.** Zeta potential measurement of clean, aminated and Janus silica particles (1  $\mu\text{m}$  diameter). Silica particles were cleaned with ethanol and water and the clean particles treated with 10vol.% of APTES. The Janus particles had two surfaces, one containing hydroxyl groups and the other - amino groups. The pH was altered by using NaOH or HCl.

## 5.4 Conclusions

The preparation method of producing Janus particles via polymerised Pickering emulsion was developed. The study started by small scale experiment to optimised the method. The emulsion stability was studied. The emulsion was stabilised with a mixture of surfactant and silica particles. The silica particles were treated with TTAB solution (0–10 mM) to tune the hydrophobicity and to allow the particles to stabilise the emulsion. The oil phase (30vol.%) was consisted of IBMA as the monomer, HDDA or EGDMA as the crosslinker, BPO as the initiator. The water phase was made of 4wt/vol.% of silica particles dispersed in TTAB solution. In the first system, the oil phase was IBMA-HDDA and the size of silica particles 2 $\mu$ m. In the second system, the oil phase was IBMA-EGDMA and the size of silica particles 1 $\mu$ m. In the third system, the oil phase was IBMA-EGDMA and the size of silica particles 0.1 $\mu$ m. The emulsion type in all the three systems was O/W emulsion (confirmed by the drop test). The emulsion stability rose with increased surfactant concentration. Emulsions were stable for hours at room temperature.

Polymerisation of the oil droplets to trap the particles at the interface occurred. During emulsification with Ultra-Turrax, the polymer beads were obtained at a low surfactant concentration of 0–0.1 mM. After that, either bulk or small pieces of polymers were produced and, at a high concentration of TTAB, 3 and 10 mM, nothing was obtained, as the polymerisation was inhibited. The coverage by silica particles of the polymer beads varied from a monolayer to a multilayer. The polymer beads were washed with pH=10 to remove the multilayer and obtain monolayer coverage. The washing removed most of the multilayer, but leaving a particle monolayer on the polymer beads. The release of silica particles from the polymer beads was optimised. The particles were removed by sonication with an ultrasonic probe. The best sonication time for the polymer beads to be dispersed in water was found to be 10 min. The immersion angle and Janus balance were measured from the SEM images and it was found that the immersion angle increased with increasing the surfactant concentration. From this method using Ultra-Turrax homogeniser the silica particles obtained after filtration were very low yield and not sufficient for further experiments.

Emulsification with an overhead stirrer was done to obtain a larger yield of polymers as well as particles. The polymerisation was successful, and the yield of polymer beads increased. The polymer beads almost fully covered with particles and there were some bare regions. The polymer beads were treated with APTES to graft amino group on the exposed surface of the silica particles. After the step of modification, the polymer beads

sonicated with ultrasonic probe to remove Janus particles. Then, Janus particles were obtained by vacuum filtration. The yield improved in comparison to the previous method with small-scale experiment. The Janus particles obtained with overhead stirrer emulsification was 0.2 g. However, this method needs further development to improve the quantity of the yield. The yield obtained from this method of emulsification with overhead stirrer was sufficient to performed further experiment.

The zeta potential measurement was performed in order to confirm the production of Janus particles. The bare silica particles and aminated silica particles were measured, as well as the Janus particles obtained. The isoelectric point of Janus particles was located midway between that of the bare silica particles and that of the aminated particles. This indicated that the Janus particles have a hydroxyl group on one side and an amino group on the other.

## 5.5 References

1. C. Kaewsaneha, P. Tangboriboonrat, D. Polpanich, M. Eissa and A. Elaissari, *Colloids Surf., A*, 2013, **439**, 35-42.
2. B. P. Binks and P. D. I. Fletcher, *Langmuir*, 2001, **17**, 4708-4710.
3. X. Pang, C. Wan, M. Wang and Z. Lin, *Angew. Chem., Int. Ed.*, 2014, **53**, 5524-5538.
4. W. Gao, A. Pei, X. Feng, C. Hennessy and J. Wang, *J. Am. Chem. Soc.*, 2013, **135**, 998-1001.
5. A. Kirillova, C. Marschelke, J. Friedrichs, C. Werner and A. Synytska, *ACS Appl. Mater. Interfaces*, 2016, **8**, 32591-32603.
6. Q. Chen, S. C. Bae and S. Granick, *Nature*, 2011, **469**, 381.
7. S. Yang, F. Guo, B. Kiraly, X. Mao, M. Lu, K. W. Leong and T. J. Huang, *Lab Chip*, 2012, **12**, 2097-2102.
8. M. Lattuada and T. A. Hatton, *Nano Today*, 2011, **6**, 286-308.
9. L. Hong, S. Jiang and S. Granick, *Langmuir*, 2006, **22**, 9495-9499.
10. S. Jiang and S. Granick, *Langmuir*, 2008, **24**, 2438-2445.
11. C. Ström, P. Hansson, B. Jönsson and O. Söderman, *Langmuir*, 2000, **16**, 2469-2474.
12. B. P. Binks, *Curr. Opin. Colloid Interface Sci.*, 2002, **7**, 21-41.
13. R. Pichot, F. Spyropoulos and I. T. Norton, *J. Colloid Interface Sci.*, 2010, **352**, 128-135.
14. T. Zhang and F. D. Blum, *J. Colloid Interface Sci.*, 2017, **504**, 111-114.

## **CHAPTER 6**

### **Summary of conclusions and future work**

The main focus of this thesis is on the preparation of macroporous polymers and Janus particles using emulsion templates. Benzoyl peroxide – dimethyl-p-toluidine (BPO-DMPT) redox-initiation couple is used to polymerise the oil phase of water-in-oil (w/o) or oil-in-water (o/w) emulsion templates at room temperature and produce macroporous polymeric materials or Janus particles, respectively.

The preparation of macroporous polymers via emulsion templating usually uses water-in-oil emulsions. The polymerisation of the oil phase is initiated either by a thermo-initiator at elevated temperature (60-80 °C) or a photo-initiator by irradiating relatively thin transparent samples with UV light. Both approaches suffer from low energy efficiency and require tedious sample preparation (removal of inhibitors, inert atmosphere). Those drawbacks are addressed by us in Chapter 3 of the thesis, where the polymerisation of w/o emulsion templates with a BPO-DMPT redox-initiation system at room temperature is investigated. The morphology and mechanical properties of the porous materials obtained are compared to those synthesised from emulsion templates using the traditional thermo-initiated polymerisation in Chapter 4.

The preparation of Janus particles in large quantities is still one of the most challenging problems in the field. Most of the preparation methods reported suffer from limited yields or Janus functionalities which could be achieved. The use of particle-stabilised (Pickering) emulsions of paraffin wax-in-water as a tool for making Janus particles introduced by the group of Granick could give large yields, but the paraffin wax causes problems due to the poor particle adhesion and the limited conditions for chemical modification. In Chapter 5, we use our knowledge for redox-initiated polymerisation of methacrylates gained in the macroporous polymer study to develop efficient and reliable procedures for the preparation of Janus particles using polymerised o/w Pickering emulsions.

The main findings and conclusions from our investigations are summarised below.

#### **6.1 Summary of main findings and conclusions**

The preparation of macroporous polymeric materials by polymerising the external oil phase of w/o emulsion templates using a BPO-DMPT redox-initiation system has been investigated and the results presented in Chapter 3. The oil phase consisted of methyl methacrylate (MMA) as a monomer, ethylene glycol dimethacrylate (EGDMA) as a crosslinker, Pluronic L-121 (PEL-121) surfactant as emulsifier, BPO as an initiator and

DMPT as an accelerator. Deionised water was used as a water phase in the emulsion templates. All chemicals have been used as received without any purification and the emulsions prepared and polymerised in air at room temperature.

The effect of water volume fraction,  $\phi_w$ , in the emulsion template on the morphology, porosity and mechanical properties of the polymeric materials has been investigated in two series of experiments at fixed concentrations of the crosslinker (15 vol.% EGDMA), BPO (1 wt/vol.%) and DMPT (1.19 vol.%). In the first series, the surfactant concentration in the oil has been kept constant at 5 wt/vol.%, therefore the amount of surfactant in the emulsion progressively decreased with the increase of the water volume fraction. In the second series of experiments, the amount of the surfactant in the oil has been adjusted to maintain its concentration with respect to the total volume of emulsion equal to 1.75 wt/vol.%. It was found that all emulsion templates with  $\phi_w$  in the range 65-90 vol.% produced macroporous polymers with open pores and porosity ranging from 70 % to 94 % depending on the water content. The median diameter (DN0.5) of voids and pore throats was also found to increase with the water fraction. In the first series of experiments, the increase of void diameter was significant: from  $9.0 \pm 0.5 \mu\text{m}$  ( $\phi_w = 65$  vol.%) to  $29.0 \pm 1.5 \mu\text{m}$  ( $\phi_w = 90$  vol.%), i.e. more than 200 % increase. A similar trend was observed for the median pore throat diameter which increased 4 times from  $1.6 \pm 0.1 \mu\text{m}$  to  $6.4 \pm 0.6 \mu\text{m}$ , respectively. This has been attributed to the decrease of the total amount of surfactant as  $\phi_w$  increases resulting in the formation of emulsion templates with bigger droplets. As expected, the elastic modulus and the strength of the materials decreased with increasing the porosity. The material with 70 % porosity had elastic modulus of  $109.6 \pm 1.8$  MPa and strength of  $8.71 \pm 0.20$  MPa, while the respective values obtained for the material with 93 % porosity were  $14.4 \pm 0.4$  MPa and  $0.57 \pm 0.01$  MPa. Similar trends for the porosity, pore diameters, elastic modulus and compressive strength were observed in the second series of experiments when the total concentration of surfactant in the emulsion was kept constant. All materials in those experiments were also with open pore structure and similar porosities. However, the variation of the void and pore throat median diameters with the water fraction was less pronounced: only 34 % increase for the void and 2 times increase for the pore throat diameters when the water volume fractions was increased from 65 to 90 vol.%. In these experiments, the larger amount of surfactant in the higher water content systems helped to generate smaller droplets and maintain the emulsion stability better during the polymerisation. The curing of emulsion templates was found to be within 20-35 minutes (longer at higher water fractions) and the temperature during

polymerisation did not exceed 39 °C. These features of the studied system suggest it could be used in applications where rapid curing at relatively low temperatures is required.

The effect of surfactant concentration in the oil phase of the emulsion template on the properties of the porous materials obtained after polymerisation have been investigated at a fixed water volume fraction of 80vol.%. The concentrations of crosslinker (15 vol.% EGDMA), BPO (1 wt/vol.%) and DMPT (1.19 vol.%) in the oil phase (MMA) were also kept constant, while the concentration of PEL-121 surfactant,  $C_{SO}$ , varied in the range 0.4-10 wt/vol.%. Again, all the materials produced had open pore structure and almost the same porosity of 83 – 84 % within the experimental error of  $\pm 2$  %. However, the void and throat diameters were significantly affected by the surfactant concentration. The median diameter of voids and pore throats monotonically decreased with the increase of surfactant concentration: from  $88.7 \pm 7.2 \mu\text{m}$  to  $11.3 \pm 0.6 \mu\text{m}$  for the voids and from  $7.38 \pm 0.54 \mu\text{m}$  to  $2.48 \pm 0.17 \mu\text{m}$  the pore throats. It was found that both the elastic modulus and compressive strength had maximum values at 1wt/vol.% of PEL-121. The elastic modulus has increased from  $58.4 \pm 1.6$  MPa at  $C_{SO} = 0.4$  wt/vol.% to  $74.2 \pm 1.1$  MPa at  $C_{SO} = 1$  wt/vol.%, and decreased at higher PEL-121 concentrations reaching  $60.9 \pm 1.0$  MPa at  $C_{SO} = 10$  wt/vol.%. Similarly, the strength was found to be  $3.31 \pm 0.14$ ,  $4.06 \pm 0.07$  and  $2.94 \pm 0.12$  MPa at 0.4, 1 and 10 wt/vol.% PEL-121, respectively. Our results suggest that the surfactant concentration in the emulsion template has a pronounced influence on the morphology and the mechanical properties of the respective microporous material. The surfactant concentration has to be adjusted to maximise the elastic modulus and strength of the macroporous polymeric materials produced by the emulsion templating method.

The effect of crosslinker concentration on the properties of the porous materials obtained from emulsion templates containing 80vol.% water have been investigated. The concentrations of PEL-121 surfactant (5 wt/vol.%), BPO (1 wt/vol.%) and DMPT (1.19 vol.%) in the oil phase (MMA) were kept constant, while the concentration of EGDMA varied in the range 5 – 35 vol.%. It was found that the median diameter of voids and pore throats decreased modestly as for voids  $18.9 \pm 1.2 \mu\text{m}$  to  $14.8 \pm 0.8 \mu\text{m}$  and pore throats  $4.2 \pm 0.20 \mu\text{m}$  to  $2.5 \pm 0.20 \mu\text{m}$ . The elastic modulus and the strength decreased slightly with increasing the crosslinker concentration. The elastic modulus decreased by 36% and the strength by 11%. The crosslinker concentration affected very strongly the curing dynamics of the emulsion templates; the gelling time has dropped from almost 2 h at 5 vol.% EGDMA to less than 13 min at 35 vol.% EGDMA. These results show that the curing time of the emulsion templates can be tuned in a broad range by adjusting the

crosslinker concentration without compromising the mechanical properties of the porous materials produced.

We demonstrated for the first time that MMA-based emulsion templates can be polymerised using BPO-DMPT redox-initiation to produce open cell macroporous polymeric materials at room temperature without the need of any complicated steps of preparation typical for other methods. Since the BPO initiator works only in the presence of the DMPT accelerator, they could be kept separated in two emulsions each containing the BPO or DMPT only. The polymerisation of the emulsion template could be initiated by mixing the two emulsions. We have successfully demonstrated this approach by making a filter in situ in water using benzyl methacrylate instead of MMA to achieve faster polymerisation. The advantages of using two emulsions are that once prepared in the lab, they could be stored for a long time and used in the field when and where needed. The stability during storage of two w/o emulsion templates with 20 vol.% oil phase made of MMA, 15 vol.% EGDMA and 5wt/vol.% of PEI-121 surfactant was investigated. The aqueous phase was either deionised water or 0.12 M CaCl<sub>2</sub>. Visible changes in the appearance of both type of emulsion templates were not detected for 9 days after their preparation. However, microscope images revealed that the median droplet diameter in the emulsion made with deionised water increased ~3.5 times after 5 days of storage due to Ostwald ripening. The increase of the droplet size in the emulsion with electrolyte was much smaller (25 % after 5 days) than that in the emulsion with deionised water. Therefore, for long-term storage, electrolyte must be added to the water phase of w/o emulsion templates to suppress the Ostwald ripening and maintain the original characteristics of the template.

In Chapter 4, the preparation of macroporous polymers from w/o emulsion templates using the thermo-initiation method at high temperature was studied and the materials obtained were compared to those produced with the redox-initiation method at room temperature. Experiments with w/o emulsion templates containing 80 vol.% internal water phase and 20 vol.% oil phase made of MMA, 15 vol.% EGDMA and 5wt/vol.% of PEI-121 surfactant were conducted. The initiator was either BPO (up to 3.5 wt/vol.%) or 1.6 wt/vol.% of AIBN in the oil phase. In both cases, the preparation of porous polymers was found to be very challenging since the emulsions destabilised during heating in the oven at 70 °C. When BPO was used, all attempts to speed up the polymerisation by removing the inhibitors from the oil phase, adding 0.12 M CaCl<sub>2</sub> in the water phase and using nitrogen atmosphere did not produce porous materials with the desired properties.

Partial success was achieved by using degassed aqueous phase (in addition to all previous measures) and conducting the polymerisation at 80 °C. Therefore, BPO is not a suitable thermo-initiator for making porous polymers by emulsion templating. Better results were obtained with the AIBN initiator but only when the preparation steps outlined above (removing the inhibitors from the oil phase, adding 0.12 M CaCl<sub>2</sub> in the degassed water phase and using nitrogen atmosphere) were followed. However, the emulsion templates with a water content of 85 vol.% or higher were partially or completely destabilised during heating in the oven and porous materials of reasonable quality were not produced. The porous materials produced from templates with 65-80vol.% water phase had an open structure; the highest porosity achieved was 88 %. It was found that the median diameter of voids and pore throats increased with the the water volume fraction from 12.9±0.6 µm to 16.5±1.0 µm for the voids and from 1.7±0.2 µm to 2.7±0.2 µm for the pore throats. The increase of the diameter of the voids (by 28%) and the pore throats (by 59%) was rather modest in comparison to that in redox-initiated systems (155 % and 131 % for the voids and throats, respectively). The materials were brittle and crushed during the compression tests. As expected, the elastic modulus and strength decreased as the porosity increased.

Our results demonstrate, that the preparation of macroporous polymers by emulsion templating using redox-initiation is simpler, faster and cheaper in comparison to that using the thermo-initiation method. The redox-initiation method shows simplicity as there is no need for any prior purification of the oil phase, degassing of the water phase, using N<sub>2</sub> atmosphere or adding electrolyte to the water phase. The emulsion templates are more stable in the redox-initiation method thus allowing for the preparation of materials with higher porosity (93 %) in comparison to the thermo-initiation method. In addition, the mechanical properties of the materials produced with the redox-initiation method are better than those produced with the thermo-initiation method. Those are significant advantages of the redox-initiation method in comparison to other techniques for making macroporous polymeric materials by emulsion templating.

A method for the preparation of Janus particles by polymerising the oil phase of o/w Pickering emulsions at room temperature has been developed (Chapter 5). As a proof of principle, small-scale experiments were initially conducted using high speed homogenisation in the emulsion preparation. The hydrophobicity of silica particles with diameters 2, 1 or 0.1 µm was tuned by using different concentrations of the TTAB cationic surfactant and used for the preparation of o/w Pickering emulsions with 30 vol.% oil phase. Isobutyl methacrylate (IBMA) with 1,6-hexanediol diacrylate (HDDA) or

EGDMA crosslinkers and BPO-DMPT redox-initiator couple were used in those experiments. Stable o/w Pickering emulsions have been obtained and successfully polymerised when the TTAB concentrations were below the CMC (3mM). Polymer beads with partially imbedded particles at their surface were obtained in the range of 0 - 0.1 mM TTAB as revealed from SEM images. The immersion angle of the particles in the polymer beads was found to increase with the surfactant concentration. Therefore, the 'Janus balance' (the ratio between the external area of the particle and the area immersed in the polymer) could be controlled by adjusting the surfactant concentration. It was demonstrated that the release of silica particles from the polymer beads could be achieved by 10 min sonication in water using an ultrasonic probe. Although the yield of particles was very small, these experiments demonstrated the feasibility of our approach for Janus particle preparation. Further experiments for scaling up the process were conducted using an overhead stirrer for making larger amounts of Pickering emulsions. MMA was used as a monomer to produce harder polymer beads which could be used in other polymeric applications after releasing the Janus particles from their surface. It was found that the particle coverage on the polymer beads was almost a complete monolayer and improved in comparison to the small-scale experiments. The exposed surface of the silica particles was treated with APTES to graft amino group and the Janus particles released in water by sonication. The particle yield was not great (~24 % of the total amount of particle used) but much bigger than that in the small-scale experiments. Further optimisation of the procedure is needed to improve the yield. Zeta potential measurement revealed that the isoelectric point of Janus particles was located midway between that of the bare silica particles and that of fully aminated particles. This indicates that Janus particles with hydroxyl-amine functionality have been successfully produced.

## **6.2 Future work**

We demonstrated that macroporous polymers can be easily produced by redox-initiated polymerisation of surfactant stabilised w/o emulsion templates at room temperature. In the future, it would be interesting to stabilise the emulsion templates with solid particles alone (or with surfactants) and study the effect on the mechanical properties and the morphology of the materials produced. In addition, the effect of different crosslinkers and/or acrylic monomers (glycidyl methacrylate, benzyl methacrylate, etc.) on the properties of macroporous polymeric materials produced by our approach could be investigated. If successful, the use of glycidyl methacrylate would allow for a post-functionalisation of the microporous polymer with potential applications in separation

and analysis. The surface density of the surfactant at the interface did not performed and it could be studied by measuring the interfacial tension and apply Gibbs equation.

The method for making Janus particles developed by us could be improved further. This should include experiments for achieving better control over the immersion depth of silica particles in the polymer (for example by using different cationic surfactants such as octyltrimethylammonium bromide or decyltrimethylammonium bromide), preparation of Janus particles with different functionalities, developing more direct methods for proving the Janus character of the particles produced and investigation of their behaviour in bulk liquids and liquid interfaces. The overhead stirrer emulsification needs further optimisation to maximise the Janus particle yield. If the zeta potential measurement would be used to prove the production of Janus particles, buffer solution should be introduced to the suspension of the particles to maintain constant pH during the experiment.